

DRIFT SPECTRA FOR INELASTIC SHEAR FRAMES

A THESIS SUBMITTED TO  
THE GRADUATE SCHOOL OF NATURAL AND APPLIED SCIENCES  
OF  
MIDDLE EAST TECHNICAL UNIVERSITY

BY

ALI ETEMADI

IN PARTIAL FULFILLMENT OF THE REQUIREMENTS  
FOR  
THE DEGREE OF DOCTOR OF PHILOSOPHY  
IN  
CIVIL ENGINEERING

AUGUST 2015



Approval of the thesis:

**DRIFT SPECTRA FOR INELASTIC SHEAR FRAMES**

submitted by **ALI ETEMADI** in partial fulfillment of the requirements for the degree of **Doctor of Philosophy in Civil Engineering Department, Middle East Technical University** by,

Prof. Dr. Mevlüde Gülbin Dural Ünver  
Dean, Graduate School of **Natural and Applied Sciences**

\_\_\_\_\_

Prof. Dr. Ahmet Cevdet Yalçiner  
Head of Department, **Civil Engineering**

\_\_\_\_\_

Prof. Dr. Hakkı Polat Gülkan  
Supervisor, **Civil Engineering Dept., Çankaya University**

\_\_\_\_\_

**Examining Committee Members:**

Prof. Dr. Kurtuluş Soyluk  
Civil Engineering Dept., Gazi University

\_\_\_\_\_

Prof. Dr. Hakkı Polat Gülkan  
Civil Engineering Dept., Çankaya University

\_\_\_\_\_

Prof. Dr. Murat Dicleli  
Engineering Sciences Dept., METU

\_\_\_\_\_

Assoc. Prof. Dr. Ayşegül Askan Gündoğan  
Civil Engineering Dept., METU

\_\_\_\_\_

Assoc. Prof. Dr. Afşin Sarıtaş  
Civil Engineering Dept., METU

\_\_\_\_\_

**Date:** 08/18/2015

**I hereby declare that all information in this document has been obtained and presented in accordance with academic rules and ethical conduct. I also declare that, as required by these rules and conduct, I have fully cited and referenced all material and results that are not original to this work.**

Name, Last name : Ali Etemadi

Signature :

## **ABSTRACT**

### **DRIFT SPECTRA FOR INELASTIC SHEAR FRAMES**

Etemadi, Ali

Ph.D., Department of Civil Engineering

Supervisor : Prof. Dr. Hakkı Polat Gülkan

August 2015, 212 Pages

In assessing the damage originating from strong ground motions in building frames, it is necessary to identify properly the post-yield hysteresis degrading behavior of structural components that are well correlated with structural response and in turn, with damage. Likewise, structural damage during the ground motion is due to excessive interstory drift ratio; hence more realistic estimation of interstory drift demands has a significant role in the seismic evaluation of frame buildings.

Existing approaches used to calculate the drift spectrum are valid in elastic ranges and cannot count for overestimated drift demands due to the post-yielding behavior of structural systems. A simple procedure to estimate the spectra of maximum interstory drift demands in shear-type frames that respond in post-elastic limits is described in this thesis, and the effect of hysteresis deterioration properties on seismic demands is clarified. Afterwards, the modification factors are proposed to incorporate the hysteresis degradation effects parametrically. These factors are defined with respect to the corresponding elastic drift demands.

The closed-form drift spectrum is adopted as reference spectrum to validate the proposed spectrum ordinates in elastic ranges. The closed-form drift spectrum is derived based on the continuous shear-beam model and wave propagation theory. To

derive the drift spectrum through the proposed method, series of simple shear frames are designed to be consistent with the continuous shear-beam models thereafter by systematic variation of their column stiffness and story mass properties, a reasonable period range (0.3-2.4 s) is obtained. When these frames are subjected to the ground motions considered, their dynamic responses are computed by time history response analysis method, and this is performed in both elastic and inelastic ranges.

A smooth hysteretic model is adopted to incorporate the nonlinearity of structural members into the nonlinear time history calculations by meaningful magnitude variations of the control parameters. In this way the different types of hysteresis degrading properties (i.e. stiffness decay, strength deterioration and hysteresis pinching) are modeled by considering the rotational springs at both ends of each column for all stories. This model is extended based on the classical differential Bouc-Wen model. Access to experimental results of the cyclic force-deformation characteristics of components typical to the structure being analyzed provides the best means of specifying the above degrading parameters.

The parametric identification study is carried out to clarify the relationship between control parameters and the response hysteresis loops as well as provide a comprehensive range of the basic parameters. This is used to formulate a model for the desired hysteresis loop where all its parameters are physically meaningful. It is assumed that these quantities are collected from the cyclic loading tests, which reflects the realistic hysteresis decay characteristics of RC columns when exposed to severe cyclic loadings.

The drift demands gained through the wave propagation solution, and the results of 105,000 response history analyses in both elastic and inelastic ranges are used for calculating the error statistics. Such massive numbers of repeated processes are very exhausting to conduct manually, and this is the underlying factor in the development of a code to perform these time-consuming processes automatically. The least squared regression analysis is conducted on the intact differences between both elastic and inelastic spectrum ordinates to get the smooth variation functions. The

modification coefficients are proposed as the function of vibration period and some other system dependent variables. In the dataset of records, a substantial number of near-fault ground motions are involved, which make large seismic demands to the structures. Such a number of selected records are an indication of the reliability of statistical results. This method could apply to the rapid seismic evaluation of the existing poor-detailed, non-ductile buildings.

**Keywords:** Drift spectrum, Smooth Hysteretic Model, Bouc-Wen model, shear-type frame, stiffness and strength degradation, hysteresis pinching, quasi static analysis, near-field ground motions

## ÖZ

### LİNEER OLMAYAN KAYMA ÇERÇEVELERİ İÇİN YAKLAŞIK KAT ARASI YER DEĞİŞTİRME SPEKTRUMU

Etemadi, Ali

Doktora, İnşaat Mühendisliği Bölümü  
Tez Yöneticisi : Prof. Dr. Hakkı Polat Gülkan

Ağustos 2015, 212 Sayfa

Şiddetli yer hareketlerinden dolayı bina çerçevelerinde meydana gelen hasar tahminlerinde, hareket sırasında oluşan, katlar arası yer değiştirmelerin yüksek değerlerinden ötürü kolonlarda meydana gelen yapısal hasarlarla ilişkili olan davranışı düzeltici parametrelerin doğru bir şekilde tanımlanması gereklidir. Ayrıca, yer hareketleri esnasında yapı sistemlerindeki yüksek oranlarda katlar arası yer değiştirme sonucunda meydana gelen yapısal hasarlar dikkate alındığında, katlar arası yer değiştirme taleplerinin daha gerçekçi tahmini, çerçeve yapıların sismik değerlendirilmesinde önemli rol oynamaktadır.

Katlar arası yer değiştirme spektrumunu hesaplamak için kullanılan mevcut yaklaşımlar elastik aralıklarda geçerli olmaktadır, dolayısıyla yapısal sistemlerin akma ötesi davranışlarının yol açtığı, tahmin ötesi yer değiştirme taleplerini kapsamamaktadır. Bu tezde, elastik ötesi limitlerdeki davranışa tepki veren kayma-tipi çerçevelerde tanımlanmış azami katlar arası yer değiştirme talep spektrumlarının tahmin edilmesi için basit bir yöntem açıklanmış ve akma ötesi histeresis azalma davranışları sonucu ile değişen sismik talepler tanımlanmıştır. Daha sonra, elastik spektrum ile elastik sınır ötesi spektrum arasındaki azalma parametrelerine bağlı olan katsayı değerleri çıkarılmıştır. Böylece, histeresis azalma özelliklerinin

spectrum ordnatlar üzerindeki etkileri parametrik olarak incelenebilmektedir. Bu katsayılar doğrusal sistemlerdeki yer değiştirme taleplerine göre tanımlanmıştır.

Kapalı form katlar arası yer değiştirme spektrumu, elastik aralıklarda önerilen spektrum ordnatlarını doğrulamak üzere referans spektrum olarak ele alınmıştır. Kapalı form katlar arası yer değiştirme spektrumu, dalga yayılma teorisi ve sürekli kesme kiriş modeli kullanılarak türetilmiştir. Katlar arası yer değiştirme spektrumunun önerilen yöntemle türetilmesi için, basit kayma-çerçeve serileri kesme kiriş modeline uyumlu olacak şekilde tasarlanmıştır ve kolon rijitliğini ve kat kütle özelliklerini sistematik olarak değiştirerek, geniş bir titreşim süresi aralığında (0.3 – 2.4 s) elde edilmiştir. Bu çerçeveler, ele alınan yer hareketlerine maruz kaldıklarında, dinamik tepkileri, elastik ve/veya elastik olmayan bölgelerde “zaman tanım alanında davranış analiz yöntemi” kullanılarak hesaplanmıştır.

Yuvarlatılmış histeresis modeli, yapısal elemanların doğrusal olmayan davranış etkilerini doğrusal olmayan zaman tanım alanı hesaplamalarına dahil edilmesi için kullanılmıştır. Bu da modeli kontrol eden parametrelerin anlamlı büyüklük varyasyonları ile gerçekleşmiştir. Böylece farklı türdeki histeretik azalma özellikleri (yani rijitlik azalması; mukavemet azalması ve histeresis daralma) tüm kat kolonlarının iki ucundaki dönme yayları kullanılarak modellenmiştir. Bu model klasik diferansiyel tabanlı Bouc-Wen formülasyonundan yola çıkılarak geliştirilmiştir. Analiz edilen binaya özgü yapı bileşenlerinin çevrimsel kuvvet-deformasyon özelliklerinin deney sonuçlarına ulaşılması, yukarıda bahsi geçen azaltıcı parametrelerin en iyi şekilde açıklanmasını sağlamaktadır.

Parametrik model tanımlama çalışmaları, modelin kontrol parametreleri ve tepkisel histeresis döngüleri arasındaki ilişkiyi netleştirmek ve modelin kontrol parametrelerine geniş kapsamlı bir dizi sağlamak amacıyla gerçekleştirilmiştir. Tüm parametreler fiziksel olarak anlamlı olmakta ve istenen histeresis döngü modelini formüle etmek için kullanılabilir. Döngüsel yükleme testlerinden çıkartılan tahmini parametre değerlerinin şiddetli çevrimsel yüklere maruz betonarme kolonların gerçekçi histeresis azalma özelliklerini yansıttığı varsayılmaktadır.

Katlar arası yer deęiřtirme talepleri dalga yayılımı çözümlü aracılıęıyla elde edilmiřtir. Deęerlendirmelerde 105,000'in üzerinde zaman tanım alanlı davranıř hesaplaması, elastik olan ve olmayan tüm alanlarda, hata istatistiklerini hesaplamak için kullanılmıřtır. Çok sayıda tekrarlanan ve çok fazla zaman alan bu hesaplamalar elle yapılamayacaęı için, iřlemi otomatik olarak uygulayan bir program hazırlanmıřtır. Elastik ve elastik olmayan spektrum koordinatları arasındaki farklardan elde edilen tam deęiřim oranlarına uygulanan en küçük kareler regresyon analizi sonucunda verileri temsil eden en ideal eęriler üretilmeye çalıřılmıřtır. Modifikasyon katsayıları, titreřim periyodu ve sisteme baęımlı bazı dięer deęiřkenler dikkate alınarak önerilmiřtir. Çalıřmadaki kayıt verilerinin oluřturulmasında, yapılar için ařırı sismik taleplere yol ačan, yakın saha deprem kayıtları kullanılmıřtır. Seçilen yer hareketi sayısı, istatistiki sonuçların güvenilirlięini arttırmaktadır. Bu yöntem, zayıf veya sünek olmayan özelliklere sahip varolan binaların hızlı onarım deęerlendirmesinde yararlı olabilmektedir.

**Anahtar Kelimeler:** Katlar arası yer deęiřtirme spektrumu, Yuvarlatılmıř histeretik modeli, Bouc-Wen modeli, Kayma-tipi Çerçeve, rijitlik ve mukavemet azalması, hysteresis daralma, yarı-statik çözümlüleme, yakın saha yer hareketleri

*To my mother...*

*for dedicating your life to me...*

## ACKNOWLEDGEMENTS

The research presented in this dissertation has been made possible with contributions from many individuals to whom I am indebted. This study was performed under the supervision of Prof. Dr. Polat H. Gülkan. I would like to express my sincere appreciation for his invaluable guidance, encouragement, support, insight and friendly cooperation that he has provided me throughout this study. I consider myself fortunate to study with such an exceptional instructor and engineer.

Special thanks to my examining committee members for their review of my thesis and for comments they made on it. This work is supported by Scientific Research and Technical Council of Turkey (TÜBİTAK) under Award No. 111M551. The funding provided by TÜBİTAK is gratefully acknowledged.

My friendship department, Abbas Abbasov, Mohammad Ahmadi-adli, Cengiz Eser, Siamak Gharahjeh, Mehran Ghasabeh, Erdinç İşbilir, Nefiseh Shaban, Reza Moonesirad, Yashar Tavakkoli Osgouei, Pouya Zoghipour, deserves thanks for all the moments shared together in campus life.

I wish to express my sincere appreciation to Merve Aygenç, Onur Doğan, Semih Kavurucu, Rıdvan Ozkerim and Kathi Wyldeck for their helps, comments and suggestions throughout this study.

I would like to particularly thank to my dear uncle Mr. Daryoush Heidarlou and his better half, dear Neşvet, for their motivation and for all the things they had done for me throughout these years.

Finally, my deepest thanks and love go to my family, Mohammad Reza Etemadi and Ziba Heidarlou and to my brother Mazdak Etemadi, for their confidence in me and for their endless love, unyielding patience, support and encouragement throughout my whole life without their support, I could never perform this study. I am greatly indebted to them for everything that they have done for me.

## TABLE OF CONTENTS

ABSTRACT .....	v
ÖZ .....	viii
ACKNOWLEDGEMENTS .....	xii
TABLE OF CONTENTS .....	xiii
LIST OF TABLES .....	xvii
LIST OF FIGURES .....	xviii
LIST OF ABBREVIATIONS AND SYMBOLS .....	xxiii
1 INTRODUCTION .....	1
1.1 General .....	1
1.2 Purpose and Scope .....	10
1.3 Thesis Outline .....	15
2 DRIFT SPECTRUM IN LITERATURE .....	17
2.1 Introduction .....	17
2.2 Alternative Idealization Models of Building Frames .....	18
2.3 Iwan Drift Spectrum .....	21
2.4 Limitation of Proposed Drift Spectrum in Inelastic Regions .....	27
3 ANALYTICAL STUDY ON HYSTERESIS CAPACITY DEGRADATION OF STRUCTURAL SYSTEMS .....	37
3.1 Introduction .....	37
3.2 Bouc-Wen Hysteretic Model .....	42

3.2.1	Stiffness and Strength Degradation.....	45
3.2.2	Pinching Function .....	47
3.2.3	Solving the Bouc-Wen Hysteretic Model in the Analytical Form...48	
3.2.4.	Variation of the Response Hysteresis Loop of the SDOF system with the Bouc-Wen Model Parameters under External Cyclic Excitation.....	50
3.2.4.1	Influence of Parameter A.....	50
3.2.4.2	Influence of Parameters $\beta$ and $\gamma$ .....	52
3.2.4.3	Influence of the Parameter $n$ .....	52
3.2.4.4	Influence of the Parameters $\delta_A$ , $\delta_\eta$ and $\delta_v$ .....	55
3.2.4.5	Influence of Parameters $\sigma_0$ and $\delta_a$ as well as $\zeta_1$ and $\zeta_2$ .....	56
3.2.5	Seismic Response of SDOF Systems with the Bouc-Wen Hysteretic Model .....	61
3.3	Formulation of the Smooth Hysteretic Model .....	64
3.3.1	Stiffness Decay of the Hysteretic Spring .....	67
3.3.2	Strength Degradation .....	69
3.3.3	Hysteretic Pinching Formulation .....	70
3.4	Identification of Hysteresis Loop Control Parameters .....	71
3.5	SHM Sensitivity to Parameter Variations .....	81
4	SHEAR FRAMES MODELS AND GROUND MOTIONS DATABASE FOR DRIFT SPECTRUM DERIVATION .....	89
4.1	Introduction .....	89
4.2	Structural System.....	90
4.2.1	Design Methodology.....	91
4.2.2	Capacity design.....	93
4.2.3	Modeling of Plastic Hinges at Columns Tips .....	99
4.3	Characterization of Ground Motions Applied in This Study .....	101

4.4	Verification of Linear Elastic Drift Spectrum Obtained through the Simulation and Iwan (1997) Formulation .....	103
4.4.1	Program Development .....	104
4.4.2	Comparison of linear drift spectra derived through the Iwan (1997) formulation with the alternative RHA method .....	108
5	DERIVATION OF MODIFICATION FACTORS FOR DRIFT SPECTRA OF INELASTIC SHEAR FRAMES .....	111
5.1	Introduction .....	111
5.2	Structural Performance Levels and Ranges.....	114
5.3	Modification Factor Function for Inelastic Drift Spectrum .....	117
5.3.1	The Modification Factor for Degraded Smooth Elastic-plastic Systems ( $C_{\text{degraded}}$ ) .....	121
5.3.1.1	The $C_{\text{degraded}}$ Variation with Smoothness Rate of Elastic-Yield Transition .....	123
5.3.1.2	The $C_{\text{degraded}}$ Variation with Post Yielding Hysteresis Degradations .....	136
5.3.2	The Modification Factor to Incorporate Hysteresis Pinching Properties ( $C_{\text{pinched}}$ ) .....	145
5.4	Effect of PGA Intensity on the $C_{\text{pinched}}$ Factor .....	148
5.5	Effect of Peak Ground (a/v) Ratio on Drift Spectrum.....	150
6	SUMMARY, CONCLUSION AND RECOMMENDATIONS FOR FUTURE STUDIES .....	155
6.1	Summary of the Study .....	155
6.2	Conclusions .....	158
6.3	Future Studies.....	162
	REFERENCES .....	165

APPENDICES .....177

    A. TABLES OF SELECTED GROUND MOTIONS.....177

    B. THE PROGRAM GENERICFRAMES .....185

CURRICULUM VITAE.....211

## LIST OF TABLES

### TABLES

Table 3.1 Structural properties and Bouc-Wen hysteretic model control parameter of a SDOF system under seismic excitation.....	62
Table 3.2 Material characteristics and reinforcement details of test specimens.....	76
Table 3.3 Displacement protocols applied to the test specimens .....	77
Table 3.4 Hysteresis degradation parameter values obtained from comparison of simulation (the quasi-Static analysis) with respected to experimental results .....	78
Table 4.1 Story mass and stiffness properties and yield base shear of single bay generic shear frames.....	99
Table 5.1 Structural performance levels and damage for columnar members as per recommended by FEMA-356.....	117
Table 5.2 Control parameters that control the $C_{\text{degraded}}$ and $C_{\text{pinched}}$ factors with different intensity levels and correlation coefficient ( $r$ ) and standard error ( $s$ ) of fitted curves at each period interval.....	127
Table 5.3 Common area of quantities for hysteretic parameters .....	137

## LIST OF FIGURES

### FIGURES

- Figure 1.1 Aerial views of a few typical RC-MRF buildings in Gölcük. Traditional and faulty construction practices with limited interstory drift capacity under near-fault ground motion led to structural instability and excessive damage, including full collapse .....8
- Figure 1.2 Changeability of two adjacent, similar building responses proceed from different limit states; post-yielding hysteresis behavior pattern; and interstory drift capacities.....8
- Figure 2.1 Alternative idealization models of building frames; (a) Typical frame and rigid frame model; (b) Equivalent shear-beam model; (c) Equivalent shear-frame model.....19
- Figure 2.2 Comparisons of the close form solution with the simple approximation method (Gülkan et al., 2002) for ground motions (a) recorded at Düzce (NS) earthquake (19 Nev., 1999),  $c = 135$  m/s,  $H = 3$ m,  $\zeta=2\%$ ; and (b) Rinaldi Receiving Station (NS), 1994 Northridge earthquake with  $c = 100$  m/s,  $H = 3$ m and  $\zeta=0.0\%$ .....28
- Figure 2.3 Comparisons of interstory drift demand estimates using Timoshenko Beam Model with the GIDS method exposed to Rinaldi record (1994).29
- Figure 2.4 Drift spectra for the un-damped shear beam model subjected to Rinaldi (NS) record (Northridge ground motion 1994) through (1) wave propagation analysis (Equation 2.7) and (2) modal history analysis including one and (3) five modes contributions.....30
- Figure 2.6 Physical configurations corresponding to Iwan (1997) shear-beam model .....31
- Figure 2.7 Response Interstory drift time series calculated for short period system ( $T=0.2$ s) damped system  $\zeta=0.05$ ) for S80W direction of the Lucerne Valley station record during the 1992 Landers event .....32

Figure 3.1 Examples of the story mechanism induced by the hinge plasticization at the column tips of RC MRF buildings.....	39
Figure 3.2 Examples of decay modes seen in the column members subjected to cyclic loading: (a) Stiffness decay, (b) Strength deterioration, (c) Pinching or slip .....	41
Figure 3.3 Schematic diagram of a SDOF hysteretic model to depict hysteretic degradation and pinching behavior.....	44
Figure 3.4 Slip-lock series hysteresis .....	46
Figure 3.5 Comparison of hysteresis restoring force component $z(t)$ vs. displacement $x(t)$ phase plane plots with different $A$ values, the parameters excluding $n$ are kept constant. ( $\zeta = 5\%$ , $\omega = 3$ , $a = 0.0$ , $n = 2$ , $\beta = 0.5$ , $\gamma = 0.5$ ) .....	51
Figure 3.6 Possible hysteresis response loops through the different combination $\beta$ and $\gamma$ , remaining parameters is kept constant and is listed in the figure.	54
Figure 3.7 Comparison of hysteresis restoring force component $z(t)$ versus displacement $x(t)$ phase plane plots with different $n$ values, the parameters excluding $n$ are kept constant. ( $\zeta = 5\%$ , $\omega = 3$ , $a = 0$ , $A = 1$ , $\beta = 0.5$ , $\gamma = 0.5$ ) .....	55
Figure 3.8 Hysteretic restoring force component $z$ vs. displacement $x$ phase plane plot with ( $\zeta = 5\%$ , $\omega = 3$ , $a = 0$ , $n = 2$ , $\beta = 0.5$ , $\gamma = 0.5$ , $v_0 = 1$ , $\delta_A = 0$ and $\delta_v = 0$ ).....	57
Figure 3.9 Hysteretic restoring force component $z$ versus displacement $x$ phase plane plots with different $\sigma_0$ quantities: (a) $z$ vs. $x_1$ ; (b) $z$ vs. $x_2$ ; (c) $z$ vs. $x$ ( $\zeta = 5\%$ , $\omega = 3$ , $a = 0$ , $A = 1$ , $n = 2$ , $\beta = 0.5$ , $\gamma = 0.5$ , $\delta_v = 0$ , $\delta_\eta = 0$ , $\delta_A = 0$ , $\delta_a = 0.05$ and $\delta_\sigma = 0$ ).....	58
Figure 3.10 Hysteretic restoring force component $z$ vs. displacement $x$ phase plane plots with different $\delta_a$ values: (a) $z$ vs. $x_1$ ; (b) $z$ vs. $x_2$ (c) $z$ vs. $x$ ( $\zeta = 5\%$ , $\omega = 3$ , $a = 0$ , $A = 1$ , $n = 2$ , $\beta = 0.5$ , $\gamma = 0.5$ , $\delta_v = 0$ , $\delta_\eta = 0$ , $\delta_A = 0$ , $\delta_0 = 0.05$ and $\delta_\sigma = 0$ ) .....	59
Figure 3.11 Hysteretic restoring force component $z(t)$ vs. displacement ( $x(t)$ ) phase plane plots with different: (a) $\zeta_1$ quantities ( $\xi_0 = 0.05$ , $\delta_\xi = 0.001$ , $\lambda = 0.006$ ); (b) $\zeta_2$ quantities ( $\zeta_{10} = 0.98$ , $p = 1$ ), the following parameters	

are identical in both cases: ( $\zeta = 5\%$ , $\omega = 3$ , $a = 0$ , $A = 1$ , $n = 2$ , $\beta = 0.5$ , $\gamma = 0.5$ , $\delta_v = 0$ , $\delta_\eta = 0$ and $\delta_A = 0$ ) .....	60
Figure 3.12 Seismic response of SDOF system under the Düzce-NS ground motion record using the Bouc-Wen hysteretic model .....	63
Figure 3.13 Parallel springs in hysteretic model.....	65
Figure 3.14 Basic components of hysteretic models .....	67
Figure 3.15 Stiffness degradation rule .....	68
Figure 3.16 Schematic view of test setup (Acun, 2010) .....	77
Figure 3.17 Displacement time series imposed on the specimen (1P2) .....	78
Figure 3.18 Comparison of simulation and experimental results for sub-standard non-conforming column specimens (Type-1).....	79
Figure 3.19 Comparison of simulation and experimental results for on standard, code compliant code (TEC 1998, 2007) column specimens .....	80
Figure 3.20 Variation of hysteresis loop shape by adding degradation properties in turn to get specimen 1D2 results: (a) Non degrading loop (b) addition of the smoothness parameter for elastic-yield transition N; (c) Stiffness degradation $\alpha$ ; (d) Strength deterioration $\beta_1$ , $\beta_2$ ; (e) and combination of them; (f) plus the pinching properties .....	83
Figure 3.21 Qualitative view of effect of pinching parameters on hysteresis loop for specimen 1D2 ( $R_s$ : Slip Length factor, $\sigma$ : Slip sharpness factor, $\lambda$ : Parameter for mean moment level of slip).....	84
Figure 3.22 Comparison of response displacement time history of SDOF system under Düzce-NS ground motion record using (a) the SHM and (b) Analytical Bouc-Wen hysteretic model .....	88
Figure 4.1 Generic single bay 3, 6, 9, 12, 15, 18 and 20 stories shear frame used in this study .....	92
Figure 4.2 Design assumptions: Uniform distribution of flexural stiffness along the frame height (kept constant), story capacities are determined according to lateral loading distribution as per of the TEC 2007 recommendations. ....	93
Figure 4.3 Schematic of generic plane single bay 12-story shear-frame: (a) Pushover analysis under uniform load pattern; (b) Moment distributions over the	

column tips throughout the height corresponding to the applied load pattern .....	96
Figure 4.4 The design yield base shear coefficient used in structures design .....	97
Figure 4.5 Equivalent lateral earthquake force distribution over the height for the shear frames with fundamental period equal to 0.6, 0.9, 1.2, 1.5, and 1.8 s. ( $T = 0.1N$ ).....	98
Figure 4.6 Typical tri-linear model form IDARC 2D element models library used for plastic hinges (Valles et al., 1996 and Reinhorn et al., 2009) .....	100
Figure 4.7 Mean and mean plus standard deviation elastic acceleration response spectrum (2%- damped) of selected ground motions and (TEC, 2007) spectrum.....	103
Figure 4.8 Program interface for calculation of inelastic drift spectrum using the generic shear frame models .....	107
Figure 4.9 Comparison of the drift spectrum ordinates calculated by both the proposed method and the Iwan (1997) formulation for ground motion records of (a) the Bolu-NS; (b) the Sakarya-EW; (c) the Kobe –NS ...	110
Figure 5.1 Proportional relation of the mean displacement between SSD and EPP systems calculated with earthquake recorded on different site classes	119
Figure 5.2 Mean and mean plus standard deviation drift spectrum for selected ground motion records (a) elastic systems; (b) smoothing elastic plastic systems ( $N=2$ ).....	126
Figure 5.3 Variation of smoothed elastic-plastic modification factor $C_{\text{degraded}}$ , over the period range for systems with different elastic–yielding transition level, $N$ . (Here $N=20$ symbolizes the sharpness transition and $N=1$ represents the smoothest transition level).....	129
Figure 5.4 Effect of elastic-post yielding smoothness transition parameter, $N$ , on the interstory drift spectrum.....	130
Figure 5.5 Story capacity (a.1, b.1 and c.1) curves and interstory drift history (a.2, b.2 and c.2); at stories with maximum IDR, the shear frames have been used in derivation of interstory drift spectrum under Sakarya-EW record (Figure 5.4). Shear frames have different smoothness transition levels	

	and their periods are 0.5 s. (a.1 and a.2), 1.2 s. (b.1 and b.2), and 2.0 s. (c.1 and c.2), respectively .....	131
Figure 5.6	The story shear versus story drift (kN-mm); and the time series of the story drift (mm-s) for the three story frame with vibration period of 0.4s under the Düzce ground motion record.....	135
Figure 5.7	The M+S.D. drift Spectrum for systems with different stiffness degradation level.....	140
Figure 5.8	Variation of hysteresis capacity degradation modification factor ( $C_{degraded}$ ) throughout the period range for different hysteresis degradation control parameter levels (a) Stiffness degradation, (b) Strength degradation, (c) Combined stiffness-degrading and strength-decay .....	141
Figure 5.9	Effect of hysteresis capacity degradation (combined stiffness and strength degradation), on the interstory drift spectrum for Sakarya-EW record	143
Figure 5.10	The story capacity (a.1, b.1 and c.1) curves and interstory drift time series (a.2, b.2 and c.2) at stories with maximum IDR, for the shear frames have been used in the derivation of the interstory drift spectrum under the Sakarya-EW record (Figure 5.9). Shear frames have hysteresis capacity degradation (combined stiffness and strength degradation) and the periods are 0.6 s. (a.1 and a.2), 1.2 s. (b.1 and b.2), and 2.0 s. (c.1 and c.2), respectively .....	144
Figure 5.11	Variation of pinching modification factor ( $C_{pinched}$ ) throughout the period range for different pinching control parameter levels (a) Slip length parameter, $R_s$ ; (b) Slip sharpness parameter, $\sigma$ ; (c) Mean moment level of slip, $\lambda$ .....	147
Figure 5.12	IDR surface as function of period for different peak ground acceleration intensity for: (a) Linear systems (b) Pinched system.....	149
Figure 5.13	Pinched modification factor variations for selected earthquake records scaled to different peak ground acceleration intensity.....	150
Figure 5.14	The M+S.D. elastic and inelastic drift spectra (including hysteresis capacity decays and pinching at response loops) for different a/v ratio ranges: (a) Low a/v; (b) Intermediate a/v; (c) High a/v ranges.....	153

## LIST OF ABBREVIATIONS AND SYMBOLS

A	parameter that controls the shape of the hysteresis loop (Bouc-Wen Model)
ATC	applied technology council
$A_0$	parameters that control tangent stiffness
$A_{0g}$	effective ground acceleration coefficient
$a$	ratio of post-yield stiffness to the initial elastic stiffness
$a,b,c$	system dependent regression constants of the modification coefficient expression (in Chapter II; the $a,b$ are used as regression constant in the Equation $T = aH^b$ )
$a/v$ ratio	ratio of the peak ground acceleration ( $a$ ) to peak ground velocity ( $v$ )
B	span length of frame
$C_0$	modification factor to relate roof displacement to first mode spectral displacement
$C_1$	modification factor to relate expected maximum inelastic displacement to displacement calculated from elastic response
$C_2$	modification factor to represent effect of pinched hysteretic loop, stiffness degradation, and strength loss
$C_3$	modification factor to represent increased displacements due to dynamic P-Delta effect
$C_{\text{degraded}}$	modification factor that is modified to the degrading smooth elasto-plastic systems
$C_{\text{pinched}}$	modification factor for systems including pinching in a response loops
$C_y$	yield base shear coefficient

$C_{\mu}$	ratio of inelastic to elastic spectral displacement
$c$	shear wave velocity traveling through a building
$c_v$	linear viscous damping coefficient
$D_i(t)$	relative displacement of a single-degree-of-freedom elastic system with the period and damping of the $i$ 'th mode
EPP	elastic, perfectly plastic system
$EA_c$	axial rigidity of column
$EI_3^{\pm}$	post yield flexural stiffness (positive/negative) as % of elastic
$EI_b, EI_c$	flexural rigidity of beam and column, respectively
$F(t)$	excitation force
$F_h$	force functions of the hysteretic spring
$F_{hy}$	yield force of the hysteretic spring
$F_i$	design seismic load acting at $i$ 'th storey in equivalent seismic load method
FEMA	federal emergency management agency
FN	fault normal
FP	fault parallel
$f(t)$	mass normalized external excitation
$f(z)$	delta function
$f'_c$	compressive strength of test specimens concrete
$f_u$	ultimate strength of longitudinal reinforcement of test specimens
$f_y$	yield strength of longitudinal reinforcement of test specimens
$G(z)$	standard Gaussian density function
$GA_c$	shear stiffness of a column
GIDS	generalized interstory drift spectrum
GSDR	ground story drift ratio
$g$	gravitational acceleration
$H$	height of the shear beam or total height of a building
$H()$	heaviside step function

$H_h$	hysteretic energy dissipated
$H_i$	height of $i$ 'th storey of building
$H_{ult}$	hysteretic energy dissipated when loaded monotonically to the ultimate curvature without any degradation
$h$	story height
$h(z)$	pinching function
$I$	building Importance factor
$ID$	interstory drift
$IDR$	interstory drift ratio
$k_0$	lateral stiffness of a single-degree-of-freedom system
$k_{comb}$	tangent stiffness of the combined system
$k_{h0}$	initial hysteretic stiffness
$k_{hd}$	degraded hysteretic stiffness
$k_{post\ yield}$	post yielding stiffness
$k_{slip}$	slip-lock stiffness
$k_{tangent}$	tangent stiffness
$L_1$	response modification parameter of the first mode
$M+S.D.$	mean plus standard deviation
$MIDR$	maximum interstory drift ratio
$MRF$	moment resisting frame
$M_1$	mass participation factor of the first mode
$M_{cr}$	cracking moment
$M_w$	moment magnitude
$M_y$	yielding moment
$m$	lumped mass of a single-degree-of-freedom system
$N$	parameter that controls the “smooth” transition between the elastic and post-elastic branch
$NEHRP$	national earthquake hazard reduction program
$N_p$	number of data points
$N_{pp}$	number of parameters in the model that is being optimized
$N_s$	total number of stories of building from the foundation level

n	parameter that controls the smoothness of the transition from linear to nonlinear range (Bouc-Wen model)
ODE	ordinary differential equation
P	rate of initial drop in slope (in the Bouc-Wen model)
PBEE	performance based earthquake engineering
PBSD	performance based seismic design
PGA	peak ground acceleration
PGV	peak ground velocity
RC	reinforced concrete
RHA	response history analysis
$R_a(T)$	seismic load reduction factor (or relative strength factor)
$R_k$	controls the stiffness degradation
$R_s$	controls the slip-length
r	correlation coefficient
$S(T)$	spectrum coefficient
SDOF	single degree of freedom
SHM	smooth hysteretic model
SMRF	steel moment resistant frame
SSD	strength degradation system
$S_a$	the response spectrum acceleration at the effective fundamental vibration period and damping ratio of the building under consideration
$S_D$	elastic spectral displacement
$\text{sign}(x)$	signum function
s	standard error
T	building natural vibration period
$T_e$	effective fundamental period of the building in the direction under consideration computed by modifying the fundamental vibration period from elastic dynamic analysis. e.g. eigenvalue analysis
TEC	Turkish earthquake code
TS 500	requirements for design and construction of reinforced

	concrete structures (Turkish Standard, 2000)
$T_A, T_B$	spectrum characteristic periods
UBC97	uniform building code (version 1997)
$u$	lateral deformation of a shear beam
$u_0, \dot{u}_0$	initial displacement and velocity of a system, respectively
$u_{cap}$	displacement ductility based on maximum displacement capacity
$\ddot{u}_g$	ground motion acceleration
$u_{max}$	maximum displacement of the system
$u_{max}^{+/-}$	maximum positive/negative displacements
$u_{max} (st. 1)$	maximum displacement of the bilinear system at story no.1
$u_y (st. 1)$	yield displacement of the bilinear system at story no.1
$v(t), z(t)$	ground velocity and displacement, respectively
$V_t$	design base shear
$V_y$	yield base shear
$W$	total weight of building calculated by considering live load participation factor
$w_i$	story weight
$x$	average height of the $j+1$ and $j$ stories
$Y_i$	an arbitrary value that nonlinear model evaluated at the $i^{th}$ data point
$Z(t)$	dimensionless hysteretic variable
$\alpha$	stiffness degradation parameter
$\alpha_0$	dimensionless parameter for lateral stiffness introduced by Miranda (1999)
$\beta$	parameter that controls the shape of the hysteresis loop (Bouc-Wen Model)
$\beta_1$	ductility-based strength degradation parameter
$\beta_2$	energy-based strength degradation parameter
$\Gamma_i$	modal participation factor of the $i^{th}$ mode of vibration
$\gamma$	parameter that controls the size and shape of the Bouc-Wen

	hysteretic loop
$\Delta F_N$	additional equivalent seismic load acting at the N'th story (top) of the structure
$\delta_A, \delta_\eta, \delta_v$	non-negative constant parameters that determine the desired rate of degradation
$\delta_t$	target displacement in the nonlinear static analysis
$\delta_\xi$	control variation rate of the $\zeta_2$
$\varepsilon(t)$	total energy dissipated through hysteresis
$\dot{\varepsilon}(t)$	rate of energy dissipated through hysteresis
$\zeta$	initial elastic viscous damping
$\zeta_1, \zeta_2$	parameter that control the severity of pinching
$\zeta_{10}$	measure of the amount of total slip (Bouc-Wen model)
$\eta$	parameter for controlling the shape of the unloading branch (SHM)
$\eta(t)$	parameter that controls the hysteresis shape and degradation of the system
$\theta(x, t)$	rotation response history at dimensionless height x
$\lambda$	factor to control mean moment level of slip
$\mu$	displacement ductility
$\nu(t)$	parameter that controls the hysteresis stiffness degradation of the system (Bouc-Wen Model)
$\xi_0$	parameter that contributes to the amount of pinching (through controlling the variation rate of $\zeta_2$ parameter)
$\rho$	beam to column stiffness ratio
$\rho_l$	reinforcement ratio
$\sigma$	parameter that governs the sharpness of the slip
$\sigma_0$	controls the sharpness of pinching
$\sigma_i$	standard deviation (uncertainty) at point i
$\varphi_i$	amplitude of the ith mode at non-dimensional height x
$\varphi_i'$	first derivative of the ith mode shape with respect to dimensionless height x

$\varphi_y$	yielding curvature
$\omega$	natural circular frequency
SSD	strength Degradation system



## CHAPTER 1

### INTRODUCTION

#### 1.1 General

The latest developments in engineering seismology and structural engineering necessitate quantified descripts of seismic demand variables that forming a significant content within the description step of seismic resistant design and safety evaluation of engineering structures. Hence, substantial number of research have been performed to comprehend the change of global and local drift demands over the building height reducing to more precisely created displacement levels that should be considered at a certain level of performance as well as seismic hazard level.

The seismic response of building frames under ground motions within a near-fault region is another issue recently of great interest. Near-field earthquakes are mostly indicated as the strong earthquake excitations of the site within a distance of around 10-15 km or less from the rupture fault. Earthquake ground motions at such stations in the direction of the fault rupture propagation are essentially different from the far-fault earthquake records. Near-field ground motions display a long-period pulse in the acceleration time series that appear as a cohesive pulse in the velocity and displacement time series, and such an emphasized pulse is not found in the earthquakes recorded at the locations far from fault rupture zones.

There are also some extra effects in these types of ground motions which are inconspicuous in more distant locations. One is that of the propagation of a stretching (shock) wave in a direction perpendicular to the fault which could be

more devastating. Significant amounts of ground deformation lead to additional effects on structural responses. The ground velocity at a close distance could exceed 50 cm/s, therefore an excessive concentration of damage is commonly observed in the buildings whose exposure to this type of ground motion. A kind of momentum in the direction of the shear increases with the “Doppler Effect” and can exert excessive forces in the stiff short-period systems. This effect is named “directivity” of ground motion. The importance of this issue is redoubled when elastic limits are exceeded, particularly for old-built engineering structures.

Observations have been received from the recent near-field earthquakes, Northridge in 1994; Kobe in 1995; Chi-Chi, Taiwan in 1999; Kocaeli, Turkey in 1999 and Wen Chuan, China in 2008. These recent events included many examples and lessons about the insufficiency of seismic performance of code-defined old-built structural systems subjected to near-fault earthquakes. Aforementioned events as the recent 22 February 2011 earthquake in Christchurch (New Zealand) showed the near-field impacts that affected the structures were in the form that cannot allow preventive measures just through detailing members to withstand prescriptive forces, and revealed the high importance of the displacements. Investigation of damage patterns demonstrated that frame buildings in the near-field had to cope with greater displacement ductility demands than could be associated with the only maximum accelerations which are used in the traditional, damage-causing capacity measure described by way of the peak value of the ground’s acceleration.

The velocity fling corresponding to a coherent superposition of the slips in the direction of fault asperities packs an impact that is not obvious right away when dynamic computations are performed applying the ordinary ground accelerogram. When building frames are exposed to these seismic actions, the customary growing of a seismic response with some modes governing the whole response probably not happen ere one of the cohesive displacement and velocity pulses propagating along the frame building as waves brings about enormous local displacements as well as following losses (Westergaard 1933; Iwan 1997).

All of these lessons and tips have indicated that it is required to reconsider the fundamental principles of performance-based earthquakes or it will even be necessary to make changes in the provision of future specifications. Some parts of these lessons relate to the calculations of relative interstory drifts.

Taking the post-yielding behavior of structures into account with calculations in a controlled manner and in terms of interstory drifts is the fundamental principle of performance-based earthquake engineering. The structural damage, or the performance given, is related to the deformations that have been suffered. Putting into practice the upper limit of column deformation, controls the design. The most familiar deformation criteria to be well-known by structural engineers are the relative interstory drift (ID) spectrum. The interstory drift refers to the relative lateral displacement between two adjacent stories; likewise, the Interstory Drift Ratio (IDR) refers to the distinction in lateral displacements for two adjacent stories normalized by the interstory height. The right and appropriate estimation on peak interstory drift is clearly consequential to seismic analysis and design of buildings. Each specification demands that the limits under the various conditions are controlled.

The response spectrum is a useful means of showing and investigating the effects of various ground motion records on different systems since its establishment (Biot 1941). The version of this used for earthquake-resistant design is referred to as the design spectrum (Housner 1947; Housner et al. 1953). The linear spectrum, as well as for the Single Degree Of Freedom (SDOF) systems, has been developed for idealized nonlinear systems in different ways. Their validity can be seen from taking place even in the scope of textbooks.

The point that should be mentioned here is that the traditional response spectrum displacement ordinates exclusively give a measure of total acceleration and displacement demands on frame buildings and do not consider concentration in displacement demands in given stories (local displacement) that generally happen in buildings, and therefore supply some prediction of the average interstory drift in

frame buildings. Nevertheless, in practice maximum interstory drift ratio (MIDR) demands are not ever distributed throughout the frame buildings height in uniform manner and therefore response spectrum ordinates do not cover a straight indicating of MIDR demands. Moreover, ordinates of the response spectrum are established upon response of a SDOF system and hence cannot numerate for the contribution of higher modes on ID demands in frame structures.

As early as the 1930s, Westergaard (1933) suggested a continuous, shear-type beam model to evaluate the lateral deformation in buildings. Rosenblueth et al. (1968) examined the shear and overturning bending in structures established upon a continuous shear-type beam model. lately, Iwan (1997) suggested a simple measure of interstory drift demands for seismic action named the drift spectrum based on wave propagation theory and a relatively simple linear model and argued that it would be particularly useful to drift demand estimation of buildings subjected to the near-field ground motions that include distinct pulses. The drift spectrum is different from the response spectrum in that it is on the foundation of a continuous shear-type beam model and not dependent upon a SDOF system.

The verity that ID demands are not distributed over the buildings height in uniform matter is an important point that should be taken into consideration into drift demand estimations. This new reliable tool considers the non uniform distribution of drift demands. The contribution of higher modes is another issue that considered as well. Hereupon, the drift spectrum leads to more precisely predictions of peak interstory drift demands than does the response spectrum.

More recently, the drift spectrum applying a continuous shear-type beam model has been a study topic for much research and some improvements have been accomplished (Chopra and Chintanapakdee, 2001; Akkar and Gülkan, 2002; Akkar et al., 2005; Huang and Iwan, 2005; Miranda and Akkar, 2006). Gülkan and Akkar (2002) demonstrated that the drift spectrum could be detected more easily through considering spectral ordinates and the fundamental mode of vibration. Following that, Miranda and Akkar (2006) generalized the drift spectrum, and they have

combined the continuous flexural-shear beam model and modal superposition technique in a way that lateral deformation pattern changing from those of a shear-type beam model to those of a flexural beam model can be intended. Therefore, it accounts for a diversified amount of deformation modes that demonstrate more accurately those of frame buildings.

The shear-type frame models and continuous shear-beam can reduce to appropriate predictions of interstory drift demands for multitude frame buildings, in particular concerning a moment resisting frame (MRF) buildings whose girders are considerably stiffer compared to columns and in addition axial deformations in the column elements can be disregarded. However, the problem is that many old-built frame buildings exhibit a wide range of generally poor seismic performance, especially once the elastic deformation limits of the concrete members are exceeded under severe ground motions. The non-ductile; poor reinforcement detailed load bearing columns exhibit nonlinear behavior and fail especially under pulse-like, near-fault ground motions.

The current drift spectrums, variants of the Iwan (1999) solution and alternative simplified approximations are proposed based on certain assumptions. One of them is the uniform stiffness distribution along the building height and the other is the linear elastic seismic response of a frame-building model under given ground motion. Whereas excluding the some low-rise structures (up to three stories), the uniform stiffness distribution assumption is not in use for most common frame buildings where, because of the non-uniform vertical distribution of ground motion caused lateral forces in frame buildings, the lateral stiffness at the top of the frame is typically minor, and in some cases remarkably smaller, compared to the lateral stiffness at the basement floor of building.

Likewise, for drift spectrum generalization, such as that proposed by Miranda and Akkar (2006), the modal responses were assumed as uncoupled (i.e. the modal responses do not interfere against each other) to be able to utilize the modal superposition technique for which this is not true for a structures when its response

extends into a nonlinear region. The modes are solely the property of linear systems; it is not possible in principle to address the modal behavior after stepping out of linearity. In inelastic zones, the modal shapes and corresponding modal participation factors can be meaningfully changed due to the stiffness decay in a structural system.

The column side-sway mechanism is a common failure mode in Reinforced Concrete moment resisting frame (RC-MRF) buildings when exposed to pulse-like, near-fault earthquakes. The existence of such structures in old and densely populated areas that include many old non-ductile building is even more critical. The situation becomes worse when the sites are close to a fault rupture resource, and the pulse associated with these ground motions lead to large scale casualties induced by serious structural damage, or even fully structural collapse, mainly arising from overestimated interstory drift demands.

Examples of such performance were seen in the 1999 Kocaeli earthquake (Turkey), Figure (1.1). In such framed buildings, the longitudinal column reinforcement bars were commonly designed to resist moments generated by code-specified lateral forces rather than the moments associated with the capacities of the column ends. These older columns are often weaker than the beams, leading to early column hinging and an undesirable column side-sways mechanism. Column hinging is undesirable because this may lead to structural instability after only a very few cycles. Similar damage examples were also seen in the past near-fault earthquakes as well.

Figure 1.2 exhibits two six-story, non-ductile, moment-resistant frame buildings in Gölcük after the 1999 Kocaeli, Turkey earthquake. As seen in the figure, one of the buildings collapsed totally, whereas the adjoining building incurred some damage only to the first story. Damage survey of the first story in both buildings illustrated that the buildings had a similar plan footmark and construction detailing. It is likely that the two buildings were identical and that both buildings may have been constructed by the same contractor. Both buildings were seemingly exposed to

identical seismic excitations levels, yet one building were intact the shakes and performed well, while the other one was fully collapsed. This is an example concerning the importance of the limit state and post yielding behavior of structural components for the extreme distinction in performance of non-ductile moment resistant frames (Sezen et al 2003) that differ in minute detail only.

It is likely that the building systems exhibit inelastic behavior and drift demands when exposed to near-field, pulse-like ground motions for some reason, such as various lateral load distributions along the height that are induced by the earthquake; or drift demands concentration in some floors, etc. As a result, it is necessary to address this problem for realistic assessment of inelastic interstory drift demands. As it has been seen, the current linear drift spectrum cannot reflect the realistic seismic demands experienced during severe ground motions for these kinds of frame buildings. This study seeks answers to these questions. The main objective of the work is to expand the drift spectrum that was previously investigated by Westergaard (1933) and later remodeled via Iwan (1997), Gülkan and Akkar (2002) and Miranda and Akkar (2006) in linear ranges to the nonlinear systems.



Figure 1.1 Aerial views of a few typical RC-MRF buildings in Gölcük. Traditional and faulty construction practices with limited interstory drift capacity under near-fault ground motion led to structural instability and excessive damage, including full collapse. [Courtesy of <http://www.koeri.boun.edu.tr/depremmuh/eski/eqspecials/kocaeli/golcuk.htm>]



Figure 1.2 Changeability of two adjacent, similar building responses proceed from different limit states; post-yielding hysteresis behavior pattern; and interstory drift capacities (Sezen et al., 2003)

Although the similarity with a shear beam is helpful for generating the spectrum of interstory drift demands for a certain earthquake action, other models may be employed. The approach used in this study is established upon nonlinear time history analyses of some simple frame building models. Sequences of frame models are designed with varying column stiffness and story mass properties in a systematic fashion, in order that distinctive periods are acquired. When these frame models are exposed to desired earthquake records, their dynamic response is computed by the Response History Analysis (RHA) method in the elastic range and then extrapolated into the inelastic range through correction factors.

The frame models are idealized similar to the shear beam models. Their height varies between 3-20 stories. Since all types of nonlinear behaviors of columns have been attributed to the representative hysteretic elements, the number of openings at frame models has ceased to be important. This process is performed on the elements that bring the shear-beam system to the original position through the extended Bouc-Wen type model that includes hysteresis properties. Thus, it has been possible to examine the realistic behavior of the structural components at all displacement levels beyond the yielding limits, through taking into account the numerous parameters that contribute to the strength deterioration and stiffness degradation and ostensible pinching of response loops. A comprehensive description of the research is given in the following section entitled "Purpose and Scope".

The hysteresis behavior of non-seismically detailed RC columns is predicted by considering the versatility and mathematical tractability of the extended Bouc-Wen model for the SDOF system and this model has been adopted with appropriate modification for the study here. The model, in its analytical forms of a group of differential equations, can capture the actual characteristics of non-ductile reinforced concrete column members, including stiffness decay and strength deterioration, softening and hardening as well as pinching. The hysteresis behavior of the non-ductile reinforced concrete column is not only contingent upon the distinct quantity of the parameters, involved in the differential equations of models, but also on their mutual actions resulting from the linear ranges. Therefore, it is seen that the most

appropriate approach is to represent the nonlinear behavior that is controlled by the model parameter in terms of divergence from the linear model. Useful results in evidence in this dissertation refer to calculating the expression of the modification coefficient that yield nonlinear drift ratios by multiplying with linear interstory drift demands. The equation and graphical form of each modification coefficient is also given.

## **1.2 Purpose and Scope**

This thesis deals with the examination of the inelastic drift demands of structural systems containing different hysteresis degradation properties exposed to a near-field ground motions excitations. Generalization of results to both elastic and inelastic drift spectra are derived and compared. To this end, the sequences of simple shear-type frames are designed, via systematic alteration of the story mass and column stiffness characteristics, and distinctive vibration periods are acquired. When these frame models are exposed to certain earthquake records, their dynamic response is calculated by response history analysis (RHA) in the elastic ranges. In this way, it becomes possible to derive spectra of the maximum inelastic interstory drift demands as well as their ratios to elastic drift demands over a wide period range (0.3 s – 2.4 s). Realization of these global objectives can be distilled into the following steps:

At the onset, elastic interstory drift spectrum is calculated through Iwan (1997) formulation. The interstory drift ratio demands obtained via Iwan (1997) formulation are accepted as the closed form solution, and the drift spectrum is re-plotted and compared with results derived by the Gülkan and Akkar (2002) approach. In this way the accuracy of the Iwan (1997) formulation is demonstrated and various differences are checked so that curves are made readily available.

The early drift spectrum was contrary to its modern idea and its multitude properties premier to the traditional response spectrum, it has some limitations. These restrictions will be discussed in detail in the following sections, but an important

issue that must be mentioned is that the Iwan (1997) drift spectrum and later alternative formulations proposed for interstory drift demands estimations are valid strictly in the elastic range; however, inelastic behavior of structural systems is reasonable in the event of pulse type, near-fault earthquakes which result in great deformation demands. In turn, these result in damage and even full collapse.

Estimating the seismic response of structural systems exposed to serious inelastic load reversal is one of the major important difficulties in structural engineering. This is particularly valid for a highly nonlinear material similar to reinforced concrete where system properties continually vary by either degrading of stiffness and strength as well as pinching. One reason for appearance of the pinching in the response loop is the repetition process of cracks opening and closing. This indicates degrading ability to dissipate energy through hysteresis behavior. The analytical model used to incorporate hysteresis degradations parametrically into RH analysis is clarified, its formulations are defined and the control parameters shaping the response hysteresis loops are investigated.

It is focused on the versatility and mathematical manageability of the Bouc-Wen model into the SDOF system in its analytical formation of a collection of differential equations. The dynamic behavior for various types of structures liable to random cyclic loading or given ground motion is solved. The “ODE 45” solvers in MATLAB platform is utilized to solve the ordinary differential equations concerned with in the model. The analytical responses under sinusoidal loads are examined; this is done to understand how hysteretic control parameters and their interactions affect the hysteresis loop shape. Furthermore, seismic response of the SDOF system subjected to given ground motion is investigated and seismic responses plotted.

The IDARC-2D platform has been adopted to follow nonlinear static and dynamic analysis; the program includes the Smooth Hysteretic Model (SHM) which is developed established upon the original Bouc-Wen model and it has the capability to simulate a number of various types of hysteresis loops employing a sole smooth hysteretic function influenced by a group of user-defined parameters through

continuous variation of stiffness caused by yielding, together with sudden alteration in consequence of unloading and degrading behavior. Therefore the three major phenomena defining the seismic response of reinforced concrete components namely; capacity deterioration and pinching (or slip) behavior can be easily modeled. A detail on the SHM formulation and scope of change of control parameters is discussed.

To properly represent the realistic restoring force behavior of RC members, it is required to evaluate control variables appropriately. Data collected from the cyclic loading test provides valuable information to estimate model parameters. To identify variable ranges, the analytical responses are compared with the experiment results. For this purpose, the analytical models are prepared analogous to test setup of the RC column specimens. In this way, an average range of parameters is deducted. It is assumed that these quantities reflect the realistic degradation characteristics of the RC columns when exposed to severe cyclic loadings. The operation is based on the SHM hysteresis loop that includes the control parameters to predict the certain experiment results with minimum error.

The quasi-static experimentation may be described as a testing protocol where cyclic loading is progressively applied to the specimens. In this method, explanation of a testing program together with the loading protocol is a fundamental issue. The quasi-static technique is nine times out of ten carried out on a deformation-controlled basis to best facilitate explanation of the results on the basis of ductility and to allow continuing the testing further than the load carrying capacity. The selected experiments belong to the quasi-static tests are conducted on cantilever reinforced concrete columns. The selected experiments belong to quasi-static tests conducted on cantilever reinforced concrete columns.

The hysteresis response relations are investigated and key parameters are clarified which are used to formulate a model for the hysteresis loop where all of its parameters are physically meaningful. The purpose underlying this is to supply a diversified amount of the control parameters to incorporate the hysteresis decay of

structural members into the following nonlinear dynamic analysis by meaningful magnitude variations. Afterwards the sensitivity of response loops to parameter variation is examined. Following that, drift spectrum is computed through seismic response of generic frame models such that via plotting the MIDR against to corresponding fundamental period, spectrum ordinates are obtained. The structural models are prepared to be consistent with the shear beam model used in Iwan (1997) formulation with which the results are compared. The close form solution is compared with other alternative spectrum ordinates to show compatibility of the results and acceptability of alternative approaches in the elastic ranges.

As a subsequent step, drift spectrum is derived using the smooth, elastic-plastic systems containing the hysteresis degradation properties beyond the yielding points. These systems reflect the nonlinear behavior of the code-defined building frames under the seismic excitations. The distribution of story capacities is defined in accordance with that lateral load pattern as per of Turkish Earthquake Code (TEC 2007). The structural members are designed such that inelastic deformations occur only at column ends and all beams remain elastic. Inelastic behavior of structural systems takes into account by consideration of nonlinear hinges at column ends using the smooth hysteretic model. The nonlinear time history analyses are conducted on 20 smooth; elastic-plastic frame models with vibration periods arranging from 0.3 s to 2.4 s.

Inasmuch as RHA method needs many analyses for different periods and if added to this hysteresis loop control parameters variation and reiterate to all selected ground motions, the number of analyses become very high and run to tens of thousands. Thus such a repetitive and time consuming operation has been coded to be conducted automatically. Reduced spectrum of drift called the inelastic drift spectrum and it reflects post yield hysteresis degradation effects into the ordinates of drift demands. Effects of the smoothness transition rate to post yielding region, and post yielding stiffness and strength degradation; as well as hysteresis pinching on drift spectrums are other issues which are clarified respectively.

The mean plus standard deviation (M+S.D) drift spectrum of selected ground motions is applied to evaluation of the drift demands. Besides, the parameter ranges of hysteretic degradation changed around the initial estimations is adapted to examine the degradation effect on the maximum interstory drift ratios. These estimates are inferred from the identification process. By comparing the mean elastic spectrum ordinates with inelastic spectra which has been drawn in this study, the modification coefficient ratios are extracted to consider individual and/or combination effects of hysteresis degradation into drift spectrum.

The best fitted curve established upon minimizing the square root of the discrepancy between inelastic drift spectrum and corresponding elastic spectrum ordinates is calculated for determining the modification factors. Thus, readily depending on the fundamental period and other system dependent parameters, the modification factors that incorporate inelastic behavior consequences are obtained. Thereupon the sensitivity of the MIDR demands to each degradation parameter is investigated in detail. It is believed that these modification factors could be considered individual and/or combination effects of hysteresis decays of structural members as they affect the drift demands. Two quantities are used to express the “goodness” of a particular curve fit; the correlation coefficient ( $r$ ); and the standard error ( $s$ ) of the estimates over each period interval. The investigation is continued on examination of ground motion characteristics impacts and the importance of peak ground velocity effects on response displacements is re-emphasized.

In the data-group of ground motion records, a substantial number of near-fault ground motions are selected. There are classified into three groups on the foundation of their  $a/v$  ratio and in recognition of the special consequence pulse-like time series which results in great seismic demands to the structural systems, are examined in detail. Thus, totally 192 records with over 60 records in each group have been assembled. Such a number of selected records are an indication of the reliability of statistical results.

### 1.3 Thesis Outline

The chapters of the dissertation are constituted as follows;

Chapter 2 includes an overview of the drift spectrum derivation process in the literature. First, an interstory drift spectral method proposed by Iwan (1997) to compute interstory drift demands directly established upon continuous shear-beam model and the theory of wave propagation theory is described and some modifications as well as criticisms dealing with drift spectrum are discussed. Later, the alternative approaches to calculating the drift spectrum in the literature are discussed and the advantages and limitations of each one are also clarified.

In Chapter 3, the hysteresis capacity decay, stiffness degradation and energy dissipation of simple nonlinear structural systems are introduced. The differential equation dependent upon the Bouc-Wen model which is used to model hysteresis response of a similar system along with the Smooth Hysteretic Model (SHM) which was developed based on this model and it has been implemented in IDARC-2D platform, is presented. Then the parameters that control model as well as derivation of equations governing the model are discussed in detail. Afterwards, a comparison is made between these analytical models with respect to analogous experimental results through matching both response loops; in which the experimental setup and corresponding analytical models are illustrated. The aim underlying this is to supply a wide range of the key parameters to incorporate the hysteresis decay of structural members into a succeeding nonlinear dynamic analysis by meaningful magnitude variations. Then, a sensitivity analysis of response loops under the variation of parameters is realized.

In chapter 4, the frame models that have been used in the simulations are explained, starting with the design methodology. The frame models are designed to satisfy the requirements of the Turkish Seismic Code (TEC, 2007). Other design assumptions are also sorted and explained in detail. In the data-set of recorded ground motions, a large number of near-fault ground motions are involved, in terms of the special importance pulse-type time series leading to large seismic demands to the buildings,

classification along with other characterization of ground motions is given at the end of the Chapter 4 and part 1-3 of Appendix A.

In chapter 5, the comparison is made between drift spectrum that is calculated with (i) the many response history analysis and (ii) the Iwan (1997) solution. Results are examined in order to validate proposed procedure performance in linear ranges. The compatibility between simulation responses and theoretical results are verified and the practicability of the recommended procedure is demonstrated. Derivation of the drift spectrum through response history calculations were needed numerous analyses, so a program is coded in the Java™ Archive (JAR) tool to pave the way for such a repetitive process and in this way, the main analyzer Platform (IDARC 2D) execution and reading responses can be conducted automatically. Following that the verification operation is performed on the spectrum obtained by the two methods.

In chapter 6, the modification factors used to compute the inelastic interstory drift ratio demands in comparison with elastic drift spectrum are derived. Thence, the expressions of the modification coefficient which incorporate each hysteresis degradation consequence are defined and the variation ranges of control parameters that represent the hysteresis degradation level are examined in detail. The approximation is accomplished by regression analysis. The sensitivity of the IDR demands to each hysteresis decay property is also investigated by varying the control parameter quantities, which in turn represents degradation severity of each material deterioration property. The modification coefficient is proposed as the function of vibration period  $T$  and some other system dependent variables. The numbers of characteristics of ground motion records along with hazard levels are other factors that are examined in this chapter as well.

Finally, in chapter 7, a brief summary of the investigation conducted together with its principal conclusions and other important findings are summarized and possible future work areas are listed.

## CHAPTER 2

### DRIFT SPECTRUM IN LITERATURE

#### 2.1 Introduction

One of the main damage demand parameters of building frames under strong ground motion loads is the Interstory Drift Ratio (IDR) and, as mentioned previously, it explains the difference in lateral displacements between two sequential stories standardized by the interstory height. Therefore, the right and convenient estimation of the peak interstory drift ratio is clearly important to design and seismic assessment of structural systems. Many researchers have used the continuous beams to model the behavior of cantilever structures when exposed to static and dynamic loads (Westergaard, 1933; Jennings and Newmark, 1960; Resenblueth, 1968; etc.). Westergaard (1933) presented a continuous shear-type beam model to evaluate the lateral deformation in building frames. Rosenblueth et al. (1968) examined the shear and overturning moment in building frames on the basis of a continuous shear-type beam model.

For multitude building frames, the shear-type frame model can reduce to sensible assessment of interstory drift demands. This is especially valid regarding the moment resisting frame buildings whose girders are considerably stiffer compared to the columns and also axial deformations in the columns are insignificant. On such an occasion, vibration modes will be comparatively identical to those of a shear-type frame. Dependent upon a continuous shear-beam model and wave propagation theory, Iwan and Chen (1994) and Iwan (1997) suggested a new and simple measure of interstory drift demands for severe seismic action named the drift spectrum and

recommended that the drift spectrum is especially beneficial for near-field ground motions that include distinct pulses.

## **2.2 Alternative Idealization Models of Building Frames**

Three alternative frame models could be applied to estimate the response of each building: rigid frame; equivalent shear-beam; and equivalent shear-frame models. The description and details of each one are explained in the following (Díaz 1994); The rigid frame model corresponds to the conventional representation of an assemblage of beams and columns with finite stiffnesses and resistances, and with the connections between structural members free to rotate as infinitely rigid elements (Figure 2.1.a).

The equivalent shear-beam model is an assemblage of structural members connected along horizontal interfaces, which coincide with the story levels. The building masses are supposed to be concentrated at the story levels. These members only suffer shear deformations when liable to lateral forces (Figure 2.1.b). The lateral stiffness of the structural element that employed to demonstrate the mechanical properties of a given story is equal to the lateral stiffness of that story, computed based on adequate assumptions regarding the deformed shape of the original frame. The yield strengths of the stories could be specified through the nonlinear static response analysis. This includes pushing the structure in accordance with a code-defined configuration of lateral deformations that are made to increase proportionally up to the point when the stories of interest reach their yield capacities.

The general geometry of the equivalent shear-frame model is identical to that of the conventional rigid frame (MRF), but being different from it in the mechanical properties of its structural members. The columns have very large axial stiffness and the beams have very large flexural strength and stiffness. As a consequence of these properties, the lateral response of the shear-frame is similar to that of a shear-type

beam, but the flexural strengths of the columns are affected by the axial forces on the columns due to both gravitational and seismic actions (Figure 2.1).

All the columns in a given story are considered to have equal cross sections, such that the lateral story stiffness of the shear-frame model is coincide with the story stiffness of the central frame of the building; The joints are presumed to be free to rotate and to displace in the horizontal and in the vertical directions in the plane of the frame. It is also assumed that all the columns in a given story have strength equal to that of the column requiring the largest reinforcement area in the story. Eventually the frame is analyzed and designed following the same criteria and methods as the conventional rigid frame, but the beams are assumed to be infinitely strong.

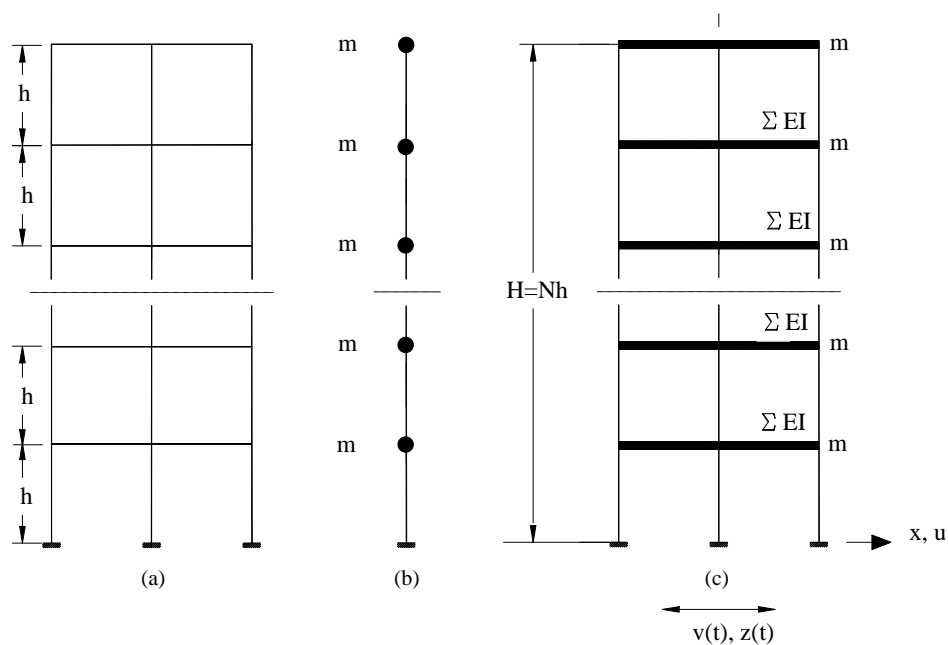


Figure 2.1 Alternative idealization models of building frames; (a) Typical frame and rigid frame model; (b) Equivalent shear-beam model; (c) Equivalent shear-frame model

The proportional relation of beam and column stiffness is the major structural parameter, denoted by  $\rho$  which governs the proportionate joint rotation in structural

frames caused by contributions of column and beam flexural stiffness at the floor levels (Blume 1968). This is the proportion of the summation of the beam rigidities  $(I/L)_b$  to column rigidities  $(I/L)_c$  at the level that is adjacent to the mid-height of the structural system. It provides beneficial knowledge for the general dynamic structural properties identical to the fundamental information dominated among the damping and fundamental mode shape. Therefore, it may be a multi-purpose variable to simulation of the structural systems to receive the important dynamic characteristics of the whole structural system. With the similar elastic modulus for columns and beams, the generalized way of  $\rho$  is shown in Equation 2.1.

$$\rho = \frac{\sum_{\text{beams}}(I/L)_b}{\sum_{\text{columns}}(I/L)_c} \quad (2.1)$$

The mode shape for  $\rho=0.0$  demonstrates deformation shape of bending. When  $\rho$  be on the rise, the deformation behaviors is regulated by both flexural and shear deformations, while as  $\rho=\infty$  the structural system works as a shear-type frame. The variation curves of the the basic mode shapes and corresponding interstory drift ratios of other  $\rho$  quantities for common frame buildings with uniform lateral stiffness along the building height was discussed in detail (Akkar et al. 2005). Akkar illustrated the ideal ordinary structural behavior with similar lateral stiffness on every floor through which a sole  $\rho$  quantity able to capture the basic mode deformation pattern in an efficient manner, in order that the rise in  $\rho$  lead to enlargement of the lateral deformation for the fundamental mode.

The peak interstory drift moves around the upper half of the building and the lower half very quickly, whenever  $\rho$  vary between 0.0 and 0.125. The greatest difference between the dominant first-mode lateral deformations and interstory drifts takes place while  $\rho$  varied between 0.0 and 0.125 quantities. (I.e. changeover from flexural behavior to composed mode shape pattern). When the first mode govern structural system acts similar to flexural cantilever ( $\rho = 0.0$ ) or in pure shear-type ( $\rho = \infty$ ), the peak interstory drift takes place at the top story or at the basement story, respectively. For the analytical models used in this study, the beam to column

stiffness ratio ( $\rho$ ) goes to infinity as a representative of ideal shear-type frame with which results are compared with those shear beam model assumption of the wave propagation solution.

### 2.3 Iwan Drift Spectrum

The drift spectrum was first introduced on the basis of the maximum shear deformation in a shear beam owing to a travelling wave. The maximum shear deformation is similar to the interstory drift ratio in building systems. The conceptual ideal shear beam model is illustrated in Figure 2.1.b. The explicit formulation of the relative drift spectrum for the basement level is expressed as follows (Iwan 1997);

Wherein the idealized form of the structural frame into the conventional shear beam is shown (see Figure 2.1.b), the frame is exposed to ground motion at the basement level. Ground velocity and ground displacement are symbolized by  $v(t)$  and  $z(t)$  respectively. The  $m$  masses are merged into each other through the frame columns. The columns are considered linear. The motion equation of the frames is illustrated by Equation (2.2).

$$\frac{\partial^2 u}{\partial t^2} - \frac{12 \sum EI}{mh} \frac{\partial^2 u}{\partial y^2} = 0 \quad (2.2)$$

Let's get auxiliary notations.

$$c = \sqrt{\frac{12 \sum EI}{mh}} \quad \omega = \frac{\pi c}{2 H} \quad \text{and} \quad T = \frac{4H}{c} \quad (2.3)$$

The solution relying on the wave propagation theory, for once horizontal displacement is non-dispersive and for damping  $\zeta$ , can be written according to Equation (2.4). The  $c$  coincides with the shear wave velocity traveling throughout

the structure height. This problem was mentioned the “telegraph” problem whilom and was examined by Courant and Hilbert (1962)

$$u(z, t) = \exp\left(-\frac{2\pi\zeta}{T}t\right) f(y \pm ct) \quad (2.4)$$

Then an interstory drift ratio becomes as Equation (2.5)

$$\frac{\partial u}{\partial z} = \exp\left(-\frac{2\pi\zeta}{T}t\right) f'(y \pm ct) \quad (2.5)$$

At ground-story, the Equation (2.5) will be similar to the Equation (2.6)

$$\left.\frac{\partial u}{\partial z}\right|_{z=0} = \pm \frac{1}{c} \left\{ \dot{u}(t) + \frac{2\pi\zeta}{T} u(t) \right\} \quad (2.6)$$

The expressions  $\dot{u}(t) = v(t)$  and  $u(t) = z(t)$  could be taken from Equation (2.6). Regardless of the wave propagation, the direction reversing should be considered as well, so that the direction will be changed when reflected from the ground story; although the sign remains unchanged while sent back from the top story level. The wave velocity in each level is shown by Equation (2.7).

$$\begin{aligned} \frac{\partial u}{\partial t} = \dot{u} &= -\frac{2\pi\zeta}{T} \exp\left(-\frac{2\pi\zeta}{T}t\right) f(y \pm ct) \pm c \exp\left(-\frac{2\pi\zeta}{T}t\right) f'(y \pm ct) \\ &= -\frac{2\pi\zeta}{T} u \pm c \frac{\partial u}{\partial y} \end{aligned} \quad (2.7)$$

Since wave reciprocating to the top level lasts  $\frac{T}{2} = \frac{2H}{c}$ , summing the contributions of the deteriorating waves traveling up and down the beam in Equation (2.6) for  $t = \frac{nT}{2}$  is given as;

$$\begin{aligned}
\text{IDR}_{\text{Iwan}} &= \frac{\partial u(T, \zeta)}{\partial y} \\
&= \max_{vt} \left| \frac{1}{c} v(t) + \frac{2\pi\zeta}{T} z(t) \right. \\
&\quad \left. + 2 \sum_{n=1}^{N \leq \frac{2t}{T}} (-1)^n e^{-n\pi\zeta} \left[ v\left(t - \frac{nT}{2}\right) + \frac{2\pi\zeta}{T} \cdot z\left(t - \frac{nT}{2}\right) \right] \right|
\end{aligned} \tag{2.8}$$

The plot of Equation (2.8) relative to fundamental period,  $T$  and for different damping quantities  $\zeta$ , brings the relative drift spectrum. This is the precise way of formulating the lateral motion within the elastic range of the conceptual multistory uniform frames (see Figure 2.1.c) using the one-dimensional wave propagation theory. The point that should be noted here is concerned with linear the superposition rule because the formulation is defined for linear systems. The ground velocity  $v(t)$  and displacement time series  $z(t)$  are required to solve the Equation (2.8). This variable is closely related with evaluation of filtered types of ground motions and may be varied. Therefore, some researchers, including the Hiedbrecht and Rutenberg (2000); Chopra and Chintanapakdee (2001); Gülkan and Akkar (2002); Kim and Collins (2002); Roberts and Lutes (2003); Huang and Iwan (2005); Collins and Lim (2006); Miranda and Akkar (2006) have developed an alternative to the Equation (2.8) without compromising accuracy of estimations. All of these are still linear. Comparison of some of these approximate results with respect to Equation (2.7) representing the closed form solution is given in the following sections.

Chopra and Chintanapakdee (2001) have acknowledged that by involving a suitable number of modes, one is able to evaluate the base level drift precisely. Kim and Collins (2002) remarked that the original formulation of the drift spectrum matches up with the cantilever shear-type beam model fastened to external springs with dampers attached firmly to a fixed point. Likewise, they pointed out the Iwan (1997) formulation terminates in residual drifts for given seismic excitations.

Gülkan and Akkar (2002) showed that the drift spectrum can be acquired using the spectral quantities quite easily, but approximately. To consider only the fundamental vibration mode and ordinates of common response displacement spectrum, an alternative simplified expression for the drift spectrum was proposed. Referring to Figure 2.1.c and considering the structural frame model, if this N-story frame comprises columns similar in their dynamic characteristics, then the shear beam expression for the first mode shape and period T can be written as Equation (2.9).

$$\varphi(z) = \sin \frac{\pi z}{2H} \xrightarrow{\text{at } z=h} \varphi(z) = \sin \frac{\pi}{2n} \quad (2.9)$$

The total height of the building is denoted by  $H = Nh$ ; N and h are the number and height of stories respectively. Since the total mass mobilizes in the first mode of the idealized shear frame and reaches approximately 80 %, therefore, only the first mode is taken into account. In most frame buildings, girders rotate at ends of column, but if the identical uniform characteristics retain throughout the frame height and the fundamental period being consistent with this generic frame, then the shear-type frame in Figure 2.1.c would still have the identical spectral displacements. The period dependent Ground Story Drift Ratio (GSDR), Equation (2.10), is obtained by combination of Equation 2.3 with the code-defined, empirically based fundamental period. As an example, the period expression ( $T = 0.08H^{3/4}$ ) as per of Uniform Building Code (UBC 1997) is adopted in Equation (2.10). With this purpose in mind that a half sine displacement pattern is employed to represent the deformed shape, the modal participation factor of the fundamental mode consider equal to 1.27. (I.e. the modal participation factor of 1<sup>st</sup> mode is  $L_1/M_1 = 4/\pi = 1.27$ ).

$$\text{GSDR}_{\text{Gülkan}} = 1.27 \cdot \frac{S_D(T, \zeta)}{h} \cdot \sin \frac{2\pi h}{Tc} \quad (2.10)$$

Presented in Figure 2.2 are the drift spectra for the two ground motions which were recorded at the Düzce (NS) during the 1999 Kocaeli (for  $\zeta=2.0$  %); and the Rinaldi Receiving Station (NS) during the 1994 Northridge earthquakes ( $\zeta=0.0$  %); determined by two methods: (1) wave propagation analysis that led to Equation 2.8;

and using  $T = 0.0853L^{3/4}$  and (2) formulation that made simpler to derive the drift spectrum as an alternative approach through taking into account common ordinates of the response displacement spectrum and with the use of only fundamental vibration mode (Equation 2.10). As shown in Figure 2.2, simple approximation can estimate drift demands in elastic ranges with good accuracy.

Later, some reviews and improvements about the versatility of the beam model were carried out. Miranda and Akkar (2006) generalized the interstory drift spectrum with the use of a combined flexural-shear beam model and modal superposition technique, such that they were able to consider lateral deformations changing from those of a flexural-type beam to those of a shear-type beam. Therefore, to use this approach one is able to estimate the drift demands for a large spectrum of deformation modes that reflect more accurately those of multistory frame buildings. They called it the generalized interstory drift spectrum (GIDS).

The beam model applied in the GISD comprise of a combination of a cantilever shear-beam and a cantilever flexural-beam deforming in shear pattern and bending configuration, respectively. The dimensionless parameter  $\alpha_0$  was introduced by Miranda (1999) to regulate the amount of participation of total shear and total flexural deforming in a simplified model of frame buildings aimed to estimate maximum interstory drift demands approximately and therefore, it governs the lateral deflected shape in its simplified structural system model. The lateral stiffness  $\alpha_0$ , is described as

$$\alpha_0 = H \sqrt{\frac{GA}{EI}} \quad (2.11)$$

Where  $EI$  is flexural rigidity of the flexural beam and  $GA$  is shear rigidity of the shear beam model. It is proper to mention that a quantity of  $\alpha_0$  equal to infinity ( $=650$ ) fit to a pure shear-beam model and  $\alpha_0 = 0$  value demonstrates a purely flexural-beam model. A mediate quantity of  $\alpha_0$ , fits to frame buildings that merged flexural and shear deformations. On the basis of calibration of detailed analytical

building models, Ruiz-Garcia and Miranda (2005) noted that the lateral deformation shapes of frame buildings whose lateral resisting system comprise only of structural walls can generally be estimated through applying the quantities of  $\alpha$  between 0 and 2; buildings with dual structural systems comprising of a composition of braced frames and moment-resisting frame buildings or a composition of shear walls and moment-resisting frames, the quantity of  $\alpha$  are usually placed on between 1.5 and 6; while MRF buildings commonly having quantities of  $\alpha$  are normally changed between 5 and 20 (Ruiz-Garcia and Miranda 2005).

The IDR at the  $j^{\text{th}}$  floor is estimated through rotation in the beam model at the level matching the halfway of the desired floor. The ordinates of GIDS are determined as the peak rotation along the building height and IDR is calculated as

$$\text{GIDS}_{(\text{Miranda et al})} = \max_{v,x,t} |\theta(x,t)| \approx \max_{v,x,t} \left| \frac{1}{H} \sum_{i=1}^{mn} \Gamma_i \phi_i'(x) D_i(t) \right| \quad (2.12)$$

Where symbolizations of the Equation 2.12 introduced by Miranda and Akkar (2006) as follow:  $x$  is the mean height of the  $j+1$  and  $j$  stories.;  $mn$  denotes the number of vibration modes measured in the spectral analysis;  $\Gamma_i$  is the modal participation factor of the  $i^{\text{th}}$  vibration mode;  $\phi_i'(x)$  symbolizes the first derivative of the  $i^{\text{th}}$  mode shape  $\phi_i(x)$  with respect to dimensionless height  $x$ ;  $D_i(t)$  represents the relative displacement response of a SDOF elastic system with the period of the  $i^{\text{th}}$  mode  $T_i$  and modal damping ratio  $\zeta_i$  exposed to a certain ground acceleration  $\ddot{u}_g(t)$  (Miranda and Akkar, 2006).

Junju Xie and Zeping Wen (2008) replaced the Timoshenko beam model instead of the combined flexural-shear beam in the GIDS derivation approach. They concluded that the drift spectrum established upon this model is restricted for evaluation of lateral drift demand for shear wall structures. Figure 2.3 illustrates the similarity of drift spectra employing the Timoshenko beam model with the GIDS when subjected to the Rinaldi, Receiving Station-NS record. Similar to the GIDR, the mode shapes

in the cantilever Timoshenko beam model are controlled by the height-width ratio (H/B).

As is shown by this Figure, the interstory drifts demands estimated on the basis of the Timoshenko beam model are lower than the corresponding results obtained by GIDS method. This is in agreement with the knowledge that the lateral resisting system such as a shear walls has decreasing effect on the interstory drift demands, which has been acknowledged by GIDS approach. It is represented that the drift spectrum based on the continuous Timoshenko beam model is limited for the assessment of lateral drift demands for shear wall frame buildings. It might not be appropriate to estimate lateral drift demands for other frame buildings when applying the simple cantilever beam model.

#### **2.4 Limitation of Proposed Drift Spectrum in Inelastic Regions**

The early drift spectrum measures ground motion demands dependent upon the wave propagation analysis of a shear beam model and it is useful particularly for near-fault ground motions. It provided beneficial information not directly could be obtained from the traditional response spectrum. Notwithstanding its new conceptuality and its multitude properties premiere to the customary response spectrum, the close form solution has some limitations.

Chopra and Chintanapakdee (2001) demonstrated that the wave propagation analysis cannot be well comprehended by structural engineers and showed the drift spectrum can also be estimated employing customary modal analysis techniques that are acquainted to design engineers with the inclusion of a proper number of modes.

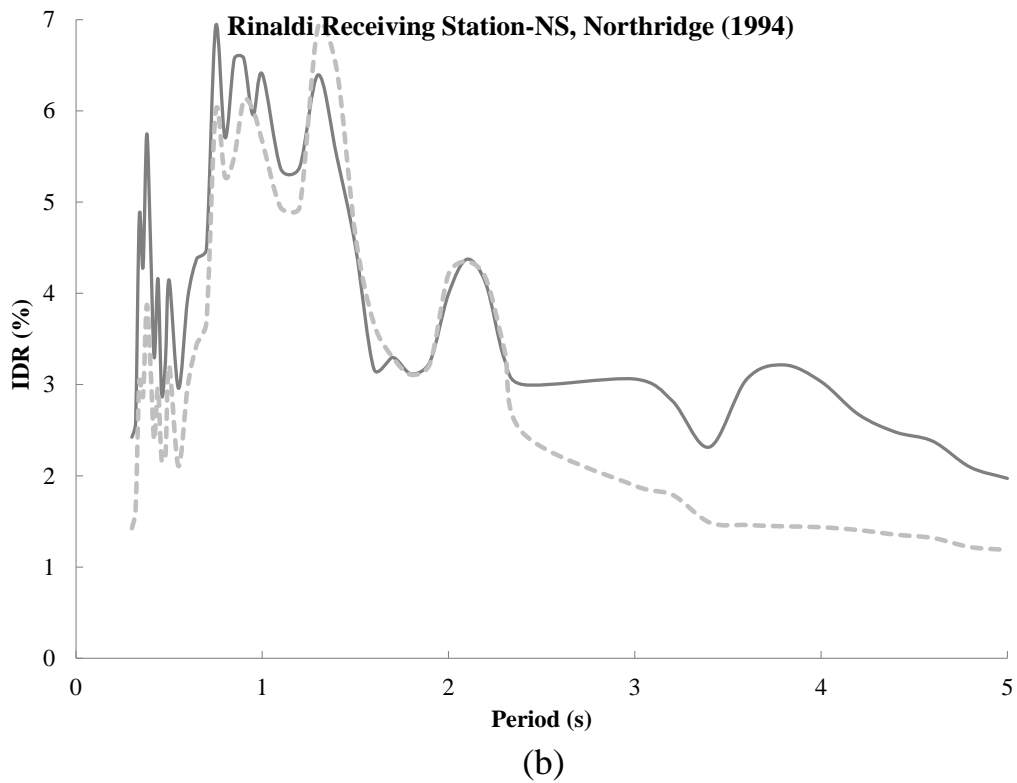
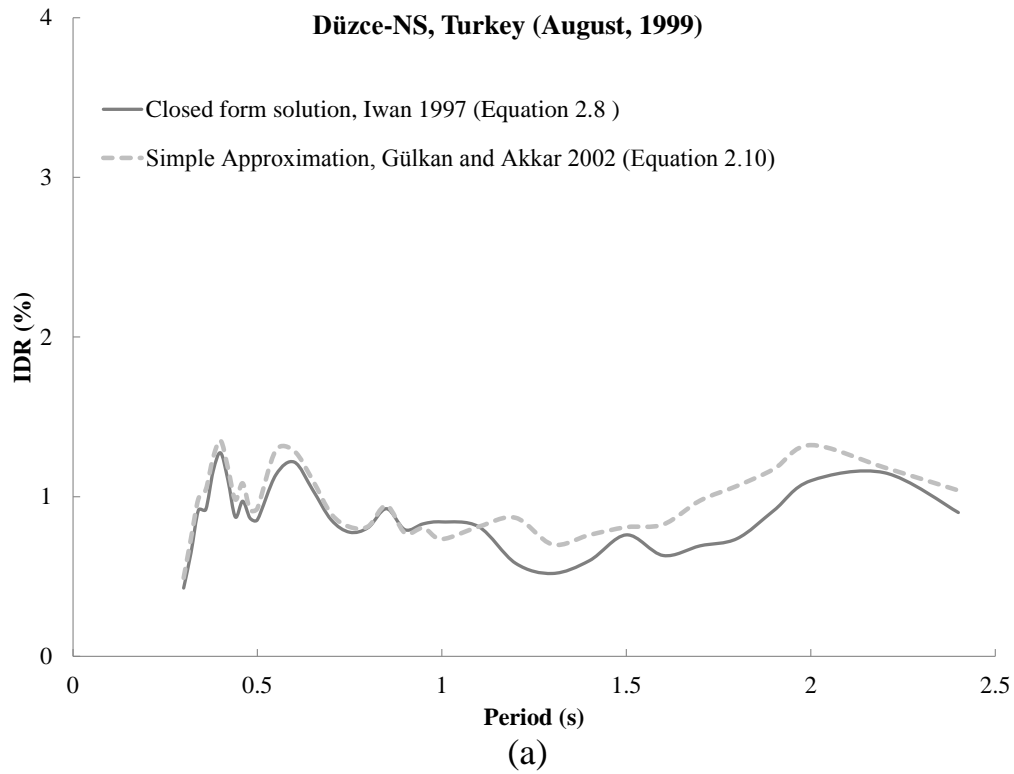


Figure 2.2 Comparisons of the close form solution with the simple approximation method (Gülkan et al., 2002) for ground motions (a) recorded at Düzce (NS) earthquake (19 Nev., 1999),  $c = 135$  m/s,  $H = 3$  m,  $\zeta = 2\%$ ; and (b) Rinaldi Receiving Station (NS), 1994 Northridge earthquake with  $c = 100$  m/s,  $H = 3$  m and  $\zeta = 0.0\%$

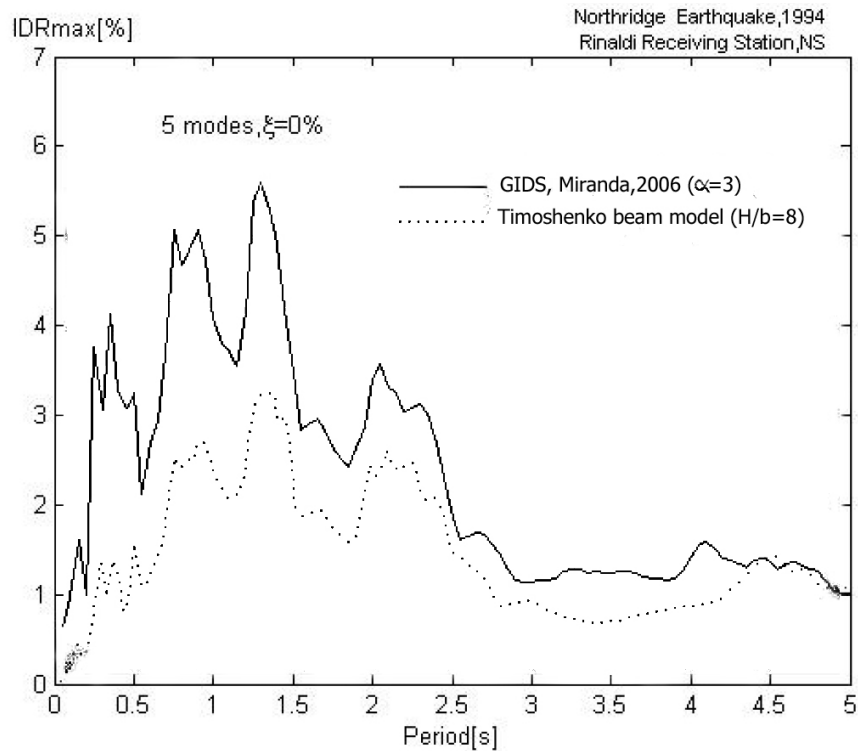


Figure 2.3 Comparisons of interstory drift demand estimates using Timoshenko Beam Model with the GIDS method exposed to Rinaldi record (1994)

Figure 2.4 shows the comparison between wave propagation analysis (Equation 2.8), which is the basis for the drift spectrum, and classical modal analysis by including the contributions of one or several modes. The spectra are plotted for un-damped shear beams under the Rindali (NS) record (1994 Northridge Earthquake). As is seen, the base level drift demand calculated by way of modal analysis will converge to the close form solution as suitable numbers of vibration modes are included, such that the discrepancy between the two sets of modal response history analysis (Modal RHA) resulted with one mode contribution and wave propagation analysis simply reflects the response contributions of modes higher than the fundamental mode.

Kim and Collins (2002) pointed out that the creative mathematical form utilized by Iwan (1997) formulation fits to a cantilever shear-beam model that is fasten to external springs with dampers attached firmly to a fixed reference point. They also demonstrated that the Iwan (1997) drift spectrum formulation leads to residual

(permanent) drifts for a given ground motion, which it is contradictory with the assumption of the linear elastic model.

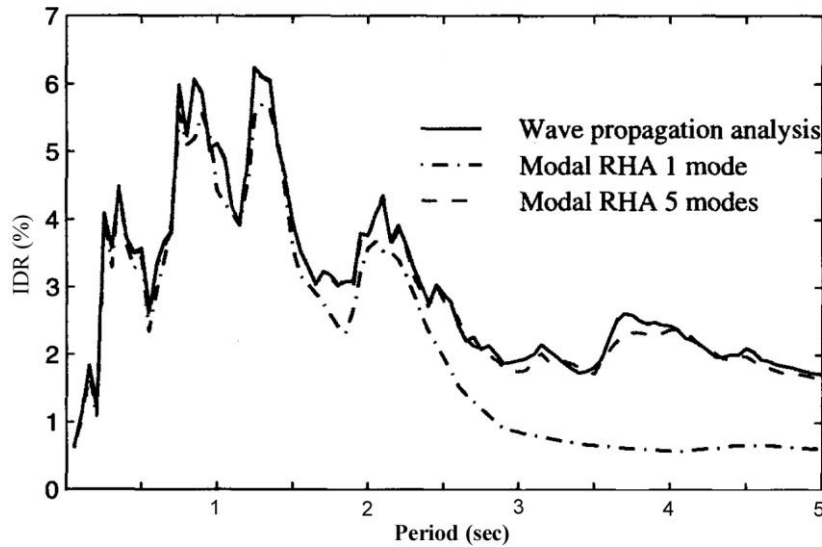


Figure 2.4 Drift spectra for the un-damped shear beam model subjected to Rinaldi (NS) record (Northridge ground motion 1994) through (1) wave propagation analysis (Equation 2.7) and (2) modal history analysis including one and (3) five modes contributions

The physical significance of the shear-beam formulation is schematically displayed in Figure 2.5. This is the physical model which forms the foundation for the solution suggested by Iwan (1997). Thus, the linear solution offered by Iwan's in Equation 2.8 does not coincide with the model in Figure 2.5 as intended. The residual drift problem rises from the springs mounted externally to beam model. An example of such a residual drift problem is demonstrated in the in Figure 2.6. This graph shows interstory drift time history using the Iwan (1997) expression (Equation 2.8) with shear-beam systems for 5 percent damped and with a vibration period of 0.2 s when exposed to a S80W direction of the ground motion recorded at the Lucerne Valley station during the 1992 Landers event. As it is seen this approach yields a residual

drift of nearly 0.5% which is incompatible with the linear behavior assumption in derivation of the Iwan (1997) drift spectrum.

It is worthy of note that the residual drift impacts the solution rather quickly, in order that it might influence the maximum drift response that takes place during the beginning of the seismic excitation. In other words, for ground motions that having features as specified permanent ground offset at the end of the ground motion record, the calculated interstory drift through the Iwan (1997) model did not return to zero as time approached infinity. Instead, the drift response goes to a non-zero constant. Whereas the Iwan (1997) formulation for the drift demand spectrum was dependent upon linear elastic behavior of a damped continuous shear-beam, therefore the drift response must eventually converge to zero after the excitation.

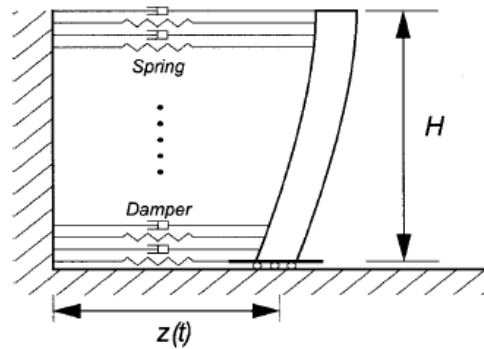


Figure 2.5 Physical configurations corresponding to Iwan (1997) shear-beam model

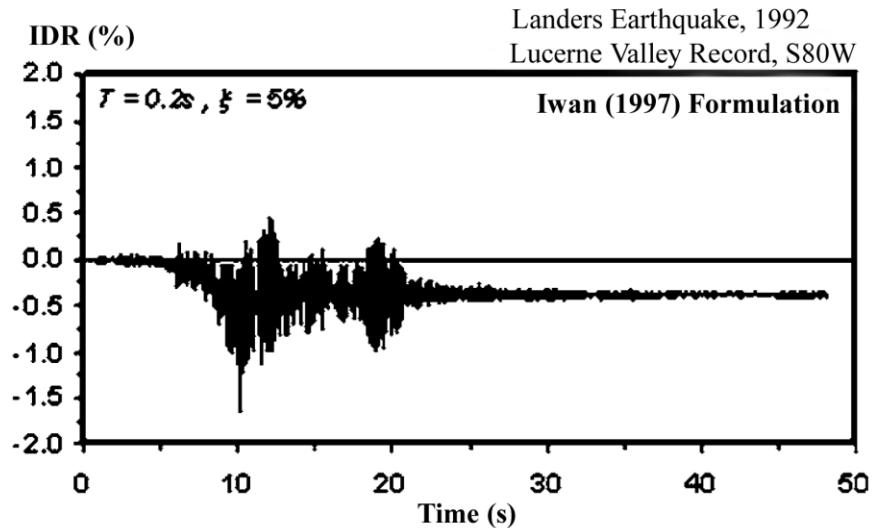


Figure 2.6 Response Interstory drift time series calculated for short period system ( $T=0.2s$ ) damped system ( $\zeta=0.05$ ) for S80W direction of the Lucerne Valley station record during the 1992 Landers event

Elastic response of SDOF systems and shear-beam models do not comprise influences of inelastic structural response and repeated cycles of inelastic deformations, which are mostly in conjunction with damage. Experimental work has shown that damages of structural members and whole systems are affected by several inelastic cycles of response (Bertero et al., 1977; Bozorgnia and Bertero, 2001). This means that, structural systems mostly become more vulnerable if they go through repeated cycles of inelastic motions. Inelastic behavior of structural system is probably in the matter of pulse-type, near-field earthquakes that demonstrate enormous deformation demands. This necessitates structural seismic performance as estimated through the inelastic dynamic analysis. In this regard, emphasis should be focused on the explanation of inelastic interstory drift limits for a more realist evaluation of structural performance. One approach to calculate the inelastic behavior of a structural system is modified the elastic response using the response modification coefficient.

Converting the elastic spectral displacement ordinates into the inelastic range can be one way of achieving the inelastic base level drift demands. In order to enhance the versatility of estimated drift ordinates, Gülkan and Yazgan (2005) extended the Equation (2.10) to achieve the inelastic drift demands using the constant ductility inelastic displacement equation, which had been proposed by (Miranda 2000). This expression is presented in Equation (2.13).

$$C_{\mu} = \frac{SD_{inelastic}}{SD_{elastic}} = \left[ 1 + \left( \frac{1}{\mu} - 1 \right) \exp(-12T\mu^{-0.8}) \right]^{-1} \quad (2.13)$$

Here  $C_{\mu}$ : indicates the modification factor of the inelastic to the elastic displacement, which is dependent on period,  $T$  and displacement ductility,  $\mu$ . It is required to note that the Equation (2.13) is in use only for elastic-plastic hysteresis behavior. The expression for the inelastic base level drift limit is provided in Equation 2.14 (Gülkan and Yazgan 2004, 2005).

$$IDR_{modified\ Gülkan} = 1.27 \cdot C_{\mu} \cdot \frac{S_D(T, \zeta)}{h} \cdot \sin \frac{\pi^b \sqrt{ah}}{2^b \sqrt{T}} \quad (2.14)$$

Gülkan and Yazgan modified Equation (2.10) by making use of code expressions. However, the proposed solution (Equation 2.14) included several drawbacks in the nonlinear zone; the Equation  $T = aH^b$ , that is used here (which first appeared in the ATC3-06 report and later UBC 97; TEC 1997, 2007 and etc.) was derived through Rayleigh's method under the following assumptions (Chopra 1995; Goel and Chopra, 1997); (1) Lateral forces were assumed to be distributed linearly along the building height (triangular variation of forces); (2) stories weight is distributed uniformly over building height; (3) the structure deflected linearly under applied lateral forces. The last assumption implies the same interstory drift for all stories which is not case for applied drift demands in inelastic ranges. Essentially, it is not possible to find the right shape for the deflection pattern particularly when structural members exceeded the elastic limits.

Moreover, in Equation (2.14) as well as other ideal building models (such as Iwan (1997) equation; GIDS approach and UBC formula) the relationships were expressed referring to the initial period using uncracked sections; a period factor; and a linear displacement response spectrum of certain equivalent damping. However, it is known that growing cracks in building frames (e.g. RC MRF and Steel Moment Resistant Frame (SMRF)) during inelastic behavior that exposed to severe ground motions reduce the stiffness of frames, which in turn enhances the fundamental period,  $T$  (Goel and Chopra 1997). Another incompetence of Equation (2.14) is related to the delegation of a proper level of damping and the mechanism by which damping is modeled, is a critical decision should be made by the user. The ratios of maximum interstory drifts for nonlinear and linear analyses are found to change meaningfully, as did the ratios between locations of these quantities. These are important topics should be assessed to improve the preciseness of the inelastic drift spectrum in predicting drift demands for real structures.

The generalized interstory drift spectrum (GIDS) extends the drift spectrum to structural system where the shear-beam model may not be suitable. Moreover, it allows one to incorporate a large spectrum of deformation modes that reflect more accurately those of frame buildings in to drift spectrum calculation. Nonetheless, it must be noted that the basic presumption underling the employed modal superposition method in the interstory drift spectrum that made general, that is it the modal responses are supposed to be uncoupled, which is not true for a structural system when its response runs into an inelastic region. In the inelastic range, the modal shapes and corresponding modal participation factors might be meaningfully changed due to the stiffness degrading in the structural system. Uniform lateral stiffness distribution is another assumption which is not the case for most common frame buildings. Owing to the non-uniform vertical distribution of earthquake-produced lateral forces in frame buildings, the lateral stiffness at the top of the structure is smaller in a characteristic manner and in some cases considerably smaller compared to the lateral stiffness at the base of the building.

All of the aforementioned issues are indicative of a shortage of current drift spectrum in nonlinear ranges. However, the inelastic behavior of structural systems is more reasonable in the case of severe ground motions, particularly when buildings are located close to fault rupture zone that exhibits large drift demands associated with pulse-like excitation, and in turn damages arising from degrading hysteresis responses occur after some restoring cycles.

Lack of realistic models of the non-ductile structural members can be damaging to reliable seismic evaluation of the RC frame buildings. Analytical models of columns subjected to seismic loading require a force displacement envelope relationship capable of yielding the realistic behavior of the structural members at each displacement levels. This is an exact requirement to taking into account the fact that the multiple parameters contributing to strength deterioration; stiffness decay and apparent pinching of response loops. Therefore, in these cases, it is very much required to estimate interstory drift demands accurately in an inelastic domain and to incorporate hysteresis capacity decay consequences into interstory drift demands. One way to account for inelastic behavior of a structural system is modified the elastic response using the response modification factor. This study will try to examine this issue in detail.



## CHAPTER 3

### ANALYTICAL STUDY ON HYSTERESIS CAPACITY DEGRADATION OF STRUCTURAL SYSTEMS

#### 3.1 Introduction

Suitable protection of structural systems from the effects of ground motions needs a precise understanding of strength capacity and displacement properties of the members and components producing the structure that provides resistance to seismic load effects. Attainable approaches established upon mechanical principles are mostly skimmed to provide trustworthy knowledge on these properties, mainly on account of the random nature of the cyclic displacement demands applied to members and the reliance of the response features on the displacement time series to that a member is exposed. Therefore, experiments with physical specimens, which regenerate the site conditions as practically as possible, are required to supply essential knowledge that may be employed to establish, improve or approve analytical models which will constitute a source for seismic safeguarding processes.

Structural systems commonly demonstrate inelastic behavior subjected to strong cyclic loading along with earthquake excitations, particularly for generously nonlinear material similar to reinforced concrete. For load factored linear elastic analysis, recommended through the design provisions, the results are wholly sufficient, nevertheless do not exhibit the realistic behavior properties of the structural system. However, whether an inelastic seismic response is considered or not, more filtered simulation models are required to obtain a pragmatic behavior.

The load-deflection envelope curve plotted subject to this inelastic excitation exhibits itself in the form of hysteresis loops. The hysteresis expression applies to the memory essence of the inelastic structural assembly, which means that the restoring force relies not just on the present deformation by the same token on the previous deformations. A measure of the energy dissipated subject to cyclic loading as a result of internal friction within the structural system and yielding of the structural components reflect in hysteresis loops. In the process of reiterated cyclic loading, deterioration in the mechanical properties of structural systems is generally seen in the inelastic response range. This is especially correct for RC materials that have high tendency to behave in nonlinear range and whereas system properties are continually being varied through both stiffness and strength deterioration or apparent pinching of hysteresis loops, pinching comes from a sudden loss of stiffness usually related to opening and closing of cracks prevalently seen in masonry and RC Frame buildings (Figure 3.1).

As seen in the figure, pure detailed columns in old built RC frame buildings are often weaker than the beams, leading to early column hinging and an undesirable column sideways mechanism. In older RC buildings, the girders are often stronger than the columns, and column hinging after only a very few seismic excursions can result in a story mechanism, producing larger P-Delta effects and inelastic rotations in the column tips. Severe failures and even fully collapse due to a story sideways mechanism can be widely observed. Analytically, capacity deterioration in mechanical properties is reflected in three different forms of the load-damage relationships. These are stiffness decay, strength degradation, and pinching at the response hysteresis loops. Important and evolutionary results from past cyclic experimentations taken from the typical RC components undergo to various kinds of hysteresis decays are illustrated in Figure 3.2.(a)-(c) (Atalay and Penzien, 1975; Takemura and Kawashima, 1997; Matamoros, 1999).

In the past years, important studies have been done in order to surmount difficulties originating in dynamic nonlinear analysis. Challenges emerge not only from the intrinsic complexity of RC systems, but also from the uncertainties identifying with

terms like material nonlinearity; dynamic loading; and hysteresis behavior. Macro-modeling of structural systems has been one of the key approaches presented to model such complex phenomena. In a macro-modeling analogy, knowledge areas related to the factual behavior of RC is embodied in the system applying an element-based method.



Figure 3.1 Examples of the story mechanism induced by the hinge plasticization at the column tips of RC MRF buildings

In the element-based method, the beam element is enhanced with a force-deformation or moment-curvature relationship defining the behavior of both end sections, a hysteresis behavior and a pertinent propagation of yielding govern for the beam which is well-founded from matrix structural analysis as well. Through the introduction of such a smooth elasto-plastic element, one is able to model the progressive change of the mechanical characteristics of the element as it transited from the elastic to the inelastic area of its response. Macro-models take advantage of the capturing general behavior equivalently without utilizing to intricate finite element discretizations.

Numerous hysteresis models include hysteresis stiffness and strength deterioration, and apparent pinching properties have been developed in recent decades to model the cyclic response of the structure. One of the most generally acknowledged models is a differential model suggested by Bouc (1967) at first and later enhanced by Wen (1976). The reason behind the wide acceptance of this model is its ability to better reflect the continuous changes in the material properties together while capturing many commonly observed types of hysteretic behavior (such as bilinear, softening, hardening, etc.) through simply tuning a few control parameters.

The early hysteresis Bouc-Wen model worked as the foundation for several evolutions of the models, Baber and Wen (1981) by introducing degradation shape functions, thereby extending the model to consider strength and stiffness decays. Baber and Noori (1985) later made general form this hysteretic model by adding the pinching behavior, (Park et al. 1987; Kunnath and Reinhorn 1995) that addresses the strain-rate-dependent characteristics of materials dependent upon plasticity theory.

In addition, Sivaselvan and Reinhorn (1999, 2000) advanced a versatile hysteretic model that can tackle with degrading of stiffness and strength as well as pinching in sections of structural components, commonly expressed by pinched hysteretic models through altering the features of component springs and their extended model called the Smooth Hysteretic model (SHM). Subsequent to these developments, many computer programs have been enhanced, able to carry out a nonlinear structural analysis like for example: IDARC (Park et al., 1978; Kunnath et al. 1992); DRAIN-2D (Kanaan and Powell 1973) and etc. The SHM is incorporated in the “IDARC 2D” platform with continuous variation of stiffness due to yielding, as well as a sharp change on account of unloading and degrading behavior. Since then, the IDARC platform and along with it SHM from its element library is adopted to consider the flexural component of the deformation beyond the yielding points in both nonlinear static and dynamic analyses.

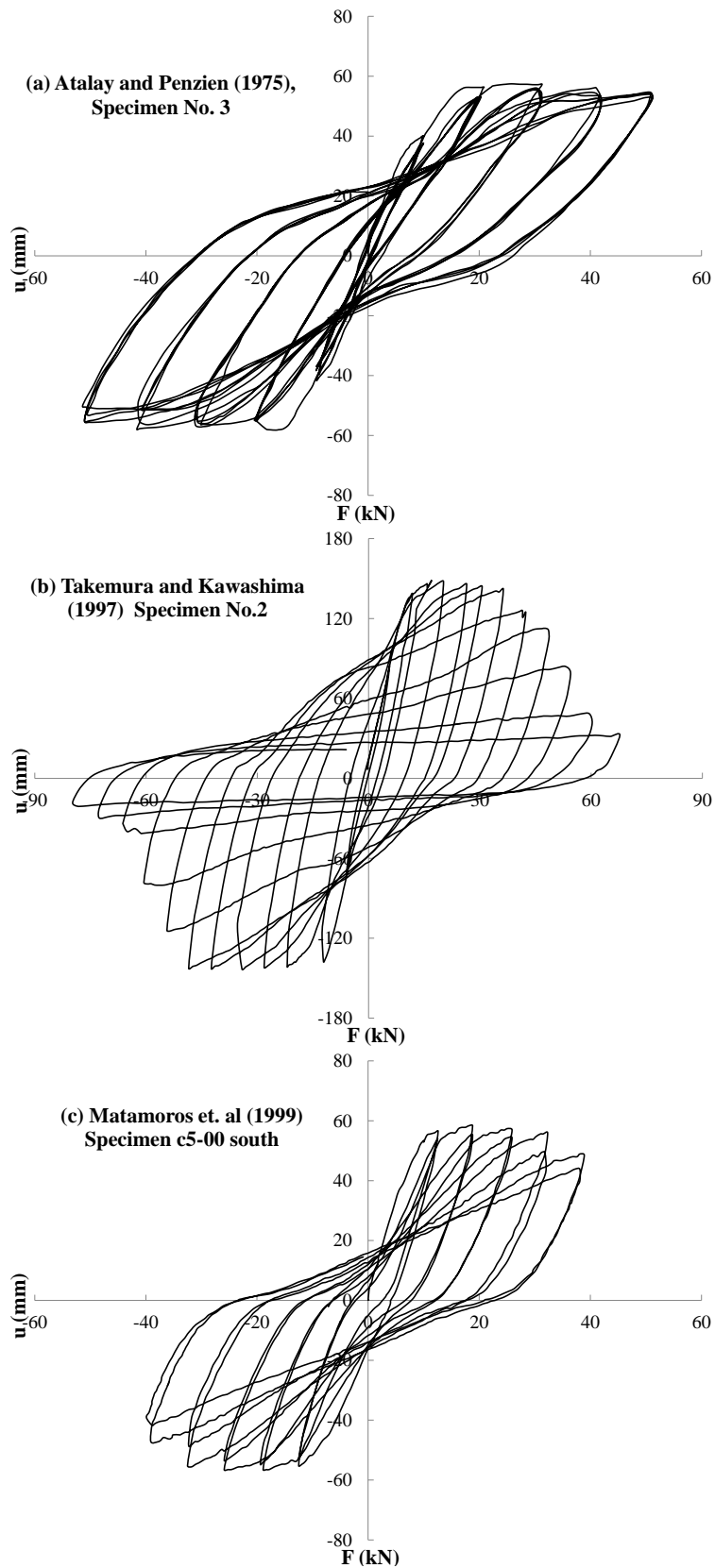


Figure 3.2 Examples of decay modes seen in the column members subjected to cyclic loading: (a) Stiffness decay, (b) Strength deterioration, (c) Pinching or slip

To correctly represent the realistic restoring force dealing of structural members, it is required to appraise parameters of the SHM appropriately. Data collected from the cyclic loading test provides valuable information to estimate model parameters. Analytical models are prepared using data presented in the input data sheet for experiments; smooth hysteretic response curves under the identical loading are computed. The hysteresis response relations are investigated and key parameters are clarified which used to formulate a model for the hysteresis loop where all its parameters are physically meaningful.

The purpose underlying this is to supply a diversified amount of the model control parameters to incorporate the hysteresis decay of structural members on following nonlinear dynamic analysis by meaningful magnitude variations. The important equations of the differential based Bouc-Wen model and the SHM which was developed based on this model are discussed. Likewise, the deviation of both models and parameters that control the model equations are examined in subsequent sections.

### 3.2 Bouc-Wen Hysteretic Model

The equation of motion govern to the SDOF hysteretic system is described by

$$m\ddot{u}(t) + c_v\dot{u}(t) + aku(t) + (1 - a)kz(t) = F(t) \quad (3.1)$$

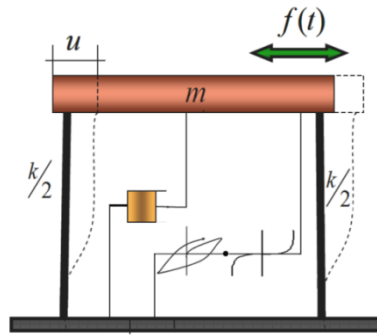
Where  $u(t)$  is the relative displacement of the mass  $m$  compared to the earthquake excitation;  $k$  denotes the linear stiffness;  $c_v$  is a linear viscous damping coefficient;  $a$  indicates proportional relation of the post-yield with respect pre-yield stiffness ( $0 \leq a \leq 1$ ) and  $F(t)$  is the excitation force while the over dot designates derivative toward the time. If Equation (3.1) is divided by  $m$ , the following equation is obtained:

$$\ddot{u}(t) + 2\zeta\omega\dot{u}(t) + \alpha\omega^2u(t) + (1 - a)\omega^2z(t) = f(t) \quad (3.2)$$

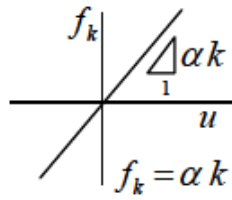
Here,  $\zeta$  and  $\omega$  symbolize the linear damping ratio ( $c/2\sqrt{k_i m}$ ) and pre-yield natural circular frequency of the system  $\sqrt{k_i/m}$  respectively; and  $f(t)$  signifies the mass normalized external excitation,  $f(t) = F(t)/m$ . It should be noted that in Equation (3.2) the term  $a\omega^2 u(t)$  is interpreted as the cycle independent linear restoring force component, whereas  $(1 - a)\omega^2 z(t)$  term represents the hysteretic restoring force component. The system is comprised of a non-pinching hysteresis element in series with a “pinching or slip-lock” element which is linked in parallel to an elastic spring (Figure 3.3). The hysteretic restoring force is a function of hysteretic displacement  $z(t)$  dimensionless hysteretic parameter, which complies with the following nonlinear differential equation (Equation 3.3).

$$\dot{z}(t) = h(z) \left[ \frac{A(t) \cdot \dot{u}(t) - v(t)(\beta|\dot{u}(t)||z(t)|^{n-1}z(t) + \gamma\dot{u}(t)|z(t)|^n)}{\eta(t)} \right] \quad (3.3)$$

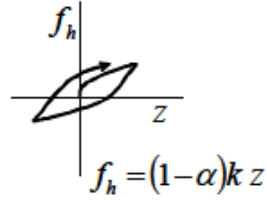
The constants  $A$ ,  $\beta$ ,  $\gamma$  and  $n$  describe the hysteresis shape;  $v(t)$  and  $\eta(t)$  along with  $A$  affect stiffness and strength degradation respectively; and  $h(z)$  symbolizes the pinching function.



a) The Schem of model



b) Undamped linear force



c) Hysteretic restoring force

Figure 3.3 Schematic diagram of a SDOF hysteretic model to depict hysteretic degradation and pinching behavior

### 3.2.1 Stiffness and Strength Degradation

The total energy absorption is employed in the model to estimate capacity deterioration of the system. The energy absorbed by the hysteretic element is the continuous integration of the hysteretic force,  $f_h$  over the entire displacement  $u$ , is declared as Equation (3.4)

$$\begin{aligned}
 \varepsilon(t) &= \int_{u(0)}^{u(t)} f_h du \\
 &= (1 - a)\omega^2 \int_{u(0)}^{u(t)} z(u, t) du \frac{dt}{dt} \\
 &= (1 - a)\omega^2 \int_{u(0)}^{u(t)} z(u, t) dt
 \end{aligned} \tag{3.4}$$

Strength deterioration and stiffness decay parameters  $v$ ,  $\eta$  and  $A$  are a function of the whole dissipated hysteresis energy as explained in following equations

$$\begin{aligned}
 A(t) &= A_0 - \delta_A \varepsilon(t) \\
 v(t) &= 1 + \delta_v \varepsilon(t) \\
 \eta(t) &= 1 + \delta_\eta \varepsilon(t)
 \end{aligned} \tag{3.5}$$

where  $\delta_A$ ,  $\delta_\eta$  and  $\delta_v$  are positive constants that define the desired rate of decay at distinctive displacement degrees. Once  $\delta_\eta$  and  $\delta_v$  quantities are zero, the structural system does not deteriorate its stiffness and strength. Here  $\varepsilon$  is the total energy dissipated through hysteresis.

$$\dot{\varepsilon}(t) = (1 - a)\omega^2 z(t) \dot{x}(t) \tag{3.6}$$

If the assumption in such a way that the pinching of system can be ascribed to a physical slipping which occurs upon reversal of loading, then hysteresis loop

pinching may be incorporated into the differential model of hysteresis by addition of a time-dependent ‘slip-lock’ element given by the rate equation (Equation 3.7):

$$\dot{x}_2 = f(z)\dot{z} \quad (3.7)$$

It is observed from Figure 3.4 that the slip-lock element acts fully in a similar manner to a hardening nonlinear spring with the particular characteristic that the ‘slip’ zone stiffness is almost zero whereas the ‘lock’ zone stiffness is closely infinity. Furthermore, the slip-zone length ( $2a$ ) may be assumed to be zero at the beginning and rise as the system deteriorates.

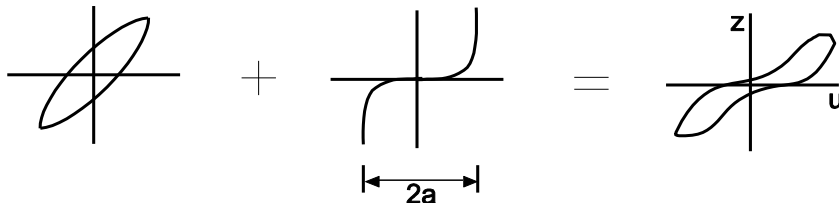


Figure 3.4 Slip-lock series hysteresis

For feasible modeling aims, the function  $f(z)$  may be given as Equation (3.8):

$$f(z) = 2aG(z) \quad (3.8)$$

Where  $G(z)$  is any finite and continued approximation to the delta function. The standard Gaussian density function expression in Equation (3.9) is one of the parameterized functions that could be led to the delta function.

$$G(z) = \frac{1}{\sigma\sqrt{2\pi}} e^{-\frac{z^2}{2\sigma^2}} \quad (3.9)$$

So that the width ( $\sigma$ ) goes to zero,  $G(z)$  approximates to the delta function. Upon substitution of the Gaussian density function into Equation (3.8), Equation (3.7) can be rewritten as

$$\dot{x}_2 = \sqrt{\frac{2a}{\pi\sigma}} e^{-\frac{z^2}{2\sigma^2}} \dot{z} \quad (3.10)$$

Where the slip magnitude and the parameter  $\sigma$  may be taken as

$$a = \delta_a \varepsilon \quad (3.11)$$

$$\sigma = \sigma_0 + \delta_\sigma \varepsilon \quad (3.12)$$

The magnitude of slip and sharpness of locking be changed with time. If all the decay parameters ( $\delta$ ) are taken as zero and  $\sigma_0$  as an adequately large quantity, the current model reduces to the non-degrading non-pinching Bouc-Wen hysteretic model.

### 3.2.2 Pinching Function

The expression of pinching function  $h(z)$  that satisfies the desired pinching characteristics is given as Equation (3.13)

$$h(z) = 1 - \varsigma_1 \exp\left(-\frac{z^2}{2\varsigma_2^2}\right) \quad (3.13)$$

Here  $\varsigma_1$  controls the severity of pinching and is limited to the interval ( $0 < \varsigma_1 < 1.0$ ). Increasing  $\varsigma_2$  spreads the region of pinching. If the total energy dissipated by hysteresis ( $\varepsilon$ ) is taken as a control on pinching,  $\varsigma_1$  and  $\varsigma_2$  can be expressed by Equations (3.14) and (3.15)

$$\varsigma_1 = \varsigma_{10}[1 - \exp(-p\varepsilon)] \quad (3.14)$$

$$\varsigma_2 = (\xi_0 + \delta_\xi \varepsilon)(\lambda + \varsigma_1) \quad (3.15)$$

The rate of energy dissipated through hysteresis can be stated as

$$\dot{\varepsilon}(t) = (1 - a)\omega^2 z(t)\dot{x}(t) \quad (3.16)$$

The progression rate of  $\varsigma_1$  controls by  $p$  and the maximum quantity of it being  $\varsigma_{10}$ . The constant  $p$  governs the rate of initial drop in slope; and also measuring the amount of total slip is carried out by  $\varsigma_{10}$  ( $0 < \varsigma_{10} < 1$ ). The development of  $\varsigma_2$  is governed by the parameters  $\xi_0$ ,  $\delta_\xi$  and  $\lambda$ ; the  $\xi_0$  is a parameter that contributes to the quantity of pinching; the  $\delta_\xi$  is implied for the desirable variation rate of  $\varsigma_2$  established upon the  $\varepsilon$ ; and  $\lambda$  is a small variable that governs the variation rate of  $\varsigma_2$  as  $\varsigma_1$  variables. If the degradation parameters  $\delta_A$ ,  $\delta_\eta$  and  $\delta_v$  and the pinching function  $h(z)$  are taken as zero, the model reduces to the non-degrading non-pinching Bouc-Wen model defined by Equations (3.2) and (3.3).

### 3.2.3 Solving the Bouc-Wen Hysteretic Model in the Analytical Form

This system of differential equations (ODE) allows for the dynamic behavior for various types of structures subjected to random cyclic loading and can be solved using the ordinary differential equation solver in MATLAB platform (Mathworks, 2009). “ODE45” function, which is the standard solver for ordinary differential equations (ODEs) of the MATLAB platform is adopted to solve the simultaneous first-order ODEs that are represented the hysteresis Bouc-Wen model in its analytical form by the Equations (3.2 - 3.16). This routine uses a variable step (the combination of the fourth- and fifth order) Runge-Kutta Method to solve differential equations numerically. The ode45 is intended to handle the following general problem

$$\frac{dy}{dt} = f(t, y), \quad y(t_0) = y_0 \quad (3.17)$$

Where  $t$  is the independent inconstant (time, position, volume) and  $y$  is a vector valued of  $t$  and  $y$  to be found. The mathematical problem is determined when the vector of functions on the right-hand side of Equation (3.17). the  $f(t, y)$  is specified and the initial conditions,  $y = y_0$  at time  $t_0$ , are assigned. Consequently, it can be inscribed that

$$\begin{Bmatrix} y_1(t) \\ y_2(t) \\ y_3(t) \\ y_4(t) \end{Bmatrix} = \begin{Bmatrix} u(t) \\ \dot{u}(t) \\ z(t) \\ \varepsilon(t) \end{Bmatrix} \quad (3.18)$$

The Bouc-Wen model equations (3.2), (3.3) and (3.4) can be rewritten on the basis of Equation (3.18) as follows:

$$\dot{y}_1 = y_2 \quad (3.19)$$

$$\dot{y}_2 = -2\zeta\omega y_2(t) - a\omega^2 y_1(t) - (1 - a)\omega^2 y_3(t) + f(t) \quad (3.20)$$

$$\dot{y}_3 = h(y_3(t)) \cdot \quad (3.21)$$

$$\left[ \frac{(A_0 - \delta_A y_4(t)) y_2(t) - (1 + \delta_v y_4(t)) (\beta |y_2(t)| |y_3(t)|^{n-1} y_3(t) + \gamma y_2(t) |y_3(t)|^n)}{1 + \delta_\eta y_4(t)} \right]$$

$$\dot{y}_4 = (1 - a)\omega^2 y_3(t) \cdot y_2(t) \quad (3.22)$$

The MATLAB platform has a couple of tools to solve the ordinary differential equations numerically. The built-in function ode45, which implement version of Runge–Kutta 4th/5th-order method, is adopted to solve these set of ODE equations.

### 3.2.4. Variation of the Response Hysteresis Loop of the SDOF system with the Bouc-Wen Model Parameters under External Cyclic Excitation

The Bouc-Wen differential based model can reflect a wide range of different hysteresis loops by appropriate designates of the parameters to control the model. The following sections elaborate on the effects of these parameters on the system behavior under incoming external cyclic excitation. In the following sections, the variables controlling the hysteresis loops of the analytical Bouc-Wen model are clarified and the influence of each one upon the hysteresis response loop is investigated.

#### 3.2.4.1 Influence of Parameter A

To examine the effect of A on the tangent stiffness in the  $x - z$  plane, the slope of the hysteresis loop ( $dz/dx$ ) may be deduced using the Equation (3.23)

$$\frac{dz}{dx} = A - (\beta \text{sgn}(\dot{x}) \text{sgn}(z) + \gamma) |z(t)|^n \quad (3.23)$$

In the interval, as  $x$  and  $z$  goes to zero, Equation (3.23) reduces to Equation (3.24). The parameter A corresponds to the slope of the hysteresis loop at  $z = 0$

$$\left( \frac{dz}{dx} \Big|_{z=x=0} = A \right) \quad (3.24)$$

The Equation (3.24) implies that A sets the initial tangent stiffness. This parameter is denoted by  $A_0$  through the manuscript. The ultimate value of  $z$ , on the other hand, can be obtained by setting  $dz/dx = 0$  and solving it for  $z$

$$z_{\max} = \sqrt[n]{\frac{A}{v(\beta + \gamma)}} \quad (3.25)$$

Note that, assuming  $\beta$  and  $\gamma$  are constant Equation (3.25) shows that  $A$  governs the yield level. In order to observe the influence of  $A$  upon the hysteretic loop, a number of structural systems with varying  $A$  values are simulated using a frequency modulated signal,  $f(t) = 8 \sin((0.03t + 0.2)t)$  as external excitation. Meanwhile, the remaining parameters are kept constant ( $\zeta = 5\%$ ,  $\omega = 3.0$ ,  $a = 0.0$ ,  $n = 2.0$ ,  $\beta = 0.5$ ,  $\gamma = 0.5$ ). Figure (3.5) shows the hysteresis restoring force vs. displacement phase plane plots for four different  $A$  values. It can be discerned from the figure, besides changing the slope and the yield level, the increase in  $A$  makes the hysteresis loops even narrower.

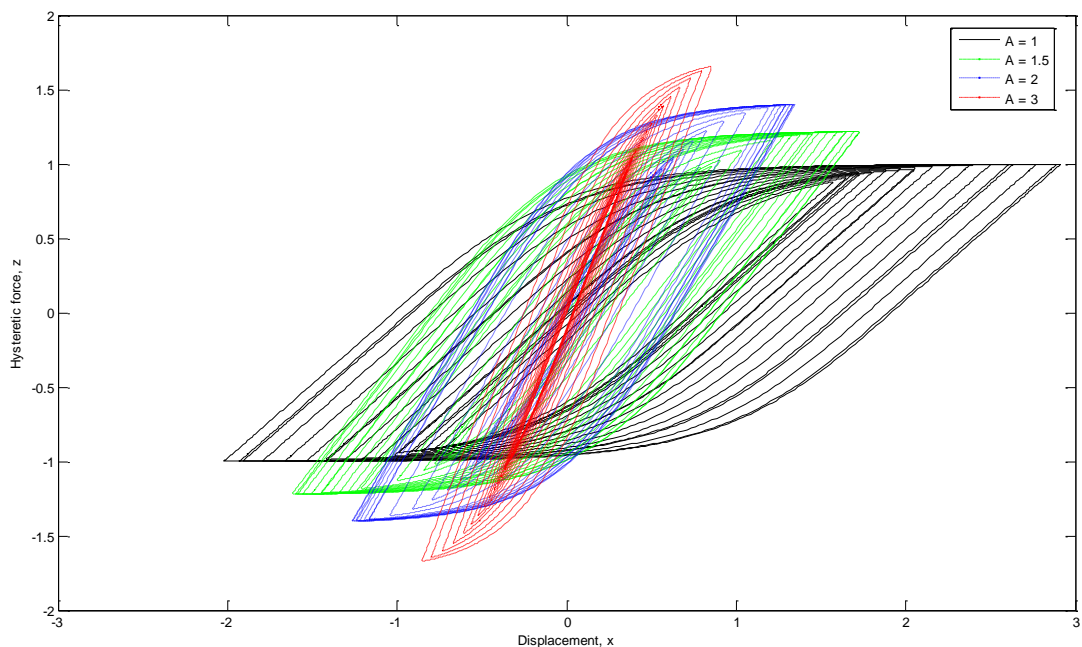


Figure 3.5 Comparison of hysteresis restoring force component  $z(t)$  vs. displacement  $x(t)$  phase plane plots with different  $A$  values, the parameters excluding  $n$  are kept constant. ( $\zeta = 5\%$ ,  $\omega = 3$ ,  $a = 0.0$ ,  $n = 2$ ,  $\beta = 0.5$ ,  $\gamma = 0.5$ )

### 3.2.4.2 Influence of Parameters $\beta$ and $\gamma$

The form of the hysteresis loop is principally controlled through the  $\beta$  and  $\gamma$  variables. A varying combination of  $\beta$  and  $\gamma$  results in a unique loop with various stiffness properties. In fact, among all the available  $\beta$  and  $\gamma$  combinations, there are only five combinations that bring about physically meaningful hysteresis loops (Wong 1994). The connection between  $\beta$  and  $\gamma$  and their influences on hysteresis response are defined below and illustrated in Figure (3.6). The effect of shape parameters in the Bouc-Wen hysteretic model is demonstrated in the graphs. In addition, it makes it possible to examine each inequality relation between  $\beta$  and  $\gamma$ . These inequalities were introduced by Baber and Wen (Baber and Wen 1981). A number of simulations are accomplished to figure out the influence of the  $\beta$  and  $\gamma$  variables. While generating the numerical responses, the parameters excluding  $\beta$  and  $\gamma$  are kept constant ( $\zeta = 5\%$ ,  $\omega = 3.0$ ,  $a = 0.0$ ,  $A = 1.0$ ,  $n = 2$ ). A frequency modulated signal is used as external excitation  $f(t) = 1000t \times \sin(2\pi t)$ , and the response is sampled at a rate of 10 Hz for a total duration of 10 s.

Figure (3.6) show the restoring force vs. displacement phase plane plots for various  $\beta$  and  $\gamma$  combinations. These figures confirm that increasing  $\beta$  values lead to wider hysteresis loops and  $\beta = 0.0$  cause the response to be non-hysteretic even though nonlinearity is still preserved in certain cases. Moreover, it is also apparent from these plots that negative  $\gamma$  values tend to cause a hardening response provided that  $|\gamma| > |\beta|$  and  $\gamma < 0.0$ .

### 3.2.4.3 Influence of the Parameter $n$

The parameter  $n$  controls the smoothness of the transition from the linear to nonlinear region. While the values of  $n$  increase, the smoothness hysteresis loading direction approaches the ideal elastoplastic function. The unloading direction comes near to a linear line. In contrast to this case, with decreasing values of  $n$ , the transition rate from the linear region to nonlinear ranges sharpens and hysteresis

loops become narrow. The foregoing discussion shows that as  $n$  approaches infinity, the hysteresis loop approaches a bilinear form. A true bilinear hysteresis will be attained if  $a > 0$ , whereas a true elasto-plastic hysteresis will result if  $a = 0$ . In hardening systems ( $\gamma < 0$ ), the hysteresis loop is narrow and the linear transition is sharp, and softening systems ( $\gamma > 0$ ) illustrate the elasto-plastic function trend.

A number of systems with altering  $n$  values are simulated under excitation  $f(t) = 3 \sin((0.03t + 0.2)t)$  conditions to find out the impact of the parameter  $n$ . While producing the numerical responses, the parameters excluding  $n$  are kept constant ( $\zeta = 5\%$ ,  $\omega = 3$ ,  $a = 0$ ,  $A = 1$ ,  $\beta = 0.5$ ,  $\gamma = 0.5$ ). The hysteresis response is sampled at a rate of 200 Hz for a total duration of 60 s (see Figure 3.7). Figure (3.7) illustrate the hysteresis restoring force vs. displacement phase plane plots for excitation forces corresponding to four different  $n$  values. It is obvious from these graphs that as  $n$  increases, the transition from elastic range to post-elastic region becomes sudden and approaching that of a bilinear model.

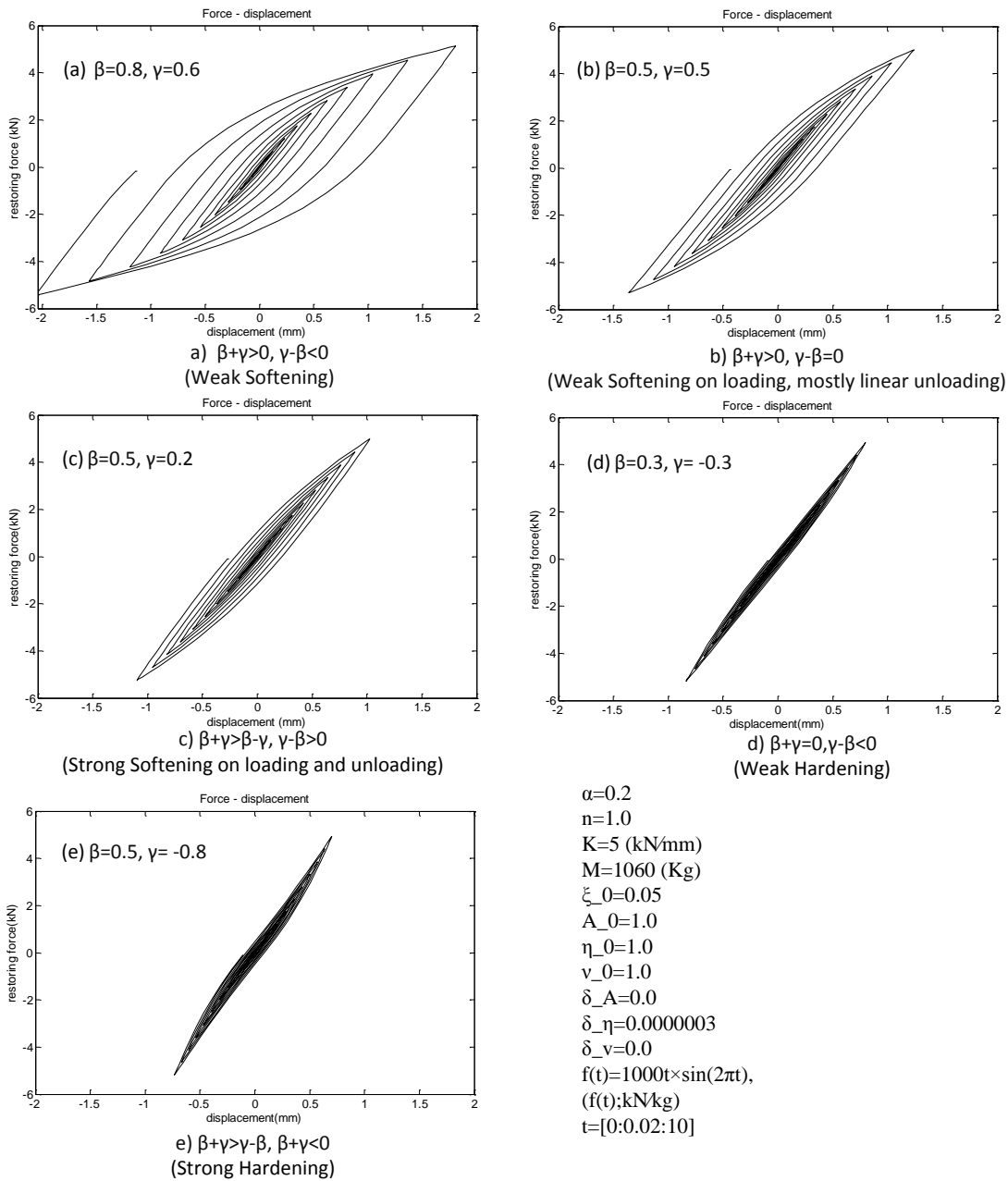


Figure 3.6 Possible hysteresis response loops through the different combination  $\beta$  and  $\gamma$ , remaining parameters is kept constant and is listed in the figure

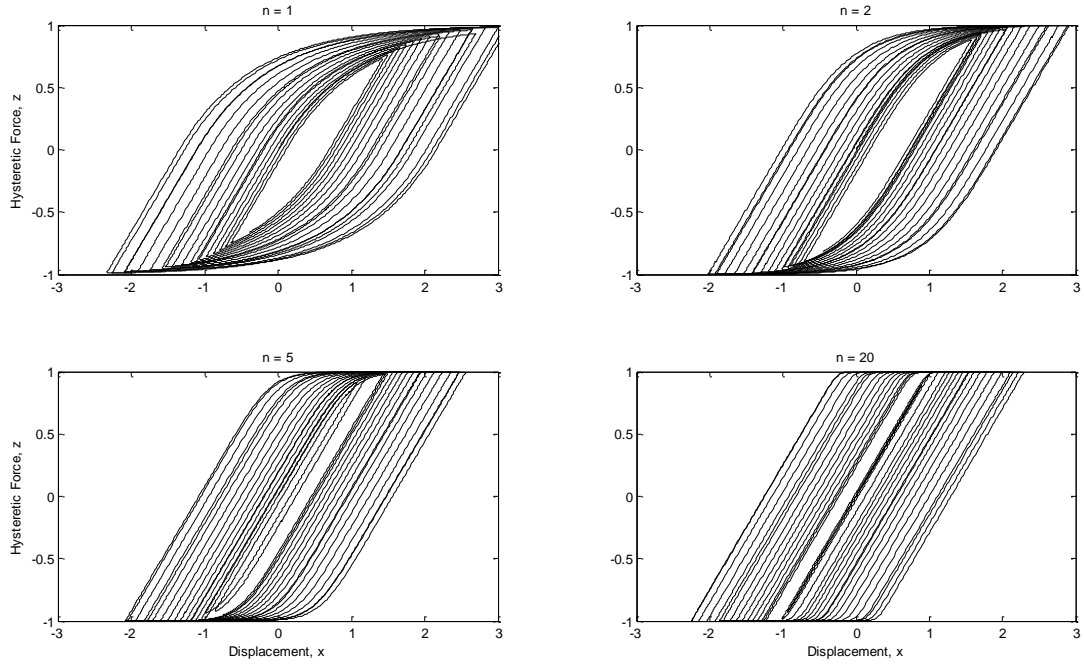


Figure 3.7 Comparison of hysteresis restoring force component  $z(t)$  versus displacement  $x(t)$  phase plane plots with different  $n$  values, the parameters excluding  $n$  are kept constant. ( $\zeta = 5\%$ ,  $\omega = 3$ ,  $a = 0$ ,  $A = 1$ ,  $\beta = 0.5$ ,  $\gamma = 0.5$ )

#### 3.2.4.4 Influence of the Parameters $\delta_A$ , $\delta_\eta$ and $\delta_v$

A system with the parameters  $\zeta = 5\%$ ,  $\omega = 3$ ,  $a = 0$ ,  $A_0 = 1$ ,  $n = 2$ ,  $\beta = 0.5$  and  $\gamma = 0.5$  is analyzed three times using a sine signal  $f(t) = 4\sin(2t)$  as external excitation. In each simulation, only one of the parameters among  $\delta_\eta$ ,  $\delta_v$  and  $\delta_A$  is changed and the remaining two are assumed to be unchanged and equal to zero. The response is sampled at a rate of 200 Hz for a total duration of 40 s (Figure 3.8). The hysteresis restoring force vs. displacement phase plane plots for each of these tests. These graphs confirm the analytical findings that  $\eta$  controls the stiffness deterioration;  $v$  governs the strength degradation behavior and  $A$  variable influences both.

### 3.2.4.5 Influence of Parameters $\sigma_0$ and $\delta_a$ as well as $\zeta_1$ and $\zeta_2$

The response of a SDOF system under sinusoidal excitation  $f(t) = 4\sin(2t)$  is analyzed through numerical Ordinary Differential Equation based Bouc-Wen solution techniques to assess the proposed pinching behavior. In the first set of simulations, all parameters except  $\sigma_0$  is kept unchanged and  $\sigma_0$  is allowed to take on four different quantities. Figure (3.9) shows the responses of the non-pinching hysteretic system, slip-lock (pinched) model and the series model for different  $\sigma_0$  quantities. Investigation of these plots reveals that  $\sigma_0$  controls the sharpness of pinching. In order that while  $\sigma_0$  decreases the ‘slip’ zone stiffness goes to zero and the ‘lock’ zone stiffness approaches infinity. So it may be concluded that the sharpness of pinching varies by contrast with  $\sigma_0$ . In the second set of simulations, the parameter  $\delta_a$  is altered with all other parameters that are kept constant. Figure (3.10) illustrates the responses of the non-pinching hysteretic system, slip-lock (pinched) model and the series model for different  $\delta_a$  quantities. It is clear from these figures that the width of the slip zone increases with  $\delta_a$ , so it can be said that this parameter is governed by the severity of pinching.

Figure 3.11.a shows the results of three simulations where  $\zeta_1$  is set to 0.80, 0.90 and 0.98 (that vary according to Equation 3.14). In each of these plots, the level of stiffness drops at the inset of the second, and successive loading cycles stay the same but the original slope is attained at rising levels of  $z$ . It may also be seen that increasing of  $\zeta_1$  quantities resulting in a decrease in minimum slopes during pinching. Figure (3.10.b) illustrates the hysteretic restoring force component versus displacement phase plane plots for three separate systems in which  $\zeta_2$  is set to 0.05, 0.08 and 0.10. These simulation consequences demonstrate that the original slope is reached at the same level of  $z$  in all cycles while the minimum slope drops at the beginning of the second and successive loading cycles. It may also be concluded that increasing  $\zeta_2$  values give rise to the area of decreased stiffness spreading.

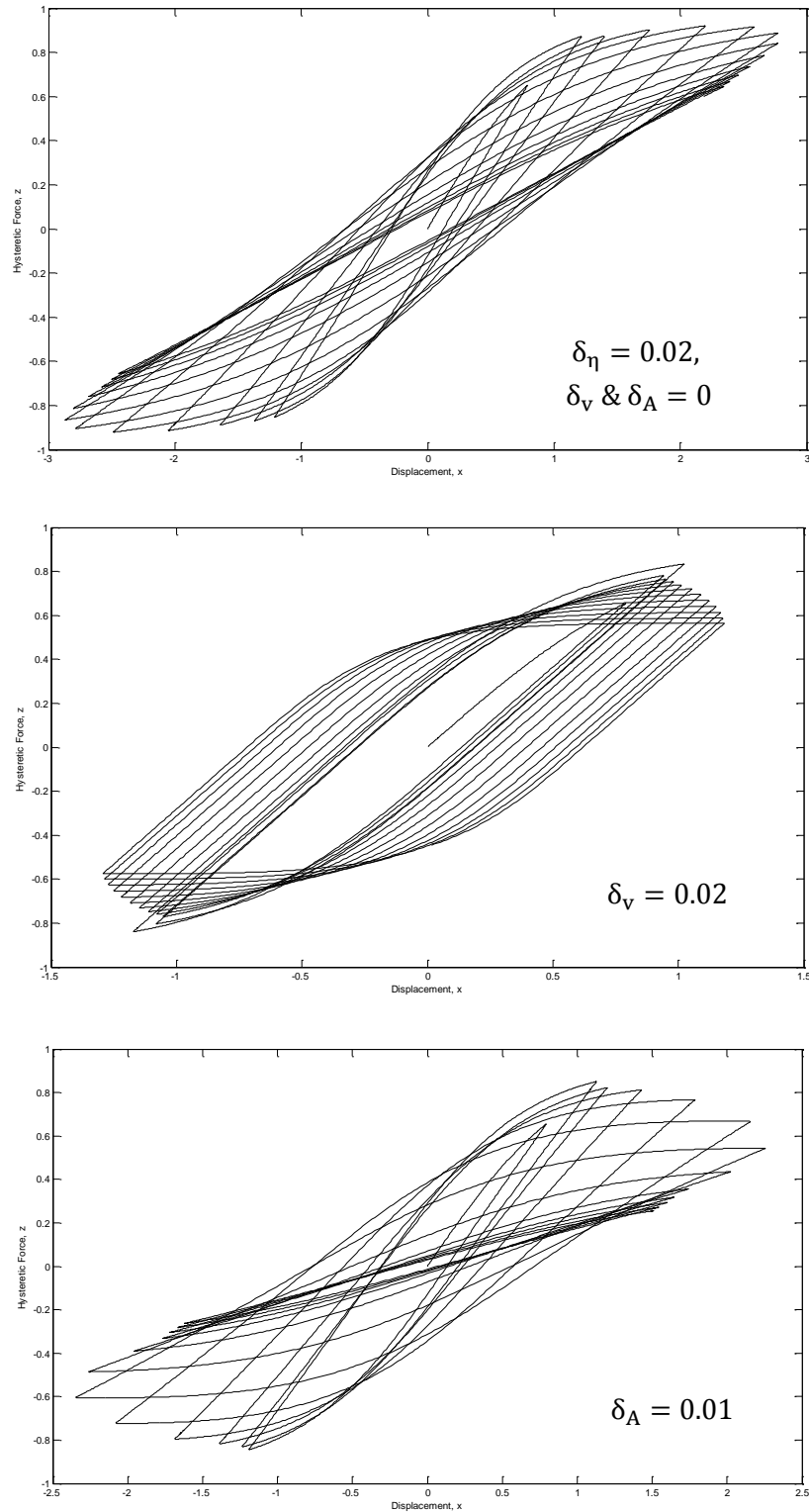


Figure 3.8 Hysteretic restoring force component  $z(t)$  vs. displacement  $x(t)$  phase plane plot with ( $\zeta = 5\%$ ,  $\omega = 3$ ,  $a = 0$ ,  $n = 2$ ,  $\beta = 0.5$ ,  $\gamma = 0.5$ ,  $v_0 = 1$ ,  $\delta_A = 0$  and  $\delta_v = 0$ )

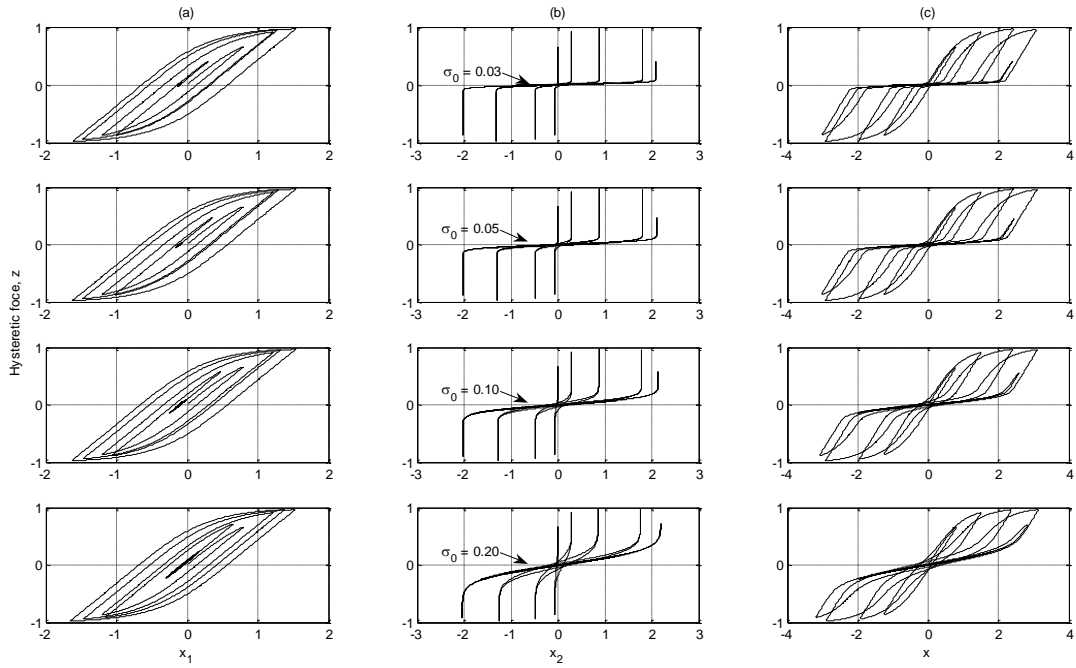


Figure 3.9 Hysteretic restoring force component  $z(t)$  versus displacement  $x(t)$  phase plane plots with different  $\sigma_0$  quantities: (a)  $z$  vs.  $x_1$ ; (b)  $z$  vs.  $x_2$ ; (c)  $z$  vs.  $x$  ( $\zeta = 5\%$ ,  $\omega = 3$ ,  $a = 0$ ,  $A = 1$ ,  $n = 2$ ,  $\beta = 0.5$ ,  $\gamma = 0.5$ ,  $\delta_v = 0$ ,  $\delta_\eta = 0$ ,  $\delta_A = 0$ ,  $\delta_a = 0.05$  and  $\delta_\sigma = 0$ )

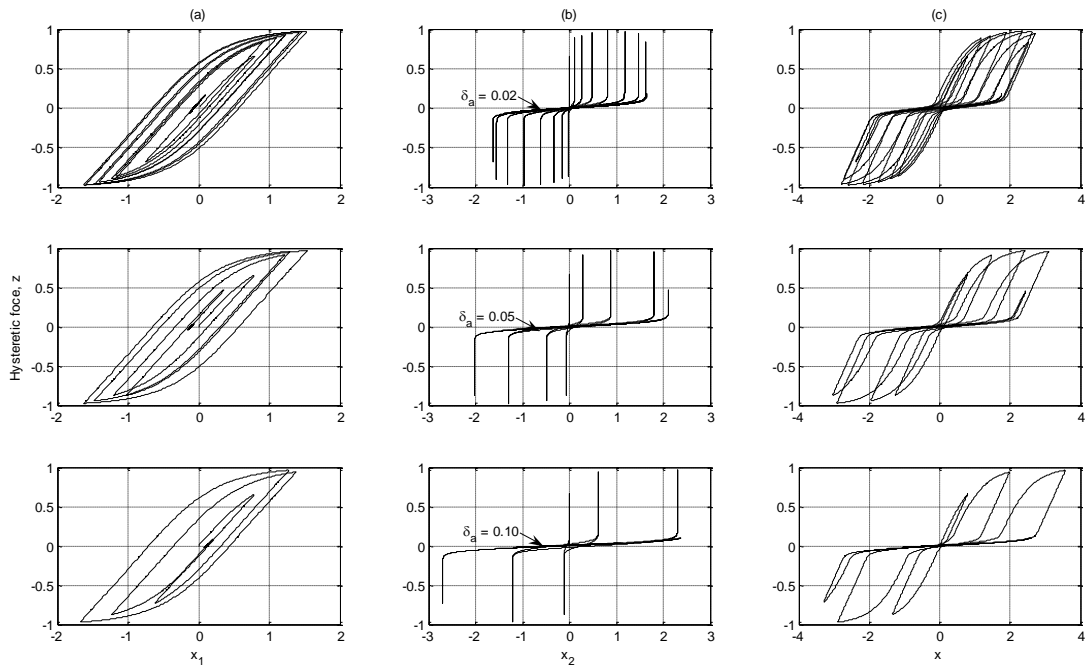


Figure 3.10 Hysteretic restoring force component  $z(t)$  vs. displacement  $x(t)$  phase plane plots with different  $\delta_a$  values: (a)  $z$  vs.  $x_1$ ; (b)  $z$  vs.  $x_2$  (c)  $z$  vs.  $x$  ( $\zeta = 5\%$ ,  $\omega = 3$ ,  $a = 0$ ,  $A = 1$ ,  $n = 2$ ,  $\beta = 0.5$ ,  $\gamma = 0.5$ ,  $\delta_v = 0$ ,  $\delta_\eta = 0$ ,  $\delta_A = 0$ ,  $\delta_0 = 0.05$  and  $\delta_\sigma = 0$ )

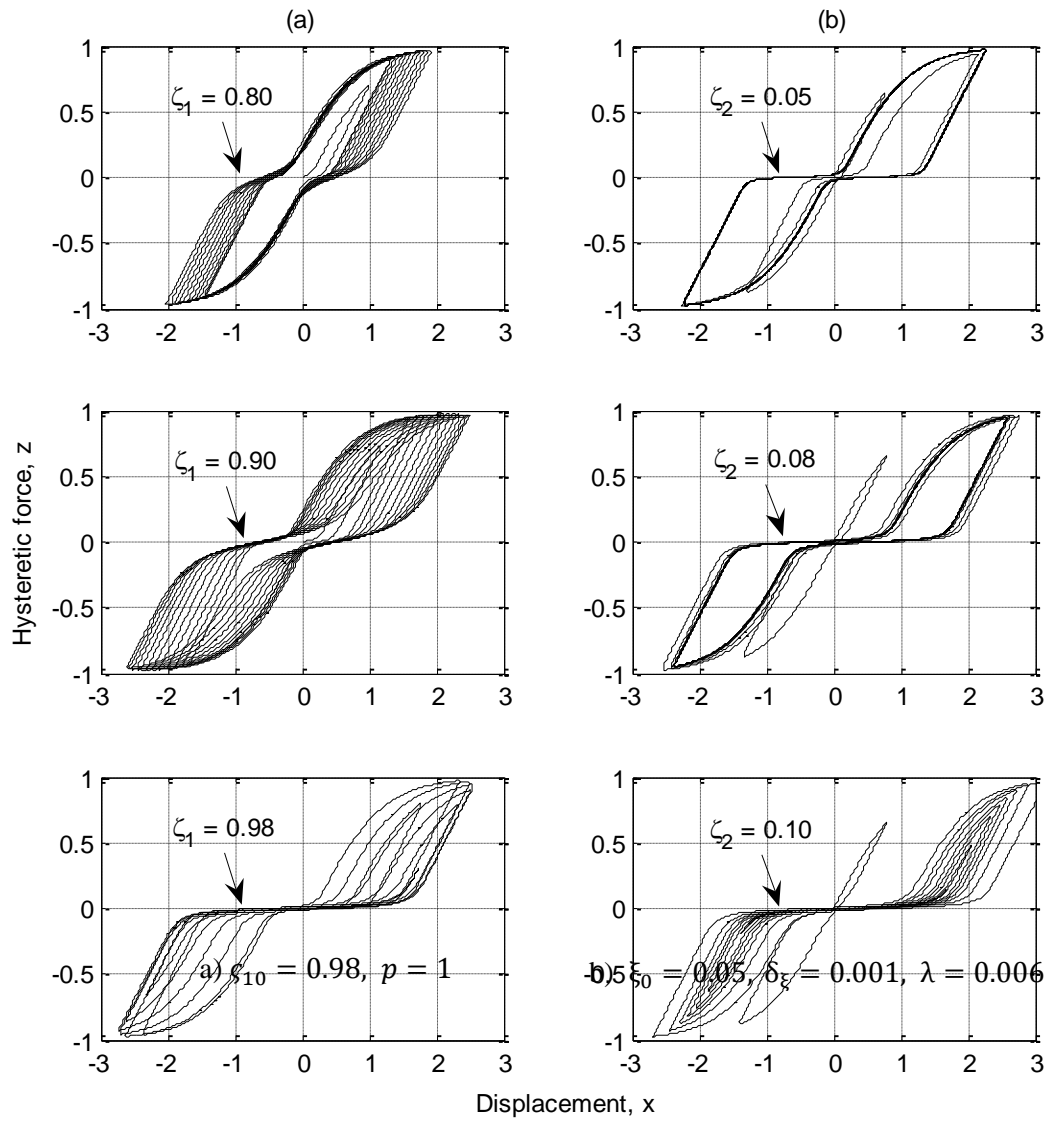


Figure 3.11 Hysteretic restoring force component  $z(t)$  vs. displacement ( $x(t)$ ) phase plane plots with different: (a)  $\zeta_1$  quantities ( $\xi_0 = 0.05$ ,  $\delta_\xi = 0.001$ ,  $\lambda = 0.006$ ); (b)  $\zeta_2$  quantities ( $\zeta_{10} = 0.98$ ,  $p = 1$ ), the following parameters are identical in both cases: ( $\zeta = 5\%$ ,  $\omega = 3$ ,  $a = 0$ ,  $A = 1$ ,  $n = 2$ ,  $\beta = 0.5$ ,  $\gamma = 0.5$ ,  $\delta_v = 0$ ,  $\delta_\eta = 0$  and  $\delta_A = 0$ )

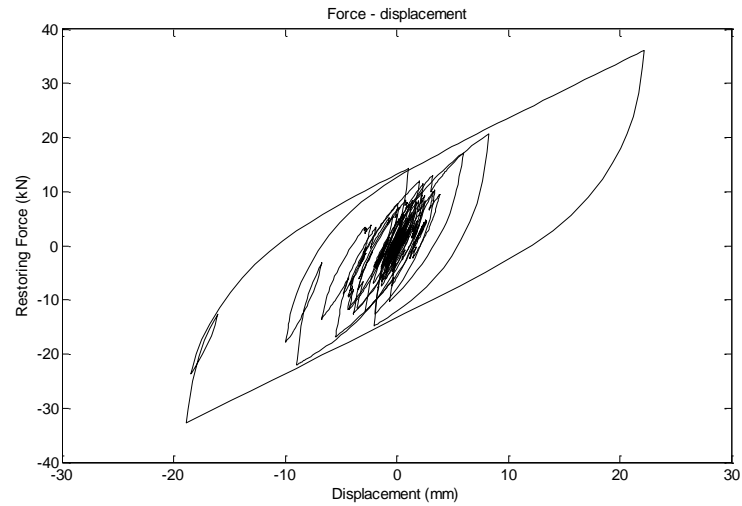
### **3.2.5 Seismic Response of SDOF Systems with the Bouc-Wen Hysteretic Model**

The Analytical Bouc-Wen hysteretic model described in Section 3.2 is extended to computing the nonlinear time history response of a SDOF system under a given ground motion. Inasmuch as a main interest of study is around the hysteresis response of structural systems under the near fault earthquakes, the ground motion recorded at the Düzce-NS (Aug, 1999), among others, is adopted to examine seismic response performance of the Bouc-Wen model such that the external load function  $f(t)$  is replaced by given earthquake record. The hysteresis response loop of the SDOF system is shown in Figure 3.12.a. The structural properties and masses as well as the Bouc-Wen model control parameter adopted are shown in Table 3.1. The displacement time histories as well as the energy dissipated by the structural system are demonstrated in Figures 3.12.b and 3.12.c, respectively.

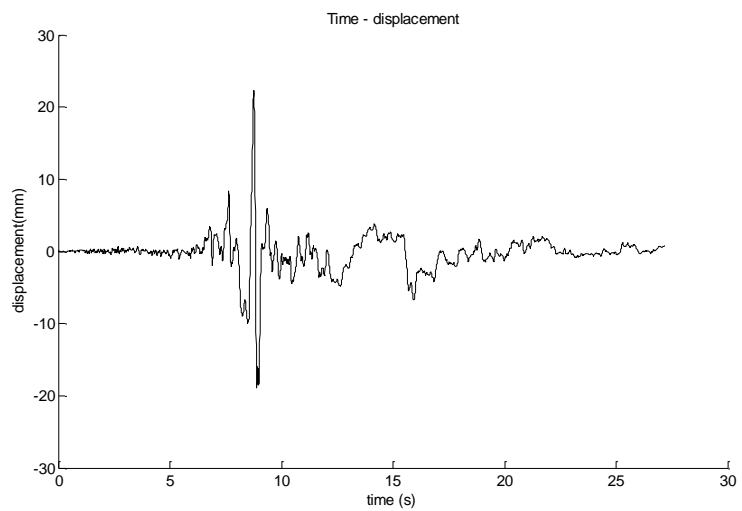
Figure 3.12 provides a good benchmark for validating that the Bouc-Wen model is implemented correctly, because it shows several diversities from the simulation. The energy dissipation is a particularly effective means to check that the implementation is correct. Therefore, the implementation of the Bouc-Wen model is accurately reproducing the expected hysteretic for the benchmark SDOF system, and can be used for a wide hysteresis variety of shapes and types of loads whether they are cyclical or given ground motions.

Table 3.1 Structural properties and Bouc-Wen hysteretic model control parameter of a SDOF system under seismic excitation

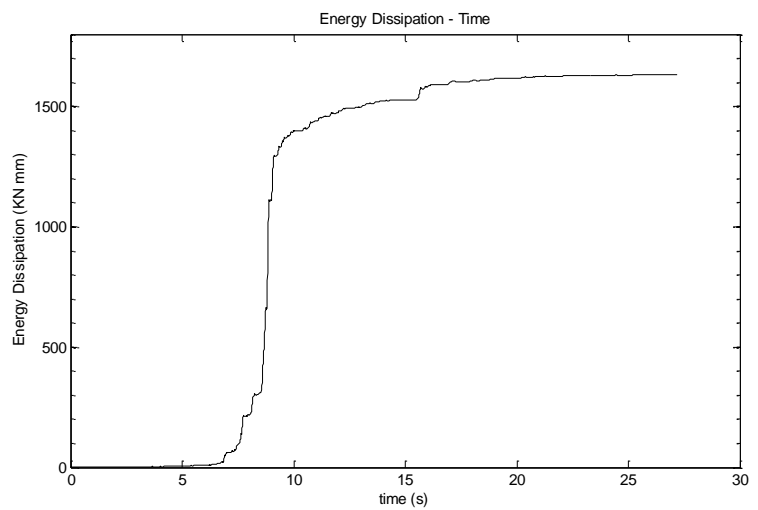
Structural properties	$k=5.7$ (Kn/mm) $m=1.06$ (ton) $\zeta=0.05$
Bouc-Wen hysteretic model shape control parameter	$\alpha=0.18$ $\beta=0.85$ $\gamma=-0.5$ $n=1$
Bouc-Wen hysteretic model pinching control parameter	$A_0=1$ $\eta_0=1$ $\delta_A=0.00$ $\delta_n=0.0000003$ $\delta_v=0.00$



a) Restoring Force – Displacement of SDOF system



b) The displacement response of SDOF system



c) The energy dissipated of SDOF system

Figure 3.12 Seismic response of SDOF system under the Düzce-NS ground motion record using the Bouc-Wen hysteretic model

### 3.3 Formulation of the Smooth Hysteretic Model

The smooth hysteretic model was improved along the original Bouc-Wen's formulation (Bouc, 1967; Wen, 1976). The restoring force  $F$ , in a nonlinear spring element for a displacement  $u$  is defined as follow (Reinhorn et al 2009; Ray and Reinhorn 2012).

$$F = ak_0u + (1 - a)k_0Z \quad (3.26)$$

and

$$\dot{Z} = A\dot{u} - \beta|\dot{u}Z|Z - \gamma\dot{u}Z^2 \quad (3.27)$$

Here,  $a$  symbolizes the post-elastic stiffness ratio and  $k_0$  is the initial elastic stiffness. The non-dimensional hysteretic variable  $Z$ , is described through the temporal differential equation (Equation 3.27). The derivatives illustrated through the dot ( $\dot{\cdot}$ ) are with respect to time;  $A$ ,  $\beta$ ,  $\gamma$  are three constants. The Bouc-Wen model is reformulated by re-establishment of the non-dimensional, time independent hysteretic  $Z$  variable. Note that  $Z$  describes the load reversal in the inelastic region and is defined as  $Z = \frac{F_h}{F_{hy}}$ . The  $F_h$  and  $F_{hy}$  are force functions of the hysteretic spring depending on the displacement and yield strength, respectively. The generalized force-displacement relationship,  $F - u$  for a system with yield strength  $F_y$  and yield displacement  $u_y$  is pointed out in Equation (3.28)

$$F = F_y \left( a \left( \frac{u}{u_y} \right) + (1 - a) \frac{F_h}{F_{hy}} \right) \quad (3.28)$$

Equation (3.28) illustrates that the whole force  $F$  at any deformation  $u$  could be stated as the summation of the two connected component springs acting in parallel as seen in Figure (3.13). The first spring is the fundamental elastic spring with linear stiffness of the post-elastic component  $ak_0u$ , and the second one is related to the hysteretic elastic perfectly plastic spring  $F_y(1 - a)Z$ . In the elastic region,  $Z$  alters with respect to  $u$  in a linear manner, while in the post-elastic region  $Z$  remains

constant. The relationship of  $Z$  and  $u$  is shown in Figure 3.14. It is worth mentioning that  $Z$  is the non-dimensional hysteresis parameter and it is described with the use of configuration seen in Figure 3.14.b and through Equation (3.29):

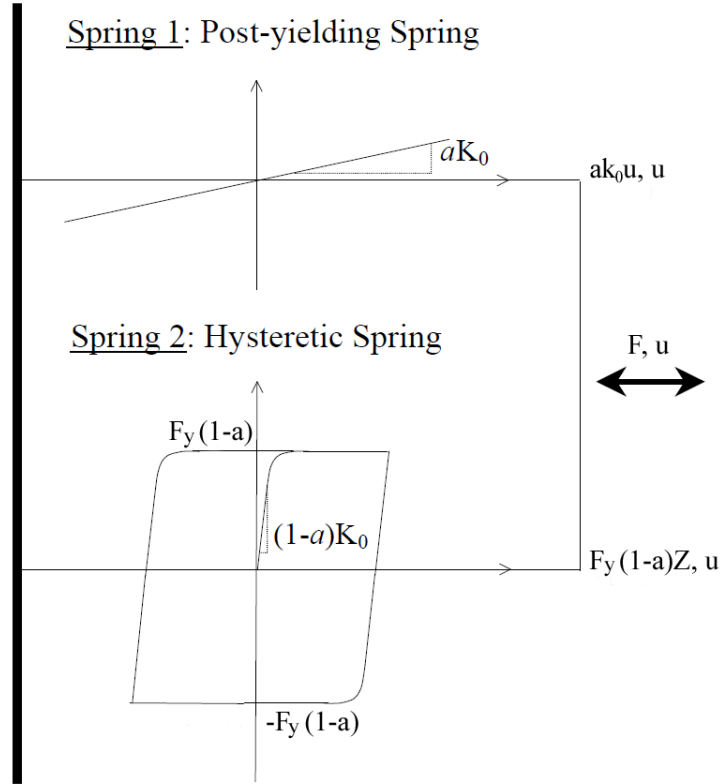


Figure 3.13 Parallel springs in hysteretic model

$$Z = \frac{F_h}{F_{hy}} = \frac{(F - ak_0u)}{[(1 - a)F_y]} \quad (3.29)$$

The change of  $Z$  variable compared to displacement  $u$  may be represented as Equation (3.30):

$$\frac{dZ}{du} = \left(\frac{1}{u_y}\right) \left[1 - |Z|^N \left\{\frac{1 + \text{sign}(Z \cdot du)}{2}\right\}\right] \quad (3.30)$$

N is the exponent that governs the “smooth” transition between the elastic and post-elastic range. The “Smooth Hysteretic Model” name was also picked out based on this property. Progressive smooth transition is made for the lower quantities ( $2 < N \leq 20$ ), while larger quantities of ( $N > 10$ ) result in sharp transition similar to the bilinear model. The signum function  $\text{sign}(x)$ , is explained through  $\text{sign}(x) = x/|x|$  for  $x \neq 0$  and  $\text{sign}(x) = 1$  for  $x = 0$ . The signum product  $Z \cdot du$  governs the load reversal as seen in Figure 3.14.b. Moreover, the continuous variation of instantaneous tangent stiffness  $K_{\text{tangent}}$  needs to be assessed in inelastic analyses of structural system. The differentiating of Equation (3.28) results in the  $K_{\text{tangent}}$  expression. Note that Equation (3.28) includes Z which is variable and defined by  $Z = \frac{F_h}{F_{hy}}$ .

The tangent stiffness  $K_{\text{tangent}}$  could be assessed in the beginning of any new calculation step applying the quantity of Z either; (a) from the past stage, or (b); through solution of the first order differential Equation (3.30) to achieve updated amount of variable Z . Appropriate approximation for instantaneous tangent stiffness equation  $K_{\text{tangent}}$  (see Equation 3.31) has been achieved using the standard semi-implicit solution of the Equation (3.30).

$$K_{\text{tangent}} = \frac{dF}{du} = k_h \left[ 1 - \left| \frac{F_y}{F_{hy}} \right|^N \left\{ \frac{1 + \text{sign}(F_h \cdot du)}{2} \right\} \right] \quad (3.31)$$

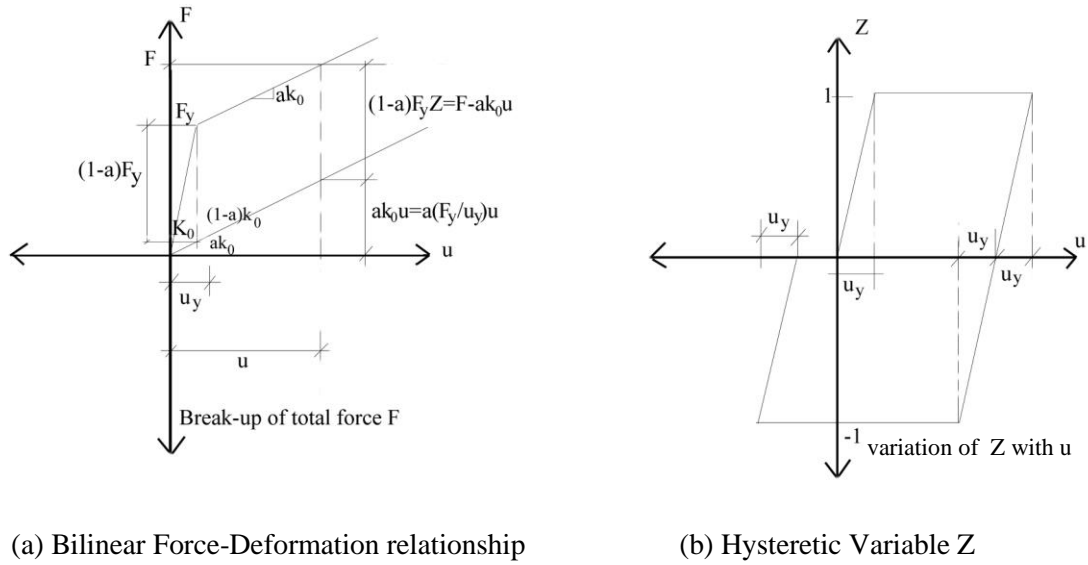


Figure 3.14 Basic components of hysteretic models

### 3.3.1 Stiffness Decay of the Hysteretic Spring

The stiffness decay can be simulated through the assumption that the unloading arm of the hysteretic spring from a positive yield direction at every unloading target to be pre-defined pivots point. This is reached through extension of the line with initial elastic stiffness (slope) on the reverse side up to the force of  $-(\alpha F_{hy})$ . As illustrated in Figure 3.15, the degraded hysteresis elastic stiffness  $K_{hd}$ , is the slope of the line linking the load reversal point  $(F_c, u_c)$  and the pivot point. The stiffness degradation factor  $R_k$  is implemented to the initial elastic stiffness  $K_{h0}$  to reach the degraded stiffness  $K_{hd}$  and it could be acquired from geometry (see Figure 3.15). The  $R_k$  factor is expressed similar to Equation (3.32).

$$R_k = \frac{(F_c + \alpha F_{hy})}{F_{h0} u_c + \alpha} \quad (3.32)$$

Here  $\alpha$  is stiffness degradation. Variation range of  $\alpha$  imply that for great quantities ( $\alpha > 200$ ), no deterioration happens, whereas lower quantities ( $\alpha < 10$ ) reduce considerable deterioration (Sivaselvan and Reinhorn, 1999).

The stiffness degradation is incorporated into the overall hysteretic model by multiplying the hysteretic stiffness by  $R_K$ , ensuring stiffness degradation is incorporated to the hysteresis component of the total tangent stiffness (Equation 3.33).

$$K_{hd} = (R_K - \alpha)k_0 \left[ 1 - \left| \frac{F_h}{F_{hy}} \right|^N \{ \eta \text{sign}(F_{hys} \cdot du) + (1 - \eta) \} \right] \quad (3.33)$$

where  $\eta$  is the parameter for controlling the shape of the unloading branch.

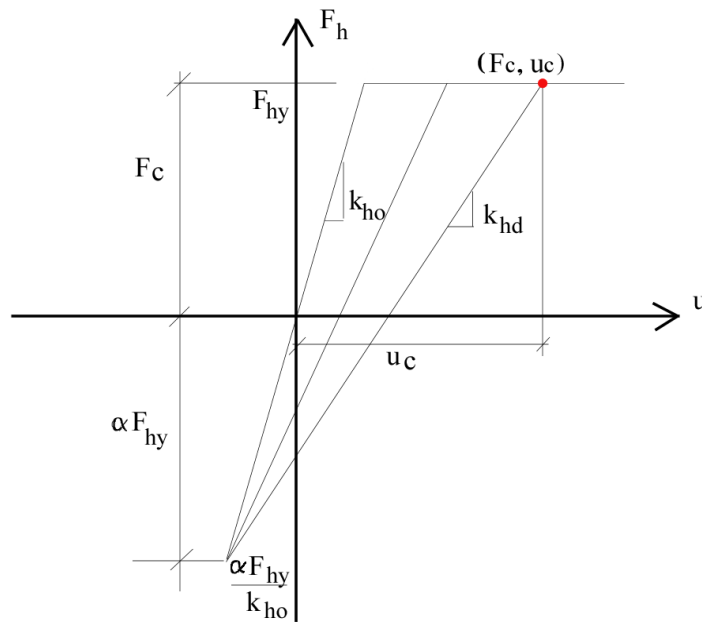


Figure 3.15 Stiffness degradation rule

### 3.3.2 Strength Degradation

Strength deterioration is described as a decay of the initial yield strength of the hysteretic component  $F_{hy0}$ . This hysteresis deterioration may be a consequence of strength loss at sections or elements level with great deformations (or high ductility demands) or owing to unrecoverable energy dissipation  $H$  by way of the cyclic treatment. The degraded yield force  $F_{hy}$  may be regulated through energy based strength degradation factor and a ductility based strength deterioration factor (Sivaselvan and Reinhorn, 2011).

$$F_{hy} = F_{hy0} \left\{ 1 - (|u_{max}|/u_{cap})^{(1/\beta_1)} \right\} \left\{ 1 - \{\beta_2/(1 - \beta_2)\}(H/H_{ult}) \right\} \quad (3.34)$$

The expression in the first braces of Equation (3.34) is the ductility basis strength deterioration ratio where  $|u_{max}|/u_{cap}$  is the displacement ductility dependent upon the peak displacement capacity  $u_{cap}$  and the latest peak displacement attained,  $u_{max}$ ; in addition  $\beta_1$  symbolizes the ductility basis strength decay factor. The expression in the second braces is the energy based strength deterioration ratio where  $\beta_2$  shows the energy based strength decay parameter. The functions  $H$  and  $H_{ult}$  are computed through the Equations (3.35) and (3.36).

$$H = \int_0^u F_h \cdot du - F_h^2 / (2R_k k_h) \quad (3.35)$$

$$H_{ult} = F_{hy0} \cdot u_y / 2 + F_{hy0} (u_{cap} - u_y) \quad (3.36)$$

Here  $H$  is the hysteresis energy dissipated and  $H_{ult}$  is hysteresis energy dissipated when loaded monotonically to ultimate displacement without any decay. Strength degradation is combined in the whole hysteresis model through modification of  $F_{hy}$  using the Equations (3.34), (3.35) and (3.36) in order to calculate the tangent stiffness  $K_{tangent}$  from the Equation (3.31).

### 3.3.3 Hysteretic Pinching Formulation

Pinching (or slip) is the variation in displacement coming from opening and closing of cracks or disappearance of bond at section components, among others. Pinching properties are merged in the hysteresis model by taking into account a supplemental stiffness component  $k_{slip}$  in series with the hysteresis stiffness component. The tangent stiffness established upon the modified Gaussian pinching model  $k_{slip}$  is exhibited according to Equation (3.37).

$$k_{slip} = \left( \sqrt{\frac{1}{2\pi}} \frac{R_s (u_{max}^+ - u_{max}^-) H(u_{max}^+ - u_{max}^-)}{\sigma F_{hy}} e^{-\frac{1}{2} \left( \frac{F_h - \lambda}{F_{hy} \sigma} \right)^2} \right)^{-1} \quad (3.37)$$

Where  $F_h$  is denoted the current hysteretic force and  $F_{hy}$  describes the yield force of the hysteretic spring; in addition  $u_{max}^+$  and  $u_{max}^-$  are the maximum positive and negative displacements, respectively;  $H(\ )$  is the Heaviside step function;  $\sigma$  is a parameter denoting the sharpness of the slip;  $R_s$  controls the slip-length; and  $\lambda$  is the factor to control mean moment level of slip. The tangent stiffness of the combined system is then obtained by Equation (3.38). Detailed model formulation and scope of change of control parameters can be found in reports published by (Reinhorn et al 2009; Güllkan and Etemadi, 2014).

$$k_{comb} = k_{postyield} + \frac{k_h \cdot k_{slip}}{k_{slip} + k_h} \quad (3.38)$$

### **3.4 Identification of Hysteresis Loop Control Parameters**

All structural components have limited capacity. Because of this, grasping their behavior under severe ground motion excitations has always been a serious objective of earthquake engineering. One method to assess the performance of structural components is through experimental evaluations using quasi-static cyclic loading technique. The relatively slow use of the load in quasi-static cyclic tests allows researchers to relate structural metrics such as top displacement, drift, hinge rotation, strains, etc. to visual damage of structural specimens (e.g. first cracking, spalling of the concrete, buckling of longitudinal reinforcement). Current earthquake resistant design procedures for structural components have been established based on experimental results using quasi-static cyclic tests. Furthermore a design codes are inclined to a relatively new design methodology called “Performance-based seismic design” (PBSD). In this design methodology the assessment of different structural components plays a fundamental role. Likewise a number of performance levels, which are frequently described in the sense of acceptable levels of damage, need to be satisfied under different levels of seismic hazards.

Numerous experimental and analytical researches have been done in order to estimate the response of structural components; and to define limit states; and acceptance criteria to be used in performance-based seismic design; as well as the inelastic response assessment of RC columns under cyclic moments in the presence of compression axial load (Takizawa and Aoyama, 1976; Otani et al., 1980; Ozcebe and Saatcioglu, 1987; Bousias et al., 1992; Ambrisi and Fillippou, 1999; Kim and Lee, 2000; Sezen, 2000; Qiu et al., 2002; Tsuno and Park, 2004; Nishida and Unjoh, 2004; Umemura and Ichinose, 2004; Kawashima et al., 2006; Chaung and Loh, 2008; Li et al., 2008; Mohammad Ali, 2009; Acun, 2010; Chang and Lai, 2010; Rodrigues, 2013). Most of these effort have been focused on a cantilever RC columns with various materials; a reinforcement detail and subjected to uniaxial or/and biaxial monotonic or cyclic (quasi-static) loading. The aim of such experiments was determination of the change in stiffness for different levels of loading and the strength and stiffness evolution upon load reversals.

In order to correctly represent a restoring force behavior of substantial structural members, it is required to have an opinion on the model variables for the smooth hysteretic model appropriately. This contains the estimation of the model constants, like for example:  $N$ ,  $\alpha$ ,  $\beta_1$ ,  $\beta_2$ ,  $R_s$  ... etc. from experimental data. The smooth hysteretic model is adopted to symbolize the system on the basis of the hysteresis behavior due to cyclic loading tests of RC columns that were designed using a different philosophy. Data gathered from the cyclic loading test of structural elements may supply important information to initial estimation of hysteresis model parameters. The thought of forming such a parameter range is particularly convenient for analytical studies to predict seismic response of structural systems including degradation in hysteresis behaviors.

To recognize the model variables, a systematic two-step system identification procedure is adopted. The first stage is assigned to a comparison of the experimental and simulation results of hysteresis behavior of RC columns in order that the average parameter value deducted from the analogy of response hysteresis curves would be used for the initial estimation for the hysteresis parameter. It should be emphasized that using such an estimated quantity for hysteresis parameters could reduce the number of iteration significantly in following nonlinear dynamic analyses which will be used to represent capacity degradations and pinching properties. In the second stage, the sensitivity of response hysteresis loops to each parameter variation is investigated and the effect of each one on the hysteresis loop under cyclic loading is clarified in detail.

The whole parametric study in this section has been undertaken to comprehend the hysteresis response (include capacity decay and pinching) of a diversified amount of column end hinges and the relationship between the parameters govern the model and response hysteresis loops. The only purpose underlying this is to supply a large spectrum of the analytical parameters to incorporate the nonlinearity of structural members such as columns into following nonlinear dynamic analysis by meaningful magnitude variation of the smooth hysteretic model factors. In this way, an average range of parameters is deducted. It is assumed that these quantities reflect the

realistic post-yield degrading characteristics of the RC columns when exposed to severe cyclic loadings.

The quasi-static technique is used for the evaluation of the degrading seismic response of a cantilever RC column imposed to increasing cyclic loads. The quasi-static technique is nearly always carried out on a deformation-controlled serve a basis to simplify an interpretation of the results in the sense of ductility and to allow the tests continuing further than the bearing capacity. Besides, in order to give an idea about initial value of SHM control parameter estimations, experimental results of specimens conforming and non-conforming to the Turkish Earthquake Code (TEC 1998, 2007) are compared with simulation results, so that applied load lateral versus tip displacement of cantilever RC columns for both experiment and simulation is plotted on the same graph and has been tried to derive hysteresis parameter values from adaptation of response diagrams. The results of experiments were conducted by Acun at the structural mechanics laboratory of the Middle East Technical University is adopted to match the response loops with experimental results (Acun 2010). Cyclic loading experiments were accomplished on the cantilever RC columns to exhibit the hysteresis response envelopes as well as flexural capacity decay of column specimens which was generated according the different design philosophies.

Both axial and lateral loads were applied to cantilever RC column specimens and tests were performed using a displacement controlled quasi-static history. The twelve column specimens were designed and detailed according to the requirements outlined in (TS 500- 2000) and (TEC 2007). Two-phase experimental programs were conducted on full-scale specimens; six sub-standard non-conforming column specimens with plain bars and low concrete strength (Type-1) were tested in the first phase. It is believed specimens may be representative of the hysteresis behavior of RC columns of existing buildings constructed before the seventies in Turkey with poor detailing and low concrete strength. The aim of the first experimental phase was to acquire data on a decay treatment of such structural components. If a broad generalization is made, it can be said that the weakest members of the existing

building stock in Turkey are in this building class. In this case, this research will also focus on poor detailed building types as it would be realistic to consider this specimen set (Type 1).

In the second phase of the experimental program another six column specimens with deformed bars reinforcement and proper detailing, (on standard) code compliant RC columns, (Type-2) were tested. Normal strength concrete was used for the second type of specimens. It is accepted that the set represent the columns those designed and detailed in accord with the current Turkish Earthquake Code recommendations (TEC 1998, 2007). The details of established test setup and scheme for instrumentation of experiments conducted by Acun are shown in Figure 3.16. The column specimen cross section dimensions were  $350 \times 350 \text{ mm}^2$  and their clear height was 1800 mm. The longitudinal reinforcements were composed of 14 No. 8 bars along the column height. The shear reinforcement comprises of No. 3 stirrups at spacing correspond to 70 mm. The material characteristics and reinforcement details of test specimens are given in Table 3.2.

Tests were begun with applying the axial load on column specimens. Once the axial load level of interest was achieved, it was kept unchanged and lateral load enforcement process was started. Either two-step constant-amplitude cyclic displacement patterns or multi-step changing-amplitude loading schemes were applied on columns. The imposed displacement protocols for each member of both types of column specimens are given in Table 3.3 in terms of both tip displacements and corresponding drift ratios. It must be pointed out that the experiments were ended either when the end of displacement protocols was achieved or a failure happened. The failure is described as the occurrence of a hoop reinforcement opening; or severe core concrete crushing; or even bar buckling.

The only test variable for Type-2 specimens was the amplitude of entered tip displacement. Four specimens were examined under fixed amplitude displacement reversals and the remaining two were tested under changing amplitude displacement

cycles. Imposed displacement time series applied to the 1P2 specimen is demonstrated in Figure 3.17.

On the other hand, the tested samples are analyzed using data presented in the input data sheet for experiments, in order that the smooth hysteresis response loops obtained from the quasi-static technique under the same loading pattern is considered. The purpose of these analyzes is to simulate an essential characteristics of hysteresis behavior and to compare it with recorded response of experiment results in order to extract the SHM parameter ranges.

On the other hand, the tested samples are analyzed using data presented in the input data sheet for experiments, so that the smooth hysteresis response loops obtained from quasi-static technique under the same loading pattern is considered. The hysteresis response relations were investigated and key parameters were clarified which are employed to formulate a model for the response hysteresis loop where all its variables are materially meaningful. In this way, the initial guess of the SHM parameters as representative of the common degradation characteristics of RC columns is estimated through comparison of response loops with those of experimental results.

A similarity between response hysteresis loops in numerical simulation (through the SHM) with those of the experiment results is plotted for sub-standard non-conforming column specimens (Type-1) and (on standard-code compliant column specimens (Type-2) specimens in Figure 3.18 and 3.19 respectively. As is seen, through tuning the rate of stiffness and strength hysteresis degradation and pinching parameters, tries to consistent the hysteresis responses that are obtained from comparison of simulation results with test responses. Such that appropriate hysteresis factors are extracted through visual comparison of response loops. The same process has been conducted for both sub-standard non-conforming specimens Figure 3.18 and on standard, code compliant specimens, Figure 3.19. The identified parameters for the SHM is deduced via visual matching of both the hysteretic loops are summarized in Table 3.4.

The values obtained may be representative of the hysteresis degrading parameters of poor detailed columns of the existing RC buildings constructed in Turkey and are used just as an initial estimation for hysteresis parameters in nonlinear dynamic analysis. The parameters given in Table 3.4 are the hysteresis parameters that controlled the Smooth Hysteresis Model Equations, Equations (3.26) – (3.38) (Gülkan and Etemadi, 2014).

Table 3.2 Material characteristics and reinforcement details of test specimens

Specimen Type	Specimen code	Concrete			Longitudinal reinforcement			Transverse reinforcement		
		Compressive strength, $f_c$ (MPa)	14 $\phi$ 8			$\phi$ 3 @ 70mm				
			Yield strength, $f_y$ (MPa)	Ultimate strength, $f_u$ (MPa)	Reinforcement ratio, $\rho_l$ ( $A_s/b_w h$ )	Yield strength, $f_y$ (MPa)	Ultimate strength, $f_u$ (MPa)	Reinforcement ratio, $\rho_t$ ( $A_{sw}/b_w h$ )		
Type-1	1P2	13.5								
	2P3	12.2								
	3P3_No.4	13.1								
	4P4	12.4	315	448	0.01	368	487	0.0026		
	5P5	11.4								
	6PV1	12.5								
	7P3_U	13.2								
Type-2	1D2	25.8								
	2D3	25.9								
	3D4	27.6	454	604	0.01	469	685	0.0061		
	4D5	24.6								
	5DV1	25.0								
	6DV2	25.3								

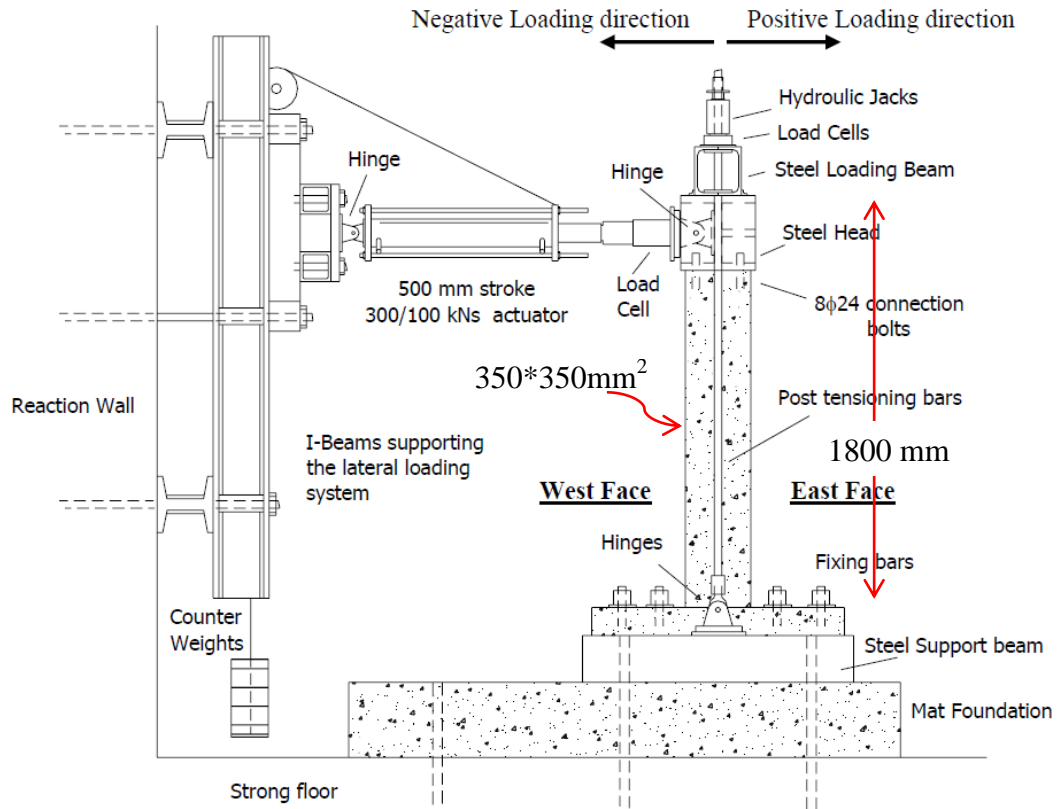


Figure 3.16 Schematic view of test setup (Acun, 2010)

Table 3.3 Displacement protocols applied to the test specimens

Cycle No	SPECIMENS												
	Type 1						Type 2						
	1P2	2P3	3P3_NO.4	4P4	5P5	6PV1	7P3_U	1D1	2D3	3D4	4D5	5DV1	6DV2
1	35 (1.75)	50 (2.5)	50 (2.5)	70 (3.5)	105 (5.25)	10 (0.5)	50 (2.5)	35 (1.75)	50 (2.5)	70 (3.5)	105 (5.25)	10 (0.5)	17.5 (0.87)
2	35 (1.75)	50 (2.5)	50 (2.5)	70 (3.5)	105 (5.25)	10 (0.5)	50 (2.5)	35 (1.75)	50 (2.5)	70 (3.5)	105 (5.25)	10 (0.5)	17.5 (0.87)
3	35 (1.75)	50 (2.5)	50 (2.5)	70 (3.5)	105 (5.25)	10 (0.5)	50 (2.5)	35 (1.75)	50 (2.5)	70 (3.5)	105 (5.25)	10 (0.5)	17.5 (0.87)
4	35 (1.75)	50 (2.5)	50 (2.5)	70 (3.5)	105 (5.25)	50 (2.5)	50 (2.5)	35 (1.75)	50 (2.5)	70 (3.5)	105 (5.25)	50 (2.5)	35 (1.75)
5	35 (1.75)	50 (2.5)	50 (2.5)	70 (3.5)	105 (5.25)	50 (2.5)	50 (2.5)	35 (1.75)	50 (2.5)	70 (3.5)	105 (5.25)	50 (2.5)	35 (1.75)
6	35 (1.75)	70 (3.5)	70 (3.5)	105 (5.25)	70 (3.5)	50 (2.5)	70 (3.5)	35 (1.75)	50 (2.5)	105 (5.25)	70 (3.5)	50 (2.5)	35 (1.75)
7	35 (1.75)	70 (3.5)	70 (3.5)	105 (5.25)	70 (3.5)	35 (1.75)	70 (3.5)	35 (1.75)	50 (2.5)	105 (5.25)	70 (3.5)	35 (1.75)	50 (2.5)
8	70 (3.5)	70 (3.5)	70 (3.5)	105 (5.25)	70 (3.5)	35 (1.75)	70 (3.5)	70 (3.5)	70 (3.5)	105 (5.25)	70 (3.5)	35 (1.75)	50 (2.5)
9	70 (3.5)	70 (3.5)	70 (3.5)	105 (5.25)	70 (3.5)	35 (1.75)	70 (3.5)	70 (3.5)	70 (3.5)		70 (3.5)	35 (1.75)	50 (2.5)
10	70 (3.5)	70 (3.5)	70 (3.5)	105 (5.25)	70 (3.5)	70 (3.5)	150 (7.5)	70 (3.5)	70 (3.5)		70 (3.5)	70 (3.5)	70 (3.5)
11	70 (3.5)	105 (5.25)				70 (3.5)	150 (7.5)	70 (3.5)	70 (3.5)			70 (3.5)	70 (3.5)
12	70 (3.5)	105 (5.25)				70 (3.5)		70 (3.5)	70 (3.5)			70 (3.5)	70 (3.5)
13	105 (5.25)	105 (5.25)				35 (1.75)		105 (5.25)	105 (5.25)			35 (1.75)	105 (5.25)
14						35 (1.75)		105 (5.25)	105 (5.25)			35 (1.75)	105 (5.25)
15						35 (1.75)		105 (5.25)	105 (5.25)			35 (1.75)	105 (5.25)
16						105 (5.25)						105 (5.25)	
17						105 (5.25)						105 (5.25)	
18						105 (5.25)						105 (5.25)	

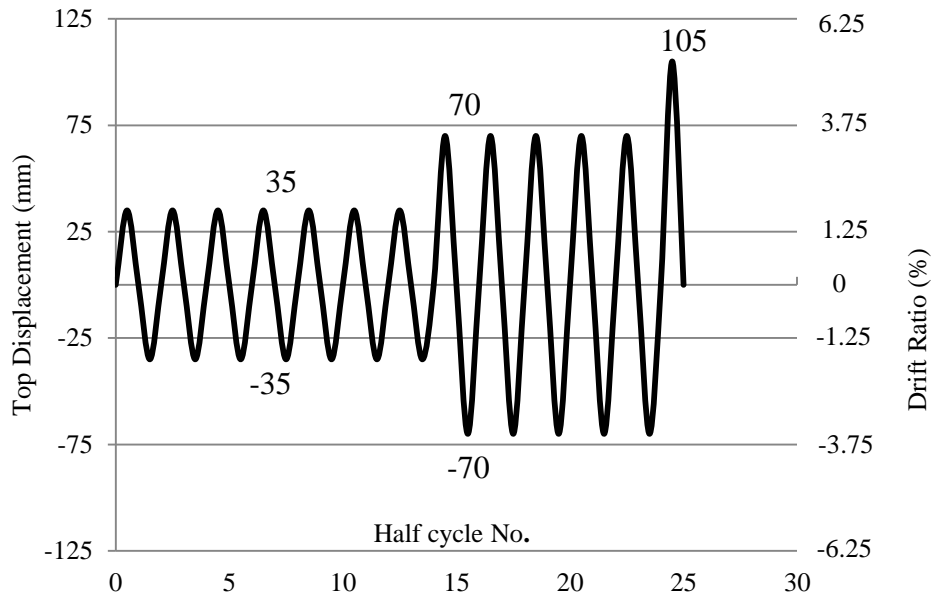


Figure 3.17 Displacement time series imposed on the specimen (1P2)

Table 3.4 Hysteresis degradation parameter values obtained from comparison of simulation (the quasi-Static analysis) with respected to experimental results

System Parameters		Non-Conforming Sub-Standard Specimens (Type-1)						Conforming Specimens according to TEC 2007, (Type-2)					
		1P2	2P3	3P3_N0.4	4P4	5P5	6PV1	1D2	2D3	3D4	4D5	5DV1	6DV2
Size and Shape Parameters	$\alpha$	2	2	1	2	2	2	2	2	2	2	2	2
	$\beta_1$	0.2	0.2	0.6	0.2	0.2	0.3	0.1	0.2	0.2	0.4	0.2	0.3
	$\beta_2$	0.28	0.28	0.47	0.28	0.28	0.4	0.1	0.28	0.28	0.45	0.28	0.4
	N	1.5	1	2	1.5	2	2	1	1	1.5	1	1.5	1.5
Pinching Parameters	$\eta$	0.5	0.5	0.5	0.5	0.5	0.5	0.5	0.5	0.5	0.5	0.5	0.5
	$R_s$	0.3	0.3	0.3	0.3	0.35	0.3	0.3	0.3	0.35	0.35	0.33	0.35
	$\sigma$	0.3	0.3	0.38	0.3	0.3	0.3	0.35	0.4	0.35	0.35	0.35	0.4
	$\lambda$	0.1	0.1	0.2	0.1	0.15	0.15	0.1	0.1	0.3	0.3	0.15	0.1

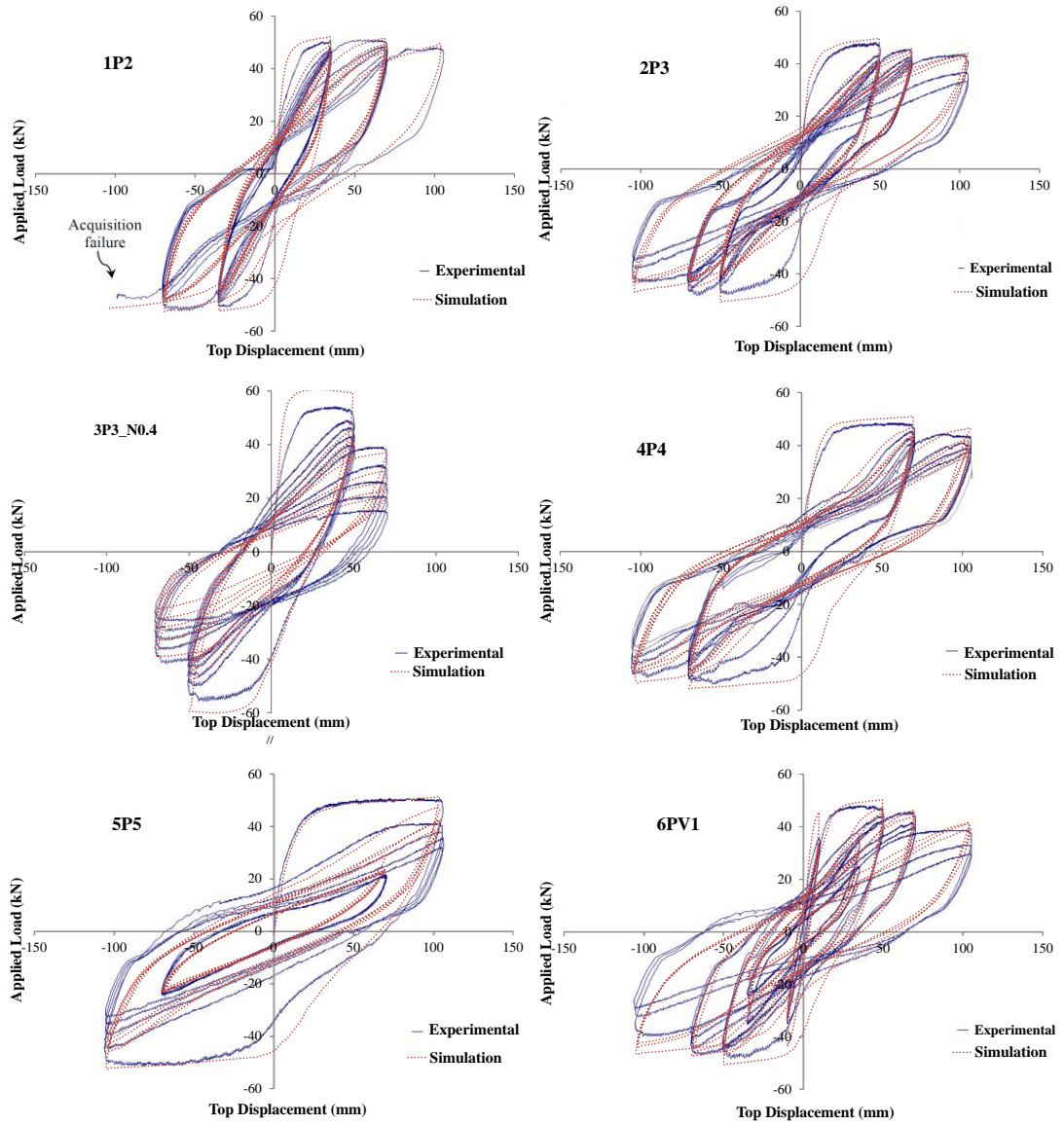


Figure 3.18 Comparison of simulation and experimental results for sub-standard non-conforming column specimens (Type-1)

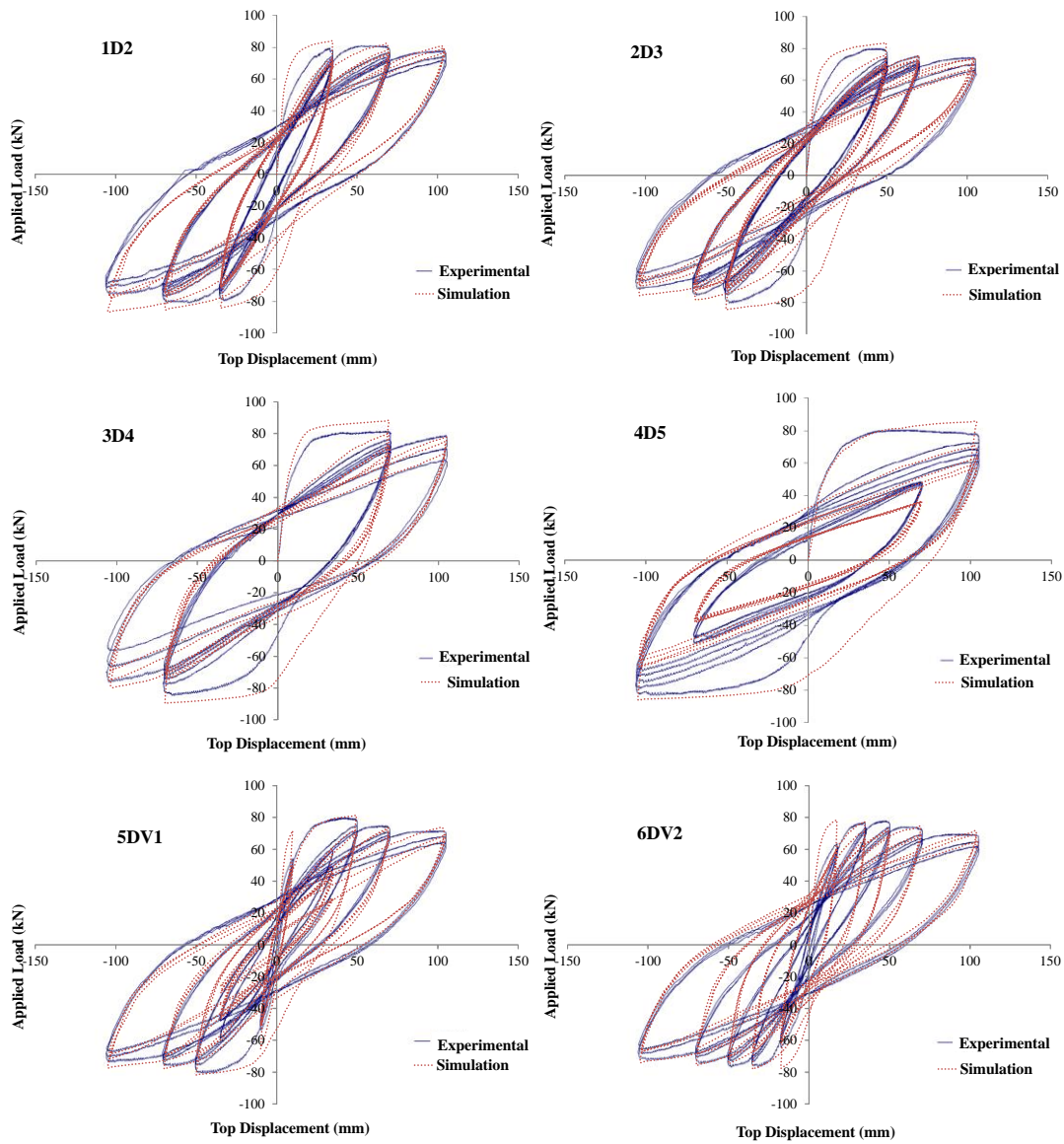


Figure 3.19 Comparison of simulation and experimental results for on standard, code compliant code (TEC 1998, 2007) column specimens

### 3.5 SHM Sensitivity to Parameter Variations

In pursuance of sensitivity assessment of the response loop of SHM to variation of model constants, a numerical example is deduced from section 3.4. The analogy results of simulation results with those of the experimental works are summarized in Table 3.4. The sensitivity of the response hysteresis loop is examined by varying the amount of each analytical variable in individual form one immediately after the other while other parameters are kept fixed in magnitude. The hysteresis response loops presented in Figures 3.20 and 3.21 indicate the susceptibility of the model to control parameters, such that Figure 3.20 displays the influences of analytical parameters related to shape of loop  $N$ ,  $\alpha$ ,  $\beta_1$ ,  $\beta_2$ . The Figure 3.21 points out the pinching parameters effects on the response loops correspondingly.

To achieve this purpose, the 1D2 specimen results are intended to verify the sensitivity of response loops under control parameter variations. For this purpose, the model is re-analyzed in the absence of hysteresis capacity decays and pinching in the loop, i.e. the non-degrading bilinear response loop similar to the Figure 3.20.a is considered; Thereafter, to alter the smoothness parameter,  $N$  (from 10 to 1) hysteresis shape changes to Figure 3.20.b; Following that, respectively, with addition the stiffness degrading property (by manipulating  $\alpha$  from 200.0 to 2.0) Figure 3.20.c; with additional strength deterioration parameters (varying the  $\beta_1$  and  $\beta_2$  from 0.013 to  $\beta_1=0.3$ ,  $\beta_2=0.4$ ) in the Figure 3.20.d; and combination of them that shown in Figure 3.20.e are obtained. Finally subjoins the pinching leads to the loop shape according to the Figure 3.20.f.

Remaining parameters are representative of the pinching effects. These factors control the magnitude of total slip in the hysteresis loop as seen in Figure 3.21. The slip length factor,  $R_s$  (see Figure 3.21.a); slip sharpness factor,  $\sigma$  (Figure 3.21.b); and the parameter for mean moment level of slip,  $\lambda$  (Figure 3.20.c) are evaluated respectively, so that variation of each slip factor or combinations of them are reflected in the hysteresis loop with experiences of more or less pinching level.

As it was pointed out that  $R_s$  is the controlled pinched length of the hysteresis loop,  $\sigma$  is related to sharpness of slip at the tips of the hysteresis loop so that increasing the  $\sigma$  reduced to a smoother transition to an unloading branch. Finally increasing the  $\lambda$  factor value leads to a wider hysteresis loop such that a very large magnitude of this parameter ( $R_s$  or  $\sigma = 100$ ) implies the absence of pinching in the hysteresis loop. It is observed that  $R_s$  is a controlled pinched length (see Figure 3.21.1);  $\sigma$  is related to sharpness of slip at the loop tips, as though increasing the  $\sigma$  variable reduces to a smoother transition to the unloading branch (Figure 3.21.2); and eventually enhancement of the  $\lambda$  argument leads to a wider hysteresis loop (Figure 3.21.3). It should be noted that very large magnitude of these parameters (i.e.  $R_s$  or  $\sigma = 100$ ) implies to the absence of pinching in hysteresis responses. To change model control parameters, one can adjust the severity of hysteresis decays in response loops, scope of parameter rate changes in following dynamic analysis fluctuate around initial guesses which is presented before in Table 3.4.

The entire parametric study in this section has been conducted to understand the hysteresis proceeding of a large spectrum of column end hinges and the relationship between the control parameters and the response hysteresis loops. The only purpose place underneath this is to provide a diversified amount of the analytical variables to incorporate the nonlinearity of structural members such as column members into following nonlinear dynamic calculations by meaningful magnitude variation of smooth hysteretic model.

The results given in this section represent difficulties associated with the nonlinear behavior of RC structures under returning effects. Each of the parameters on its own helps to simulate phenomenological observations. It is quite obvious that there are some interactions among these parameters in order that the same macro behavior can be achieved by altering a single parameter or there may be alterations of two or more parameters leading to the same result. In other words, the parameters are not the fixed and stable most appropriate tool. In this research by taking into account this fundamental fact, to oversee the purpose of bringing to the forefront the easiest rather than the most correct, parametric combinations.

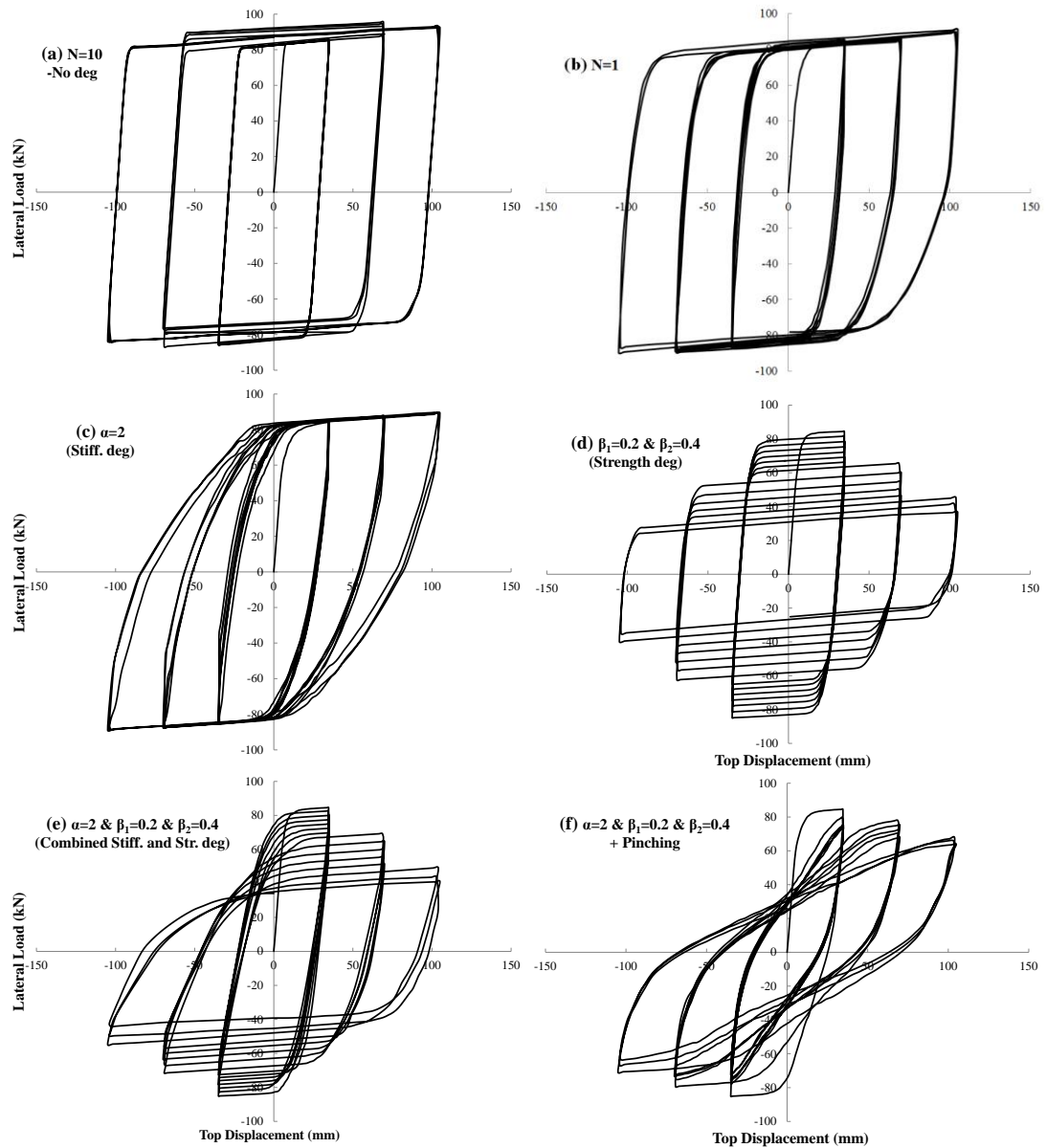


Figure 3.20 Variation of hysteresis loop shape by adding degradation properties in turn to get specimen 1D2 results: (a) Non degrading loop (b) addition of the smoothness parameter for elastic-yield transition  $N$ ; (c) Stiffness degradation  $\alpha$ ; (d) Strength deterioration  $\beta_1, \beta_2$ ; (e) and combination of them; (f) plus the pinching properties

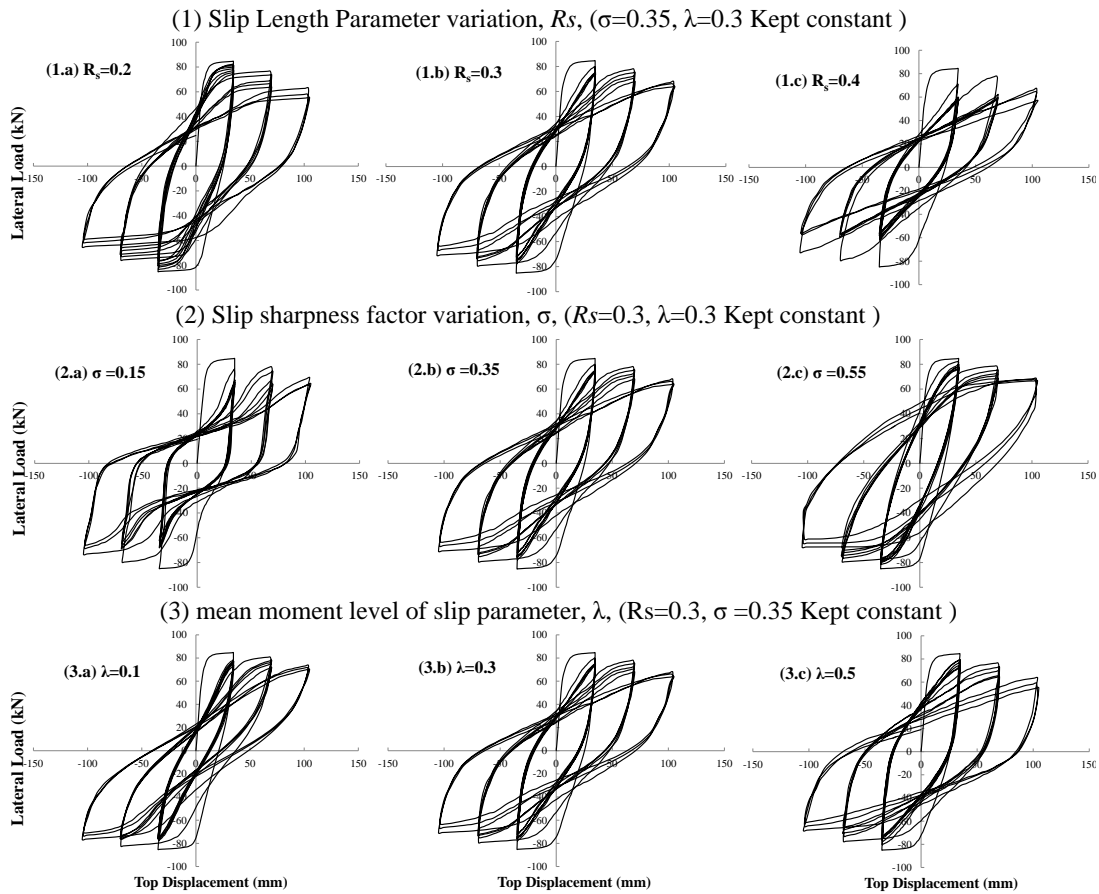


Figure 3.21 Qualitative view of effect of pinching parameters on hysteresis loop for specimen 1D2 ( $R_s$ : Slip Length factor,  $\sigma$ : Slip sharpness factor,  $\lambda$ : Parameter for mean moment level of slip)

The other important issue is related to the effects of different displacement paths of the quasi-static approach for both the axial and lateral loading directions that provide the benchmark data for dynamic and large-scale tests and to appraise existing analytical methods and material models. The impacts of an axial load and loading patterns were seen to be considerable in the flexural strength capacity; the mechanism of post-yield flexural failures and ductility and deformation of the columns. The plastic hinge formation was substantially different in a matter of a variable axial load, indispensability to a modification of the existing plastic hinge models, likewise identified SHM parameters could be affected (Esmaily-Gh. and

Xiao, 2002; Umemura and Ichinose, 2004; Jerry Shen J. et al., 2004; Booker, 2008; Krawinkler, 2009; Rodrigues, 2010; Bazaez and Dusicka, 2013).

The existing cyclic loading protocols are developed on the basis of statistic studies on ground motion responses and the considerations of gaining a maximal amount of knowledge from testing one or a few specimens. It is obvious no single protocol can represent all ground motions and their characteristics. The general ground motion response is made simpler with a cyclic loading format with only three variables: number of cycles, amplitude and succession of cycles. The selection of each variable determines the properties of a ground motion in program simulates. The number of cycles and displacement amplitude of these protocols is chosen to best represent the ground motion characteristics of chosen seismic zone and to achieve on the basis of the statistical studies of ground motion responses.

Every loading protocol will always be a compromise that will produce displacement time series which in reality will rely on many factors. Real time series, as experienced in ground motions, will be contingent upon the frequency content (distance, magnitude and soil condition dependence) moreover the intensity of the earthquake excitation and the particular assembly will be liable to within the frame of the structural system. Likewise, the count and magnitude of cycles, the component will experience rely on the configuration, stiffness, strength and modal characteristics (i.e. vibration periods and factors of participation) of the building and on degrading properties of buildings and its structural components. It is necessary to emphasize that there is no singular and finest loading pattern; this is because no two ground motions are similar as well as the fact that the specimen can be as a part of very distinct structural configurations.

The consequential questions that should be clear to reach reliable response assessment are as follows; what are the deformation amplitudes, how many cycles, and what succession of cycles should be employed to evaluate seismic performance or how can the results of distinctive experimental series be examined and interpreted in order that full advantage can be taken of a combined empirical information

generated by distinct laboratories. For the reasons listed, there are multitude parameters and steps tending to adjudication and to evaluate compromise loading history that is conservative but representative of the large spectrum of earthquake excitations and structural system configurations from a statistical standpoint.

Many loading pattern protocols were suggested in the literature (ATC-24 1992; FEMA-461 2007 and etc.) which are open to argument; The loading protocols in accord with the ATC-24 are dependent upon a statistical assessment of inelastic time series analyzes conducted with SDOF systems and employing far-field earthquakes (distance from fault rupture longer than about 20 km to elude near-fault impacts) from ground motions of magnitudes 7 or smaller. Seismic excitations from earthquakes greater than magnitude 7 are not included (due to insufficient number of records). This brings up the subject of long duration excitation, which, if in fact dominant, would enhance the count of large inelastic excursions.

It can be said that, excluding to earthquake records at soft soil sites; the long duration issue may not dominate the loading history. The reasoning is that the long return period hazard in seismically prone areas of two major urban areas is dominated either by near-fault ground motion records with forward directivity, which are short-term or by great ground motions from a larger distance, which affect mainly the long period chain of the spectra. Therefore the number of inelastic excursions is fairly small because of the few great cycles' experienced by a structural system with a long period.

Accordingly, the loading protocol issue includes tips and assumptions that necessitate be justified through more researches. The variation of response hysteresis loops, and in turn, identified model parameters for plural specimens with identical design setup and subjected to various loading histories are some of these issues that require further investigation. A monotonic, bi-directional, uni-directional and constant width loadings; variable amplitude loadings with samples for different types of loading time series. An important issue to examine is whether the identified

model parameters remain valid when specimens are subjected to loading patterns those are not in symmetric configurations.

### **3.6 Performance of the SHM under Ground Motion Excitation**

The seismic performance of the SHM described in section 3.3 is investigated by way of the nonlinear time history response of the SDOF system under given ground motion. The near-fault ground motion, Düzce-NS (Aug, 1999) earthquake record, among others, is adopted to examine seismic response performance of the SHM. The results are compared with those one obtained from the analytical Bouc-Wen hysteretic model. Structural properties and masses as well as the Bouc-Wen model control parameters were used in analysis are shown in Table 3.1. The response displacement time series of the SDOF system calculated by both models is illustrated in Figure 3.22. As can be seen in graph of displacement history, permanent displacement that is ignored in the original Bouc Wen hysteretic model is included in the improved SHM; such that it reflects a more realistic estimation of real (nonlinear) behavior of structural systems when exposed to severe ground motion. Therefore the SHM that incorporated into the IDARC 2D platform seems to be a reliable tool with sufficient accuracy to estimate the seismic behavior over the linear ranges.

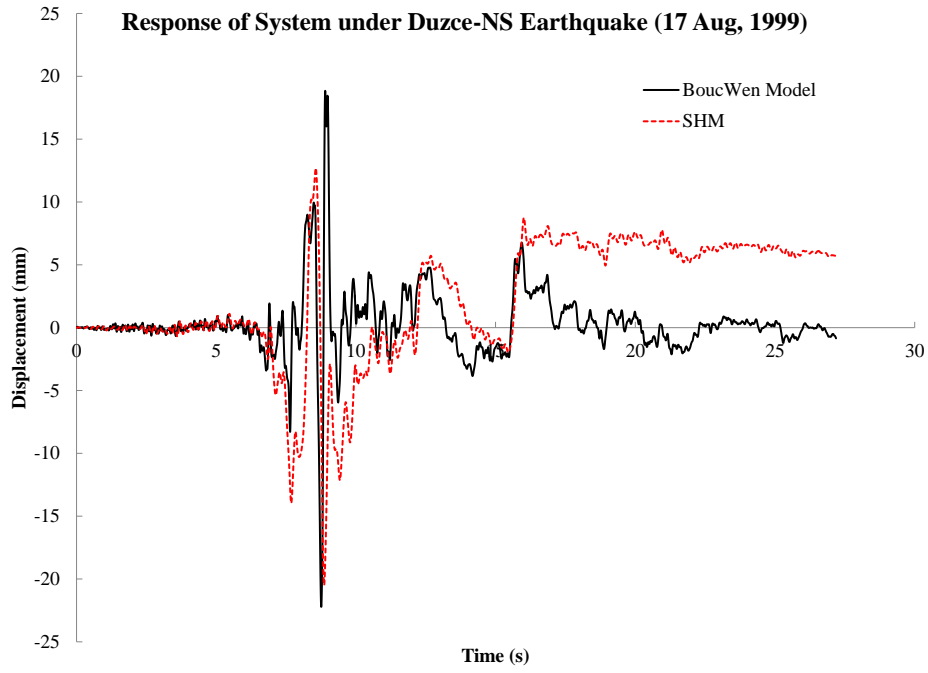


Figure 3.22 Comparison of response displacement time history of SDOF system under Düzce-NS ground motion record using (a) the SHM and (b) Analytical Bouc-Wen hysteretic model

## CHAPTER 4

### SHEAR FRAMES MODELS AND GROUND MOTIONS DATABASE FOR DRIFT SPECTRUM DERIVATION

#### 4.1 Introduction

Derivation of the drift spectrum for a certain earthquake excitation through the similarity with a shear-beam model is a practical method, but inevitably it is associated with some inaccuracy. Other models can be put to practical use; one of these possible approaches which are considered here is the design of a sequence of simple shear-type frame models, and to alter their story mass and column stiffness attributes systematically in order that distinctive fundamental periods are acquired. Whereas frame models are exposed to the earthquake excitation, their dynamic response can be calculated through the nonlinear time-history approach in both the elastic or/and inelastic ranges. That such lengthy calculations may be avoided is the important advantage that is exploited in the current study.

In the following sections, the shear type frame model to be utilized in drift spectra generation is introduced. The frames are two-dimensional, single-span structures. Likewise, other design assumptions and details related to structural properties are clarified. The manner of stiffness distribution and capacity design along the building height are important issues that are discussed. Later, some major characteristics of dataset of records are presented. The ground motion dataset has included a sizable quantity of near field records, considering the importance of the pulse-like time series in bringing about enormous seismic demands to the structural systems.

Since the generation of drift spectra through response history calculations required several analyses and added to this, the hysteretic parameters and ground motion considered the number of analyses became very high and run to the thousands, hence such repetitive and time consuming processes became very difficult to conduct manually and it is necessary procedure being implemented automatically. For this purpose, the analyzer program execution and reading response process is coded in the Java™ Archive (JAR) tool to be able to plot drift spectra more rapidly. The algorithm for the calculation procedure and code prepared for this aim is clarified.

Later the drift spectrum is plotted through both the Iwan (1997) formulation and the current method (RHA) and results are compared throughout the wide period ranges. This is essential to verify the results of the new approach with those of the closed form solution. Verification is possible only in linear ranges. The model identification process improves our confidence in the drift demand results, which is crucial in the following steps that coefficient ratios would be extracted for taking into account the inelastic behavior effects into drift spectra. In particular for this reason that the modification factors suggested with respect to the linear elastic spectral ordinates.

## **4.2 Structural System**

The structural systems being used to evaluate the seismic performances are single-bay plane RC frames. These generic shear-type frames are designed so that by varying the column stiffness and story mass properties a reasonable period range (0.3 -2.4 s) are obtained. Frames are prepared to make it consistent with the structural model with continuous shear-beams had been used in those wave propagation theory-based spectra. Likewise, corresponding elastic-plastic frame systems are designed according to weak-column/strength beam philosophy, so that beams and columns are designed such that inelastic deformations occur only at column ends and all beams remain elastic when frames are subjected to a predefined lateral load distribution. The loading pattern in pushing the structures is similar to the equivalent seismic lateral load distribution of design base shear recommended by TEC (2007). The post yielding degradation behavior is intended through plastic

hinges at the column ends and to use the smooth hysteretic model. Further details of structural properties; design and modelling assumptions of the frame considered in this study are provided in subsequent sections.

#### **4.2.1 Design Methodology**

The structural models used to estimate the seismic responses, or in particular IDR demands, are a family of single bay planer shear frame models with seven variant heights (3, 6, 9, 12, 15, 18 and 20 Stories). Each story has a height equal to 3.65m and the bay length of each frame is 7.32 m. In the design phase, through story mass and column properties variation, the fundamental vibration period is tuned to reach a period range extending from 0.3 s to 2.4 s. with adjust at a period interval of 0.1 s. In this way, a total of twenty two frames with periods of 0.3, 0.4 (three story), 0.5, 0.6, 0.7 (six story), 0.8, 0.9, 1.0 (nine story), 1.1, 1.2, 1.3 (twelve story), 1.4, 1.5, 1.6 (fifteen story), 1.7, 1.8, 1.9 (eighteen story), 2.0, 2.1, 2.2, 2.3, 2.4 (twenty story) seconds are generated (Figure 4.1). The flexural story stiffness is distributed uniformly (kept equal) along the height of the frames (Figure 4.2). It is necessary to mention that the same mass is assigned to each story at all six generic frames considered in this study.

On the other hand, the columns are designed to have very large axial stiffness; and the beams have very large flexural strength and stiffness toward the columns, and it is supposed that using these policies, a generic frame will be behave essentially as ideal shear frame models. In addition to the axial deformation, shear deformation of columns is neglected. To this end, the shear stiffness and axial stiffness are considered as infinite quantities ( $GA_c \rightarrow \infty$  and  $EA_c \rightarrow \infty$ ). The gravity load moments and the effects of axial column forces on bending strength are not considered.

In addition to these properties, P-Delta effects have been overlooked and 2% Rayleigh damping has been assigned to the following nonlinear time history analyses. As a consequence of these assumptions, the lateral response of the shear-frame considered here is similar to that of the shear-beam model of the Iwan (1997)

formulation principles with which the drift demand obtained from both approaches are compared.

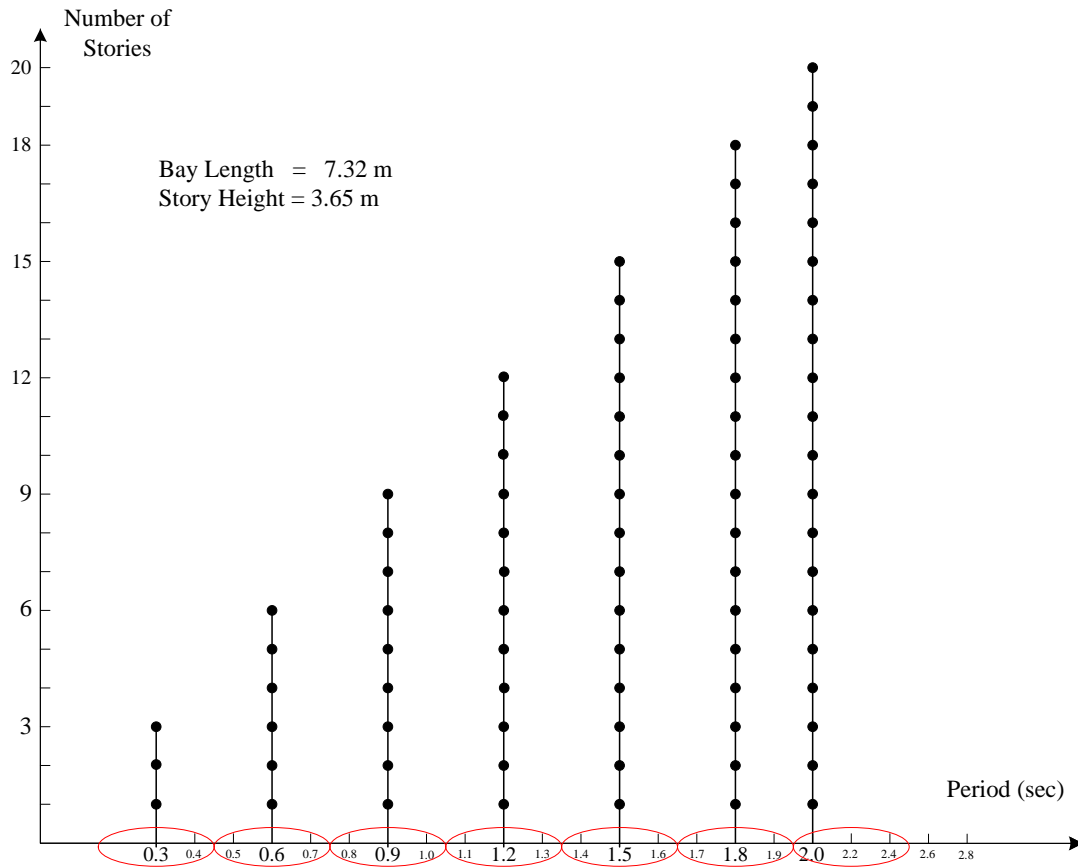


Figure 4.1 Generic single bay 3, 6, 9, 12, 15, 18 and 20 stories shear frame used in this study

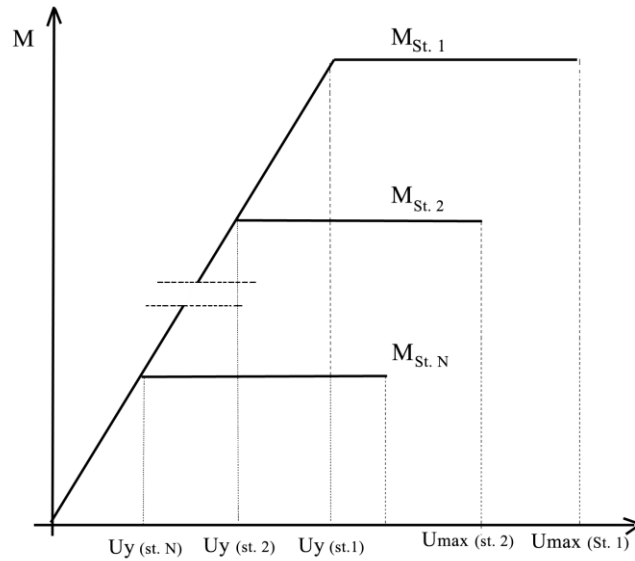


Figure 4.2 Design assumptions: Uniform distribution of flexural stiffness along the frame height (kept constant), story capacities are determined according to lateral loading distribution as per of the TEC 2007 recommendations.

#### 4.2.2 Capacity design

Corresponding to elastic systems, the smooth elastic-plastic frame systems are designed in accord with the philosophy of weak-column/strength beam, which mainly lead to the column-sway type of plastic mechanism when exposed to lateral forces. The structural members are designed such that inelastic deformations occur only at column tips, and all beams remain elastic.

Through nonlinear static analysis (pushover), the structure modeled with plastic hinges is pushed under a linear load pattern (the inversed triangle load pattern which is suggested by the TEC (2007)). Strength distribution throughout the frame height is supposed and tuned such that simultaneous yielding occurred at all story columns. Reduced moment quantities are considered as a yield moment amounts in following nonlinear dynamic calculations. Detail about the strength distribution over the frame height is given in the following section.

The nonlinear static (Pushover) approach is an appropriate tool to predict (and here design) the capacity of the structure; and its individual component members prior to a nonlinear dynamic analysis. In this way, the possible sequences of component yielding can be identified and the potential ductility capacity and the total global lateral strength could be evaluated. In the same manner, the yield moment  $M_y$  of plastic hinges at the column tips and corresponding curvature capacities  $\phi_y$  (i.e., story yield capacities) are calculated and tuned to reach simultaneous yielding along the height (Figure 4.3). The moment distributions obtained over the column tips throughout the height under applied loads are considered in the yield moments calculation procedure (Figure 4.3.b).

The design strength distribution along the structures intended in this research is established upon the base shear formula which is determined as per the recommendations of the TEC (2007). The base shear composition in TEC (2007) illustrates the prevalent practice of assessing seismic resistant design forces on the basis of a single design spectrum having scales by maximum site acceleration. The considered load patterns according to the code are employed to distribute the design base shear (the total equivalent seismic lateral load acting on the building),  $V_t$ , along the height but with the difference that the yield base shear  $V_y$  equated to the code-defined design base shear  $V_t$ . In accordance to TEC (2007)  $V_t$ , for a buildings is expressed by Equation (4.1) as the sum of equivalent seismic loads acting at story levels.

$$V_t = \frac{W \cdot A_0 \cdot I \cdot S(T)}{R_a(T)} \geq 0.1A_0IW \quad (4.1)$$

Where  $W$  denotes the whole weight of building computed in light of live load participation factor; and  $I$  denote the building Importance factor;  $S(T)$  imply to the spectrum coefficient;  $R_a(T)$  is the seismic load reduction factor; the spectral acceleration coefficient  $A_0$  described as the proportional relation of regional peak ground acceleration relative to the acceleration of gravity, (i.e. it is reflected a measure of expected severity of seismic action at a given site and is designated at the

annual probability of exceedance of 0.01. This probability level in seismic risk mapping is not directly in connection with the probability of exceedance associated with the design base shear). The yield base shear  $V_y$  is determined by Equation (4.2)

$$V_y = 1.0V_t \quad (4.2)$$

Likewise,  $V_y$  can be expressed as the sum of equivalent seismic loads acting at story levels (Equation 4.3).

$$V_y = \Delta F_N + \sum_{i=1}^N F_i \quad (4.3)$$

Where additional equivalent seismic load applying at the N'th story (top story) of the structure shown by  $\Delta F_N$ . This load is implemented for buildings higher than 25 m by taking into account the higher mode effects pursuant to Equation (4.4). Excluding to the  $\Delta F_N$  remaining part of the entire equivalent seismic load have been distributed to the stories of building frame (including top floor) in conformity with Equation (4.5)

$$\begin{cases} H_N > 25\text{m} \Rightarrow \Delta F_N = 0.07T_1 V_y \leq 0.2V_y \\ H_N < 25\text{m} \Rightarrow \Delta F_N = 0 \end{cases} \quad (4.4)$$

$$F_i = (V_y - \Delta F_N) \frac{w_i H_i}{\sum_{j=1}^N (w_j H_j)} \quad (4.5)$$

Here  $w_i$  and  $H_i$  are the story weight and the story elevation, respectively. The ratio of the yield base shear to total weight of a structure is called yield base shear coefficient and denoted by  $C_y$ . This coefficient has been used in the nonlinear static analysis as part of the design process of frame structures. Variation of the  $C_y$  over the period ranges is shown in Figure 4.4.

$$C_y = \frac{V_y}{W_{\text{Total}}} \quad (4.6)$$

The structural analysis and design of prepared frames is accomplished in agreement with the TEC (2007), for the conditions corresponding to buildings resting on the stiff clay formation (seismic zone I, according to the code); the effective ground acceleration coefficient,  $A_{0g}$ , is given as 0.4; soil considered to be type C ( $Z_3 \Rightarrow T_A = 0.15, T_B = 0.6$ ); and the seismic load reduction factor (to account for nonlinear ductile behavior) taken for RC buildings with nominal ductility level  $R_a(T) = 4$ . The structural properties of prepared frames are listed in Table 4.1. After determination of the base shear force as per TEC 2007 recommendations (see Table 4.1), base shear is distributed along the building height and is imposed to structures during the pushover analyses. Equivalent lateral earthquake force distribution along the height for the shear frames with fundamental period equal to 0.6, 0.9, 1.2, 1.5, and 1.8 s. ( $T=0.1N$ ) is drawn in Figure 4.5.

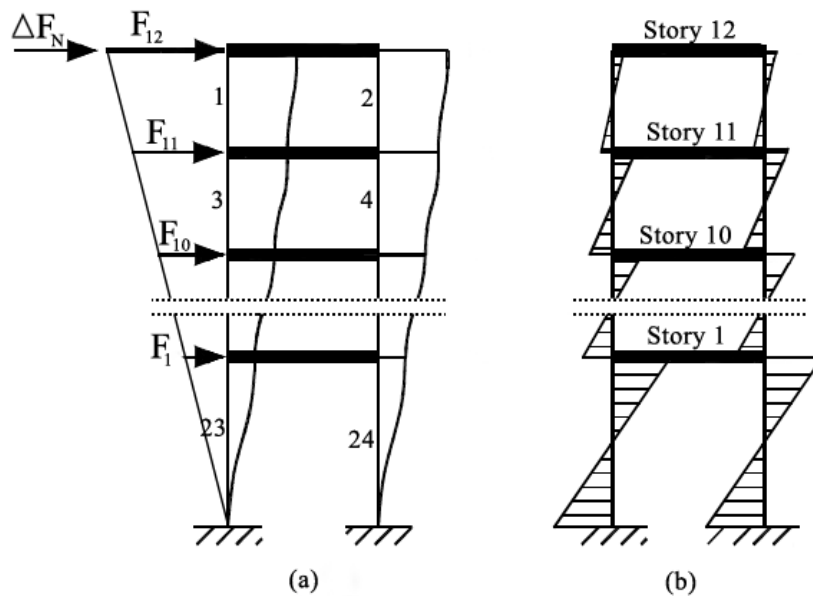


Figure 4.3 Schematic of generic plane single bay 12-story shear-frame: (a) Pushover analysis under uniform load pattern; (b) Moment distributions over the column tips throughout the height corresponding to the applied load pattern

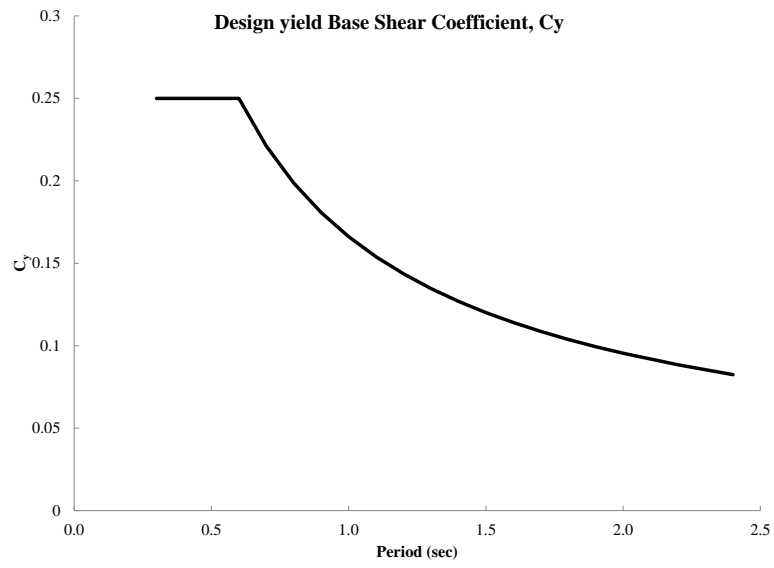


Figure 4.4 The design yield base shear coefficient used in structures design

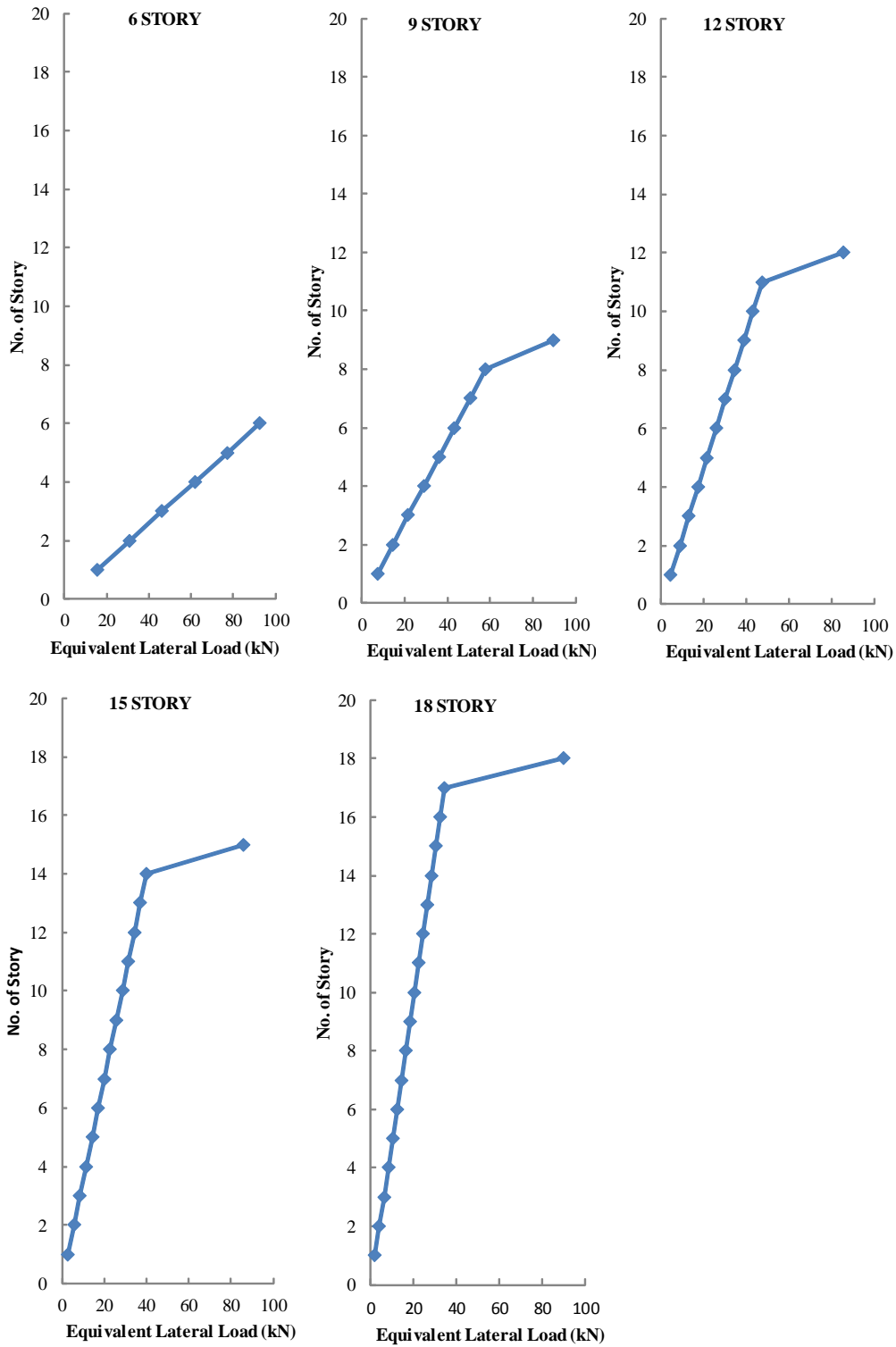


Figure 4.5 Equivalent lateral earthquake force distribution over the height for the shear frames with fundamental period equal to 0.6, 0.9, 1.2, 1.5, and 1.8 s. ( $T = 0.1N$ )

Table 4.1 Story mass and stiffness properties and yield base shear of single bay generic shear frames

No.	Period (s)	No. of Story	Story mass (Ton)	Story stiffness (kN/mm)	$V_y$ (kN)	$C_y$	$\Delta F_N$ (kN)
1	0.3	3	15.61	34548.62	114.83	0.250	0.00
2	0.4		27.75		204.08	0.250	0.00
3	0.5		12.72		187.11	0.250	0.00
4	0.6	6	18.32		269.46	0.250	0.00
5	0.7		24.93		324.17	0.221	15.88
6	0.8		15.28		267.94	0.199	15.00
7	0.9	9	19.34		308.59	0.181	19.44
8	1.0		23.88		350.18	0.166	24.51
9	1.1		16.71		302.66	0.154	23.30
10	1.2	12	19.88		335.99	0.144	28.22
11	1.3		23.33		369.81	0.135	33.65
12	1.4		17.61		328.81	0.127	32.22
13	1.5	15	20.21		357.13	0.120	37.50
14	1.6		23.00		385.87	0.114	43.22
15	1.7		18.23		349.66	0.109	41.61
16	1.8	18	20.44		374.50	0.104	47.19
17	1.9		22.77		399.59	0.099	53.15
18	2.0		20.55		384.58	0.095	53.84
19	2.2	20	24.86		431.18	0.088	66.40
20	2.4		29.59		478.65	0.082	80.41

### 4.2.3 Modeling of Plastic Hinges at Columns Tips

The inelasticity in generic frames being considered is modeled at two ends of the columns of all the stories. The moment-curvature hysteretic behavior of the rotational spring of the column tips is represented by symmetric, bi-linear rotational spring model with 2 % strain hardening. In this study, the tri-linear model is reduced to a bilinear model through the artifice of considering the cracking moment to equal 99.0 % of the yielding moment ( $M_{cr} = 0.99 M_y$ ) to satisfy elastic behavior in the pre-yield region and to provide the requisite of smaller post cracking slope with respect to yielding slope yield curvature considered a hundred two percent of cracking moment over flexural rigidity ratio ( $U_y = 1.02 M_{cr}/EI$ ). The same curvature ductility is applied for all frame members. A schematic diagram of the moment–curvature relationship of a typical tri-linear model is shown in Figure (4.6).

To compute the yielding moment,  $M_y$  and corresponding yielding curvature  $\phi_y$  for the column end hinges, through non-linear static analysis a structure is modeled with plastic hinges pushed under linear load pattern according to Equation (4.5) and strength distribution throughout the frame height tuned such that simultaneous yielding occurs at all stories column end hinges columns. To this aim, at the beginning and for a given structure, the yield base shear,  $V_y$  as well as the equivalent lateral forces at all stories are determined from Equations (4.1)-(4.5). Then after through the static analysis under the lateral load distribution corresponding values of bending moment and curvature are derived. Shear frame models designed according to the assumptions mentioned above have been applied in the following response history analyses.

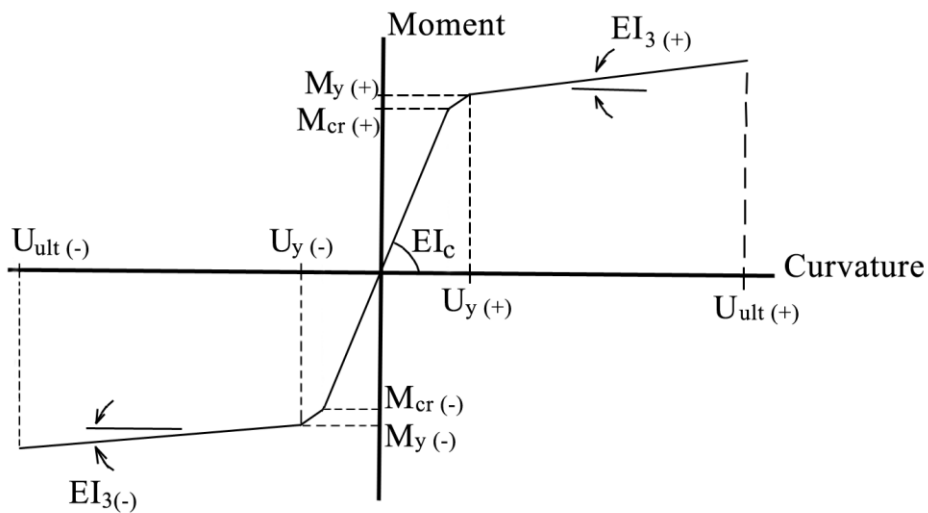


Figure 4.6 Typical tri-linear model form IDARC 2D element models library used for plastic hinges (Valles et al., 1996 and Reinhorn et al., 2009)

### 4.3 Characterization of Ground Motions Applied in This Study

It has been well known that the characteristics of seismic excitations vary strongly from record to record. The duration of intense excitation; the intensity; and the frequency content of the ground motions are contingent upon numerous parameters involving the magnitude of the seismic excitation; the local site conditions; the epicentral distance. The variations in the specifications of the seismic excitations can result in major discrepancies in the seismic response of buildings. One substantial parameter that has important influences on response of structures is the frequency content of the seismic excitations. A basic strategy established upon the peak ground acceleration to peak ground velocity ratio ( $a/v$  ratio) is prevalently approved for the frequency content assessment of seismic actions. From a statistical standpoint, ground motion records with high  $a/v$  ratios are usually related to intermediate to strong earthquake ground motions at short epicentral distances, and ground motions with small  $a/v$  ratios are in relationship with great ground motions at vast epicentral distances (Heidebrecht and Lu 1988).

Near-field ground motions are mostly applied as the ground motion records of sites in the distance of around 20 km from the rupture fault that vary considerably originating with those at far-fault regions. The different specifications of near fault earthquakes come from the rupture forward directivity; the fling-step result, the hanging wall impact, etc. In consequence of the earlier two impacts, the near-fault earthquake excitations generally show two important properties: a pulse-like velocity wave form and a permanent ground displacement, whichever bring about serious structural damage by transmitting high energy to the building at the beginning of the ground motion.

In the data-set of ground motion records, gathered to evaluate interstory drift demands on the structural system given in previous sections, a large quantity of near-field ground motions are included, in terms of the characteristic consequence, pulse-like histories creating large earthquake demands on the buildings. In total, the 193 near field records are collected. The majority of ground motions are larger than

magnitude 6 ( $M_w$ ) with short epicentral distances of less than 20 km. The ground motions are arranged into three groups on the basis of their  $a/v$  ratio. The ground motions with ( $a/v < 0.8$  g/m/s) are sorted into low ranges, where as those with ( $a/v > 1.2$  g/m/s) are grouped into the high ranges. Intermediate ranges are grouped ( $0.8$  g/m/s  $< a/v < 1.2$  g/m/s),  $a$  is in g, and  $v$  unit is m/s. Important features of the ground-motion data include the peak ground acceleration to velocity ( $a/v$  ratio), magnitude as well as a site condition, in each of three groups which are listed in Tables A.1, A.2 and A.3 in the Appendix.

To make the ground motion records comparable, uniform intensity strategy are adopted to scaling the selected records. Several ground motion parameters may be employed as the scaling factor, and henceforth, Peak Ground Acceleration (PGA) is scaled to 0.35g to give a comparison of drift demands reduced from both the Iwan (1997) formulation and the response history analyses results. Figure 4.7 shows the mean elastic acceleration spectrum (2 % - damped) of the chosen records having scales as well as the (TEC, 2007) spectrum. To reaffirm, in the following response history analyses all ground motions are scaled to PGA of 0.35g, that is adopted to introduce a sufficient level of nonlinear response.

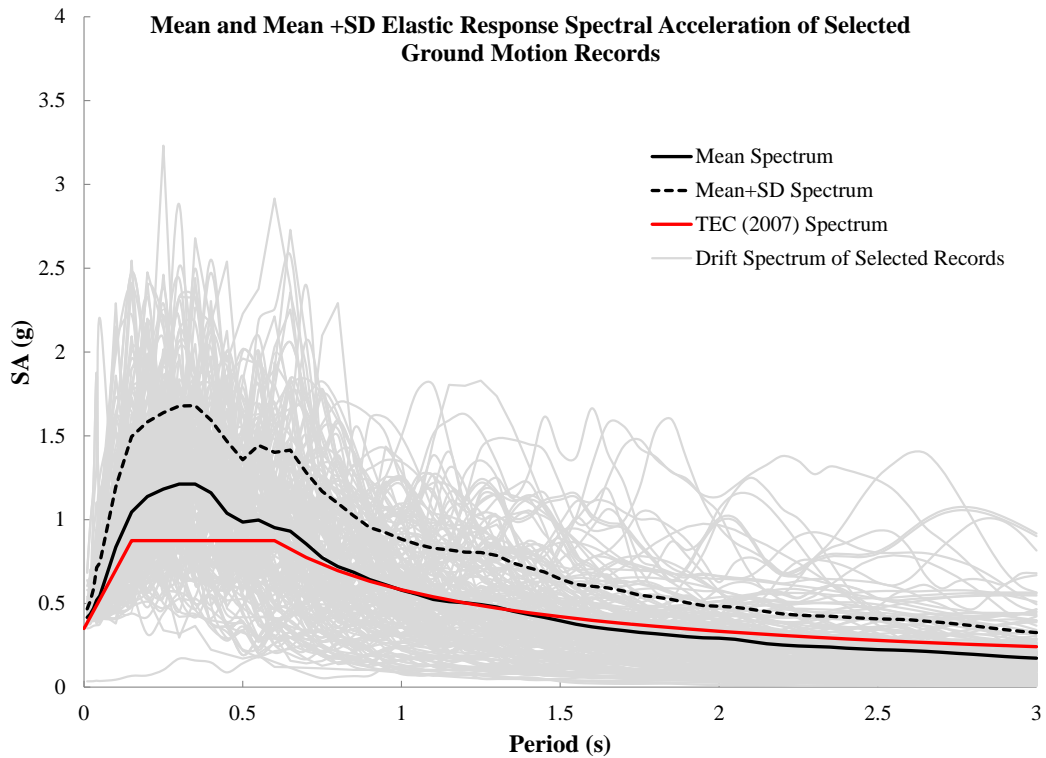


Figure 4.7 Mean and mean plus standard deviation elastic acceleration response spectrum (2%- damped) of selected ground motions and (TEC, 2007) spectrum

#### 4.4 Verification of Linear Elastic Drift Spectrum Obtained through the Simulation and Iwan (1997) Formulation

The elastic drift spectrum derivation based on the shear-beam is useful in the preliminary prediction of drift demands, but does not reveal the characteristics of the realistic behavior of the structures under strong action. Many structural damages during the ground motion arise from excessive IDR, therefore it is necessary to estimate the MIDR with greater precision, amplified by the post yielding hysteresis degradation properties. The drift spectrum can be derived via other approaches, and the dynamic elastic or/and inelastic response of simple shear-type frame under the given ground motions is used to calculate the drift spectrum. Through the systematic regulation of column stiffness and story mass properties, the desired period is achieved. This approach is called the Response History Analysis (RHA) method.

The RHA calculations are conducted through the nonlinear analyzer platform, which is used to inelastic damage analysis of reinforced concrete frame (IDARC-2D, ver.7.0) (Park et al., 1987; Valles et al. 1996 and Reinhorn et al. 2009).

Inasmuch as the drift spectrum is calculated through both methods, the (closed form) Iwan (1997) formulation and response history analysis is compared to obtain any coefficient ratio of inelastic response with respect to the linear elastic spectrum ordinates and therefore it is required that the drift spectrum be reduced from simulation processes in linear ranges to validate with those of the linear elastic Iwan (1997) formulation results. It should be noted the drift spectrum ordinates that are achieved by the Iwan (1997) formulation are considered as the base (as exact estimation measures) to compare results with alternative methods in linear ranges. Deriving the drift spectrum through response history calculations required many analyses and by adding hysteretic parameters and given ground motion alteration, the number of calculations ran to thousands. Such massive numbers of repeated processes are very exhausting to conduct manually and that issue was also the underlying factor in the preparation of a code to perform these time-consuming operations automatically.

In the following sections, the algorithm used in developing the program is examined and its implementation in the windows operating system is clearly explained. Thereafter, drift spectra are plotted through both the Iwan (1997) and RHA methods and the results are compared in terms of some examples. Eventually, coverage of the spectrum ordinates and the reasons underlying the differences between the two results are discussed.

#### **4.4.1 Program Development**

The derivation of the drift spectrum through the response history calculations needed several analyses. This spectrum is obtained through plotting the maximum drift demands of the building system exposed to given seismic excitation, relative to the vibration period of the corresponding structure. The number of analyses changes

depending on considered period range and if added to this hysteretic parameters and ground motion variation, the number of analyses become very high and run into thousands of analyses. Such repeated and time-consuming processes are very difficult to conduct manually. For this reason, the analyzer program execution and reading response process are coded in The Java™ Archive (JAR) tool, in the manner that by using this program, drift spectrum for desired hysteresis parameters and ground motions are able to be drawn more rapidly with different given PGA intensities.

Using this program, consecutive operations of (1) updating the input file of the main analyzer platform (IDARC 2D) with desired hysteresis quantities and ground motion intensities, (2) its execution, (3) reading the max interstory drift ratio demand from output sheet and (4) transmission of them is provided on the spreadsheet page, having been coded. Therefore, such time-consuming operations have been conducted automatically. The graphical user interface of the prepared program is shown in Figure 4.8.

The program is run irrespective of selected frames, i.e. in the first step we can prepare the generic frames with the desired period, drop them into the same folder, and of course with the interest period interval (see Figure 4.8.a), the code is written so that the folder can be read and the analyzer executed with updating the hysteresis parameters and inputting the ground motion (Figure 4.8.b). Afterwards, calculations are repeated for frames with lower periods to higher period ranges. At each step, the maximum interstory drift ratio is calculated and plotted into an output Excel sheet corresponding to the related frame period (Figure 4.8.c) and this procedure is done for other frames, respectively.

As mentioned above, this program works independently of the IDARC 2D input files and the only changes are applied in the hysteresis parameters line and input ground motion then analyses are repeated for all frames. Similarly, linear analysis is conducted by updating design properties of desired frames into the IDARC 2D input file and the remaining steps are the same for all combinations of input variables.

To execute the program, it is necessary to copy the "GenericFrames.jar" into the same place as the frame folders, which are included the IDARC 2D input files. It is necessary to ensure the "ground motion" folder exists near the "jar" file and the folder includes the wave files that you want to run. There are two ways to execute the program. (1) Double click on "GenericFrames.jar"; and (2) open "cmd.exe". Enter the folder address you work in. (i.e. cd <folder\_name>), following that enter the folder command "java -jar GenericFrames.jar". Using this option, it will appear what happens behind of execution process for each step. All source codes and methods (subroutines) for Java based computation program "Generic Frames.jar", which is used to derive the drift spectrum through the generic shear frames are available in Appendix B. Likewise, The Java™ (JAR) based implementation of the program and related subroutines can be found in the CD attached to the thesis.

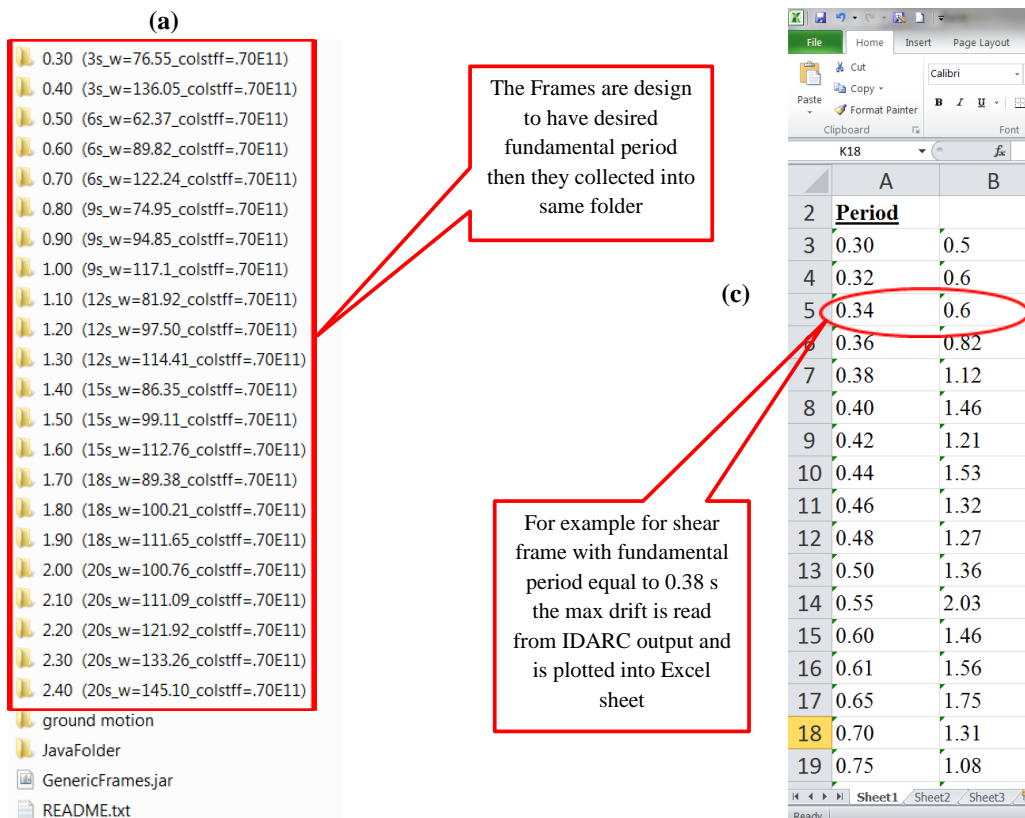
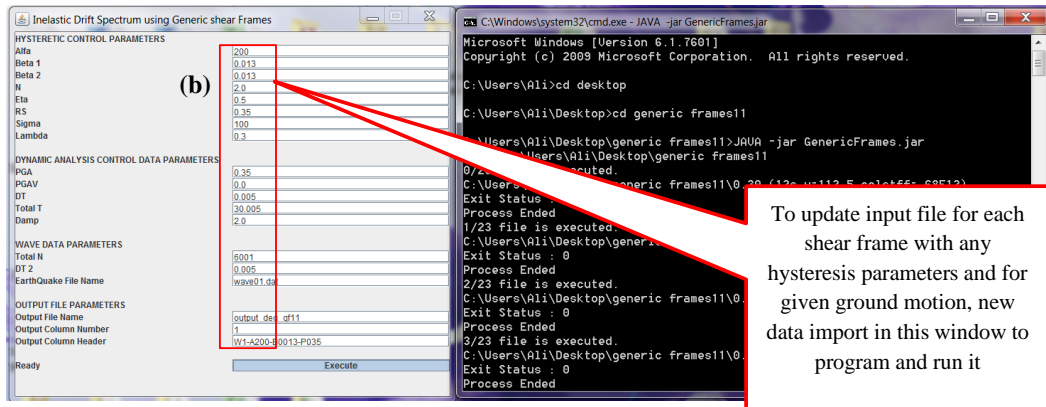


Figure 4.8 Program interface for calculation of inelastic drift spectrum using the generic shear frame models

#### **4.4.2 Comparison of linear drift spectra derived through the Iwan (1997) formulation with the alternative RHA method**

The Drift Spectrum ordinates obtained through both methods, the Iwan (1997) formulation (closed form solution) and the response history analysis, are compared to examine the performance of the proposed method and also to get any coefficient ratio of inelastic response with respect to those of the linear elastic spectrum ordinates. This is also dictated to validate the drift spectrum reduced from the simulation processes in linear ranges with those of the linear elastic Iwan (1997) formulation. This comparison is itself provided to form the basis of the following analyses to extract coefficient ratios in between the linear demands and drift ratio in elastic ranges including the individual and/or combination effects of hysteresis degradation behavior (stiffness degradation, strength deterioration, as well as pinching) in drift spectrum estimations.

The elastic drift spectrum ordinates derived from the Iwan (1997) formulation are treated as exact solution values. These quantities are taken to compare and check the compatibility of the proposed model's results in elastic regions. Figures 4.9.a - 4.9.c demonstrate the drift spectra (for  $\zeta=2\%$  damped) obtained through both approaches in linear elastic regions for structural models that subjected to four typical ground motion records. These are belonging to the ground motions recorded in the cities of Bolu (November 1999, NS), Sakarya (August 1999, EW), Hanshu (June 1973, NS) and Kobe (January 1995, NS) respectively. The closed form solution is calculated with the following assumptions;  $T = 0.0853H^{3/4}$ ,  $C = 146$  m/s,  $H = 3.65$  m.

The validation process shows whether the drift demands estimations are in good agreement or not. Likewise, it can illustrate the accuracy of such a simple modeling procedure. The spectrum ordinates achieved from the proposed method and wave propagation based approach are shown in Figure 4.9. It is shown that except for a slight deviation in the spectrum trend, the results are overlapped and there are reasonably consistent with each other, in such a way that drift demands of the RHA method are underestimated at the lower period and conversely are higher for frames with larger periods.

It should be noted that differences between the two adjacent IDR demands may result from the derivation process of each one. The Iwan (1997) formulation requires that the time histories for the ground displacement and velocity should be available, which does not always apply due to a drawback in the integration process of ground acceleration time series. Besides, buildings height is assumed to be invariant along the period range and therefore the same shear wave velocity is used in the Iwan (1997) formulation, whereas it seems illogical to generate the frames over such period ranges keeping the height constant, because there are substantial differences between structural properties of 15-story and 45-story building frames. On the other hand the moment of inertia of masses at story levels are varied, which this is dictated by the mass and stiffness variation process required to reach a desired period that in turn reduces to deviation in the drift spectrum trend. Another point that should be mentioned here is that the closed form solution gives the peak interstory drift ratio at the ground story, although most of the time the MIDR seen in ground story but yet the proposed RHA approach provides the maximum IDR along the frame height.

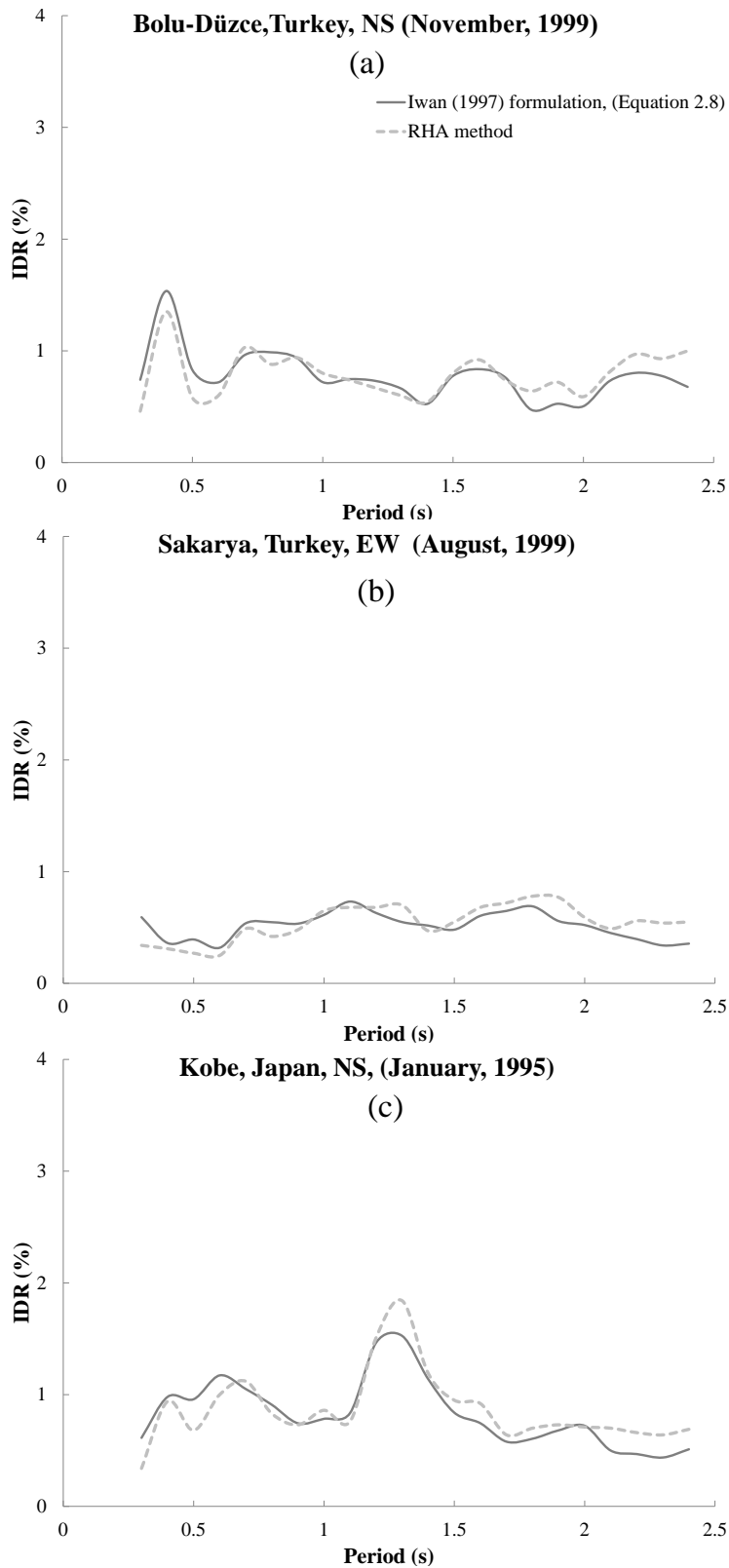


Figure 4.9 Comparison of the drift spectrum ordinates calculated by both the proposed method and the Iwan (1997) formulation for ground motion records of (a) the Bolu-NS; (b) the Sakarya-EW; (c) the Kobe -NS

## CHAPTER 5

### DERIVATION OF MODIFICATION FACTORS FOR DRIFT SPECTRA OF INELASTIC SHEAR FRAMES

#### 5.1 Introduction

The characterization of the seismic behavior of multistory frame buildings exposed to strong earthquakes needs the investigation of the seismic response at local and global levels. This is because it can be characterized through high demands for inelastic displacement and energy dissipation that frequently bring about damage concentration in some places of the buildings, as soft or weak stories.

An assessment of the demand patterns as function of structural properties of building frames and earthquake record is needed to conduct comprehensive analytical parameter studies. With the intention to comprehend and determine magnitude of seismic response demands for a large spectrum of ground motion records and structural system properties, a simple discrete shear-type frame model with lateral stiffness, inertial and strength properties approximating those of the analogous frame building and changing of height wise is adopted in the present context. These simplified generic frame models are employed to perform step-by-step dynamic analyses. Through a full nonlinear analysis the contribution of all vibration modes of buildings may be implicitly incorporated to estimate the inelastic seismic responses. Likewise, height wise distribution of interstory drift ratio may be suitably characterized. A validation of the elastic range results of the dynamic shear frame analyses is made by means of comparisons with those results of the closed form Iwan (1997) formulation. The influence of hysteresis models for detection of a limited set of structural properties and behavior patterns, which are essential for a

proper characterization of global and local responses of frame buildings, have been pointed out.

Seismic demands on generic shear frame systems have been examined in terms of maximum interstory drift ratios in the elastic and inelastic ranges, and at local and global levels for several post yielding hysteresis behaviors. In predicting the damage resulting from severe earthquake excitations in building frames, it is essential to correctly recognize the influence of degrading behavior parameters over the yielding locations of all structural components, which are mutually connected with seismic response and in turn with structural failures.

Inasmuch damage of buildings during seismic excitation mostly comes from excessive interstory drift ratio (IDR), it is required to estimate the MIDR's in inelastic region to incorporate modified IDR's that affected by hysteresis capacity degradations, such as stiffness and strength decays and pinching properties when exposed to ground motions. This issue is particularly true for pulse like near field ground motions that leads to large IDR demands. This is major reason underlying the unacceptable structural damages. This issue is double the importance of IDR estimations more realistically, in particular when structural systems enter into the inelastic regions.

For this purpose, a drift spectrum in the both elastic and inelastic ranges is calculated through the nonlinear response history method for all selected 193 ground motion records, the majority of which are near field ground motions including long period pulses. Current drift spectrum derivation in both elastic and inelastic ranges is established through the RHA approach using twenty smooth elastic-plastic frame models with different vibration periods under given ground motions. The RHA method needs several analyses for each drift spectrum and if one adds to this alteration of other hysteresis variables as well as repetitions for all selected ground motions, the number of analyses become very high and can run to thousands. As already mentioned in section 4.4.1 the program is developed to perform such

repeated and time consuming operations automatically. The total number of analyses conducted through current procedure reaches up to 105,000 separate calculations.

The specifications of earthquake records change strongly from record to record. The frequency content, the intensity and the duration of the ground motion rely on a number of parameters involving the local site conditions: the magnitude of the earthquake and topography. The mean (M) and mean plus standard deviation (M+S.D.) drift spectrum of all 193 ground motions are used to investigate the influence of stiffness or strength degradation and pinching on drift demands. This is essential, one to minimize uncertainties raised from the above effects and other to making reliable judgment on results. Seismic responses of structural systems that have the same hysteresis degradation properties are utilized to construct the drift spectra in inelastic ranges which hereinafter can be called “Inelastic Drift Spectrum” as well. The M (or M+S.D.) drift spectrum is constructed by interlinking the response MIDR’s throughout the period ranges (Figure 5.1).

The modification factors are derived from comparison of (M+S.D.) inelastic drift spectrum ordinates with respect to the corresponding elastic drift spectrums. Thereafter, using statistical methods, smooth variation has been expressed using a simple modification expression. The least squared regression analysis is used on the intact differences between both elastic and inelastic spectrum ordinates to calculate the smooth variation functions. These modification factors can be used to estimate the maximum interstory drift ratios when structural systems exhibit the inelastic behavior due to post yielding hysteresis degradations. The modification ratios are proposed toward correcting the elastic drift demands, like as closed form solution (Iwan, 1997) drift spectrum. The smooth curves fitted and the expressions for the modifying factors as well as variation of maximum interstory drift demands for different  $(a/v)$  ratios are given in subsequent sections in detail.

## 5.2 Structural Performance Levels and Ranges

Recent studies have manifested that common criteria used as the basis of the seismic resistant design of new buildings and likewise the seismic evaluation of existent ones, may be meaningfully improved by way of a definite account of lateral drift demands. Particularly, uncomplicated but trustworthy approaches which permit us to derive benefit from the results of linear elastic analyses for the assessment of the peak inelastic demands have been proving themselves to be obligatory tools of analysis. In recent times a renewed interest has emergent in the correlation between the peak inelastic drift demands and the corresponding elastic drift demands.

Lately, (Miranda E., 2000; Decanini et al., 2003; Decanini et al., 2004; Ruiz-Garcia and Miranda, 2004; Chopra and Chintanapakdee, 2004; Mollaioli et al., 2007; Mollaioli and Bruno, 2008) have derived a sequence of results for statistical studies with the aim of increasing understanding of the implementations and performance of the proportional relation of the peak inelastic to the peak elastic displacement for both SDOF and multistory systems in the analysis of structural behavior over the short to longer period ranges. Indeed, the results obtained show that for short to intermediate period ranges, the peak inelastic drift demands may be meaningfully higher than the peak elastic drifts, contingent upon the properties of the earthquake as well as on the ductility of the structural system.

In some instances, the global displacement demands on a structure may be evaluated from the seismic demand achieved in equivalent SDOF systems. However, in other cases an SDOF model cannot be employed to develop an opinion on the story and local seismic demands in multistory frame buildings; owing to the presence of local effects, similar to interstory drifts, end rotations, hysteresis degradations, etc. The way these local effects take place is established upon the ground motion and on system properties, so that it cannot be predicted through simplified SDOF responses. It would be perfect to carry out seismic demand studies on three dimensional multistory frame buildings because the dynamic behavior of actual frame buildings is contingent upon many factors. Although, some of the researchers (Krawinkler et

al., 2003; Medina, 2004; Medina and Krawinkler, 2005; Mollaioli et al., 2007) have suggested to concentrate the analyses on simplified multistory models in order to acquire insight into basic dynamic response patterns, especially in inelastic regions.

The assessment of the demand patterns as a function of the specifications of multistory frame buildings and given ground motion record is needed to carry out comprehensive parametric investigations, with the intention to grasping and quantifying seismic demands for diversified amount of ground motion records and building frame properties. In the current context, a simplified distinct generic shear-type frame model with lateral stiffness; inertial and strength properties, approximating those of the corresponding frame buildings are used. These simplified models are used in drift spectrum derivation through the RHA method.

In several pioneering publications and guidelines (ATC-32, 1996a; ATC-40 1996b; NEHRP, 1997; FEMA-356, 2000) exist in which the concept of Performance Based Earthquake Engineering (PBEE) was presented. PBEE can be defined as a design for the access of distinctive results rather than subordination to particular technologies. In PBEE, multiple performance objectives are fulfilled when building is exposed to various levels of hazard, which is an iterative procedure between design and performance assessment.

The recommended building performance objectives chart founded on FEMA 365 provides a large spectrum of structural performance necessities that might be demanded by owner of the buildings. The system performance objectives presented to hold a view on the drift demands and damage states for vertical elements may suffer by vertical members when present in structures fulfilling the explanations of the structural performance levels. Each global performance objective is detailed in terms of the performance of individual structural elements. It is accepted that if all individual frame elements meet the predefined strength and serviceability criteria, the global performance of the structural system is satisfied.

The four structural performance levels delineated in FEMA 356 standard have been chosen to correlate with the most prevalently itemized structural performance necessities. Table 5.1 makes a connection between these structural performance levels and the restricting damage states for prevalent vertical members of sideways force resisting systems (Note that Table C1-3 of FEMA-356 is replicated). Indeed, structural performance levels translate qualitative performance levels into damage states expected for structural and nonstructural systems. The discrete performance levels of structural systems are Immediate Occupancy (S-1), Life Safety (S-3), and Collapse Prevention (S-5) (FEMA 356, 2000). The pointed out quantities are predesignated to be qualitative explanations of the estimated structures behavior fulfilling the designated levels. Other guidelines such as EC-8 may use different descriptions. Opinions differ between the quantification figures as well.

Besides, damage states displayed in Table 5.1 are provided to allow a grasping of the severity of damage that may be suffered by various structural elements. The drift ratios given in the table are typical values that are provided to illustrate the overall structural response associated with various structural performance levels. The drift capacities exemplified may be given insight about the correlation of structural damages with transient and residual (or permanent) drift ratio demands. In other words, they are indicative of the range of drift demands, which generic building having the indicated structural members may experience when responding within the diverse performance levels of structural systems.

Table 5.1 Structural performance levels and damage for columnar members as per recommended by FEMA-356

Elements	Type	Structural Performance Levels		
		Collapse Prevention S-5	Life Safety S-3	Immediate Occupancy S-1
Concrete Frames	Primary	Extensive cracking and hinge formation in ductile elements. Limited cracking and/or splice failure in some nonductile columns. Severe damage in short columns.	Extensive damage to beams. Spalling of cover and shear cracking (<1/8" width) for ductile columns. Minor spalling in nonductile columns. Joint cracks <1/8" wide.	Minor hairline cracking. Limited yielding possible at a few locations. No crushing (strains below 0.003).
	Secondary	Extensive spalling in columns (limited shortening) and beams. Severe joint damage. Some reinforcing buckled.	Extensive cracking and hinge formation in ductile elements. Limited cracking and/or splice failure in some nonductile columns. Severe damage in short columns.	Minor spalling in a few places in ductile columns and beams. Flexural cracking in beams and columns. Shear cracking in joints <1/16" width.
	Drift	4% transient or permanent	2% transient; 1% permanent	1% transient; negligible permanent
Steel Moment Frames	Primary	Extensive distortion of beams and column panels. Many fractures at moment connections, but shear connections remain intact.	Hinges form. Local buckling of some beam elements. Severe joint distortion; isolated moment connection fractures, but shear connections remain intact. A few elements may experience partial fracture.	Minor local yielding at a few places. No fractures. Minor buckling or observable permanent distortion of members.
	Secondary	Same as primary.	Extensive distortion of beams and column panels. Many fractures at moment connections, but shear connections remain intact.	Same as primary.
	Drift	5% transient or permanent	2.5% transient; 1% permanent	0.7% transient; negligible permanent

### 5.3 Modification Factor Function for Inelastic Drift Spectrum

Prevalent nonlinear static proceeding in the ATC-40, FEMA-356 and FEMA-440 regulations, need formation of a pushover curve that is explained as the relationship between the base shear force and horizontal displacement of a control node. The structural system is pushed statically to a target displacement  $\delta_t$  at the control node to examine for the satisfactory level of structural performance. So that force and displacement corresponds to the displacement of control node equally or passing the target displacement should be conformed to approval criteria at desired performance level. The FEMA-356 suggests the following equation for calculating the target displacement  $\delta_t$ .

$$\delta_t = C_0 \cdot C_1 \cdot C_2 \cdot C_3 \cdot S_a \cdot \frac{T_e^2}{4\pi^2} g \quad (5.1)$$

Spectral displacement  
↓

The target displacement  $\delta_t$  obtains from multiplication of some modification factors to spectral displacement ordinates. One of these factors is  $C_2$ , which is represented influence of pinched hysteretic loop, stiffness decay and strength degradation. The remaining coefficients are presented in the following;  $C_0$  symbolizes the modification factor to make a connection between roof displacement and first mode spectral displacement;  $C_1$  is the modification factor to interrelate awaited maximum inelastic displacement to displacement computed from elastic response; and  $C_3$  represents the modification factor to demonstrate raised displacements on account of dynamic P-Delta impact. On the other hand in Equation 5.1, the  $T_e$  represents effective fundamental period of the structural system in the direction in prospect calculated through adopting the fundamental vibration period from elastic dynamic analysis. For example eigenvalue analysis;  $S_a$  is the acceleration response spectrum at the efficient fundamental vibration period and damping ratio of the structural system under consideration and  $g$  is gravitational acceleration.

The  $C_2$  modification factor is obtained from displacement ratio of the stiffness, strength degradation system (SSD) to elastic-perfectly plastic systems (EPP), i.e.  $\Delta_{SSD}/\Delta_{EPP}$ . It means that inelastic displacement should go up for SSD systems relative to EPP systems. The mean value of  $\Delta_{SSD}/\Delta_{EPP}$  for 240 ground motions and for all site classes are seen in Figure 5.1. The graph of mean displacement ratio of SSD to EPP systems are plotted for different seismic load reduction factors. This is taken from Figure 3-21 of the FEMA 440.

A similar approach has been used in this study to incorporate the hysteresis degradation effects into drift spectrum ordinates through the multiplication of some modification factors on corresponding elastic drift demands. It is necessary to note that presence of more than one effect to derivate inelastic responses from corresponding elastic behavior presupposes the multiplication of the several  $C_{xx}$

modification factors, which shows a matter of multiple factors. For the sake of interactive relation between the degradation parameters and definite judgment on the effect of each parameter one by one separately, therefore it is preferable to combine the capacity deterioration effects into one factor.

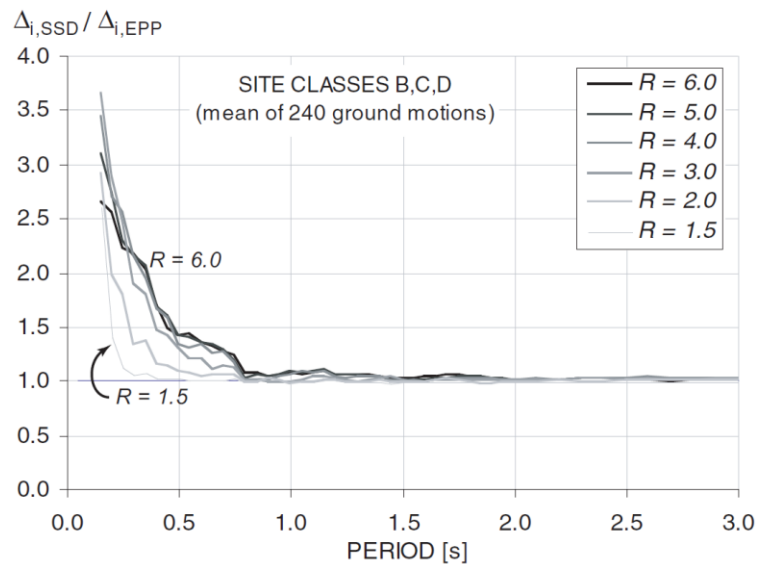


Figure 5.1 Proportional relation of the mean displacement between SSD and EPP systems calculated with earthquake recorded on different site classes

An inelastic seismic response of generic shear frames is considered to plot inelastic drift spectrum. This spectrum is reflected in many commonly observed types of hysteretic behavior at structural members to drift demands. The current approach enables one to incorporate each hysteresis decay effect (or combination of them) into drift spectrum ordinates, one by one simply by tuning a few parameters.

The mean and mean plus standard deviation drift spectrum is generated from interlinking of the mean (or M+S.D.) maximum interstory drift ratios. As a result of their analogues over the period ranges, both elastic or/and inelastic mean drift spectrum is obtained. The reason underlying the non-smooth mean spectrum is that

despite the Iwan (1997) formulation which IDR's are derived from the equation, in the proposed method drift demands are calculated individually for each period and later interlinked to each other throughout the considered period ranges. The best estimate curves among the figures correspond to mean plus standard deviation (M+S.D.) values. The standard deviation of the mean is generally more relevant when plotting a data series to be contrasted with another data series or to some theoretical model. The M+S.D. curves of the spectrum are drawn to consider scatter in data around the regression line and to demonstrate the prediction band corresponds to the probability of 84 percentile.

The ratios of M+S.D. drift spectrum ordinates, which include hysteresis deterioration properties of interest, with respect to the corresponding M+S.D. elastic spectrum are considered to get the modification factor expressions. As a result of regression analyses, a best-fitted curve established upon minimizing the squared root of the variations between the intact changes of the drift ordinates and the curve fits is provided, thus, readily depending on the period modification factors that take into account inelastic behavior is obtained. The smooth variation trend along the wide period range could be represented by the simple modification expressions shown in Equations (5.2) – (5.3).

$$\text{IDR}_{\text{degraded}}(T, \zeta) = C_{\text{degraded}} \times \text{IDR}_{\text{elastic}}(T, \zeta) \quad (5.2)$$

$$\text{IDR}_{\text{pinched}}(T, \zeta) = C_{\text{pinched}} \times \text{IDR}_{\text{elastic}}(T, \zeta) \quad (5.3)$$

In these equations; the term  $\text{IDR}_{\text{degraded}}(T, \zeta)$  reflects drift spectrum ordinates affected due to yielding of structural members of the smooth elastic-plastic systems; effects of the smoothness rate for elastic-yield transition; and stiffness degradations over the yielding point are important properties that are reflected in the degraded spectrum; likewise, the  $\text{IDR}_{\text{pinched}}(T, \zeta)$  represents inelastic drift spectrum for the structural systems including a pinching in response loops.

To calculate the modification factor expressions (Equations 5.2 and 5.3), a best-fitted curve on the basis of minimizing the squared root of the errors between the intact changes is employed. In this way, readily depending on the fundamental period and some other system dependent parameters the modification factors to taking into account an inelastic behavior are obtained. In Equations (5.2) and (5.3) - the term  $C_{\text{degraded}}$  indicates the modification factor that modifies the smooth elasto-plastic system responses. Correction ratio provided with respect to linear elastic ordinates. This factor reveals the effect of hysteresis capacity degradations beyond the yielding points.  $C_{\text{Pinched}}$  is a hysteresis pinching modification factor and can be employed to incorporate pinching consequences on drift spectrum ordinates.

What is necessary to note is that the presence of the more than one effect that deviates from elastic behavior. The multiplication of the several  $C_{\text{xx}}$  factors shows a matter of multiple factors, which in turn make it hard to offer an explanatory comment. That is why; it is preferred to represent the yielding and post yielding degradation consequences only into one factor rather than the multiplication of several adaptation factors.

### **5.3.1 The Modification Factor for Degraded Smooth Elastic-plastic Systems ( $C_{\text{degraded}}$ )**

The drift spectrum ordinates can be enhanced due to yielding at elastic-plastic systems. This enhancement varies relying on many parameters; the smoothness elastic-yield transition rate,  $N$ , and the post-yielding hysteresis deterioration in stiffness and/or strength. The difference between the M+S.D. drift spectrums for both elastic and inelastic systems is extrapolated to obtain the rate of drift demands enhancement. The smoothness parameter for elastic-yield transition  $N$  is mutated from the sharp transition rate ( $N = 20.0$  or  $10.0$ ) to the smooth transition ( $N = 1.0$ ). Then a mean plus standard deviation drift spectrum of all selected ground motions for each case is calculated. The reduced spectrum is compared with the corresponding elastic M+S.D. drift spectrum, and thus the differences between them

are found. As a result of the regression analysis on intact variation ratios between them, the best fitted smooth curves are calculated. Hereby, depending on vibration period and some other variables, the smoothed elastic plastic modification factor that takes into account the inelasticity rise from rate of the smoothing elastic plastic transition is obtained readily. The M and M+S.D. drift spectra belong to the smooth elastic-plastic systems while  $N=2.0$  are shown in Figure (5.2).

The “CurveExpert Professional” which is a cross-platform solution for curve fitting and data analysis is adopted for regression analyses (Hyams, 2014). Data can be finely-modelled with the use of desired toolbox, such as smoothing methods, linear and nonlinear regression models, or different types of splines and/or more than 60 models are resident but user defined regression models could also be defined. Full-featured graphing ability of the program permits full investigation of the curve fit as well. The procedure of looking for the best fit could be automated by letting CurveExpert compare the desired data collection to each model to pick out the best fitted curve.

In CurveExpert, the nonlinear models have been divided into families based on their characteristic behavior. The Power Family involves raising one or more parameters to the power of the independent variable, or raising the dependent variable to the power of a given parameter. The result shows that the “Modified Hoerl model” from the power low function family gives the best fitted curves to discrepancies between the modified IDR ordinates when compared to corresponding elastic demands (Hoerl and Kennard, 1970). The simple expression for the degraded smooth elastic plastic systems ( $C_{\text{degraded}}$ ) is given in Equation (5.4).

$$C_{\text{degraded}} = ab^{1/T}T^c \quad (5.4)$$

Where a, b and c are the system-dependent parameters estimated by least squares curve fitting and the fundamental period of intended frame structure, a, b, c parameters and performance of fitted curves related to  $C_{\text{degraded}}$  expression is

examined in two phases (1) for non-degraded smooth elastic plastic model and (2) for degrading smooth elastic-plastic model.

### **5.3.1.1 The $C_{\text{degraded}}$ Variation with Smoothness Rate of Elastic-Yield Transition**

Both (1) the parameter to smoothness transition rate of elastic to yielding and (2) hysteresis decays over the yielding point are incorporated through the  $C_{\text{Degraded}}$  factor. In the first step, only the N parameter is changed and the consequence of transition rate variation on drift demands is investigated thereafter the results of the post-yielding hysteresis decay variations are clarified.

The a, b, c constants and performance of fitted curves related to the  $C_{\text{degraded}}$  expression is listed in Table 5.2. To facilitate comparison and to examine the performance of the fitted curve, the period range is divided into five intervals (0.3-0.5 s, 0.6-1.0 s, 1.1-1.5 s, 1.6-2.0 s and 2.1-2.4 s). These five period intervals will be indicated as very short, short, medium, long and very long period intervals, respectively. For each period ranges coefficient correlation (r) and standard error (s) are listed in Table 5.2. The table presents the quantities of parameters a, b, c along with the correlation coefficient (r) value for different smoothness rates and post yielding degradation levels.

The error section in Table 5.2 gives information on the curve fit performance. Two quantities are used to declare the “goodness” of a particular curve fit: the correlation coefficient (r), and the standard error (s) of the estimate. Generally, the correlation coefficient varies from 0 to 1, with a correlation coefficient of 1 being the best. The standard error will be strictly positive, with smaller standard error representing the better curve fit. In the course of calculating the standard error of the estimate and correlation coefficient, an accumulation of differences between the curve fit and data points and the mean and the data points takes place. The standard error of the estimate is a measure for the accuracy of predictions. The standard error and the chi-

square value are very similar, but defined differently. The chi square is explained in Equation (5.5):

$$X^2 = \sum \left( \frac{Y - Y_i}{\sigma_i} \right)^2 \quad (5.5)$$

While the standard error is defined as Equation (5.6)

$$S = \sqrt{\sum \frac{(Y - Y_i)^2 / \sigma_i^2}{(N - N_p)}} \quad (5.6)$$

Using Equations (5.5) and (5.6) the Equation (5.7) is obtained.

$$S = \sqrt{\frac{X^2}{(N_p - N_{pp})}} \quad (5.7)$$

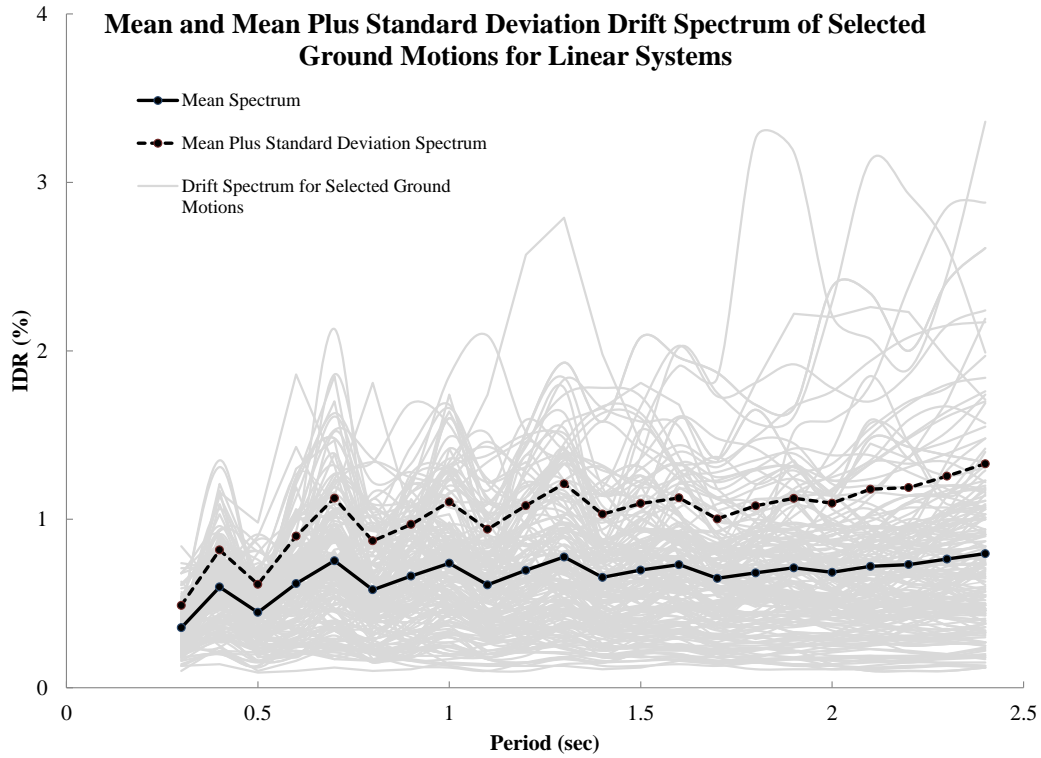
Symbolization is used in Equations 5.5 -5.7, were defined by Hyams (2014) as follow:  $N_p$  is the number of data points;  $\sigma_i$  is the standard deviation (uncertainty) at point  $i$ ;  $N_{pp}$  is the number of variables in the model that is being optimized; and  $Y_i$  is an arbitrary nonlinear model appraised at the  $i$ 'th data point (Hyams, 2014). This merit function simply measures the accord between the parametric model and the data points; a smaller quantity for the merit function symbolizes better conformity. Prevalently, this merit function is named the chi-square or/and standard error.

The drift spectrum ordinates can be enhanced due to yielding at elastic plastic systems and this enhancement can be varied depending on many parameters. The difference between the M+S.D. drift spectrums for both elastic systems and inelastic systems, with different smoothness rate for elastic-yield transition, is handled to calculate the modification coefficients. Figure 5.2.a and 5.2.b illustrates the Mean and Mean plus standard deviation drift spectrum with (1) elastic systems and (2) non-degrading elastic-plastic systems with the smoothness transition of  $N=2.0$ . Likewise, the post yielding hysteresis degradation (i.e. decay at stiffness and/or

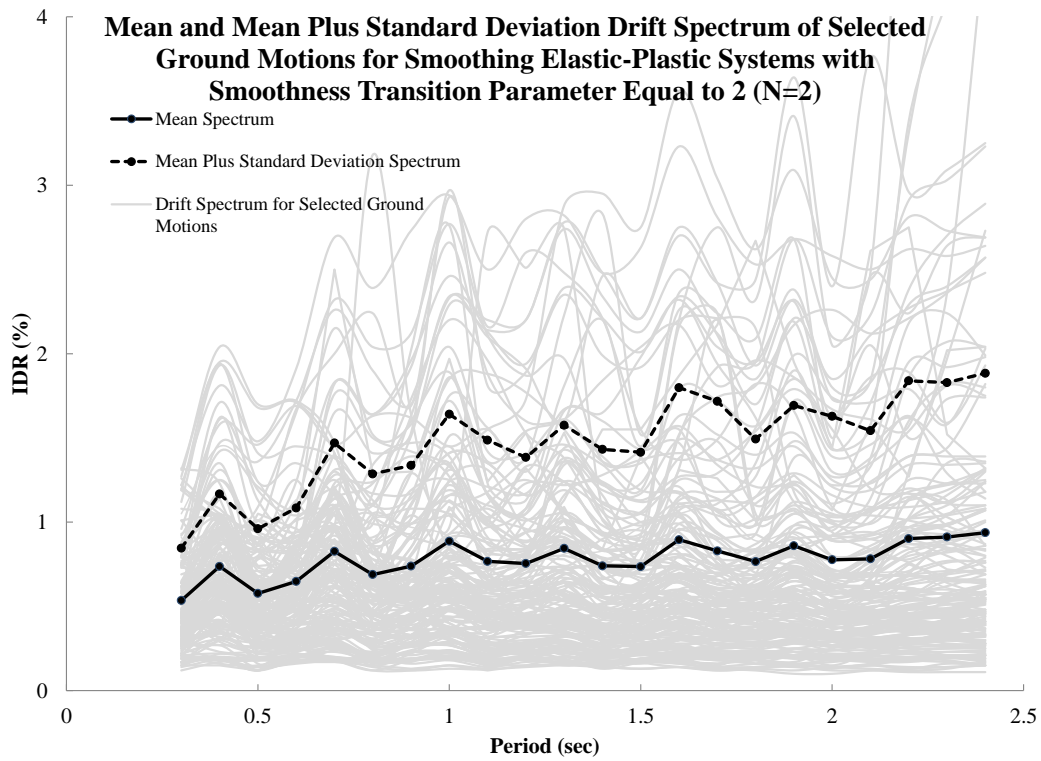
strength) are not included in spectrum calculations. The peak ground acceleration of all selected records that are applied in drift spectrum derivation process is scaled to (PGA=0.35g). As already mentioned, the M (and M+S.D.) drift spectra are constructed from interlinked mean MIDR's of individual periods. The M+S.D. drift spectrum of various cases are selected as baseline relative to corresponding elastic demands and those are used to extract the modification coefficient ratios. The process in kind will be conducted and repeated in the following sections, in order to extract the correction factors for structural systems exhibiting inelastic behavior when subjected to severe cyclic loading, but to save space such repetitive tasks are not shown and only the comparison of results will be provided.

Figure 5.3 illustrates the variation trend of the  $C_{\text{degraded}}$  factor throughout the wide period ranges (0.3 s - 2.4 s) for systems with different smoothness transition rates. The hysteresis degradation (i.e. decay at stiffness and/or strength) is not included in these graphs of functions.  $N = 20$  symbolizes the sharp elastic to post-yielding transition level, similar to the bilinear type, and  $N = 1$  represents the smoothest transition rate. It is observed that the IDR demand for smooth transition rates climbs around 130-150 percent and this enhancement proportion almost levels out over the wide period range for the elastic-plastic systems with smooth transition in the vicinity of 1-2. I.e., through the consideration of the elastic-plastic system with smooth elastic-yielding transition, response drift demands can be increased about 130- 150 percent relative to drift demands of linear systems.

Nonetheless, a steep rise in the response demand trend is seen for sharp transition level ( $N = 10$  or/and 20). This increment stepping up in the IDR demands exceeds 200 percent for flexible systems with long periods. Such steep rise does not seem to be reasonable or caused by the smooth transition level itself, neither in terms of energy entry to the structure nor material properties changes. None of them can lead to such augmentation on the response IDR ordinates. To get a closer look at this unexpected behavior, IDRs at the story capacity curves level are discussed in Figures 5.4 and 5.5.



**(a) Linear Systems**



**(b) Smoothing Elastic Plastic Systems (N=2)**

Figure 5.2 Mean and mean plus standard deviation drift spectrum for selected ground motion records (a) elastic systems; (b) smoothing elastic plastic systems (N=2)

Table 5.2 Control parameters that control the  $C_{\text{degraded}}$  and  $C_{\text{pinched}}$  factors with different intensity levels and correlation coefficient (r) and standard error (s) of fitted curves at each period interval.

Definition	Param.	System dependent Parameters			Period Interval (s)											
					Overall Period		0.3-0.5		0.6-1.0		1.1-1.5		1.6-2.0		2.0-2.4	
		a	b	c	r	s	r	s	r	s	r	s	r	s	r	
<b>Elastic–yielding Transition Level in Non Degrading Smooth Elastic–Plastic Systems</b>																
Elastic–Yielding Transition Level	N=20.0	1.747	1.049	0.295	0.834	0.073	0.614	0.052	0.835	0.058	0.583	0.055	0.356	0.032	0.688	
	N=10.0	1.496	1.137	0.367	0.814	0.010	0.880	0.007	0.996	0.067	0.186	0.059	0.152	0.045	0.272	
	N=4.0	1.309	1.180	0.310	0.701	0.064	0.397	0.014	0.905	0.039	0.292	0.030	0.630	0.029	0.315	
	<b>N=2.0</b>	<b>1.147</b>	<b>1.211</b>	<b>0.216</b>	<b>0.458</b>	<b>0.114</b>	<b>0.712</b>	<b>0.006</b>	<b>0.873</b>	<b>0.011</b>	<b>0.549</b>	<b>0.014</b>	<b>0.541</b>	<b>0.013</b>	<b>0.304</b>	
	N=1.5	1.103	1.215	0.177	0.644	0.113	0.807	0.014	0.824	0.005	0.299	0.005	0.837	0.005	0.816	
	N=1.0	1.021	1.216	0.141	0.757	0.106	0.853	0.023	0.750	0.002	0.315	0.003	0.635	0.003	0.840	
<b>Hysteresis Capacity Degradation while N is equal to 2.0</b>																
Stiffness Decay	$\alpha=10.0$	1.218	1.149	0.183	0.412	0.079	0.606	0.004	0.463	0.013	0.447	0.012	0.669	0.013	0.177	
	$\alpha=4.0$	1.195	1.156	0.170	0.441	0.096	0.555	0.004	0.874	0.006	0.838	0.012	0.422	0.009	0.610	
	$\alpha=2.0$	1.148	1.185	0.169	0.584	0.123	0.614	0.009	0.843	0.007	0.277	0.007	0.744	0.008	0.519	
	$\alpha=1.0$	1.201	1.166	0.158	0.517	0.112	0.595	0.009	0.798	0.007	0.392	0.008	0.665	0.009	0.317	
Strength Deg.	$\beta_1=0.3, \beta_2=0.15$	1.239	1.148	0.142	0.386	0.093	0.680	0.006	0.883	0.007	0.183	0.005	0.834	0.006	0.659	
	$\beta_1=0.6, \beta_2=0.6$	1.224	1.178	0.194	0.406	0.097	0.708	0.003	0.921	0.013	0.213	0.014	0.422	0.012	0.436	
Combined Stiff. and Str. Deg.	$\alpha=2.0, \beta_1=0.3, \beta_2=0.15$	1.169	1.171	0.154	0.530	0.119	0.591	0.009	0.867	0.005	0.438	0.007	0.682	0.008	0.348	
	$\alpha=2.0, \beta_1=0.6, \beta_2=0.6$	1.114	1.210	0.196	0.611	0.136	0.599	0.013	0.685	0.006	0.740	0.010	0.604	0.008	0.653	
<b>Hysteresis Pinching</b>																
Slip Length	$R_s=0.2$	2.207	0.229	-0.133	0.907	0.274	0.674	0.056	0.852	0.019	0.928	0.029	0.445	0.015	0.705	
	$R_s=0.3$	2.175	0.256	-0.110	0.901	0.151	0.919	0.053	0.813	0.018	0.901	0.023	0.559	0.015	0.543	
	$R_s=0.4$	2.141	0.249	-0.124	0.907	0.260	0.763	0.071	0.707	0.021	0.888	0.023	0.647	0.015	0.635	
Slip Sharpness	$\sigma=0.1$	1.680	0.294	-0.057	0.810	0.134	0.907	0.019	0.870	0.010	0.819	0.011	0.139	0.006	0.670	
	$\sigma=0.35$	2.127	0.273	-0.095	0.892	0.106	0.965	0.041	0.853	0.015	0.907	0.021	0.467	0.015	0.278	
	$\sigma=0.55$	2.318	0.270	-0.091	0.857	0.256	0.760	0.067	0.555	0.017	0.890	0.020	0.575	0.015	0.315	
Mean Moment Level of Slip	$\lambda=0.1$	2.635	0.297	-0.048	0.824	0.166	0.939	0.032	0.772	0.013	0.841	0.010	0.738	0.010	0.110	
	$\lambda=0.3$	2.130	0.275	-0.092	0.890	0.105	0.966	0.040	0.853	0.015	0.907	0.020	0.467	0.012	0.544	
	$\lambda=0.5$	1.938	0.235	-0.154	0.922	0.258	0.781	0.089	0.593	0.018	0.934	0.026	0.591	0.015	0.692	

To investigate the reason, why the variation of N parameter can be led to such extreme fluctuations on interstory drift ratios, the spectra are plotted under 1999, Sakarya-EW ground motion record to discuss the drift demands in story level in detail. The drift spectrum dissimilarities with different N are shown in Figure 5.4. The spectra are plotted for the Sakarya ground motion record. The N parameter varies from smooth (N=1, 2) to sharp transition (N=10, 20). The drift spectrum graphs show a local hump in the period around 1.2 s for systems with sharp transition rates. Accordingly, drift demand at the story capacity level is investigated in detail.

The nonlinear time history analyses of the shear frames with period correspond to 0.5, 1.2 and 2.0 s. when exposed to the same ground motion record are conducted. In this way, the capacity curve of each story as well as the interstory drift time at the story that maximum interstory drift occurs (in most cases ground suffered to such interstory drift ratio level) are plotted. To represent the story capacity curve, the story shear force is normalized to cumulative upper story weights then it is depicted versus the IDRs. The story capacity curves (Figures 5.5.a.1, 5.5.b.1 and 5.5.c.1) are drawn at the ground story for the frames with low (0.5 s.), medium (1.2 s.) and high periods (2.0 s.), respectively. In addition the IDR time histories are plotted for the same stories and different smoothness transition levels (see Figures 5.5.a.2, 5.5.b.2 and 5.5.c.2).

As understood from Figure 5.5 in the cases with sharp transition rates, large residual drift is observed which in turn reflects extreme interstory drifts demands on the drift spectrum. The N parameter in SHM in addition to control geometric yielding transition shape but against long odds is closely related to residual drifts. Aside from being an in constant amplitude loop, the hysteresis curve follows a path on the elastic plastic trajectory while the oval shape is of secondary importance. The response hysteresis curve calculated under ground motions will lead to/ or not lead to such residual drifts, that seem to be closely related with this variable.

Likewise, in accordance with experimental results (see Table 3.4), the smooth transition rate,  $N$ , around ( $N=1-2$ ) seems to be appropriate to represent the true behavior of RC column members more realistically. Conformity between the response loops of both the simulations and those of experimental test results confirms this conclusion as well. It is noted that the estimation of residual drift demands includes larger levels than that at assessing maximum drift demands, which indicates that changeability will reduce to larger uncertainties in the residual drift demands estimations. In terms of imposed energy exchange, the smoothness transition rate cannot be led to such an extreme increase at interstory drift response and may be arising from numerical calculation errors.

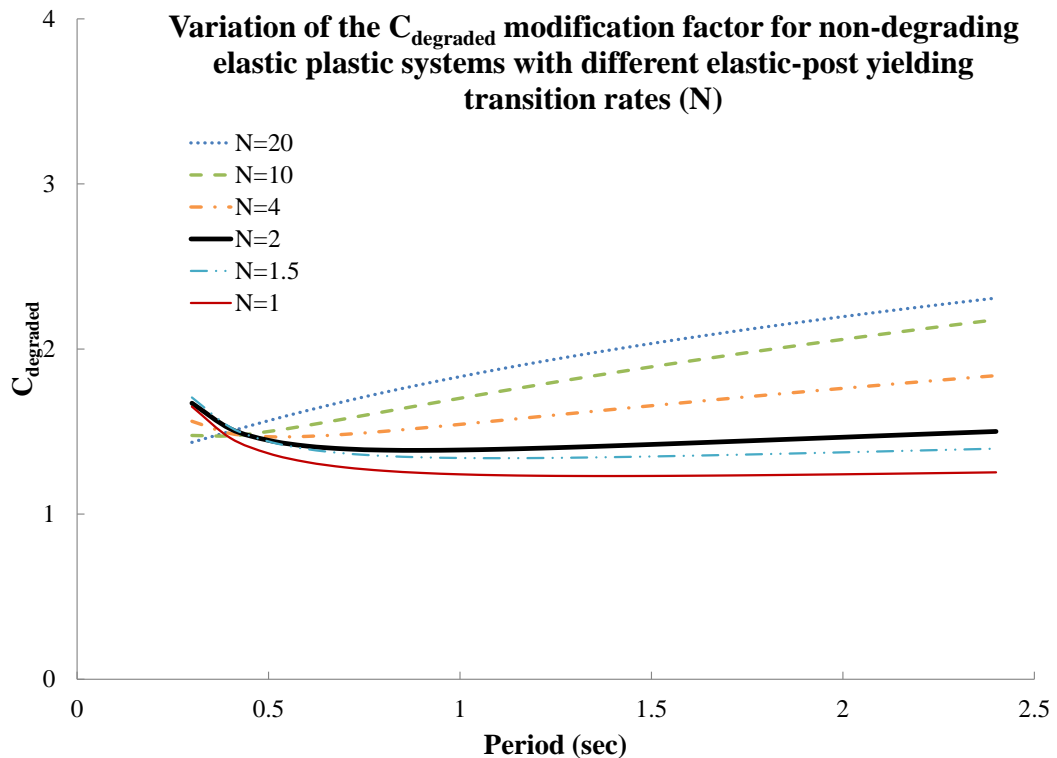


Figure 5.3 Variation of smoothed elastic-plastic modification factor  $C_{\text{degraded}}$ , over the period range for systems with different elastic-yielding transition level,  $N$ . (Here  $N=20$  symbolizes the sharpness transition and  $N=1$  represents the smoothest transition level).

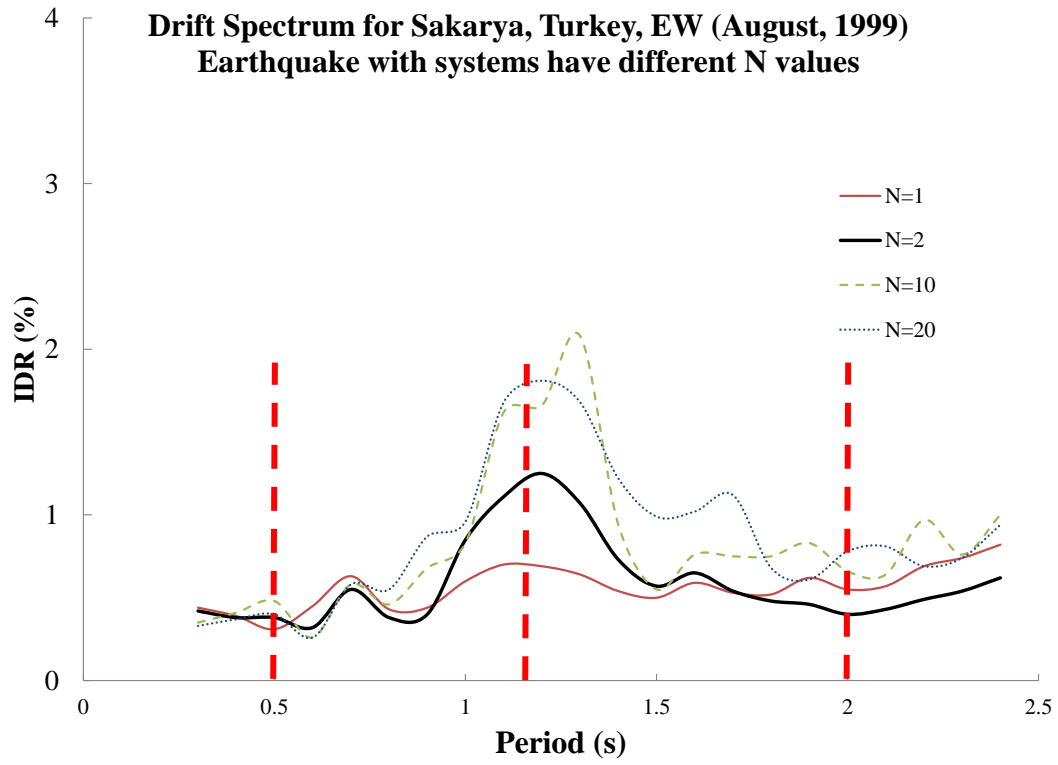


Figure 5.4 Effect of elastic-post yielding smoothness transition parameter, N, on the interstory drift spectrum

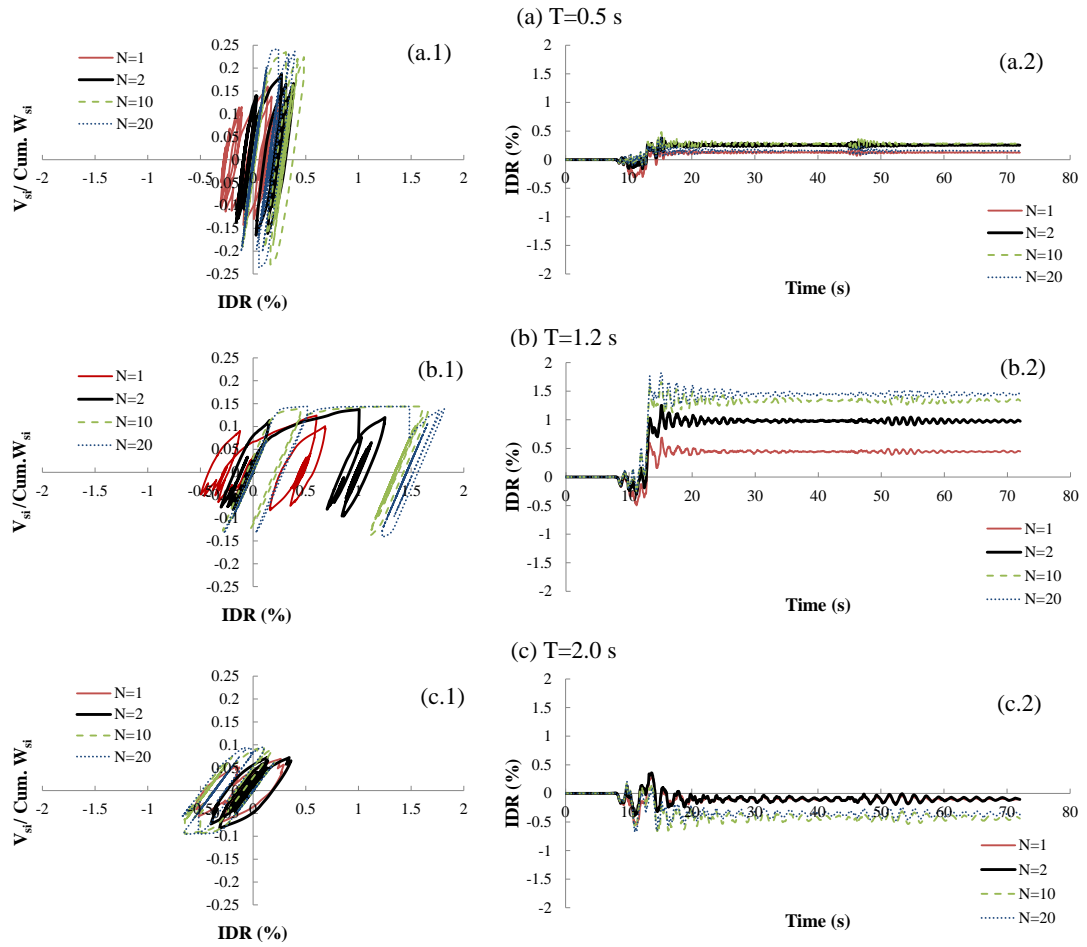


Figure 5.5 Story capacity (a.1, b.1 and c.1) curves and interstory drift history (a.2, b.2 and c.2); at stories with maximum IDR, the shear frames have been used in derivation of interstory drift spectrum under Sakarya-EW record (Figure 5.4). Shear frames have different smoothness transition levels and their periods are 0.5 s. (a.1 and a.2), 1.2 s. (b.1 and b.2), and 2.0 s. (c.1 and c.2), respectively

The important observation revealed here is that the drift spectrum of a linear system returns to zero drift at the end of the ground motion, whereas nonlinear systems at post linear regime may find themselves a new baseline. The residual (permanent) drift represents a measure of the damage exhibited in systems subjected to ground motion. The location of baseline shifting is near to pulses place associated with ground velocity histories.

The damaged buildings may need to be destroyed as a result of extreme permanent horizontal deformation at ground motions (or residual drifts), even though they did not expose extreme damage or partial structural collapse. Therefore, the appraisal of residual drift demands perform a very consequential role in determination of practical knowledge and financial capability of rehabilitation or even retrofitting of buildings that have been damaged due to severe seismic excitations. Besides, a suitable prediction of residual drift demands has demonstrated to be significant in appraising the structural residual capacity and evaluation of probable mechanisms throughout severe ground motions. In particular, the residual drift demands can be prominent when it is considered that the same buildings are subjected to a set of main-shock and following aftershock seismic sequences.

There have been some investigations with the aim of studying the magnitude of residual drift demands, which was derived from the nonlinear dynamic responses of structural systems (Christopoulos and Pampanin, 2003; Pampanin and Christopoulos, 2003; Ruiz-Garcia and Miranda, 2006a and 2006b; Ruiz-Garcia and Negrete-Manriquez, 2011). Some of them were brought to a focus nonlinear response of SDOF systems. Ruiz-Garcia and Miranda (2006) conducted an analytical examination to appraise residual drift demands of nonlinear SDOF systems with predetermined horizontal strength. They stated that residual drift demands normalized relative to maximum elastic drift demands are very impressionable to post yielding stiffness ratio and unloading stiffness on stiffness decay systems; however, they are not much affected with alterations in the ground motion magnitude or epicentral distance ranges. Furthermore, they pointed out that the effect of dispersion (record to record variability) and soil conditions in evaluating the central tendency of residual drift demands is greater rather than the estimation of the peak inelastic drift (or displacement) demands.

Ruiz-Garcia and Miranda (2006b) demonstrated the amplitude and height wise distribution of residual drift demands is considerably affected according to type element hysteresis modelling. They also showed that multistory buildings with elements showing stiffness-decay hysteresis behavior are awaited to experience

lower residual drift demands relative to those structural systems involving elements with non-deteriorating hysteresis properties, due to the fact that they tend to unload with respect to the origin during cyclic excitation. Especially, the level of element unloading stiffness has consequential impact on residual drift demands (that is to say residual drift demands tend to diminution as the unloading stiffness in stiffness-deteriorating models detracts).

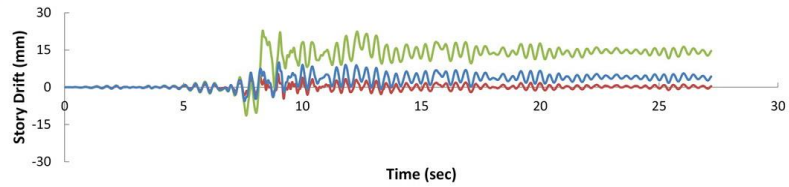
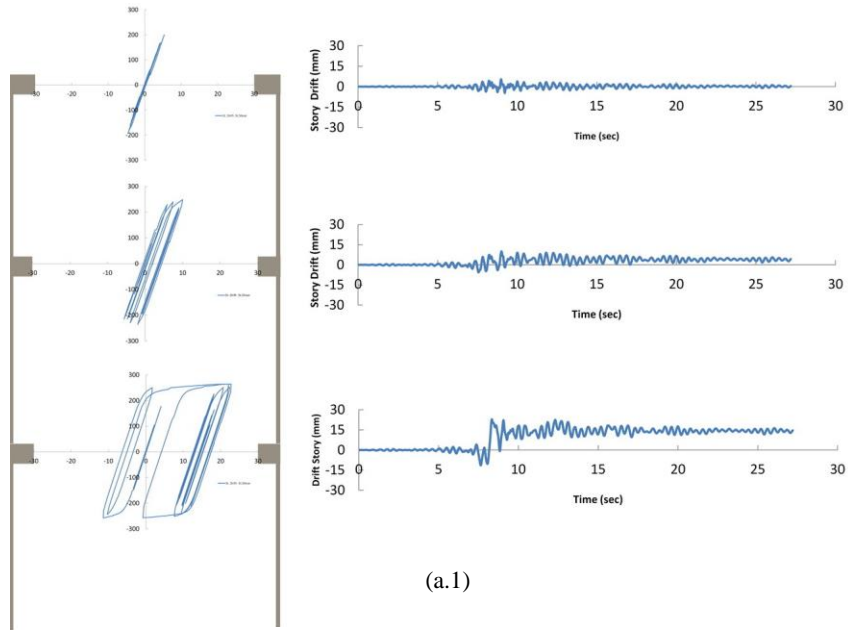
Likewise, they demonstrated that sort of building frame mechanism development under ground motion has a serious impact on the amplitude and distribution of residual drift demands along the frame height. For instance, for building with the identical number of floors, though distinctive vibration periods, building frame mechanism has further effect on flexible structural system (with higher period) toward their rigid complements. In other words, building models undergoing development of an ideal beam-hinge mechanism (weak beam–strong column philosophy) endure modest residual drift demands and a more uniform distributing of residual drift demands when compared with buildings undergoing development of ideal column-hinge or full-hinge frame mechanism (i.e. rigid beam, shear frames which is used in this study).

The other important issue is that residual drift is a good representation for damage but is sensitive to parametric variation throughout the calculations. The new baseline in a very sensitive manner depends on the system parameters, which are at hand and not stable. The effect of parameters that control the smoothness transition rate of elastic to yielding seems to be better than others. Thus a higher  $N$  quantity, which implies a sharp transition rate, amplifies the shift level of the permanent drift. Figure 5.6 illustrates the comparison of the story capacity curves along with the IDR histories for the three story shear frames with fundamental period of 0.4 s. subjected to the Düzce ground motion record. The peak ground acceleration is scaled to 0.3g.

The Figure 5.6 demonstrates the comparison of the time series of drift at the base level under the same record. As seen in the figure the shift level of the base line for the non-degrading system is more than the systems include the degradation

properties, which implies drift demands in addition to ground motion characteristics, and are interlinked with the model parameters, particularly the parameter controlling the rate of smoothness transition from elastic to post yielding region. In other words, the structural system that exhibiting the hysteresis stiffness degradation experience smaller residual drift demands than those those buildings involving members with non-decay hysteresis properties. This is in agreement with the results of Ruiz-Garcia and Miranda (2006b).

It is certain that the residual drift demands assessment includes greater levels of record-to-record mutability compared to assessing maximum interstory drift demands; this implies that the variation will result in greater uncertainty in the evaluation of residual drift demands and it must be clearly taken into consideration while evaluating permanent interstory drift demands in performance based seismic assessment protocol of structural systems. Residual drift is a notoriously difficult quantity to calculate.



(a) Non-degrading system

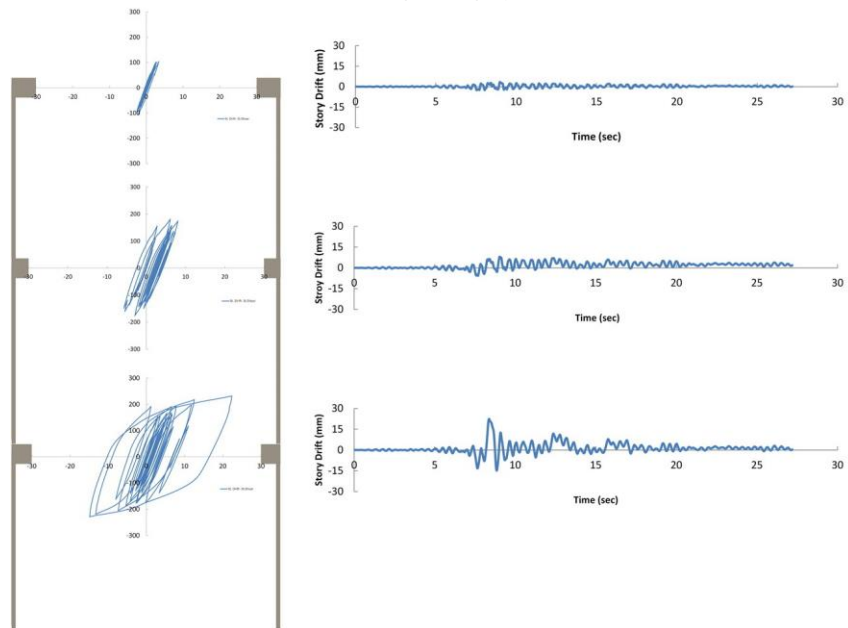


Figure 5.6 The story shear versus story drift (kN-mm); and the time series of the story drift (mm-s) for the three story frame with vibration period of 0.4s under the Düzce ground motion record.

### 5.3.1.2 The $C_{\text{degraded}}$ Variation with Post Yielding Hysteresis Degradations

The choice of a given type of hysteresis behavior in the shear-type frame permits an approximate estimation of the measure of local inelastic drift demand and to provide insight into the overall potential plastic mechanism that may happen during cyclic loading in actual structures. Besides, post yield properties of structural component such as degradation in strength and deterioration in stiffness may meaningfully affect the response to earthquake excitation.

A SHM is taken to model the cyclic response form of the frame columns in each of the floors. This model is expressed precisely in characteristic manner through the model control parameters whichever control the shape of the response loops. This also allows us to calibrate and match the response hysteresis loop with those observed in experimental testing. The force-deformation relationship in RC structures is affected by multitude factors like, the characteristics of the seismic response and the degree of reinforcement details. In situations like this, it is necessary to incorporate over the one form of hysteresis degradation behavior to simulate the hysteresis response as expected.

Hysteresis capacity of material may be decayed over the yielding point after some cycles, such that degradation of the stiffness or the strength or combination of them can be exhibited in response loops, which leads to overestimate drift demands and unexpected damages. The variation of  $C_{\text{degraded}}$  under the influence of post yielding hysteresis degradation is clarified in the following steps. The point that should be mentioned here is that, whereas hysteresis decays of stiffness and strength are examined, the  $N$  parameter is kept constant at  $N = 2$ . Otherwise, this process is also required to identify other parameters better through reducing the number of calculations. The numbers of calculations greatly increased when smoothness rates are changed and if this is added to the changes related to the pinching properties, the number of calculations runs to the thousands or tens of thousands, which make it difficult to draw any certain result. The residual drifts seen in drift demands at sharp transition rates are other reasons to keep  $N$  constant in lower ranges.

The material properties of the structure are changed during the strong ground motions. In particular, in near field ground motion due to pulse type characterizations, the hysteresis capacity of material can be decreased seriously. The stiffness decay and strength degradation are common inelastic behaviors that give rise to over estimations of interstory drift demands and finally lead to critical damages, and ignoring the impact of these behaviors on the IDR demands cannot be done in confidence. Typical ranges of parameters values for hysteresis degradation intensity have been provided by Reinhorn (2007) (Table A-1), and is re-summarized in Table 5.3 in this section, in order to examine the stiffness degradation effect on the drift spectrum, system without stiffness degradation ( $\alpha=200$ ) compared with systems include various stiffness degradation levels ( $\alpha=10, 4, 2, 1$ ).  $\alpha=1$  symbolizes system with severe stiffness degrading.

Table 5.3 Common area of quantities for hysteretic parameters

Parameter	Meaning	Value	Effect
$\alpha$	Stiffness degrading parameter	4	Severe degrading
		10	Moderate degrading
		15	Mild degrading
		200	No degrading (Default)
$\beta_1$	Strength degrading parameter (Ductility- based)	0.6	Severe degrading
		0.3	Moderate degrading
		0.15	Mild degrading
		0.01	No degrading (Default)
$\beta_2$	Strength degrading parameter (Energy -controlled)	0.6	Severe degrading
		0.15	Moderate degrading
		0.08	Mild degrading
		0.01	No degrading (Default)

Structural performance may be affected by decreasing the strength capacity across the reloading phase that also brings about a reduction of the area enveloped through the hysteresis cycles. This behavior can be established upon a progressive development of strength degradation, which is quantified as a function of the hysteresis energy dissipation during inelastic cycles.

The  $C_{\text{degraded}}$  factor also includes the stiffness deterioration,  $\alpha$ ; and the strength degradation ( $\beta_1, \beta_2$ ) properties effectiveness on IDR demands. To investigate the consequence of hysteresis capacity decays (i.e. stiffness deterioration,  $\alpha$ ; strength degradation, including ductility based strength degradation,  $\beta_1$  and hysteresis energy based decay parameter,  $\beta_2$  and combinations of them) on the  $C_{\text{degraded}}$  factor variation, at first the M+S.D. drift spectrum includes hysteresis degradation for selected ground motions are computed and compared with corresponding elastic spectrum ordinates. In this manner the rate of variation is obtained through regression analyses, best fitted smooth curves are found. In doing so, the variables related to degraded modification factor  $C_{\text{degraded}}$  that reflects the influence of post yielding hysteresis deterioration of capacity is easily obtained.

The system-dependent a, b, c variables are listed in Table 5.2, estimated by least squares curve fitting for each degrading level, and controls the degraded modification expression  $C_{\text{degraded}}$  that is given in Equation (5.4). Table 5.2 presents the quantities of constants a, b, c along with the correlation coefficient (r) value for different degradation levels. The performance of the fitted curve is provided for period intervals ranging from very short to very large i.e. (0.3-0.5 s., 0.6-1.0 s., 1.1-1.5 s., 1.6-2.0 s. and 2.1-2.4 s.).

Figure 5.7 illustrates the M + S.D. inelastic drift spectrum with different levels of stiffness degradation in addition to elastic drift spectrum. The Mean and M +S.D. drift spectrums are obtained from interlinking the mean IDR value at each period, which is why the spectrum trends fluctuate over the period ranges. And inasmuch as ordinates alteration with respect to elastic spectrum is desired, therefore the smooth best fitted curves are considered in the calculation of modification factors. What is clear from the figure is that, the stiffness degradation level by itself does not change IDR demands so much.

Figure 5.8 illustrates the change of the  $C_{\text{degraded}}$  over the period ranges length from 0.3 to 2.4 s. Figures 5.8.a, 5.8.b and 5.8.c demonstrate the impacts of stiffness, strength, and combined stiffness and strength deteriorations on the  $C_{\text{degraded}}$

modification factors, respectively. In Figure 5.8.a, the stiffness degradation level is sorted from  $\alpha=200.0$  (no stiffness decay) to severe stiffness degrading, e.g.  $\alpha=10, 4, 2$  and  $1$ .  $\alpha=1$  connotes the system with severe stiffness degradation. Likewise, the strength deterioration with moderate ( $\beta_1 = 0.30, \beta_2 = 0.15$ ) and severe level ( $\beta_1 = 0.60, \beta_2 = 0.60$ ) is reflected in Figure 5.7.b. eventually, the combination of both stiffness and strength degradation is examined in view of the severe stiffness decay of  $\alpha=2$  associated with moderate and severe strength deteriorations (see Figure 5.8.c).

It is seen that similar to the case of non-degrading systems the  $C_{\text{degraded}}$  shows the IDR demands enhancement around 150 percent relative to the elastic drift demands and this rate almost remains steady over the period ranges, i.e. for the systems with low period (stiff structures) going towards the higher period systems (flexible structures). Such increases in drift demands arise from yielding structural members in smooth elastic-plastic systems. It is also understood that strength or/and stiffness deterioration with any severity does not have any considerable effect on drift demands. This is especially true for strength deterioration.

Change in  $C_{\text{degraded}}$  factor under the stiffness decay and strength degradation in different severity over the periods for ranging from 0.3 s. to 2.4 s. is shown in Figure 5.8. The curve in Figure 5.8.a implies that stiffness decays have a little impact on drift demands, so that the trend of  $C_{\text{degraded}}$  change is more or less identical throughout the period ranges. The situation is similar for hysteresis strength degradation or even a combination of them, i.e., the stiffness or/and strength degradation and combination themselves do not show appreciable effect (increase) on the IDR demands. The increase of 150 percent in drift demands might be more relevant to inelastic behavior of smooth elastic-plastic systems than to hysteresis degradation at post-yielding regions.

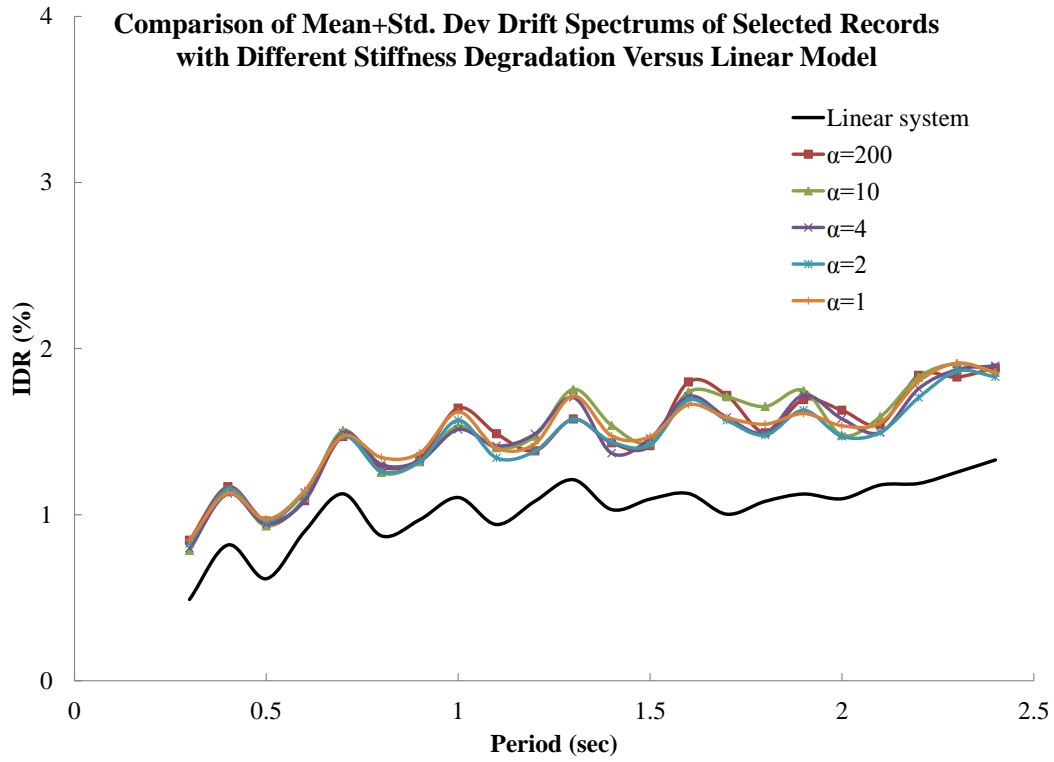


Figure 5.7 The M+S.D. drift Spectrum for systems with different stiffness degradation level

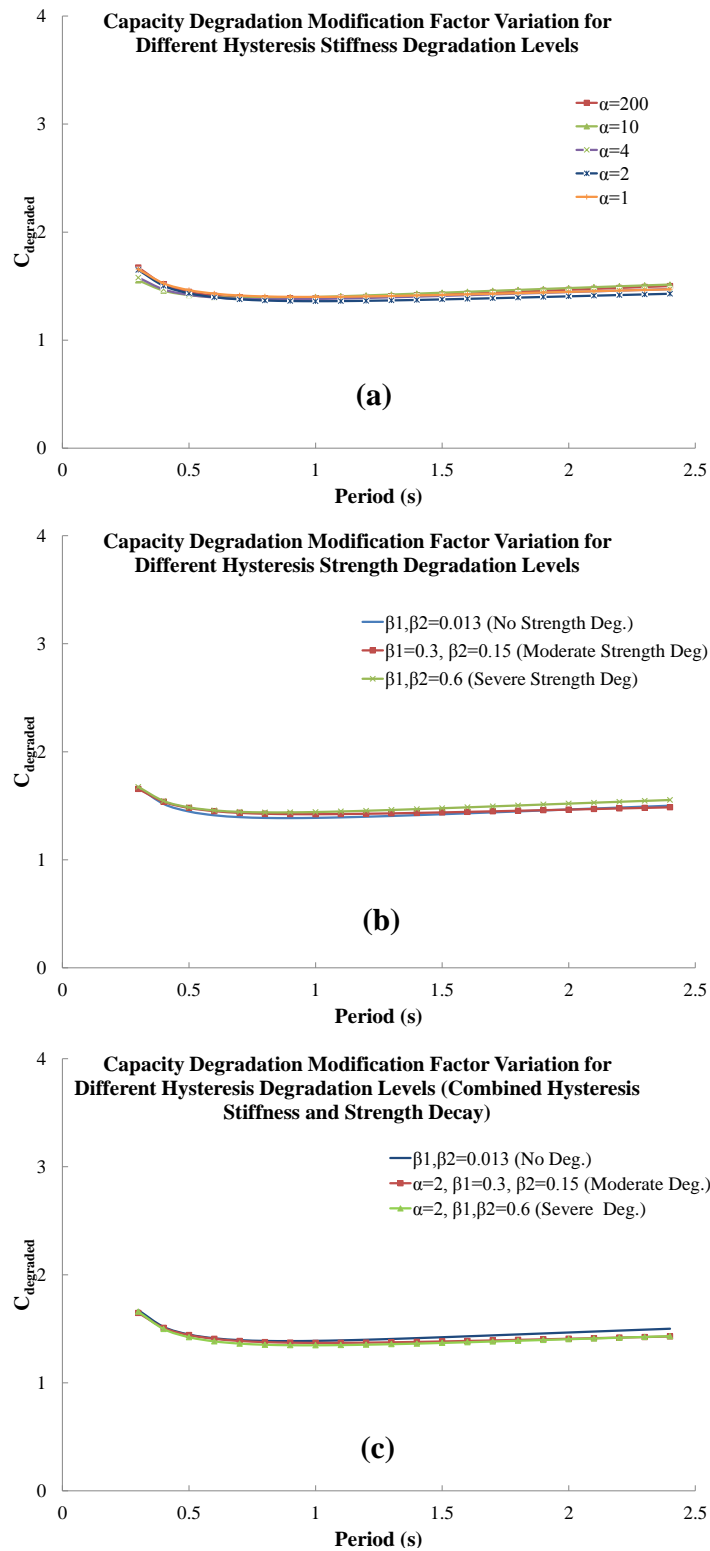


Figure 5.8 Variation of hysteresis capacity degradation modification factor ( $C_{\text{degraded}}$ ) throughout the period range for different hysteresis degradation control parameter levels (a) Stiffness degradation, (b) Strength degradation, (c) Combined stiffness-degrading and strength-decay

In order to examine this observation in more detail, the elastic drift spectrum as well as the inelastic drift spectrum including the hysteresis capacity degradation (combined stiffness and strength degradation) for the Sakarya-EW (1999) earthquake record is pointed out in Figures 5.9 and 5.10. The combination of both stiffness and strength degradation is examined in view of the severe stiffness decay of  $\alpha=1$  associated with severe level strength deterioration ( $\beta_1 = 0.50$ ,  $\beta_2 = 0.55$ ) in Figure 5.9. The drift spectrum for non-degrading systems as well as the system including the severe capacity degradation is shown in Figure 5.9.

The curves in Figures (5.10.a.1, 5.10.b.1 and 5.10.c.1) show the story capacity curves for shear frame systems with low period (0.6 s.), medium period (1.2 s.), and high period (2.0 s.), respectively. Likewise, Figures 0.6 (5.10.a.2), 1.2 (5.10.b.2) and 2.0 s. (5.10.c.2) are related to the corresponding the IDR time history series for the same structural systems. In order to depict a story capacity curve, a story shear force is normalized to cumulative upper story weights and the result is plotted versus IDRs. These graphs are drawn for a closer look at the behavior of post-yielding hysteresis capacity decay effects and its reflections on the IDR's time series. What is reaffirmed is that hysteresis stiffness or/and strength decays or even combined deterioration behavior do not play an important role in the drift demands.

Near fault ground motion records are less affected by deterioration of strength, as they state solely one or two strong pulses at the beginning of time series. However, the IDR demand may be significantly affected by both stiffness and strength deterioration for long-term earthquakes, especially if the time series contain several pulses of identical amplitude, in order that the later pulses may cause to further degradation of strength. In general, the influence of strength degradation or/and stiffness deterioration are minor where the drift demand is concerned.

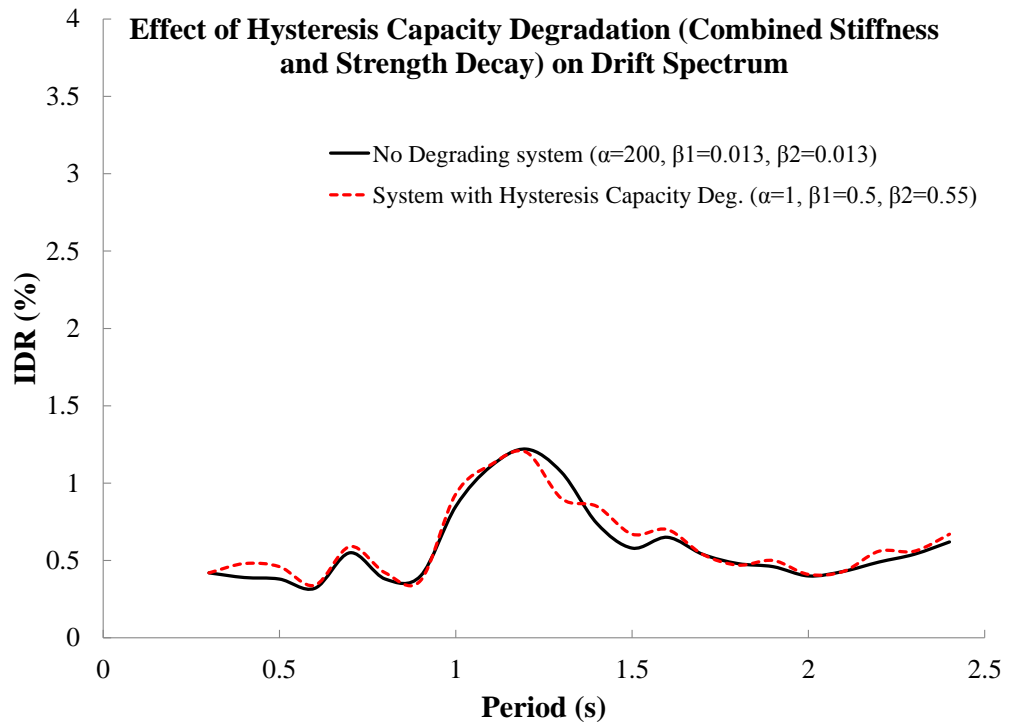


Figure 5.9 Effect of hysteresis capacity degradation (combined stiffness and strength degradation), on the interstory drift spectrum for Sakarya-EW record

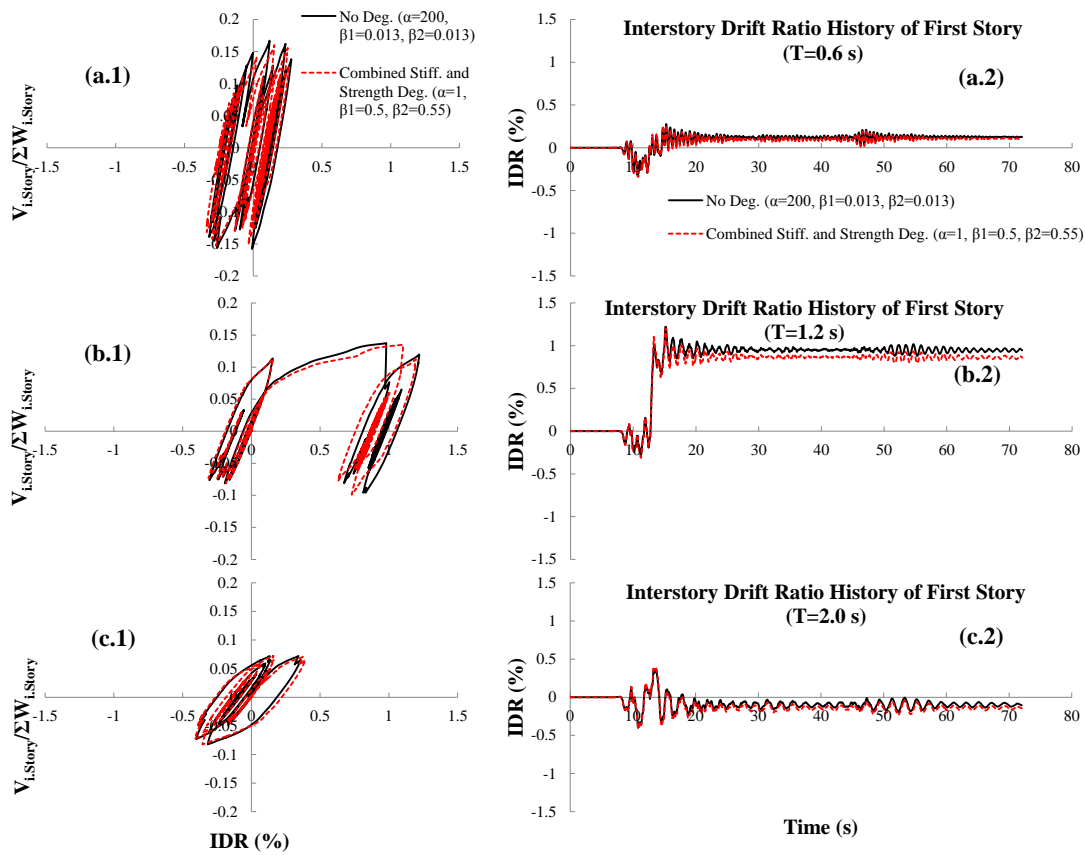


Figure 5.10 The story capacity (a.1, b.1 and c.1) curves and interstory drift time series (a.2, b.2 and c.2) at stories with maximum IDR, for the shear frames have been used in the derivation of the interstory drift spectrum under the Sakarya-EW record (Figure 5.9). Shear frames have hysteresis capacity degradation (combined stiffness and strength degradation) and the periods are 0.6 s. (a.1 and a.2), 1.2 s. (b.1 and b.2), and 2.0 s. (c.1 and c.2), respectively

### 5.3.2 The Modification Factor to Incorporate Hysteresis Pinching Properties

( $C_{\text{pinched}}$ )

Pinching is another principal attribute for hysteresis behavior. The hysteresis loop pinching is as a result of the opening and closing the cracks in reinforced concrete elements or bolt connection slip in steel members under load reversal. Apparent pinching in response loop is characterized in the SHM through three parameters;  $R_s$  Slip Length;  $\sigma$  Slip sharpness; and  $\lambda$  mean moment level of slip, such that the adjustment of each one or a combination of them shapes the response loops. The hysteresis pinching modification factor  $C_{\text{pinched}}$  is used to incorporate the influence of the systems including apparent pinching in response loops with different intensities, into the drift spectrum ordinates. Meanwhile, the  $C_{\text{pinched}}$  factor is also represented with respect to the elastic drift demands.

In order to investigate the effect of hysteresis pinching properties of structural systems on drift spectrum ordinates, the related model parameters are varied around the identified values those have been obtained from comparison of the analytical models with experimental results (see Table 3.4). These parameters reflect the pinching intensities and enable us to adjust pinching to desired rates. In the examination process for each of the parameters, the other quantities are kept unchanged.

In order to derive the correction factor between the elastic and inelastic drift demands, the M +S.D. drift spectrum of each one is compared. As result regression analysis is adopted to best fit a smooth curve that represents the changes toward the elastic drift demands. The regression analysis shows that best fitted smooth curve function for this coefficient is the “Shifted Power Model” (Hyams, 2014). The simple expression for  $C_{\text{pinched}}$  is shown in Equation (5.8).

$$C_{\text{pinched}} = a(T - b)^c \quad (5.8)$$

The system-dependent  $a$ ,  $b$ ,  $c$  constants and performance of fitted curve for the  $C_{\text{pinched}}$  factor expression that represent different pinching levels are listed in Table 5.2. The parameters are assessed by least squares curve fitting. For evaluation of the fit curves, the overall period ranges are divided from very short to very long periods (0.3-0.5s, 0.6-1.0s, 1.1-1.5s, 1.6-2.0s and 2.1-2.4s). A high correlation coefficient resulting for each period interval implies that the fitted curve reflects the variation ratios with high accuracy.

The  $C_{\text{pinched}}$  variation graphs along with the period ranges are plotted in Figure (5.11). Figures 5.11.a, 5.11.b and 5.11.c belong to the slip length, slip sharpness and mean moment level of slip effects respectively. The parameters change around the values that were obtained during the identification procedure (see Table 3.4), and somehow they reflect the intensities of related properties that are apparent in the response loop. The concept clearly understood from this graph is that in general, pinching properties affect the drift demands very strongly. According to pinching rates drift spectrum ordinates can be increased up to 170-270 percent when compared relative to corresponding elastic demands. It is shown that the least influences belong to the slip length factor in analogy to other pinching parameters. Likewise, the slip length biases the IDRs slightly around 5 percent; however, slip sharpness and mean moment severity altered the drift demands respectively up to 30 percent and 60 percent. In the meantime, the seismic responses of stiff systems increase much more than high-period flexible structure demands. The general trend of the  $C_{\text{pinched}}$  factor is that it decreases when going to higher periods.

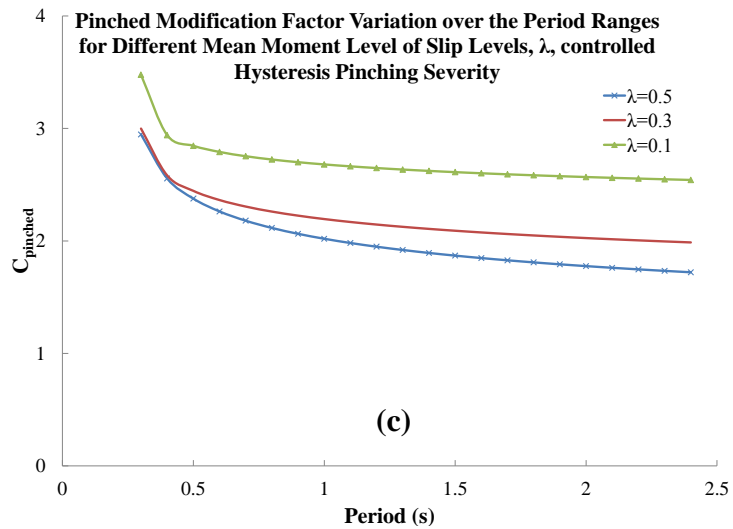
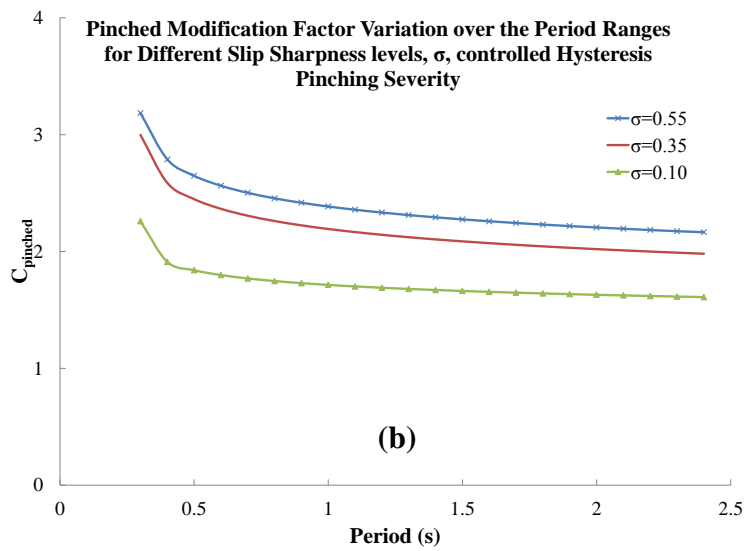
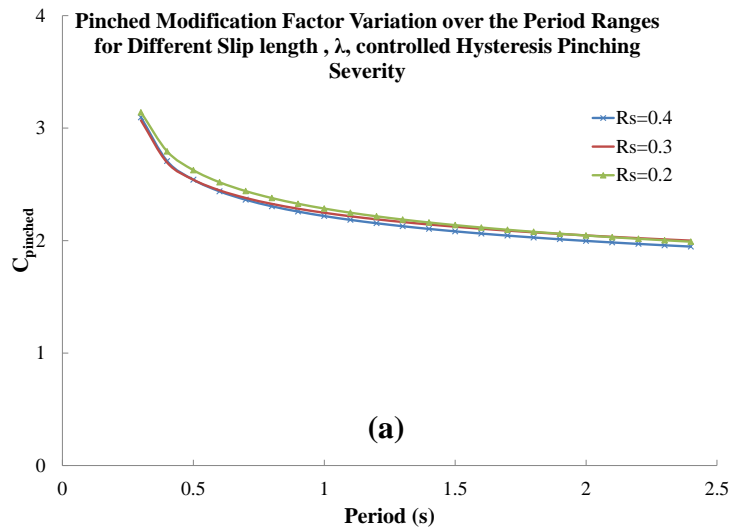


Figure 5.11 Variation of pinching modification factor ( $C_{\text{pinched}}$ ) throughout the period range for different pinching control parameter levels (a) Slip length parameter,  $R_s$ ; (b) Slip sharpness parameter,  $\sigma$ ; (c) Mean moment level of slip,  $\lambda$

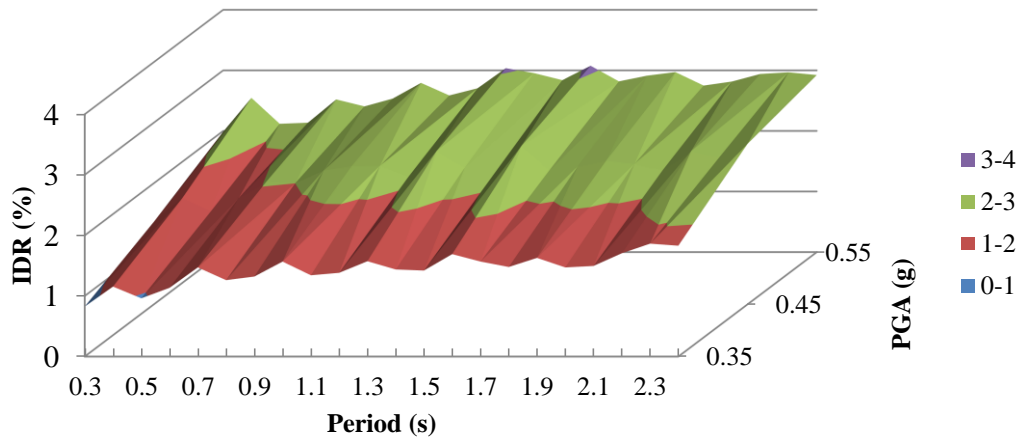
#### 5.4 Effect of PGA Intensity on the $C_{\text{pinched}}$ Factor

To answer the question, how much the  $C_{\text{pinched}}$  factor affected when structural systems are exposed to earthquakes at distinctive hazard levels, calculations are repeated for ground motions with PGA scaled to 0.35g, 0.45g and 0.55g, respectively. The modification factors are calculated from differences between the M+S.D. drift spectrum of inelastic systems and corresponding elastic spectrum ordinates.

Figure 5.12 shows the M + S.D. drift spectrum surface as a function of period and scaled factor intensities for the structural systems containing pinching in their response loop. It is seen that the gradual increasing trend is identical at each hazard level in order that high intensity results in large IDR demands. The elastic IDR ordinates for high risk level are located between 2-3 percent whereas this ratio range varies around the 3-4 percent for systems including the pinching properties. This implies that for the current hazard level onset of inelasticity in the systems containing the pinching is as expected.

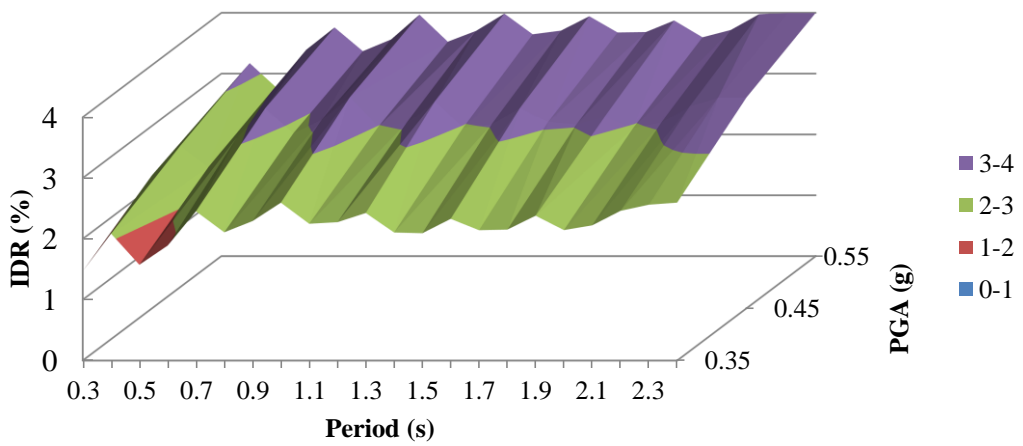
Figure 5.13 illustrates the variation trend for the  $C_{\text{pinched}}$  factor at different hazard levels. It should be noted that this factor symbolizes the modification rates between the drift demands of smooth elastic-plastic systems include the pinching at response loops, relative to the linear systems demands. It is observed that the  $C_{\text{pinched}}$  remains unchange and the system dependent parameters that control the factor expression are valid for higher hazard levels as well.

**Surface of Linear Drift Spectrum as a Function of PGA's of Scaled Selected Records**



(a) Elastic Systems

**Surface of Drift Spectrum of Pinched systems as a Function of PGA's of Scaled Selected Records**



(b) Pinched Systems

Figure 5.12 IDR surface as function of period for different peak ground acceleration intensity for: (a) Linear systems (b) Pinched system

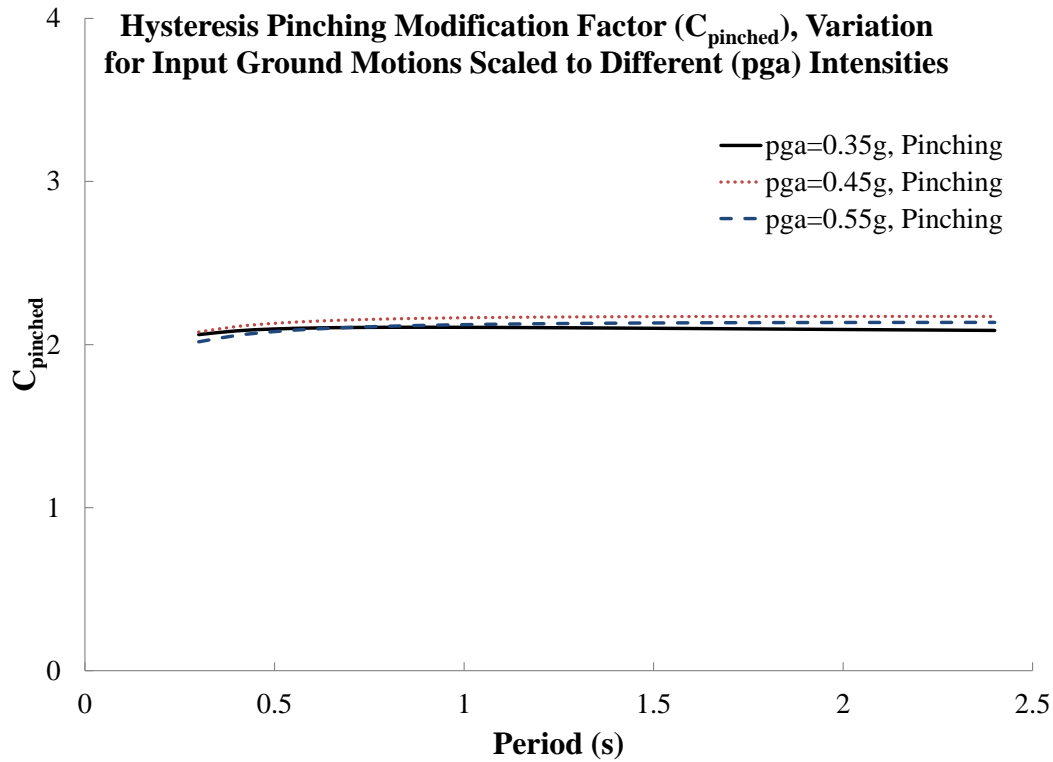


Figure 5.13 Pinched modification factor variations for selected earthquake records scaled to different peak ground acceleration intensity

### 5.5 Effect of Peak Ground (a/v) Ratio on Drift Spectrum

The peak ground acceleration to peak ground velocity ratio (a/v ratio) is broadly acknowledged as an estimator for the frequency content of ground motion records. a is in g, and v is in m/s. The a/v ratio characteristics of ground motion records are used to reveal the influence of frequency content on seismic demands. In the data collection of earthquake records, three sets of near field ground motion records are picked out to represent records in low, intermediate, and high a/v ranges with over 60 records in each group. This number of ground motions is an indication of the reliability of statistical examination. Here it is necessary to be reminded that the ground motions with (a/v < 0.8 g/m/s) are systematically arranged as the low range, whereas those with (a/v > 1.2 g/m/s) are arranged into the high ranges, between these quantities are sorted into intermediate ranges (0.8 g/m/s < a/v < 1.2 g/m/s).

The M+S.D. drift spectra of elastic and inelastic systems are computed for each group (see Figure 5.14). These sequences of operations are conducted for; (1) the linear elastic systems; (2) the non-degrading smooth elastic plastic system ( $N = 2$ ,  $\alpha = 200$ ,  $\beta_1$  and  $\beta_2=0.013$ ); (3) the smooth elastic plastic systems containing the stiffness degradation in hysteresis loop ( $N = 2$ ,  $\alpha=2$ ,  $\beta_1$  and  $\beta_2 = 0.013$ ); (4) including severe strength deterioration ( $N = 2$ ,  $\alpha = 200$ ,  $\beta_1$  ,  $\beta_2=0.6$  ); and (5) apparent pinching in response loops ( $N = 2$ ,  $\alpha = 200$ ,  $\beta_1$  and  $\beta_2=0.013$ ,  $R_s =0.3$  ,  $\sigma = 0.35$ ,  $\lambda=0.3$ ). At this stage, for all calculations ground motion intensities are scaled to PGA on the 0.35.

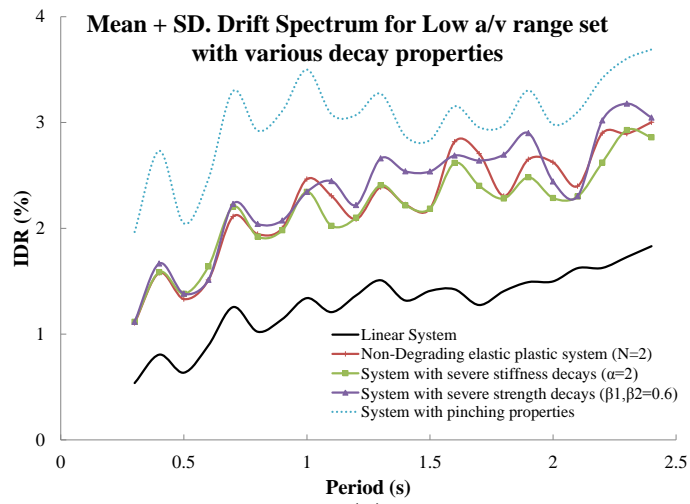
Figure 5.14.a illustrates the M+S.D. drift spectrum for the low  $a/v$  range group. Various hysteresis properties that are commonly seen in existing RC buildings are incorporated into the structural model during the drift spectrum generation procedure. It is important to note that due to the grade of excellence of materials and skillfulness of constructions attainable for RC buildings in multitude regions, it is probable that columns will form end yielding at IDRs less than 1 percent. Poor reinforcement detail and the ductility situation of columns at connection locations and some other reasons can be mentioned to adopt such preparations. As is seen in the graphs, the elastic drift spectrum ordinates exceed 1 percent over the period ranges for the low  $a/v$  range group. In passing this limit, the probability of incidence of nonlinearity could be increased. A general conclusion can be formed that ground motions with low  $a/v$  has great potential to push the structures into inelastic regions. This issue is also confirmed by an abrupt rising of the IDR ordinates arising from yielding of structural members at corresponding elastic plastic systems. It can be seen that post yielding hysteresis degradations are shaded a seismic responses to a negligible amount. An apparent pinching at response loops impresses drift demands considerably (see Figure 5.14). The pinching degradation of the smooth elastic-plastic system elevates IDR ordinates up to 130 percent.

Figure 5.14.b shows the M+S.D. drift spectrum for all systems which are exposed to ground motion records with an intermediate  $a/v$  range. The drift spectrum ordinates for both elastic and non-degrading elastic-plastic systems fluctuate about (almost

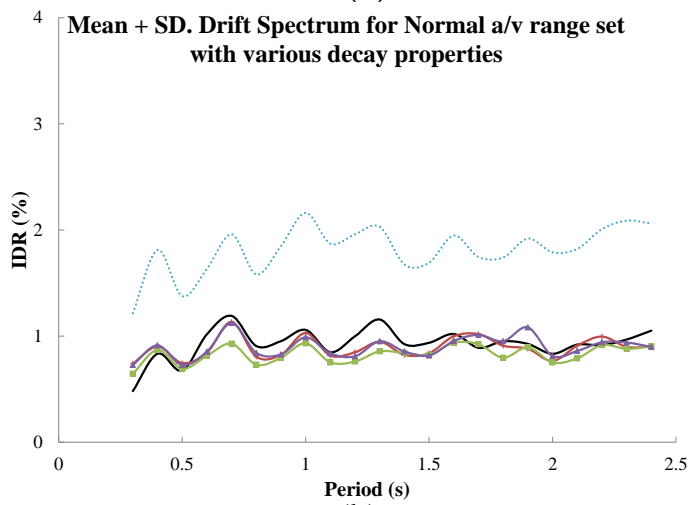
below) the 1 percent, which implies records with intermediate  $a/v$  in this hazard level do not push the code-specified structures into inelastic ranges. However, the pinching at response loops raised the IDR ordinates to 2 percent and this rate makes them prone to severe system damages.

Finally the M+S.D. drift spectra records set with high  $a/v$  ratio are plotted in Figure 5.14.c. The spectrum ordinates imply that all degrading or non-degrading elastic-plastic systems respond to ground motion actions below 1 percent. Although apparent pinching in response loops on system members increase the spectrum ordinates it can be said that the overall behavior of the systems include that the pinching properties remain elastic, such that they more likely do not experience severe nonlinearity behavior during the ground motion with high  $a/v$  ratio.

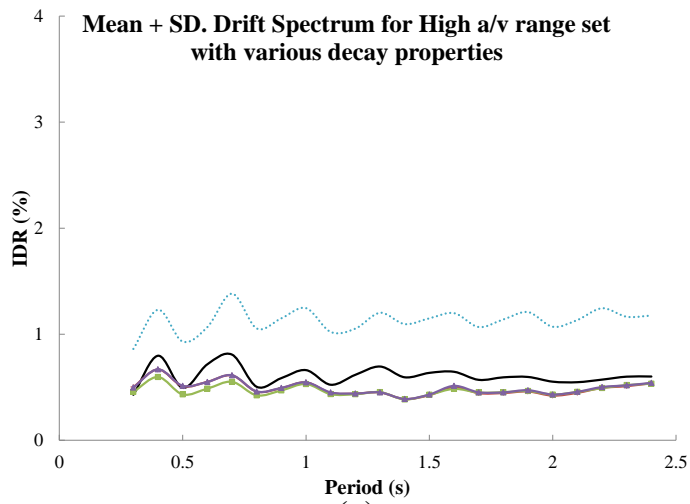
Accordingly it can be said that the peak  $a/v$  ratio is very important from the standpoint of destructive structural effects, i.e. the over-estimated IDR demands lead to severe damages when buildings are exposed to ground motion with lower  $a/v$  ratio. The main reason underlying high destruction capability of records placed in this group is high magnitude ground velocity. The  $v(t)$  term in Equation 2.8 refers to the significance of ground velocity on IDR demands. The comparison of basement plane drift spectra for far-field and near-field earthquakes in linear ranges confirmed the importance of high velocity magnitude on drift spectrum ordinates (Gülkan and Akkar, 2002). The high velocity ground motions (or lower  $a/v$  ratio at ground motion with similar intensities) reduce to higher IDR demands and in turn raised the probability of occurrence of nonlinearity and structural failures.



(a)



(b)



(c)

Figure 5.14 The M+S.D. elastic and inelastic drift spectra (including hysteresis capacity decays and pinching at response loops) for different  $a/v$  ratio ranges: (a) Low  $a/v$ ; (b) Intermediate  $a/v$ ; (c) High  $a/v$  ranges



## CHAPTER 6

### SUMMARY, CONCLUSION AND RECOMMENDATIONS FOR FUTURE STUDIES

#### 6.1 Summary of the Study

During the earthquake ground motions, the structural systems move away from linearity and begin to behave in a nonlinear style and this is established upon different reasons. The exposure of the material to deformation in the partially plastic area or the emergences of second-order effects are non-linear behavioral styles that have been handled by engineering science. In the RC structures, interaction of the two components that form a material manifests itself. Sign-changing displacement and the stiffness and/or capacity degradation, as well as poor adherence and hysteresis pinching are the issues that are not easy to physically formulate. It is difficult to make generalizations about this incident brought about from short overlap lengths or without rib reinforcement and laboratory work is sufficient to act as a general indicator. It is necessary to keep in mind that even if it is possible to insert such nonlinearity constituting rules into the equations results this may yet be outside of the facts.

The problem was decoded for linear shear frames analytically by Westergaard in the 1930s, enabling a rational explanation for the steel frame damage during the 1994 earthquake near field Northridge (e.g., Iwan, 1997). In this study, a generic nonlinearity represented by the Bouc-Wen model is applied. The model originally formulated by Bouc (1967) was later made general and expanded by Wan (1976). To be appropriate for the differential equations this formulation has been very helpful. In this study, maximum interstory drift spectrum (or shortly drift spectrum) which is

used to represent the deformation of linear systems subjected to earthquake motion has been extended to systems with nonlinear behavior through period dependent correction factors. Since, the same can be said for linear drift spectrum, there is no closed form equation to express the drift demands by inserting the ground motion characteristics and periods of shear frames. Therefore, after the nonlinear discrete systems were initially designed, thereafter for the case that systems are linear; the consistency of the results with demand estimates of the Iwan formulation (1997) has been confirmed. The shear frames with different features were produced and exposed to different ground motions. This way, the variation trend between the various maximum interstory drift ratio spectrums is calculated as a function of main period and column properties including the different nonlinear characteristics. For example, the interstory drift demands can be obtained from the combination of more than one parameter, whereas the linear drift spectrum for shear frame with certain ground motion records and certain damping ratios leads to the same value.

In other words, the feature that distinguishes the linear from the nonlinear behavior of structures is the maximum interstory drift that emerges as a simple behavioral indicator, affected by the parameters that do not have a unique combination. The variables discussed in this study, are stiffness, strength, and hysteresis energy loops in terms of pinching and the Bouc-Wen modelling adopted for this aim. The capacity was described on the basis of the document TEC (2007) and for the conditions corresponding to buildings resting on the stiff clay formation, such that the capacity of frame structures were determined for the seismic Zone I; while the effective ground acceleration coefficient and load reduction factor correspond to  $A_0 = 0.4$  and  $R_a = 4$ , respectively.

The shear force capacity of stories in various levels of the frame systems were distributed along the building height according to the requirements provided in the seismic code. In addition, selected ground motions were classified based on peak ground a/v ratios, where 'a' is peak ground acceleration and 'v' is peak ground velocity. Thus, in order to make generalizations, up to a hundred thousand of parameter combinations were examined and the results were extracted. To

generalize results and to achieve a significant consequence at the end of study, the inelastic drift spectrum ratio with respect to corresponding linear systems drift spectrum ordinates was selected to express the method of modifications. Thus the results of thousands of nonlinear/linear ratios through regression analyses were returned to in practice calculations.

In summary, through the selection of an adequate shear frame model, there is the capacity to give a fair appraisal of the seismic response of structural systems at local and global level, several parametric analyses were carried out on many distinctive structural system, and exposed to recorded seismic action of several specifications. This was conducted in the event of acquiring a spectral representation of the most prominent parameters of seismic demand, elastic and inelastic demands in the sense of peak interstory drift ratio, which represents a measure of the influence of post yielding hysteresis behaviors on the drift demands. Interstory drift measures are mutually related with earthquake damage in actual frame buildings and interstory drift restraining suggests that both nonstructural and structural loss is impressively controlled.

A type of nonlinear amplification factor or the linear modification was introduced; these factors were shown as mean + standard deviation curves among scaled ground motion drift spectrums. Since the scattering is intended to refer to the value for each period, therefore the separate tabular forms are required to represent the variables which have “heteroscedastic” characteristics (different variance for each period). Instead of this, the power law expression consequence of each parameter is summarized in a table which is a more simple and effective approach to incorporating this in the accounts. The ratios obtained in this way depend on the vibration period, without the characteristics of ups and downs, so that any results obtained have a smooth curve. The final yield modification factor is the multiplier (usually amplification) factor in reference to the linear drift spectrum.

The most important observation revealed in the present study is that the drift spectrum of linear system is consequent to the termination of the ground motion,

whether there is no residual (permanent) drift or the structural system returns to zero drift, whereas nonlinear systems within a post linear regime may find themselves a new baseline. As an example, Figure 5.5.b shows the new baseline in a very sensitive manner depends on the system parameters which are at hand and not stable. The signs can be changed and the minor variation can be reduced to facilitate great changes in the results. On the one hand, the residual drifts are a good representation for damage but on the other hand their sensitivity to parametric variation throughout the calculations brings to mind thoughts that may mean the proposed modification factor in the report is not the sole correction factor and it is also possible that the calculations lead to slightly different modification factors in the case of using another ground motion set. The residual displacements seem to have probabilistic distributions in themselves, so that they would need to be examined in a separate study.

## **6.2 Conclusions**

This study has been concerned with the question of how the linear drift spectrum may be modified to derive estimates for inelastic systems that may be described with the Bouc-wen type of nonlinearity. There is a wide range of interacting parameters that define the seismic response of shear-type frame structures. When ground motion attributes are included in the range of variables the number of discrete representations increases exponentially. The task was handled through an automated response calculation setup. Inevitably, modification factors fall within statistically definable bands, so that mean and mean plus sigma factors need to be derived.

It is important to mention that the quantitative amounts are presented herein solely for the purpose of giving the idea about the average rates of drift demands variations and the precise percentage values of changes are not concerned. In other words, what is more important in this regard is showing how the variations

occur and which parameter is more effective. The main results obtained from the study are listed as follows:

- (i) The elastic drift spectrum is derived using both the elastic (Iwan, 1997) formulation and response time history analysis method. The proposed derivation is validated using the closed form solution. The validation processes of both methods have shown that the results are in good agreement. It should be noted that slight errors between two adjacent IDR demands may have arisen from the derivation process of each one. The Iwan (1997) formulation requires that the time histories for the ground displacement and velocity should be at hand; which does not always apply because it is a function of the filter exerted to the acceleration time series, and may have drawbacks in integration process.  
Likewise, the same shear wave velocity is used in close form solution which means that the building's height is assumed invariant along the period range, whereas this is unreasonable to develop the generic frame models over such broad period ranges to keep the height unchanged, because there are substantial differences between structural properties of 15-story and 45-story building frames. In the meantime, the different moment of inertia at story levels, which is dictated through story mass and column stiffness variation, leads to deviation in the drift spectrum trend (see Figure 4.9).
- (ii) Yielding of members at the smooth elastic-plastic systems pushes the structures to the inelastic response zone and raises the IDR ordinates. This enhancement is dependent on the smoothness transition rate. For the systems with  $N=2$ , the response shows increases of around 150 percent towards the corresponding elastic IDR ordinates (Figure 5.3). It is seen that the sharp transition rate (i.e.  $N=10$  or  $20$ ) leads to a steep rise in trend of response demands (over the 200 percent) and this is due to abrupt jumps in residual drifts. This abnormality most probably have emanated from cumulative numerical errors in calculations. Such a sudden increase in demand does not seem reasonable; so that neither in terms of input energy nor changes in

mechanical properties of materials, will not lead to such abrupt variations of the drift demands (Figure 5.3).

It is implied that  $N$  parameter in addition to controlling geometric yielding transition shape is also closely related with residual drifts (see Figure 5.5.b). The smooth transition rate in the vicinity of 1-2 is understood to represent the RC column member behavior. Experimental results confirmed this deduction as well (Table 3.4). It is also understood that the strength or/and stiffness deterioration with any severity does not have any considerable effect on drift demands (Figures 5.7 and 5.8).

- (iii) Inelastic drift spectrum ordinates (for a structural system including the hysteresis degradation of stiffness and strength in the response loops) are in high levels, approximately 150 percent, in comparison to the corresponding elastic drift spectrum (Figure 5.8). The variation of the  $C_{\text{Degraded}}$  factor shows the drift demands enhancement is almost constant throughout the period ranges.
- (iv) Increasing of the drift spectrum ordinates is related to yielding of elastic plastic members and it is not because of the hysteresis stiffness degradation over the yielding points (see Figure 5.7). In other words, the post-yield hysteresis capacity degradations (i.e. stiffness or/and strength decay) do not have any significant effect on IDR demands. This is especially valid for hysteresis strength deterioration with any intensity (Figure 5.8).
- (v) Apparent pinching at response loops impresses the seismic demands in high level which makes them prone to serious damages and according to model parameter, the IDR demands for systems include the pinching and can be increased up respectively, within 120 – 180 percent relative to the non-degrading smooth elastic plastic system ordinates and 170- 270 percent with respect to the elastic IDR demands, depending on the parameters that control pinching intensities (see Figure 5.11). It is needed to be reminded again the

quantitative amounts are presented herein just to give an idea about the average rates of drift demands changes and the precise percentage values of changes are not concerned.

- (vi) Between the parameters that control the hysteresis pinching, the least impact belongs to slip length in comparison with other two parameters (Figure 5.11). This effect is maybe below 1 percent.
- (vii) It is seen that the proposed modification factors for capacity decays and pinching properties  $C_{\text{degraded}}$  is valid to ground motions at higher hazard levels (see Figure 5.13).
- (viii) It is observed that the peak ground acceleration to velocity (a/v) ratio is an important index for seismic responses assessment. Lower a/v ratios (or high velocity ground motions) plays a crucial role on abrupt enhancement of the IDR demands and in turn the probability of nonlinearity incidence (initiation of yielding in the system). The IDR responses of the structural systems exposure to the recorded ground motions accompanied by low a/v ratio passed the 1 percent limit, which means that some of the members will be entered into the post yielding zone. The high ground velocity of near fields ground motions lies behind the overestimate drift demands of structural systems.

This result is not surprising to find and is confirmed by ground velocity terms of closed form solution as well (Equation 2.11). The implication is that, the elastic drift spectrum ordinates are placed in higher level for ground motions with low a/v ratio (or high ground velocity) in contrast with records that have moderate or high a/v ratios (see Figure 5.14). The structural systems with apparent pinching behavior in response loops are more vulnerable when subjected to strong ground motions, such that their IDR ordinates for high and intermediate a/v record groups climbs around 200

percent and 300 percent respectively with respect to corresponding IDR elastic demands (Figure 5.14).

### **6.3 Future Studies**

In this study, the drift spectrum using the smooth elastic-plastic structural systems are investigated in terms of various hysteresis degradation properties to determine how well the IDR demands represent the actual building responses when exposed to strong ground motions. Variations of drift demands are clarified with respect to corresponding linear drift spectrum ordinates. Based on the outcomes of this study some future studies are discussed below:

- (i) The various scaling factors could be applied to scaling the ground motion records in order to introduce a sufficient level of nonlinear response of code compliant building models, as an example the energy based scaling method (the Arias intensity factor) could be compared with the uniform peak ground acceleration in the IDR demands estimations when buildings are exposed to ground motions with different hazard level.
- (ii) Various loading patterns might be imposed to derivation of the SHM (or Bouc-Wen model) parameters. In particular, asymmetric loading pattern is the issue that should be examined in detail. Such that the identified control parameter ranges of the SHM, which can be used as initial estimations of desired hysteresis properties during the dynamic analyses, can be examined and updated for different circumstances.
- (iii) The performance of the modification factors can be examined for the generic frames that are subjected to real ground motion records or artificially generated time series that including the impulsive properties. In this manner effect of various specifications of near field earthquake actions, on drift spectrum ordinates can be clarified. The duration of strong shaking;

intensity; magnitude; pulse effects; as well as other frequency contents of the ground motions like, fling step; forward directivity are some of the key parameters that affecting the drift demands. Parametric modelling of a single (or multiple) pulses along with artificial time series is another interesting issue, which can be used to investigate the drift responses under the excitations with different characteristics.

- (iv) Both the degraded and pinched modification factor derivation can be also extended to other types of frame buildings and this can be done by changing the Beam-column stiffness ratio  $\rho$ . Such that for  $\rho \approx 0$  the dominant first mode governing the structure acts as a flexural cantilever; and  $\rho \approx \infty$  refers to the pure shear frames. The parametric variation of this property in turn leads to the strength-beam/weak-column or the weak-column/strength-beam mechanism philosophies. The various  $\rho$  quantities can be examined and the difference between them will be reported. As an example; 0.1, 0.125 (where the dominant first mode governing the structure acts as a flexural cantilever); 0.45, 0.55 (as representative common structures); and goes to infinity (Pure shear frame).
- (v) Effects of some other structural component properties can be considered into the IDR demands calculations as well. Namely, the masonry infill walls and the semi rigid connection of beams (or columns) occupy an important place on IDR demands and can be considered into the calculations.
- (vi) The stiffness distribution patterns are not uniformly throughout the height in most of the buildings due to architectural limitations and etc. In such circumstances (or different stiffness pattern) the modification factors can be affected and this is one key issue that should be studied. In this study uniform stiffness distribution is adopted in frame design. Hence, the distribution of relative stories rigidity is tuned in order that whereas the frame building is exposed to a triangular load configuration, uniform distribution of story drifts throughout the building height is obtained.

- (vii) The residual drift demands can be investigated for the same building that is subjected to a set of main shock and following aftershock seismic sequences. The maximum and permanent (residual) drift demands in the long run of ground motions can be adopted to measure the response of the frame buildings. Likewise, the influence of aftershocks on maximum and residual drift demands of frame models in connection with the frequency content of the major-shock and the major aftershock can be examined. The study do not specifically examine the question of residual displacements, but given that damage quantification must eventually encompass permanent drifts, statistical bound for that variable might be derived.
- (viii) The seismic load reduction factor (or the relative strength factor)  $R_a$ , described as the proportional relation of the necessitate elastic strength demands with respect to the yielding strength of the structural systems and is calculated as  $R_a(T) = \frac{A_0 \cdot I \cdot S(T)}{V_y/W}$ . It is used to define the inelastic demands on structures. In this research  $R_a$  is given equal to 4 for all period ranges, as representative of RC building behavior with nominal ductility level. The degraded modification factor derivation can be repeated for the  $R_a$  values of 2, 6 and 8. It is expected that for short periods structures, the  $C_{xx}$  value be exposed to slight changes depending on the  $R_a$  quantity for all site classes and can be very high for short period and high relative strength structural systems, as it can be seen for modification factor used in target displacement calculations according to the FEMA 356 method (Figure 5.1).

## REFERENCES

- Acun B., 2010. “Energy based seismic performance assessment of reinforced concrete columns”, Ph.D Thesis, Middle East Technical University, Turkey.
- Akkar S. and Gülkan P., 2002. “A Critical near-field accelerograms from the sea of Marmara region earthquakes”, *Bulletin of the Seismological Society of America*, 92(1), pp.428–447.
- Akkar S. and Gülkan P., 2000. “Examination of selected recent ground motion records from Turkey in terms of displacement design procedures”, *Sixth International Conference on Seismic Zonation*.
- Akkar S., Gülkan P. and Yazgan U., 2004. “A simple procedure to compute the interstory drift for frame type structures”, *Thirteenth World Conference on Earthquake Engineering*, Paper No. 2274, Vancouver, B.C., Canada.
- Akkar S., Yazgan U. and Gülkan P., 2005. “Drift estimates in frame buildings subjected to near-fault ground motions”, *Journal of Structural Engineering*, Vol. 131, No. 7, pp. 1014–1024.
- Alavi B. and Krawinkler H., 2004. “Behavior of moment-resisting frame structures subjected to near-fault ground motions,” *Earthquake Engineering and Structural Dynamics*, Vol. 33, pp. 687–760.
- Ali S. M., 2009. “Study of energy dissipation capacity of RC bridge columns under seismic demand”, Ph.D Thesis, N-W.F.P. University of Engineering and Technology, Peshawar, Pakistan.
- Atalay, M. B. and Penzien, J., 1975. “The seismic behavior of critical regions of reinforced concrete components as influenced by moment, shear and axial force”, Report No. UCB/EERC-75/19, Earthquake Engineering and research center, University of California, Berkeley, California.
- Applied Technology Council (ATC-3-06), 1978. “Tentative provisions for the development of seismic regulations for buildings”, Report No. ATC-3-06, Redwood City, California.

Applied Technology Council (ATC-32), 1996. "Improved seismic design criteria for California bridges: provisional recommendations", Report No. ATC-32, Redwood City, California.

Applied Technology Council (ATC 24), 1992. "Guidelines for cyclic seismic testing of components of steel structures for buildings", Report No. ATC-24, Redwood City, California.

Applied Technology Council (ATC 40), 1996. "Seismic evaluation and retrofit of concrete buildings", Report No. ATC 40, Volume I, Redwood City, California.

Baber, T.T. and Wen, Y.K., 1981. "Random vibration of hysteretic, degrading systems", *Journal of Engineering Mechanics*, Vol. 107, No.6, pp. 1069-1074.

Baber, T.T. and Noori, M.N., 1985. "Random vibration of degrading, pinching systems", *Journal of Engineering Mechanics*, Vol. 111, No. 8, pp. 1010-1026.

Baber, T.T. and Noori, M.N., 1986. "Modeling general hysteresis behavior and random vibration application", *Journal of Vibration, Acoustics, Stress, and Reliability in Design*, Vol. 108, No. 4, pp. 411-420.

Bazaez R., and Dusicka P., 2014. "Development of cyclic loading protocol for bridge columns considering subduction zone mega earthquakes", Tenth U.S. National Conference on Earthquake Engineering Frontiers of Earthquake Engineering (10NCEE), Anchorage, Alaska.

Bertero, V. V., E.P. Popov, T.Y. Wang, and J. Vallenias, 1977. "Seismic design implications of hysteretic behavior of reinforced concrete structural walls", *Proceedings, Sixth World Conference on Earthquake Engineering, India*, Vol. II, pp.1898-1904.

Blume, J. A., 1968. "Dynamic characteristics of multi-story buildings", *Journal of the Structural Division, ASCE*, Vol. 94, pp. 337-402.

Booker A. J., 2008. "Performance of continuous and segmented post-tensioned concrete filled fiber tubes", Master Thesis, Washington State University, Pullman, WA, United States.

Bouc, R., 1967. "Forced vibration of mechanical systems with hysteresis", *Proceedings of the Fourth Conference on Nonlinear Oscillations*, Report No. 315, Prague, Czechoslovakia.

Bousias S. N., Verzelletti G., Fardis M. N., and Magonette G., 1992. "RC columns in cyclic biaxial bending and axial load", Tenth World Conference on Earthquake Engineering, pp. 3041-3046, Madrid.

Bozorgnia Y. and Bertero V. V., 2001. "Improved shaking and damage parameters for post-earthquake applications", Proceedings of the SMIP01 Seminar on Utilization of Strong-Motion Data, Los Angeles, California, pp. 1-22.

Bray J. D. and Rodriguez-Marek A., 2004. "Characterization of forward-directivity ground motions in the near-fault region", Soil Dynamics and Earthquake Engineering, Vol. 24, No. 5, pp. 815–828.

Browning J., Warden B., Matamoros A., Lepage A., 2008. "Global and local seismic drift estimates for RC frames", Engineering Structures, Vol. 30, pp. 1262–1271.

Building Seismic Safety Commission (BSSC), 1997a. "NEHRP Guidelines for the seismic rehabilitation of buildings", Report No. FEMA 273, Washington, DC.

Building Seismic Safety Commission (BSSC), 2000. "Prestandard and commentary for the seismic rehabilitation of buildings", Report No. FEMA 356, Washington, DC.

Building Seismic Safety Commission (BSSC), 2005. "Improvement of nonlinear static seismic analysis procedures", NEHRP, Department of Homeland security, Federal Emergency Management Agency, Report No. FEMA 440, Washington, DC.

Building Seismic Safety Commission (BSSC), 2007. "Interim protocols for determining seismic performance characteristics of structural and nonstructural components through laboratory testing", Report No. FEMA 461, Washington, DC.

Chang Ja-Sh. and Lai T-Wu, 2001. "Experimental study on behavior of RC columns under axial compression with bidirectional eccentricities", First International Conference on Steel & Composite Structures, Pusan, Kroea, pp.897-904.

Chang S. Y., 2010. "Experimental studies of reinforced concrete bridge columns under axial load plus biaxial bending", Journal of Structural Engineering, ASCE, pp. 12-25.

Chopra A. K. and Chintanapakdee C., 2001. "Drift spectrum vs. modal analysis of structural response to near-fault ground motion", Earthquake Spectra, Vol. 17. No. 2, pp. 221–234.

Chopra, A.K. and Goel R. K., 2000. “Building period formulas for estimating seismic displacements”, Earthquake Spectra, Vol. 16, No. 2, pp. 533-536.

Chopra. A. K., 1995. “Dynamics of structures: theory and applications to earthquake engineering”, Prentice-Hall. Inc., Upper Saddle River, N. J.

Chopra, A.K. and Goel R.K., 1999. “Capacity-demand diagram methods based on inelastic design spectrum”, Earthquake Spectra, Vol. 15, No. 4, pp. 637-656.

Chopra A.K. and Chintanapakdee C., 2004. “Inelastic deformation ratios for design and evaluation of structures: Single-Degree-Of-Freedom bilinear systems”, Journal of Structural Engineering, Vol.130, No. 9, pp.1309-1319.

Christopoulos C., Pampanin S., and Priestley MJN., 2003. “Performance-based seismic response of framed structures includes residual deformations”, Part I: single-degree-of-freedom systems, Journal of Earthquake Engineering, Vol. 7, No. 1, pp. 97–118.

Consortium of Organizations for strong Motion Observation Systems (COSMOS Strongth-Motion Vitrual Data Center)

[www.cosmos-eq.org](http://www.cosmos-eq.org)

<http://www.strongmotioncenter.org/vdc/scripts/earthquakes.plx>

[Last accessed on 7/30/2014].

Courant R. and Hilbert D., 1962. “Methods of mathematical physics”, Vol. II, pp 192-193, John Wiley and Sons, NY.

D'Ambrisi, A. and Filippou F., 1999. “Modeling of cyclic shear behavior in RC members”, Journal of Structural Engineering, Vol. 125, No. 10, pp. 1143–1150.

Daniel G. Hyams, CurveExpert Professional Documentation, Release 2.0.4.

<http://www.curveexpert.net/>

[Last accessed on 11/03/2014].

Decanini L., Liberatore L. and Mollaioli F., 2003. “Characterization of displacement demand for elastic and inelastic SDOF systems”, Soil Dynamics and Earthquake Engineering, Vol. 23, pp. 455–471.

Decanini L. D., Mollaioli F. and Mura A., 2004. “Simplified shear –type model for that evaluation of the influence of ductility and stiffness distribution patterns on multi-story structures”, XI congress Nazionale (L'ingegneria Sismica in Italia), Genova 25-29 Gennaio.

Díaz O., Mendoza E. and Esteva L., 1994. "Seismic ductility demands predicted by alternate models of building frames", *Earthquake Spectra*, Vol. 10, No. 3, pp. 465-487.

Esmaily-Gh. A. and Xiao Y., 2002. "Seismic behavior of bridge columns subjected to various loading patterns", PEER Report 2002/15, Pacific Earthquake Engineering Research Center, University of California, Berkeley, California.

Goel R K, Chopra A. K. 1997. "Period formulas for moment resisting frame buildings." *Journal of Structural Engineering*, ASCE, Vol.123, No. 4, pp.454-61.

Gülkan P. and Akkar S., 2002. "A simple replacement for the drift spectrum", *engineering structures*, Vol. 24, No. 11, pp. 1477-1484.

Gülkan P. and Yazgan U., 2004. "Inter-story drift requirements for near-field earthquakes", OECD Nuclear Energy Agency-NIED CSNI Workshop on Seismic Input Motions Incorporating Recent Geological Studies Tsukuba, Japan, pp. 15-19.

Gülkan P. and Yazgan U., 2005. "Raised drift demands for framed buildings during near-field earthquakes" J.G. Anderson (eds.), *Directions in Strong Motion Instrumentation*, Springer, Printed in the Netherlands, pp. 61-81.

Heidebrecht, A. C. and Lu, C.Y., 1988. "Evaluation of the seismic response factor introduced in the 1985 edition of the national building code of Canada", *Canadian Journal of Civil Engineering*, Vol. 15, pp. 382-338.

Heidebrecht, A. C. and Naumoski N. D., 1997. "Development and application of a displacement-based design approach for moment resisting frame structures", *Seismic Design Methodologies for The Next Generation of Codes*, P. Faifar, and H., Krawinkler, eds., Balkema, Rotterdam, The Netherlands, pp. 217-228.

Heidebrecht, A. C. and Rutenber A., 2000. "Applications of drift spectra in seismic design", *Proceedings of the Twelfth World Conference on Earthquake Engineering*, Paper No. 290, Auckland, New Zealand.

Hoerl A. E., Kennard R. W., 1970. "Ridge regression: biased estimation for nonorthogonal problems". *Technometrics*, Vol. 12, pp. 55-67.

Hoerl A. E. and Kennard, R. W., 1970. "Ridge regression: applications to nonorthogonal problems". *Technometrics*, Vol.12, pp. 69-82, correction 12, p. 723.

Huang CT., 2003. “Considerations of multimode structural response for near-field earthquakes”, *Journal of Engineering Mechanics*, Vol.129, No. 4, pp. 458–67.

Huang CT. and Iwan WD., 2005. “Generalized damped wave approach for evaluating seismic shear demands”, *Journal of Engineering Mechanics*, Vol.131, No. 12, pp. 1248–1256.

Iwan WD. and Chen X., 1994. “Important near-field ground motion data from the landers earthquake”, *Proceedings of the Tenth European Conference on Earthquake Engineering*, Balkema, Rotterdam, The Netherlands, pp. 229–234.

Iwan W.D., 1997. “Drift Spectrum: measure of demand for earthquake ground motions”, *Journal of Structural Engineering*, Vol.123, No. 4, pp. 397–404.

Java <sup>™</sup> Archive (JAR), a general-purpose, concurrent, class-based, object-oriented computer programming language. Available online; <http://www.oracle.com/technetwork/java/javase/downloads/jdk7-downloads-1880260.html>

[Last accessed on 10/13/2013].

Java <sup>™</sup> Tutorials, The practical guides for programmers who want to use the Java programming language to create applications. Available online; <http://docs.oracle.com/javase/tutorial/>

[Last accessed on 10/13/2013].

Jennings, R. L. and Newmark, N. M., 1960. “Elastic response of multistory shear beam type structures subjected to strong ground motion”, *Proceedings of the 2nd World Conf. on Earthquake Engineering*, Vol. II, Science Council of Japan, Tokyo, pp. 699–717.

Jia-Dzwan J. Sh., YEN W. Ph. and O’Fallon J., 2004. “Handbook for seismic performance testing of bridge piers”, *Thirteenth World Conference on Earthquake Engineering*, Paper No. 1682, Vancouver, B.C., Canada.

Kalkan E. and Kunnath S. K., 2006. “Effects of fling step and forward directivity on seismic response of buildings”, *Earthquake Spectra*, Vol. 22, No. 2, pp. 367–390.

Kanaan, A.E. and Powell, G.H., 1973. “General purpose computer program for inelastic dynamic response of plane structures”, Report No. EERC 73-6, Earthquake Engineering Research Center (EERC), University of California, Berkeley.

Kawashima K., Ogimoto H., Hayakawa R., and Watanabe G., 2006. "Effect of bilateral excitation on the seismic performance of reinforced concrete bridge columns", 8th U.S. National Conference on Earthquake Engineering (100<sup>th</sup> Anniversary Earthquake Conference, Paper No. 567, San Francisco, CA.

Kim J. K. and Lee S. S., 2000. "The behaviour of reinforced concrete columns subjected to axial force and biaxial bending", *Engineering Structures*, Vol. 23, pp. 1518-1528.

Kim J. K. and Collins K.R., 2002. "Closer look at the drift demand spectrum", *Journal of Structural Engineering*; Vol. 128, No. 7, pp. 942–945.

Kim J. K., Collins K.R. and Lim Y.M., 2006. "Application of internally damped shear beam model to analysis of buildings under earthquake: Robust procedure for quick evaluation of seismic performance", *Journal of Structural Engineering*, Vol.132, No.7, pp.1139–1149.

Krawinkler H., 2009. "Loading histories for cyclic tests in support of performance assessment of structural components", *Third International Conference on Advances in Experimental Structural Engineering*, San Francisco.

Krawinkler H, Medina R and Alavi B., 2003. "Seismic drift and ductility demands and their dependence on ground motions", *Engineering Structures*, Vol. 25, pp. 637–653.

Kunnath, S. K., Reinhorn, A. M. and Lobo, R.F, 1992. "IDARAC Version 4.0: A program for the inelastic damage analysis of reinforced concrete structures", *Technical Report NCEER-92-0022*, New York at Buffalo, N.Y.

Li L., Mander J. B., and Dhakal R. P., 2008. "Bidirectional cyclic loading experiment on a 3D beam-column joint designed for damage avoidance", *ASCE Journal of Structural Engineering*, vol. 134, No. 11, pp. 1733-1742.

Liao W. I., Loh CH and Wan S., 2001. "Earthquake response of RC moment frames subjected to near-fault ground motions", *The Structural Design of Tall Buildings*, Vol.10, pp. 219–29.

Matamoros, A. B., 1999. "Study of drift limits for high-strength concrete columns", *Ph.D Thesis*, University of Illinois at Urbana-Champaign, Urbana, Illinois.

Medina R. A., 2004. "Story shear strength patterns for the performance based seismic design of regular frames", ISET Journal of Earthquake Technology, Paper No. 442, Vol. 41, No. 1, pp. 101-125.

Medina R. A. and Krawinkler H., 2005. "Strength demand issues relevant for the seismic design of moment-resisting frames", Earthquake Engineering Research Institute, Earthquake Spectra, Vol. 21, No. 2, pp. 415–439.

Ministry of Public Works and Settlement, 2007. "Specification for structures to be built in disaster areas", Government of Republic of Turkey, (Deprem Bölgelerinde Yapılacak Binalar Hakkında Yönetmelik "DBYBHY", Bayındırlık ve İskân Bakanlığı).

Miranda, E., 1999. "Approximate lateral deformation demands in multistory buildings", Journal of Structural Engineering, Vol. 125, No. 4, pp. 417-425.

Miranda, E., 2000. "Inelastic displacement ratios for displacement-based earthquake resistant design", Proceedings of the twelve World Conference on Earthquake Engineering, Paper No. 1096, New Zealand.

Miranda E., 2000. "Inelastic displacement ratios for structures on firm sites", ASCE Journal of Structural Engineering, Vol. 126, No. 10, pp. 1150–1159.

Miranda, E. and Carlos J.R., 2002. "Approximate lateral drift demands in multistory buildings with nonuniform stiffness", Journal of Structural Engineering, Vol. 128, No. 7, pp. 840-849.

Miranda E. and Akkar S., 2006. "Generalized interstory drift spectrum", Journal of Structural Engineering, Vol.132, No. 6, pp. 840–852.

Mollaioli F., Mura A., and Decanini L. D., 2007. "Assessment of the deformation demand in multistory frames", Journal of Sustainable Energy & Environment (JSEE), Vol. 8, No.4, pp. 203-219.

Mollaioli F. and Bruno S., 2008. "Influence of site effects on inelastic displacement ratios for SDOF and MDOF systems", Computers and Mathematics with Applications, Vol.55, pp.184–207.

Montes R. and Rosenblueth E., 1968. "Shears and over turning moments in chimneys", Proceedings of the 2<sup>nd</sup> Mexican Conference on Earthquake Engineering, Mexican Society of Earthquake Engineering, Veracruz Mexico.

Naumoski N., Saatcioglu M., and Amiri-Hormozaki K., 2004. "Effects of scaling of earthquake excitations on the dynamic response of reinforced concrete frame buildings", 13<sup>th</sup> World Conference on Earthquake Engineering, paper No. 2917, pp. 15.

Naumoski, N., Tso, W.K., and Heidebrecht, A.C., 1988. "A selection of representative strong motion earthquake records having different A/V ratios", EERG Report 88-01, Earthquake Engineering Research Group, McMaster University, Hamilton, Ont., pp. 1-60.

Nishida H. and Unjoh S., 2004. "Dynamic response characteristic of reinforced concrete column subjected to bilateral earthquake ground motions," Thirteenth World Conference on Earthquake Engineering, Paper No. 576, Vancouver, British Columbia, Canada.

Naumoski, N., 2008. "Representative ensembles of strong earthquake records", University of Ottawa, Ottawa, Ontario.

Otani S., Cheung V. W. T., and Lai S. S., 1980. "Reinforced concrete columns subjected to biaxial lateral load reversals," The Seventh World Conference on Earthquake Engineering, Istanbul, Turkey, Vol. 6, pp. 525-532.

Pampanin S., Christopoulos C. and Priestley MJN., 2003. "Performance-based seismic response of framed structures including residual deformations", Part II: Multiple-Degree-Of-Freedom systems, Journal of Earthquake Engineering; Vol.7, No. 1, pp. 119–147.

Park, Y. J., Reinhorn, A. M. and Kunnath, S. K., 1987. "IDARC: Inelastic damage analysis of reinforced concrete frame - shear-wall structures", Technical Report NCEER, University at Buffalo, SUNY.

PEER, 2012. (NGA), Strong Motion Database, Pacific Earthquake Engineering Research Center, University of California, Berkeley.

[http://peer.berkeley.edu/peer\\_ground\\_motion\\_database/](http://peer.berkeley.edu/peer_ground_motion_database/)

[Last accessed on 7/23/2012].

Qiu F., Li W., Pan P., and Qian J., 2002. "Experimental tests on RC columns under biaxial quasi-static loading", Engineering Structures, Vol. 24, pp. 419-428.

Reinhorn A. M., M. Sivaselvan H. Roh, Kunnath S.K., Valles R.E., A. Madan, C. Li, Lobo R. and Park Y.J., 2009. "IDARC2D Version 7.0: A program for the inelastic damage analysis of structures", Technical Report MCEER-09-0006. University at Buffalo, SUNY.

Roberts M.W. and Lutes L.D., 2003. "Potential for structural failure in the seismic near field", *Journal of Engineering Mechanics*, Vol. 129, No. 8, pp. 927–934.

Rodrigues H., Arêde A., Varum H. and Costa A.G., 2010. "Experimental study on the biaxial bending cyclic behavior of RC columns", Fourteenth European Conference on Earthquake Engineering (14 ECEE), Ohrid, Macedonia.

Rosenblueth E., Elorduy J and Mendoza E., 1968. "Shears and over turning moments in shear buildings during earthquakes", *Proceedings of the 2<sup>nd</sup> Mexican Conference on Earthquake Engineering*, Mexican Society of Earthquake Engineering, Veracruz Mexico.

Ruiz-Garcia J. and Miranda E., 2004. "Inelastic displacement ratios for design of structures on soft soil sites", *ASCE Journal of Structural Engineering*, Vol. 130, No. 12, pp. 2051–2061.

Ruiz-Garcia J. and Miranda E., 2005. "Performance-based assessment of existing structures accounting for residual displacements", Report No. 153, the John A. Blume Earthquake Engineering Center, Department of Civil and Environmental Engineering, Stanford University.

Ruiz-García J, Miranda E., 2006. "Residual displacement ratios for assessment of existing structures", *Earthquake Engineering and Structural Dynamics*, Vol. 35, No. 3, pp. 315–336.

Ruiz-García J. and Miranda E., 2006. "Evaluation of residual drift demands in regular multi-story frames for performance-based seismic assessment", *Earthquake Engineering and Structural Dynamics*, Vol.35, pp. 1609–1629.

Ruiz-García and Negrete-Manriquez, 2011. "Evaluation of drift demands in existing steel frames under as-recorded far-field and near-fault mainshock–aftershock seismic sequences", *Engineering Structures*, Vol. 33, pp. 621–634.

Saatcioglu M. and Ozcebe G., 1989. "Response of reinforced concrete columns to simulated seismic loading", *ACI Structural Journal*, Vol. 86, Issue 1, pp. 3-12.

Sasani M., Makris N., Bolt B.A., 2006. “Damping in shear beam structures and estimation of drift response”, *Journal of Engineering Mechanics*; Vol. 132, No. 8, pp. 851–858.

Sezen H., 2000. “Seismic behavior and modeling of reinforced concrete building columns”, Ph.D. Thesis, University of California, Berkeley.

Sezen H., Whittaker A.S., Elwood K.J., Mosalam K.M., 2003. “Performance of reinforced concrete buildings during the August 17, 1999 Kocaeli, Turkey earthquake, and seismic design and construction practise in Turkey”, *Journal of Engineering Structures*, Vol. 25, pp. 103-114.

Sivaselvan, M. and Reinhorn, A. M., 2001. “Hysteretic models for deteriorating inelastic structures”, *ASCE Journal of Engineering Mechanics*, Vol. 126, No.6, pp. 633-664.

Rinne, J. E., 1960. “Design criteria for shear and overturning moment”, *Proceedings of the 2nd World Conference on Earthquake Engineering*, Vol. III, Science Council of Japan, Tokyo.

Takemura H., Kawashima, K., 1997. “Effect of loading hysteresis on ductility capacity of bridge piers”, *Japan Journal of Structural Engineering*, Vol. 43A, pp. 849–858.

Takizawa H., and Aoyama M., 1976. “Biaxial effects in modelling earthquake response of RC structures”, *Earthquake Engineering and Structural Dynamics*, Vol. 4, pp. 523-552.

TR-KYH, Strong Ground Motion Database of Turkiye (2012). <http://kyh.deprem.gov.tr/ftpe.htm> [Last accessed on 4/5/2012].

Tsuno K. and Park R., 2004. “Experimental study of reinforced concrete bridge piers subjected to bi-directional quasi-static loading”, *Structural Engineering Structures*, JSCE, vol. Vol. 21, No 1, pp. 11-26.

Umemura H. and Ichinose T., 2004. “Experimental study on the effects of loading history on the ductility capacity of reinforced concrete members”, Paper No. 1301, 13<sup>th</sup> World Conference on Earthquake Engineering, Vancouver, B.C., Canada.

Valles R. E., Reinhorn A. M., Kunnath S. K., Li C., and Madan A., 1996, “IDARC 2D Version 4.0 : A Computer Program for the Inelastic Damage Analysis of

Buildings”, Technical Report NCEER- 96-0010, State University of New York at Buffalo.

Wen, Y.K., 1976. “Method for random vibration of hysteretic systems”, *Journal of Engineering Mechanics*, Vol.102, No. 2, pp. 249-263.

Westergaard H. M., 1933. “Earthquake-shock transmission in tall building”, *Eng. News-Rec.*, Vol. 111: pp. 654–656.

Wong, C.W., Ni, Y.Q., and Ko J.M., 1994. “Steady-state oscillation of hysteretic differential model. II: Performance analysis”, *Journal of Engineering Mechanics*, Vol. 120, No. 11, pp. 2299-2325.

Xie J. and Wen Z., 2008. “A measure of drift demand earthquake ground motions for based on timoshenko beam model”, *Fourteenth World Conference on Earthquake Engineering*, Beijing, China.

Yang D., Pan J. and Li G., 2010. “Interstory drift ratio of building structures subjected to near-fault ground motions based on generalized drift spectral analysis”, *Soil Dynamics and Earthquake Engineering*, Vol. 30, pp. 1182–1197.

Zembaty Z., 2007. “Non-stationary random vibrations of a shear beam under high frequency seismic effects”, *Soil Dynamics and Earthquake Engineering*; Vol. 27: pp. 1000–1011.

## APPENDIX A

### TABLES OF SELECTED GROUND MOTIONS

List of ground motion records used in the study with low  $a/v$  ratio ( $a/v < 0.8$ ) (Table A.1); intermediate  $a/v$  ratio ( $0.8 < a/v < 1.2$ ) (Table A.2); and high  $a/v$  ratio ( $1.2 < a/v$ ) (Table A.3) are presented. The one hundred ninety three records have been picked in order to select different seismic conditions in terms of magnitude; source to site distance; fault mechanism factors that affect the signal nature by a considerable amount.

The selection of the records have made on the basis of their damage potential, according to following features; (1) the most records have been taken in the near-fault region typically characterized by long duration pulses (note that in the tables distance denoted the closest distance from fault rupture); (2) Magnitude between 5.3 and 8.1; (3) The ground motions have been recorded on different types of soil; (4) peak ground acceleration (PGA) lies between 1.174 g. and 0.044 g.; (5) Peak ground velocity (PGV) is between 0.016 m/s and 1.749 m/s. And so the faulting mechanisms of strike-slip; reverse; oblique-reverse; thrust, for rock ( $760 \text{ m/sec} < V_{S,30} < 1500 \text{ m/sec}$ ); stiff ( $360 \text{ m/sec} < V_{S,30} < 760 \text{ m/sec}$ ); and soft ( $180 \text{ m/sec} < V_{S,30} < 360 \text{ m/sec}$ ) ... sites are tabulated.

#### LIST OF ABBREVIATIONS

SS	: Strike-Slip Faulting
R	: Reverse Faulting
T	: Thrust Faulting
RO	: Reverse-Oblique

Table A.1 List of ground motion records used in the study with low a/v ratio ( $a/v < 0.8$ )

No.	Earthquake and Date	Comp.	Soil Cond. <sup>2</sup>	Mech. <sup>1</sup>	Mag. ( $M_w$ )	Dist. (km)	PGA (g)	PGV (m/s)	a/v Ratio (g/m/s)
1	Düzce, Aug. 1999	NS	Soil	SS	7.5	17.06	0.337	0.606	0.56
2	Düzce, Aug. 1999	EW	Soil	SS	7.5	17.06	0.383	0.496	0.77
3	Düzce, Aug. 1999	FP	Soil	SS	7.5	17.06	0.273	0.485	0.56
4	Düzce, Aug. 1999	FN	Soil	SS	7.5	17.06	0.398	0.677	0.59
5	Bolu-Düzce, Nov.1999	NS	Soil	SS	7.1	8.23	0.410	0.658	0.62
6	Bolu-Düzce, Nov.1999	EW	Soil	SS	7.1	8.23	0.513	0.861	0.60
7	Bolu-Düzce, Nov.1999	FP	Soil	SS	7.1	8.23	0.503	0.843	0.60
8	Bolu-Düzce, Nov.1999	FN	Soil	SS	7.1	8.23	0.412	0.626	0.66
9	Erzincan, Mar. 1992	F45P	Soil	SS	6.7	4.40	0.456	0.583	0.78
10	Gebze, Aug. 1999	NS	Rock	SS	7.5	7.74	0.269	0.456	0.59
11	Gebze, Aug. 1999	EW	Rock	SS	7.5	7.74	0.143	0.347	0.41
12	Gebze, Aug. 1999	FN	Rock	SS	7.5	7.74	0.245	0.370	0.66
13	Imperial Valley, May. 1940	EW	Soil	SS	6.5		0.214	0.365	0.59
14	Imperial Valley, Oct. 1979	S40E	Soil	SS	6.5		0.339	0.665	0.51
15	Imperial Valley, Oct. 1979	S40E	Soil	SS	6.5		0.338	0.509	0.66
16	Imperial Valley, Oct. 1979	S50W	Soil	SS	6.5		0.459	1.125	0.41
17	Izmit, Aug. 1999	NS	Rock	SS	7.5	4.26	0.167	0.320	0.52
18	Izmit, Aug. 1999	EW	Rock	SS	7.5	4.26	0.227	0.543	0.42
19	Izmit, Aug. 1999	FP	Rock	SS	7.5	4.26	0.223	0.548	0.41
20	Izmit, Aug. 1999	FN	Rock	SS	7.5	4.26	0.168	0.309	0.54
21	Kobe, June 1995	F45N	Stiff Soil	SS	6.9	3.40	1.086	1.606	0.68
22	Kobe, Takatori, June 1995	F45N	Soil	SS	6.9	4.50	0.784	1.749	0.45
23	Kobe, Takatori, June 1995	F45P	Soil	SS	6.9	4.50	0.423	0.635	0.67
24	Northridge, Sylmar County Hospital, Jan. 1994	EW	Soil	R	6.7		0.604	0.769	0.79
25	Northridge, Olive View, Jan. 1994	F45N	Soil	T	6.7	6.40	0.724	1.195	0.61
26	Northridge, Rinaldi, Jan. 1994	F45N	Soil	R	6.7	7.50	0.891	1.745	0.51
27	Northridge, Rinaldi, Jan. 1994	F45P	Soil	R	6.7	7.50	0.399	0.608	0.66
28	Sakarya, Aug. 1999	EW	Rock	SS	7.4	3.20	0.407	0.798	0.51
29	Tabas, Iran, Sept.1978	F45N		R	4.4		0.827	1.135	0.73
30	Landers, Lucern, June 1992	EW	Soil	SS	7.3	1.10	0.245	0.508	0.48
31	Landers, Lucern, June 1992	NS	Soil	SS	7.3	1.10	0.152	0.290	0.52
32	Yarimca, Aug. 1999	NS	Soil	SS	7.5	3.28	0.322	0.796	0.40
33	Yarimca, Aug. 1999	FN	Soil	SS	7.5	3.28	0.318	0.780	0.41
34	C. Mendocino, Petrolia, April1992	F45N	Stiff Soil	R	7.0		0.624	1.267	0.49
35	C. Mendocino, Petrolia, April1992	F45P	Stiff Soil	R	7.0		0.615	0.898	0.69
36	Santa Cruz Mtns, Loma Prieta, Holliste, Oct. 1989	NS	Soil	RO	6.9	8.70	0.369	0.628	0.59
37	Santa Cruz Mtns, Loma Prieta, Holliste, Oct. 1989	EW	Soil	RO	6.9	8.70	0.178	0.309	0.58
38	Landers, Lucern, Jan. 1992	EW	Soil	SS	7.3	1.10	0.284	0.427	0.66
39	Loma Prieta, Oakland Outer H. Wharf, Oct. 1989	EW		RO	6.9	8.70	0.276	0.376	0.73
40	Northridge, Newhall, Jan. 1994	EW	Soil	R	6.7		0.583	0.748	0.78
41	Northridge, Newhall, Jan. 1994	NS	Soil	R	6.7		0.590	0.947	0.62
42	Loma Preita , Oakwh, Oct. 1989	EW	Stiff Soil	RO	6.9		0.276	0.376	0.73
43	Loma Preita, Oakwh, Oct. 1989	NS	Stiff Soil	RO	6.9		0.220	0.354	0.62
44	Cape Mendocino, Petrolia, April1992	EW	Stiff Soil	R	7.0		0.662	0.895	0.74
45	San Fernando, 8244 Orion Blvd., Feb.1971	NS	Stiff Soil	R	6.6		0.134	0.239	0.56
46	Scse Valve Hall Groind Floor, Jan. 1994	N11E	Stiff Soil	R	6.7		0.831	1.220	0.68
47	Scse Valve Hall Groind Floor, Jan. 1994	N79W	Stiff Soil	R	6.7		0.453	0.743	0.61
48	San Fernando, Sta241, Feb.1971	EW	Stiff Soil	R	6.6		0.134	0.238	0.56
49	Sylmar, Scse Valve Hall Groind Floor, Jan. 1994	N52E		R	6.7		0.604	0.122	0.50
50	Sylmar, Scse Valve Hall Groind Floor, Jan. 1994	S38E		R	6.7		0.754	0.108	0.69
51	Symar, Hosp, Jan. 1994	EW		R	6.7		0.604	0.769	0.79
52	Symar, Hosp, Jan. 1994	NS		R	6.7		0.843	0.129	0.65
53	Chi-Chi, Taiwan, TCU065, Sept.1999	EW	Soil	RO	7.6	0.60	0.814	0.126	0.64
54	Chi-Chi, Taiwan, TCU067, Sept.1999	EW	Soil	RO	7.6	0.60	0.503	0.796	0.63
55	Chi-Chi, Taiwan, TCU072, Sept.1999	EW	Soil	RO	7.6	7.00	0.489	0.718	0.68

Table A.1 continued

<i>No.</i>	<i>Earthquake and Date</i>	<i>Comp.</i>	<i>Soil Cond.<sup>2</sup></i>	<i>Mech.<sup>1</sup></i>	<i>Mag. (M<sub>w</sub>)</i>	<i>Dist. (km)</i>	<i>PGA (g)</i>	<i>PGV (m/s)</i>	<i>a/v Ratio (g/m/s)</i>
56	Long Beach California, Mar. 1933	N51W	Rock		6.3	59.00	0.097	0.237	0.41
57	Lower Calif., Dec.1934	S00W	Stiff Soil		6.5	58.00	0.160	0.209	0.77
58	San Fernando California, Feb.1971	N61W	Stiff Soil	R	6.4	40.00	0.101	0.193	0.52
59	San Fernando California, Feb.1971	EW	Stiff Soil	R	6.4	39.00	0.132	0.216	0.61
60	San Fernando California, Feb.1971	S37W	Stiff Soil	R	6.4	41.00	0.129	0.186	0.69
61	San Fernando California, Feb.1971	S90W	Stiff Soil	R	6.4	39.00	0.114	0.186	0.61
62	San Fernando California, Feb.1971	N15E	Stiff Soil	R	6.4	38.00	0.117	0.215	0.54
63	San Fernando California, Feb.1971	S38W	Rock	R	6.4	41.00	0.119	0.173	0.69
64	San Fernando California, Feb.1971	NS	Stiff Soil	R	6.4	32.00	0.106	0.170	0.62
65	Erzincan, Mar. 1992	F45N	Soil	SS	6.7	2	0.432	0.118	0.37

Table A.2 List of ground motions with intermediate  $a/v$  ratio ( $0.8 < a/v < 1.2$ )

No.	Earthquake and Date	Comp.	Soil Cond.	Mech.	Mag. ( $M_w$ )	Dist. (km)	PGA (g)	PGV (m/s)	$a/v$ Ratio (g/m/s)
1	Bolu, Düzce, Nov.1999	FN	Soil	SS	7.1	20.41	0.771	0.669	1.15
2	Imperial Valley, May. 1940	EW	Soil		6.5		0.348	0.323	1.08
3	Kern, Taft Lincoln School Tunnel, July 1952	N69E	Soil	R	7.4		0.156	0.157	0.99
4	Kern, Taft Lincoln School Tunnel, July 1952	N21W	Soil	R	7.4		0.179	0.177	1.01
5	Kobe, Jan. 1995	F45P	Stiff Soil	SS	6.9	4.30	0.576	0.718	0.80
6	Northridge, Arleta And Nordhoff F. Sta., Jan. 1994	EW	Soil	R	6.7		0.344	0.404	0.85
7	Northridge, Olive View, Jan. 1994	F45P	Soil	T	6.7	6.40	0.579	0.533	1.09
8	Tabas, Iran, Sept.1978	F45P		R	7.4		0.887	0.109	0.81
9	Bolu, Düzce, Nov.1999	FN	Soil	SS	7.4		0.771	0.669	1.15
10	Afyon Sultandag, Mar. 2002	EW					0.094	0.867	1.09
11	Afyon Sultandag, Mar. 2002	NS					0.113	0.124	0.91
12	Santa Cruz Mtns, Loma Prieta, Corralit, Oct. 1989	NS	Soil	RO	7.1		0.630	0.552	1.14
13	Santa Cruz Mtns, Loma Prieta, Corralit, Oct. 1989	EW	Soil	RO	7.1		0.479	0.475	1.01
14	Landers, Lucern, June 1992	NS	Soil	SS	7.4	1.10	0.274	0.271	1.01
15	Northridge, LACC_NOR, Jan. 1994	NS	Soil	R	6.7		0.222	0.251	0.88
16	Northridge, MOORPARK, Jan. 1994	EW	Soil	R	6.7		0.193	0.204	0.95
17	Pacoima Dam, Feb.1971	N74W		R	6.6		1.171	0.113	1.03
18	San Fernando-8244 Orion Blvd., Feb.1971	EW		R	6.6		0.255	0.297	0.86
19	San Fernando, Sta241, Feb.1971	NS		R	6.6		0.255	0.298	0.86
20	Chi-Chi, Taiwan, TCU089, Sept.1999	EW	Soil	RO	7.6	8.90	0.333	0.309	1.08
21	Imperial Valley California, May. 1940	NS	Stiff Soil		6.6	8.00	0.348	0.334	1.04
22	Kern County California, July 1952	S69E	Rock	R	7.4	56.00	0.179	0.177	1.01
23	Kern County California, July 1952	N21E	Rock	R	7.4	56.00	0.156	0.157	0.99
24	Borrego Mtn. California, April1968	N57W	Stiff Soil		6.5	122.00	0.046	0.042	1.10
25	Borrego Mtn. California, April1968	N33E	Stiff Soil		6.5	122.00	0.041	0.037	1.11
26	San Fernando California, Feb.1971	S90W	Rock	R	6.6	24.00	0.150	0.149	1.01
27	San Fernando California, Feb.1971	EW	Stiff Soil	R	6.6	35.00	0.211	0.211	1.00
28	San Fernando California, Feb.1971	EW	Stiff Soil	R	6.6	39.00	0.165	0.166	0.99
29	San Fernando California, Feb.1971	NS	Rock	R	6.6	31.00	0.180	0.205	0.88
30	San Fernando California, Feb.1971	N37E	Stiff Soil	R	6.6	41.00	0.199	0.167	1.19
31	Near East Coast Of Honshu,Japan, Nov.1974	NS	Stiff Soil		6.1	38.00	0.070	0.072	0.97
32	Near East Coast Of Honshu,Japan, Aug.. 1971	EW	Stiff Soil		7.0	196.00	0.078	0.068	1.15
33	Monte Negro Yugoslavia, April1979	NS	Rock		7.0	17.00	0.171	0.194	0.88
34	Mexico, Sept.1985	NS	Rock		8.1	230.00	0.105	0.116	0.91
35	Mexico, Sept.1985	EW	Rock		8.1	44.00	0.123	0.105	1.17
36	Loma Prieta/S. C. Mtns, Santa T. Hills, Oct. 1989	S45W	Stiff Soil	RO	7.0	11.9	0.275	0.262	1.05
37	Loma Prieta/S. C. Mtns, S. Teresa Hills, Oct. 1989	N45W	Stiff Soil	RO	7.0	11.9	0.228	0.206	1.11
38	Loma Prieta/S. C. Mtns,Gilroy #2, Oct. 1989	NS	Stiff Soil	RO	7.0	4.5	0.351	0.333	1.05
39	Loma Prieta/S. C. Mtns, Gilroy #2, Oct. 1989	EW	Stiff Soil	RO	7.0	4.5	0.323	0.392	0.82
40	Loma Prieta/S. C. Mtns, C. L.Dam, S.W.Abut., Oct. 1989	S15W	Fill over Rock	RO	7.0	16.9	0.152	0.151	1.00
41	L. Prieta/S. C. Mtns, Coyote L. Dam - Downstream, Oct. 1989	N75W	Fill over Rock	RO	7.0	16.9	0.178	0.210	0.85
42	L. Prieta/S. C. Mtns,Gilroy #3, Oct. 1989	EW	Stiff Soil	RO	7.0	6.3	0.369	0.438	0.84
43	L. Prieta/S. C. Mtns, Gilroy #4, Oct. 1989	NS	Stiff Soil	RO	7.0	7.9	0.416	0.391	1.06
44	L. Prieta/S. C. Mtns, Gilroy #6, Oct. 1989	NS	Rock	RO	7.0	12.2	0.114	0.131	0.87
45	L. Prieta/S. C. Mtns, H. Valley, G. Park, Oct. 1989	NS	Stiff Soil	RO	7.0	28	0.131	0.125	1.04
46	L. Prieta/S. C. Mtns, H. Valley – G. Park, Oct. 1989	NS	Stiff Soil	RO	7.0	28	0.112	0.137	0.82

Table A.2 continued

<i>No.</i>	<i>Earthquake and Date</i>	<i>Comp.</i>	<i>Soil Cond.</i>	<i>Mech.</i>	<i>Mag. (M<sub>w</sub>)</i>	<i>Dist. (km)</i>	<i>PGA (g)</i>	<i>PGV (m/s)</i>	<i>a/v Ratio (g/m/s)</i>
47	L. Prieta/S. C. Mtns, Agnew, Oct. 1989	EW	Stiff Soil	RO	7.0	21	0.161	0.182	0.88
48	L. Prieta/S. C. Mtns, Stanford Univ., Oct. 1989	NS		RO	7.0	20.5	0.288	0.284	1.01
49	L. Prieta/S. C. Mtns, A. Dam - C. Crest, Oct. 1989	N63E		RO	7.0	16.9	0.404	0.438	0.92
50	L. Prieta/S. C. Mtns, A. Dam - C. Crest, Oct. 1989	N27W		RO	7.0	16.9	0.320	0.281	1.14
51	L. Prieta/S. C. Mtns, A. Dam - Crest, Oct. 1989	S63W		RO	7.0	16.9	0.388	0.467	0.83
52	L. Prieta/S. C. Mtns, A. Dam, Mid-dam C, Oct. 1989	S63W		RO	7.0	16.9	0.152	0.177	0.86
53	L. Prieta/S. C. Mtns, A. Dam Right Crest, Oct. 1989	N27W		RO	7.0	16.9	0.315	0.314	1.00
54	L. Prieta/S. C. Mtns, A. Dam - Toe, Oct. 1989	N27W		RO	7.0	16.9	0.119	0.120	0.99
55	Chi-Chi, Taiwan, CHY006, Sept. 1999	NS	Stiff Soil	RO	7.6	14.5	0.359	0.421	0.85
56	Chi-Chi, Taiwan, CHY028, Sept. 1999	NS	Stiff Soil	RO	7.6	8.7	0.707	0.848	0.83
57	Chi-Chi, Taiwan, CHY028, Sept. 1999	EW	Stiff Soil	RO	7.6	8.7	0.594	0.606	0.98
58	Loma Prieta/S. C. Mtns, Corralitos, Sept. 1989	NS	Landslide Deposits	RO	7.0	2.8	0.630	0.552	1.14
59	Loma Prieta/S. C. Mtns, Corralitos, Oct. 1989	EW	Landslide Deposits	RO	7.0	2.8	0.479	0.475	1.01
60	Chi-Chi, Taiwan, TCU045, Sept. 1999	NS	Stiff Soil	RO	7.6	24.7	0.476	0.464	1.03
61	Chi-Chi, Taiwan, TCU045, Sept. 1999	EW	Stiff Soil	RO	7.6	24.7	0.459	0.478	0.96
62	Chi-Chi, Taiwan, TCU078, Sept. 1999	NS	Stiff Soil	RO	7.6	8.3	0.308	0.336	0.92
63	Chi-Chi, Taiwan, TCU078, Sept. 1999	EW	Stiff Soil	RO	7.6	8.3	0.442	0.409	1.08
64	Chi-Chi, Taiwan, TCU089, Sept. 1999	EW	Stiff Soil	RO	7.6	12.8	0.354	0.353	1.00

Table A.3 List of ground motions used in the study with high a/v ratio ( $1.2 < a/v$ )

No.	Earthquake and Date	Comp.	Soil Cond.	Mech.	Mag. ( $M_w$ )	Dist. (km)	PGA (g)	PGV (m/s)	a/v Ratio (g/m/s)
1	Bolu, Düzce, Nov.1999	NS	Soil	SS	7.1	20.41	0.754	0.583	1.29
2	Bolu, Düzce, Nov.1999	EW	Soil	SS	7.1	20.41	0.822	0.669	1.23
3	Bolu, Düzce, Nov.1999	FP	Soil	SS	7.1	20.41	0.817	0.568	1.44
4	Northridge, Santa Monica C. H Grounds, Jan. 1994	EW	Soil	R	6.7		0.883	0.417	2.12
5	Santa Cruz Mtns, Loma Prieta, Capitola, Oct. 1989	NS	Soil	RO	6.9		0.472	0.361	1.31
6	Santa Cruz Mtns, Loma Prieta, Capitola, Oct. 1989	EW	Soil	RO	6.9		0.398	0.307	1.30
7	Santa Cruz Mtns, Loma Prieta, Gilroygc, Oct. 1989	N67E	Soil	RO	6.9		0.356	0.289	1.23
8	Santa Cruz Mtns, Loma Prieta, Gilroygc, Oct. 1989	N23W	Soil	RO	6.9		0.316	0.229	1.38
9	Northridge, LACC_NOR, Jan. 1994	EW	Soil	R	6.7		0.256	0.214	1.20
10	Northridge, MOORPARK, Jan. 1994	NS	Soil	R	6.7		0.292	0.203	1.44
11	Pacoima Dam, Feb.1971	S16W		R	6.6		0.781	0.574	1.36
12	Parkfield, June 1966	N40E		SS	6.2		0.237	0.108	2.19
13	Parkfield, June 1966	S50W		SS	6.2		0.275	0.118	2.34
14	Cape Mendocino, Petrolia, April 1992	NS	Stiff Soil	R	7.0		0.590	0.483	1.22
15	Santa Monica, City Hall Grounds, Jan. 1994	EW		R	6.7		0.883	0.417	2.12
16	Santa Monica, City Hall Grounds, Jan. 1994	NS		R	6.7		0.370	0.249	1.48
17	Chi-Chi, Taiwan, TCU071, Sept.1999	EW	Soil	RO	7.6	5.30	0.567	0.445	1.27
18	Chi-Chi, Taiwan, TCU078, Sept.1999	EW	Soil	RO	7.6	8.20	0.444	0.393	1.13
19	Chi-Chi, Taiwan, TCU079, Sept.1999	EW	Soil	RO	7.6	11.00	0.740	0.612	1.21
20	Parkfield, California, June 1966	N65W	Rock	SS	5.6	7.00	0.269	0.145	1.86
21	Parkfield, California, June 1966	N85W	Rock	SS	5.6	5.00	0.434	0.254	1.70
22	San Francisco California, Mar. 1957	S80E	Rock		5.3	11.00	0.105	0.046	2.28
23	San Francisco California, Mar. 1957	S09E	Stiff Soil		5.3	17.00	0.085	0.050	1.67
24	Helena Montana, Oct. 1935	NS	Rock		6.0	8.00	0.146	0.072	2.03
25	Lytle Creek, Sept.1970	S25W	Rock		5.4	15.00	0.198	0.096	2.06
26	Oroville California, Aug.. 1975	N53W	Rock		5.7	13.00	0.084	0.044	1.91
27	San Fernando California, Feb.1971	S74W	Rock	R	6.6	4.00	1.075	0.577	1.86
28	San Fernando California, Feb.1971	S21W	Rock	R	6.6	26.00	0.146	0.085	1.72
29	Nahannin.W.T., Canada, Dec.1985	FP	Rock		6.9	7.50	1.101	0.462	2.38
30	Central Honshu, Japan, Feb.1971	FN	Stiff Soil		5.5	27.00	0.151	0.059	2.56
31	Near E. Coast Of Honshu, Japan, May. 1972	NS	Stiff Soil		5.8	33.00	0.146	0.060	2.43
32	Honshu Japan, April 1966	NS	Stiff Soil		5.4	4.00	0.270	0.111	2.43
33	Monte Negro Yugoslavia, April 1979	NS	Rock		5.4	12.50	0.042	0.016	2.63
34	Banja Luka Yugoslavia, Aug. 1981	EW	Rock		6.1	8.50	0.074	0.032	2.31
35	Loma Prieta/S. C. Mtns, C.L Dam – DS., Oct. 1989	S15W	Soil	RO	7.0	16.9	0.158	0.127	1.25
36	Loma Prieta/S. C. Mtns, Gilroy #3, Oct. 1989	NS	Stiff Soil	RO	7.0	6.3	0.542	0.345	1.57
37	Loma Prieta/S. C. Mtns, Gilroy #6, Oct. 1989	EW	Soil	RO	7.0	12.2	0.170	0.139	1.22
38	Loma Prieta/S. C. Mtns, A. Dam - Crest, Oct. 1989	N27W		RO	7.0	16.9	0.270	0.220	1.23
39	Loma Prieta/S. C. Mtns, A. Dam – D.S., Oct. 1989	S63W		RO	7.0	16.9	0.250	0.223	1.12
40	Loma Prieta/S. C. Mtns, A. Dam – D.S. , Oct. 1989	N27W		RO	7.0	16.9	0.244	0.196	1.25
41	Loma Prieta/S.C, Mtns, A.Dam, M.D, Oct. 1989	N63E		RO	7.0	16.9	0.222	0.168	1.32
42	Loma Prieta/S. C. Mtns, A. Dam, M.D , Oct. 1989	S27E		RO	7.0	16.9	0.171	0.134	1.27
43	Loma Prieta/S. C. Mtns, A.Dam,R. Crest, Oct. 1989	N63E		RO	7.0	16.9	0.420	0.288	1.46
44	Chi-Chi, Taiwan, WNT, Sept.1999	NS	Stiff Soil	RO	7.6	2.2	0.619	0.336	1.84
45	Chi-Chi, Taiwan, WNT, Sept.1999	EW	Stiff Soil	RO	7.6	2.2	0.956	0.621	1.54

Table A.3 continued

<i>No.</i>	<i>Earthquake and Date</i>	<i>Comp.</i>	<i>Soil Cond.</i>	<i>Mech.</i>	<i>Mag.</i>	<i>Dist.</i>	<i>PGA</i>	<i>PGV</i>	<i>a/v</i>
				<i>h.</i>	<i>(M<sub>w</sub>)</i>	<i>(km)</i>	<i>(g)</i>	<i>(m/s)</i>	<i>Ratio</i>
									<i>(g/m/s)</i>
46	Loma Prieta/S. C. Mtns, Capitola, F.Sta., Oct. 1989	NS	Soil	RO	7.0	15.9	0.472	0.361	1.31
47	Loma Prieta/S. C. Mtns, Capitola, F.Sta., Oct. 1989	EW	Soil	RO	7.0	15.9	0.398	0.307	1.30
48	Loma Prieta/S. C. Mtns, UCSC/L. Lab, Oct. 1989	NS	Rock	RO	7.0	18.8	0.442	0.212	2.08
49	Loma Prieta/S. C. Mtns, UCSC/L. Lab, Oct. 1989	EW	Rock	RO	7.0	18.8	0.409	0.212	1.93
50	Loma Prieta/S. C. Mtns, S. - Aloha Ave., Oct. 1989	NS	Stiff Soil	RO	7.0	4.1	0.504	0.413	1.22
51	Loma Prieta/S. C. Mtns, Gilroy, G.Coll., Oct. 1989	N67E	Soil	RO	7.0	3	0.356	0.289	1.23
52	Loma Prieta/S. C. Mtns, Gilroy, G.Coll., Oct. 1989	N23E	Soil	RO	7.0	3	0.316	0.230	1.38
53	Loma Prieta/S. C. Mtns, Gilroy #7, Oct. 1989	NS	Stiff Soil	RO	7.0	15.6	0.210	0.166	1.26
54	Loma Prieta/S. C. Mtns, Gilroy #7, Oct. 1989	EW	Stiff Soil	RO	7.0	15.6	0.321	0.163	1.97
55	Loma Prieta/S. C. Mtns, P.A.VA - B. 1 B. Oct. 1989	S32W	Stiff Soil	RO	7.0	16.7	0.386	0.405	0.95
56	Loma Prieta/S. C. Mtns, Palo Alto VA Hosp - Bldg 1 bsm, Oct. 1989	N58W	Stiff Soil	RO	7.0	16.7	0.348	0.230	1.52
57	Loma Prieta/S. C. Mtns, Palo Alto VA Hosp - Bldg 1 rf, Oct. 1989	S32W	Stiff Soil	RO	7.0	16.7	0.839	0.651	1.29
58	Loma Prieta/S. C. Mtns, Palo Alto VA Hosp - Bldg 1 rf, Oct. 1989	N58W	Stiff Soil	RO	7.0	16.7	1.174	0.661	1.78
59	Chi-Chi, Taiwan, CHY010, Sept. 1999	EW	Stiff Soil	RO	7.6	22.4	0.225	0.186	1.21
60	Chi-Chi, Taiwan, CHY041, Sept. 1999	NS	Stiff Soil	RO	7.6	21.9	0.631	0.371	1.70
61	Chi-Chi, Taiwan, CHY041, Sept. 1999	EW	Stiff Soil	RO	7.6	21.9	0.303	0.204	1.49
62	Chi-Chi, Taiwan, TCU088, Sept. 1999	NS	Rock	RO	7.6	13.2	0.505	0.331	1.52
63	Chi-Chi, Taiwan, TCU088, Sept. 1999	EW	Rock	RO	7.6	13.2	0.517	0.136	3.81



## **APPENDIX B**

### **THE PROGRAM GENERICFRAMES**

In this appendix, all source codes and methods (subroutines) for Java based computation program, for derivation of the drift spectrum using generic shear frames, are presented.

The Java platform is a general-purpose computer programming language that is object-oriented, class-based, and particularly designed to have as few implementation dependencies as possible. It is developed by Sun Microsystems and thereafter acquired by Oracle Corporation in January, 2010. It is designated to let application developers “write once, run anywhere” (WORA), this means that compiled Java code can run on all platforms that support Java without the need for recompilation, in other words, it is architecture independent.

In software, JAR (Java Archive) is a package file format characteristically utilized to round up many Java class files and collaborated metadata and resources (text, images, etc.) into one file to administrate application software or libraries on the Java platform. JAR files are basically archive files, built on the ZIP file format and have the .jar file extension. A JAR file lets Java runtimes to deploy a series of classes and their connected resources in an efficient manner. The elements in a JAR file can be compressed, which together with the capacity to download an whole application in a single requisition, makes downloading a JAR file much more serviceable than individually downloading the many uncompressed files which would form a one Java application.

An executable Java program can be packaged in a JAR file, associated with any libraries the program uses. Microsoft Windows operating systems can run these

directly when clicked. The typical invocation is "java -jar foo.jar" from a command line. (c:\users\[computer name]\[Folder includes the frame models and IDARC analyser]> JAVA -jar GenericFrames.jar), Wherein "GenericFrames.jar" is the program used to generate the drift spectrums using generic shear Frames.

All Java programs start as text files with the suffix 'java'. This means that any text editor can be utilized to generate these text files. This file is employed to create a runnable program with the suffix '.class'. Java source code files (files with a \*.java extension) are compiled into a format named bytecode (files with a \*.class extension), which can then be executed by a Java interpreter. In other words, a Java class file is generated through a Java compiler from Java programming language source files (.java files) including Java classes. In Java, everything is given in a class, and class has methods. So, to define a unit that does your own computation means defining a class, and a method inside the class.

As already mentioned each subroutine in java must be defined inside some class. This makes Java rather unusual among programming languages, since most languages allow free-floating, independent subroutines. One purpose of a class is to group together related subroutines and variables. Perhaps the designers of Java felt that everything must be related to something. A Java program potentially has access to a large number of subroutines created by many different programmers. The fact that those subroutines are assembled into named classes (and classes are assembled into named "packages") helps control the complexity that might cause by so many distinct names.

A subroutine that is a member of a class is often called a method, and "method" is the term that often is used for subroutines in Java. The source codes (methods) for a class, interface, counting, or annotation type in a text file whose name is the simple name of the type and whose extension is "\*.java". The source codes of methods/subroutines for updating the input file of main analyzer IDARC-2D Platform (Frames.java) with interface to import desired data, hysteresis quantities and ground motion intensities, (Display.java), likewise, the source code for reading

the MIDR demand from output sheet and transmission them to provided spreadsheet page are given in (DoubleString.java), (WaitThread.java) and (WriteExcel.java) methods.

```
import java.io.BufferedReader;
import java.io.DataInputStream;
import java.io.File;
import java.io.FileInputStream;
import java.io.FileNotFoundException;
import java.io.FileOutputStream;
import java.io.IOException;
import java.io.InputStream;
import java.io.InputStreamReader;
import java.io.OutputStream;
import java.io.PrintWriter;
import java.io.UnsupportedEncodingException;
import java.net.URISyntaxException;
import java.net.URL;
import java.util.ArrayList;
import java.util.regex.Matcher;
import java.util.regex.Pattern;
import javax.swing.JFrame;
import jxl.write.WriteException;

/*
 * Inelastic Drift Spectrum for shear frames
 * PhD thesis Ali Etemadi
 * June 2015
 *
 * */
public class Frames {
    private static ArrayList<String> folderList;
    public static ArrayList<DoubleString> datas;
    public static String path;
    public static String javaFolder = "JavaFolder";
    public static String outFolder = "OutputFiles";
    public static String waveFolder = "ground motion";
    public static String parameterFile = "Parameters.txt";
    public static Display display;

    private static String getInputFileName(String folderPath){
        File idarc = new File(folderPath + "\\\" + "IDARC.DAT");
        FileInputStream fis;
        String inputFileName = null;
        try {
            fis = new FileInputStream(idarc);
            DataInputStream in = new DataInputStream(fis);
            BufferedReader br = new BufferedReader(new InputStreamReader(in));
            inputFileName = br.readLine();
        }
    }
}
```

```

        in.close();
    } catch (IOException e) {
        // TODO Auto-generated catch block
        e.printStackTrace();
    }
    return folderPath + "\\" + inputFileName;
}

private static DoubleString getOutputFileName(String folderPath){
    String period;

    File idarc = new File(path + "\\" + folderPath + "\\" + "IDARC.DAT");
    FileInputStream fis;
    String outputFileName = null;
    try {
        fis = new FileInputStream(idarc);
        DataInputStream in = new DataInputStream(fis);
        BufferedReader br = new BufferedReader(new InputStreamReader(in));
        br.readLine();
        outputFileName = br.readLine();
        in.close();
    } catch (IOException e) {
        // TODO Auto-generated catch block
        e.printStackTrace();
    }

    String outPath = path + "\\" + folderPath + "\\" + outputFileName;
    period = getPeriod(outPath);
    DoubleString ds = new DoubleString(period, outPath);
    return ds;
}

private static String getPeriod(String filePath) {
    // TODO Auto-generated method stub
    File file = new File(filePath);
    if(!file.exists()){
        System.out.println(file.getName() + " file can not find!");
        System.exit(0);
    }
    FileInputStream fis;
    String line;
    double period = -1;
    try {
        fis = new FileInputStream(file);
        DataInputStream in = new DataInputStream(fis);
        BufferedReader br = new BufferedReader(new InputStreamReader(in));
        line = br.readLine();
        int index = line.indexOf("PERIOD");
        while(index!=-1){

```

```

        line = br.readLine();
        index = line.indexOf("PERIOD");
    }
    line = br.readLine();
    line = br.readLine();

    while(line.equals("")){
        line = br.readLine();
    }
    period = getRatio(line);
    in.close();
} catch (IOException e) {
    // TODO Auto-generated catch block
    e.printStackTrace();
}
return Double.toString(period);
}

private static void modifyInputFile(String pathInputFile){
    File inputFile = new File(pathInputFile);
    File temp = new File(path + "\\ " + javaFolder + "\\ " + "temp.txt");
    try {
        temp.createNewFile();
        FileInputStream fis = new FileInputStream(inputFile);
        DataInputStream in = new DataInputStream(fis);
        BufferedReader br = new BufferedReader(new InputStreamReader(in));
        PrintWriter writer = new PrintWriter(temp, "UTF-8");

        String line = br.readLine();
        while(line.indexOf("Hysteretic Control")==-1){
            writer.println(line);
            line = br.readLine();
        }

        for(int i=0; i<2; i++){
            writer.println(line);
            line = br.readLine();
        }

        // Modify line and write to temp
        writer.println(modifyHC(line));

        line = br.readLine();
        while(line.indexOf("Dynamic Analysis Control Data")==-1){
            writer.println(line);
            line = br.readLine();
        }

        writer.println(line);
    }
}

```

```

line = br.readLine();

// Modify line and write to temp
writer.println(modifyDACD(line));

line = br.readLine();
while(line.indexOf("Wave data")==-1){
    writer.println(line);
    line = br.readLine();
}

writer.println(line);
line = br.readLine();

// Change line
// Modify line and write to temp
writer.println(modifyWD(line));

line = br.readLine();
while(line.indexOf("TAFT - EARTHQUAKE")==-1){
    writer.println(line);
    line = br.readLine();
}

writer.println(line);
line = br.readLine();

// Change line
writer.println(Display.earthQuakeFile);

while(br.ready()){
    line = br.readLine();
    writer.println(line);
}

in.close();
writer.close();

inputFile.delete();
temp.renameTo(inputFile);

} catch (IOException e) {
    // TODO Auto-generated catch block
    e.printStackTrace();
}

}

private static boolean isContains(File [] list, String txt) {

```

```

        for(File f : list) {
            if(f.getName().toUpperCase().trim().equals(txt.toUpperCase().trim()))
return true;
        }
        return false;
    }

private static void copyWaveDataFile(String folderName, String waveDataName){
    File f1 = new File(path + "\\\" + waveFolder + "\\\" + waveDataName);
    File f2 = new File(path + "\\\" + folderName + "\\\" + waveDataName);

    try{
        if(!f2.exists()){
            f2.createNewFile();
        }

        InputStream in = new FileInputStream(f1);
        OutputStream out = new FileOutputStream(f2);

        byte[] buf = new byte[1024];
        int len;
        while ((len = in.read(buf)) > 0){
            out.write(buf, 0, len);
        }
        in.close();
        out.close();
    } catch(FileNotFoundException ex){
        ex.printStackTrace();
        System.exit(0);
    } catch(IOException e){
        e.printStackTrace();
    }
}

private static void keepFolders(File dir) {
    folderList = new ArrayList<String>();
    File [] list = dir.listFiles();
    for(File f : list) {
        if(f.isDirectory()) {
            File [] subList = f.listFiles();
            if(isContains(subList,"IDARC.DAT") && isContains(subList,
"iDarc2d_7.0.exe")){
                folderList.add(f.getName());
            }
        }
    }
}

private static void createParameterFile(File file) {

```

```

// HC Parameters
double hc_alfa_default = 2.0;
double hc_beta1_default = 0.013;
double hc_beta2_default = 0.013;
double hc_N_default = 10.0;
double hc_eta_default = 0.5;
double hc_RS_default = 0.35;
double hc_sigma_default = 100;
double hc_lambda_default = 0.3;

// DACD Parameters
double dacd_pga_default = 0.1;
double dacd_pgav_default = 0.0;
double dacd_dt_default = 0.005;
double dacd_TotalT_default = 27.19;
double dacd_damp_default = 2.0;

// Wave Data Parameters
int wd_totalN_default = 5438;
double wd_dt2_default = 0.005;

// Ground Motion Earthquake
String earthquakeFile_default = "wave05.dat";

// Output File Parameters
String outputFileName_default = "output" ;
String outputColumnNumber = "0";

PrintWriter writer;
try {
    writer = new PrintWriter(file, "UTF-8");
    writer.println(hc_alfa_default);
    writer.println(hc_beta1_default);
    writer.println(hc_beta2_default);
    writer.println(hc_N_default);
    writer.println(hc_eta_default);
    writer.println(hc_RS_default);
    writer.println(hc_sigma_default);
    writer.println(hc_lambda_default);
    writer.println(dacd_pga_default);
    writer.println(dacd_pgav_default);
    writer.println(dacd_dt_default);
    writer.println(dacd_TotalT_default);
    writer.println(dacd_damp_default);
    writer.println(wd_totalN_default);
    writer.println(wd_dt2_default);
    writer.println(earthquakeFile_default);
    writer.println(outputFileName_default);
    writer.println(outputColumnNumber);
    writer.close();
}

```

```

    } catch (FileNotFoundException e) {
        // TODO Auto-generated catch block
        e.printStackTrace();
    } catch (UnsupportedEncodingException e) {
        // TODO Auto-generated catch block
        e.printStackTrace();
    }
}

public static void main(String [] args) {
    Display.Report = "Ready";

    URL url = Frames.class.getProtectionDomain().getCodeSource().getLocation();
    // if your Test.java is on the filesystem and not in a jar...
    File testJava;
    try {
        testJava = new File(url.toURI());
        path = testJava.getParent();
        System.out.println("Path: " + path);
    } catch (URISyntaxException e1) {
        // TODO Auto-generated catch block
        e1.printStackTrace();
    }

    File dir = new File(path);
    keepFolders(dir);

    String javaFolderPath = path + "\\\" + javaFolder;
    File javaFolderFile = new File(javaFolderPath);
    if(!javaFolderFile.exists()){
        javaFolderFile.mkdir();
    }

    String parameterPath = path + "\\\" + javaFolder + "\\\" + parameterFile;
    File parameterFile = new File(parameterPath);
    if(!parameterFile.exists()){
        try {
            parameterFile.createNewFile();
        } catch (IOException e) {
            // TODO Auto-generated catch block
            e.printStackTrace();
        }
        createParameterFile(parameterFile);
    }
}

```

```

final JFrame frame = new JFrame ("Inelastic Drift Spectrum using Generic shear
Frames");

```

```

display = new Display();
frame.setDefaultCloseOperation( JFrame.EXIT_ON_CLOSE );
frame.add( display )           ;
frame.pack()                   ;
frame.setVisible( true )      ;
    frame.setResizable(false) ;
    frame.setLocation(50, 50);
}

public static void execute() {
    datas = new ArrayList<DoubleString>();

    for(int i=0; i<folderList.size(); i++){
        Display.Report = i + "/" + folderList.size() + " file is executed." ;
        System.out.println(Display.Report);
        modifyInputFile(getInputFileName(path + "\\" + folderList.get(i)));
        copyWaveDataFile(folderList.get(i), Display.earthQuakeFile);
        if(executeOneFile(folderList.get(i)){
            getDataFromOutput(folderList.get(i));
        }
    }

    createExcelFile();
    Display.Report = "Ready";
    System.out.println(Display.Report);
}

private static boolean executeOneFile(String folderPath) {
    Process p;
    String exePath = path + "\\" + folderPath;

    try {
        ArrayList<String> cmd = new ArrayList<String>();
        cmd.add(exePath + "\\" + "idarc2d_7.0.exe");

        ProcessBuilder pb = new ProcessBuilder(cmd);
        pb.directory(new File(exePath));
        System.out.println(pb.directory().getAbsolutePath());
        pb.redirectErrorStream(true);

        Process process = pb.start();
        process.getInputStream().close();
        process.waitFor();
        process.getOutputStream().flush();
        process.getOutputStream().close();
        //copy(process.getInputStream(), System.out);
        System.out.println("Exit Status : " + process.exitValue());
        System.out.println("Process Ended");
        if(process.exitValue()==0){

```

```

        return true;
    } else {
        return false;
    }

    /*
    p = pb.start();
    p.waitFor();
    System.out.println("no wait");
    OutputStream inpStr = p.getOutputStream();
inpStr.flush();
inpStr.close();
*/

    /*
    String [] cmds = new String[2];
    cmds[0] = exePath + "\\\" + "idarc2d_7.0.exe";
    cmds[1] = "\\n";
    System.out.println("p is running");
    //p = Runtime.getRuntime().exec(exePath + "\\\" + "idarc2d_7.0.exe", null ,
new File(exePath) );
    p = Runtime.getRuntime().exec(cmds, null , new File(exePath) );
    System.out.println("p wait");
    p.waitFor();
    System.out.println("p no wait");
    OutputStream inpStr = p.getOutputStream();
    System.out.println("got stream");
inpStr.flush();
System.out.println("flushed");
inpStr.close();
*/

    //Thread.sleep(35000);
    //WaitThread wt = new WaitThread(p);
    //wt.start();
    //p.destroy();
    } catch (IOException e) {
        // TODO Auto-generated catch block
        e.printStackTrace();
        return false;
    } catch (InterruptedException e) {
        // TODO Auto-generated catch block
        e.printStackTrace();
        return false;
    }
}

private static String modifyHC(String line){
    int firstIndex = line.indexOf(',');
    firstIndex = line.indexOf(',', firstIndex +1);

```

```

String first = line.substring(0, firstIndex );

first += ", " + Display.hc_alfa;
first += ", " + Display.hc_beta1;
first += ", " + Display.hc_beta2;
first += ", " + Display.hc_N;
first += ", " + Display.hc_eta;
first += ", " + Display.hc_RS;
first += ", " + Display.hc_sigma;
first += ", " + Display.hc_lambda;

int secondIndex = line.lastIndexOf(',', line.length()-1);
String second = line.substring(0,secondIndex);
secondIndex = second.lastIndexOf(',', second.length()-1);
second = line.substring(0,secondIndex);
secondIndex = second.lastIndexOf(',', second.length()-1);
second = line.substring(0,secondIndex);
second = line.substring(second.length());

return first + second;
}

private static String modifyDACD(String line){
    int secondIndex = line.lastIndexOf(',', line.length());
    String second = line.substring(secondIndex);
    String first = Display.dacd_pga;
    first += ", " + Display.dacd_pgav;
    first += ", " + Display.dacd_dt;
    first += ", " + Display.dacd_TotalT;
    first += ", " + Display.dacd_damp;
    return first + second;
}

private static String modifyWD(String line) {
    int firstIndex = line.indexOf(',');
    firstIndex = line.indexOf(',', firstIndex +1);
    String first = line.substring(0, firstIndex );
    first += ", " + Display.wd_totalN;
    first += ", " + Display.wd_dt2;
    return first;
}

private static void getDataFromOutput(String folderPath) {
    DoubleString ds = getOutputFileName(folderPath);
    String outputFileName = ds.str;
    String data = getMaxDriftRatio(outputFileName);
    datas.add(new DoubleString(ds.period, data));
}

private static String getMaxDriftRatio(String outputFileName) {

```

```

File file = new File(outputFileName);
FileInputStream fis;
double max = Integer.MIN_VALUE;
try {
    fis = new FileInputStream(file);
    DataInputStream in = new DataInputStream(fis);
    BufferedReader br = new BufferedReader(new InputStreamReader(in));
    String line = br.readLine();
    int index = line.indexOf("DRIFT RATIO");
    while(index!=-1){
        if(!br.ready()) { return "0"; }
        line = br.readLine();
        index = line.indexOf("DRIFT RATIO");
    }
    line = br.readLine();
    line = br.readLine();
    line = br.readLine();
    line = br.readLine();
    line = br.readLine();
    while(!line.equals("")){
        double temp = getRatio(line);
        if(temp > max){
            max = temp;
        }
        line = br.readLine();
    }
    in.close();
} catch (FileNotFoundException e) {
    // TODO Auto-generated catch block
    e.printStackTrace();
} catch (IOException e) {
    // TODO Auto-generated catch block
    e.printStackTrace();
}
return Double.toString(max);
}

private static double getRatio(String line) {
    double value = 0;
    Matcher matcher = Pattern.compile( "[-+]?\\d*\\.?\\d+([eE][-+]?\\d+)?" ).matcher( line );
    for(int i=0; i<3 && matcher.find(); i++){
        value = Double.parseDouble( matcher.group() );
    }
    return value;
}

private static void createExcelFile(){
    String outputFolderPath = path + "\\\" + javaFolder + "\\\" + outFolder ;
    String outputFilePath = outputFolderPath + "\\\" + Display.outputFileName + ".xls";
}

```

```

File folder = new File(outputFolderPath);
File file = new File(outputFilePath);
try {
    if(!folder.exists()){
        folder.mkdir();
    }
    if(!file.exists()){
        file.createNewFile();
        WriteExcel.write(outputFilePath);
    } else {
        WriteExcel.modify(outputFilePath);
    }
} catch (WriteException e) {
    // TODO Auto-generated catch block
    e.printStackTrace();
} catch (IOException e) {
    // TODO Auto-generated catch block
    e.printStackTrace();
}
}
}

```

..... (Display.java) .....

```
import java.awt.Dimension;
import java.awt.Graphics;
import java.awt.GridLayout;
import java.awt.event.ActionEvent;
import java.awt.event.ActionListener;
import java.io.BufferedReader;
import java.io.DataInputStream;
import java.io.File;
import java.io.FileInputStream;
import java.io.FileNotFoundException;
import java.io.IOException;
import java.io.InputStreamReader;
import java.io.PrintWriter;
import javax.swing.JButton;
import javax.swing.JLabel;
import javax.swing.JPanel;
import javax.swing.JTextField;
```

```
public class Display extends JPanel {
```

```
    static String Report;
```

```
    // HC Parameters
```

```
    static String hc_alfa;
    static String hc_beta1;
    static String hc_beta2;
    static String hc_N;
    static String hc_eta;
    static String hc_RS;
    static String hc_sigma;
    static String hc_lambda;
```

```
    // DACD Parameters
```

```
    static String dacd_pga;
    static String dacd_pgav;
    static String dacd_dt;
    static String dacd_TotalT;
    static String dacd_damp;
```

```
    // Wave Data Parameters
```

```
    static String wd_totalN;
    static String wd_dt2;
```

```
    // Earthquake Ground Motion
```

```
    static String earthquakeFile;
```

```
    // Output File Parameters
```

```

static String outputFileName;
static String outputColumnNumber;
static String columnHeader;

public void construct ()
{
    readOldParameters();

//
    this.setLayout(new BorderLayout(this, BorderLayout.PAGE_AXIS));

    this.setLayout(new GridLayout(30,2));

    // HC Parameters
    add(new JLabel("HYSTERETIC CONTROL PARAMETERS"));
    add(new JLabel(""));

    add(new JLabel("Alfa"));
    final JTextField alfa = new JTextField(hc_alfa, 10);
    add(alfa);

    add(new JLabel("Beta 1"));
    final JTextField beta1 = new JTextField(hc_beta1, 10);
    add(beta1);

    add(new JLabel("Beta 2"));
    final JTextField beta2 = new JTextField(hc_beta2, 10);
    add(beta2);

    add(new JLabel("N"));
    final JTextField N = new JTextField(hc_N, 10);
    add(N);

    add(new JLabel("Eta"));
    final JTextField eta = new JTextField(hc_eta, 10);
    add(eta);

    add(new JLabel("RS"));
    final JTextField RS = new JTextField(hc_RS, 10);
    add(RS);

    add(new JLabel("Sigma"));
    final JTextField sigma = new JTextField(hc_sigma, 10);
    add(sigma);

    add(new JLabel("Lambda"));
    final JTextField lambda = new JTextField(hc_lambda, 10);
    add(lambda);

    // DACD Parameters

```

```

add(new JLabel(""));
add(new JLabel(""));
add(new JLabel("DYNAMIC ANALYSIS CONTROL DATA
PARAMETERS"));
add(new JLabel(""));

add(new JLabel("PGA"));
final JTextField pga = new JTextField(dacd_pga, 10);
add(pga);

add(new JLabel("PGAV"));
final JTextField pgav = new JTextField(dacd_pgav, 10);
add(pgav);

add(new JLabel("DT"));
final JTextField dt = new JTextField(dacd_dt, 10);
add(dt);

add(new JLabel("Total T"));
final JTextField TotalT = new JTextField(dacd_TotalT, 10);
add(TotalT);

add(new JLabel("Damp"));
final JTextField damp = new JTextField(dacd_damp, 10);
add(damp);

// Wave Data Parameters
add(new JLabel(""));
add(new JLabel(""));
add(new JLabel("WAVE DATA PARAMETERS"));
add(new JLabel(""));
add(new JLabel("Total N"));
final JTextField totalN = new JTextField(wd_totalN, 10);
add(totalN);
add(new JLabel("DT 2"));
final JTextField dt2 = new JTextField(wd_dt2, 10);
add(dt2);
add(new JLabel("EarthQuake File Name"));
final JTextField earthQuake = new JTextField(earthQuakeFile, 20);
add(earthQuake);
add(new JLabel(""));
add(new JLabel(""));
add(new JLabel("OUTPUT FILE PARAMETERS"));
add(new JLabel(""));
add(new JLabel("Output File Name"));
final JTextField outputFile = new JTextField(outputFileName, 20);
add(outputFile);
add(new JLabel("Output Column Number"));

```

```

        final JTextField outputColumn = new
JTextField(Integer.toString((Integer.parseInt(outputColumnNumber)+1)), 2);
        add(outputColumn);

        add(new JLabel("Output Column Header"));
        final JTextField header = new JTextField("", 25);
        add(header);
        add(new JLabel(""));
        add(new JLabel(""));
        add(new JLabel(Report));
        JButton executeButton = new JButton("Execute");
        executeButton.addActionListener(new ActionListener() {
            public void actionPerformed(ActionEvent e) {
                // Execute
                // HC Parameters
                hc_alfa = alfa.getText();
                hc_beta1 = beta1.getText();
                hc_beta2 = beta2.getText();
                hc_N = N.getText();
                hc_eta = eta.getText();
                hc_RS = RS.getText();
                hc_sigma = sigma.getText();
                hc_lambda = lambda.getText();

                // DACD Parameters
                dacd_pga = pga.getText();
                dacd_pgav = pgav.getText();
                dacd_dt = dt.getText();
                dacd_TotalT = TotalT.getText();
                dacd_damp = damp.getText();

                // Wave Data Parameters
                wd_totalN = totalN.getText();
                wd_dt2 = dt2.getText();

                // Earthquake Ground Motion
                earthQuakeFile = earthQuake.getText();

                // Output File Parameters
                outputFileName = outputFile.getText();
                outputColumnNumber = outputColumn.getText();

                columnHeader = header.getText();
                saveParameters();
                Frames.execute();
            }
        });
        add(executeButton);
    }
    public Display(){

```

```

        construct();
    }

    private void saveParameters() {
        String parameterPath = Frames.path + "\\\" + Frames.javaFolder + "\\\" +
Frames.parameterFile;
        File file = new File(parameterPath);
        try {
            if(!file.exists()){
                file.createNewFile();
            }
            PrintWriter writer;
            writer = new PrintWriter(file, "UTF-8");
            writer.println(hc_alfa);
            writer.println(hc_beta1);
            writer.println(hc_beta2);
            writer.println(hc_N);
            writer.println(hc_eta);
            writer.println(hc_RS);
            writer.println(hc_sigma);
            writer.println(hc_lambda);
            writer.println(dacd_pga);
            writer.println(dacd_pgav);
            writer.println(dacd_dt);
            writer.println(dacd_TotalT);
            writer.println(dacd_damp);
            writer.println(wd_totalN);
            writer.println(wd_dt2);
            writer.println(earthQuakeFile);
            writer.println(outputFileName);
            writer.println(outputColumnNumber);
            writer.close();

        } catch (FileNotFoundException e) {
            // TODO Auto-generated catch block
            e.printStackTrace();
        } catch (IOException e) {
            // TODO Auto-generated catch block
            e.printStackTrace();
        }
    }

    private static void readOldParameters() {
        String parameterPath = Frames.path + "\\\" + Frames.javaFolder + "\\\" +
Frames.parameterFile;
        File file = new File(parameterPath);
        if(file.exists()){
            try {
                FileInputStream fis = new FileInputStream(file);
                DataInputStream in = new DataInputStream(fis);

```

```

        BufferedReader br = new BufferedReader(new
InputStreamReader(in));
        readParameters(br);
        in.close();
    } catch (FileNotFoundException e) {
        // TODO Auto-generated catch block
        e.printStackTrace();
    } catch (IOException e) {
        // TODO Auto-generated catch block
        e.printStackTrace();
    }
}
}

```

```

private static void readParameters(BufferedReader br){
    // HC Parameters
    hc_alfa = getStringFromLine(br);
    hc_beta1 = getStringFromLine(br);
    hc_beta2 = getStringFromLine(br);
    hc_N = getStringFromLine(br);
    hc_eta = getStringFromLine(br);
    hc_RS = getStringFromLine(br);
    hc_sigma = getStringFromLine(br);
    hc_lambda = getStringFromLine(br);

    // DACD Parameters
    dacd_pga = getStringFromLine(br);
    dacd_pgav = getStringFromLine(br);
    dacd_dt = getStringFromLine(br);
    dacd_TotalT = getStringFromLine(br);
    dacd_damp = getStringFromLine(br);

    // Wave Data Parameters
    wd_totalN = getStringFromLine(br);
    wd_dt2 = getStringFromLine(br);

    // Earthquake Ground Motion
    earthquakeFile = getStringFromLine(br);

    outputFileName = getStringFromLine(br);
    outputColumnNumber = getStringFromLine(br);
}

```

```

private static double getDoubleFromLine(BufferedReader br){
    String strLine;
    double d = 0;
    try {
        if((strLine = br.readLine()) != null) {
            d = Double.parseDouble(strLine);
        }
    }
}

```

```

    } catch (NumberFormatException e) {
        // TODO Auto-generated catch block
        e.printStackTrace();
    } catch (IOException e) {
        // TODO Auto-generated catch block
        e.printStackTrace();
    }
    return d;
}

private static String getStringFromLine(BufferedReader br){
    String strLine = "";
    try{
        strLine = br.readLine();
    } catch (NumberFormatException e) {
        // TODO Auto-generated catch block
        e.printStackTrace();
    } catch (IOException e) {
        // TODO Auto-generated catch block
        e.printStackTrace();
    }
    return strLine;
}

@Override
public Dimension getPreferredSize ()
{
    // Preferred size for the display

    return new Dimension(600,500 );
}

public static void step(){
    //repaint() ;
    try {
        Thread.sleep( 50 );
    } catch (InterruptedException e) {
        // TODO Auto-generated catch block
        e.printStackTrace();
    }
}
}
}

```

..... (DoubleString.java) .....

```
public class DoubleString{
    public String period;
    public String str;
    public DoubleString(String p, String s){
        period = p;
        str = s;
    }
};
```

..... (WaitThread.java) .....

```
import java.io.IOException;
import java.io.OutputStream;

public class WaitThread extends Thread {

    Process p;
    OutputStream inpStr;
    public WaitThread(Process p){
        this.p = p;
    }

    public void run(){
        double startTime = System.currentTimeMillis();
        double currentTime = System.currentTimeMillis();
        double waitTime = 35000;
        while(currentTime - startTime < waitTime){
            currentTime = System.currentTimeMillis();
        }
        try {
            inpStr = p.getOutputStream();
            inpStr.flush();
            inpStr.close();
            p.destroy();
        } catch (IOException e) {
            // TODO Auto-generated catch block
            e.printStackTrace();
        }
        this.interrupt();
    }
}
```

..... (WriteExcel.java) .....

```
import java.io.File;
import java.io.IOException;
import java.util.Locale;
import jxl.CellType;
import jxl.CellView;
import jxl.Workbook;
import jxl.WorkbookSettings;
import jxl.format.CellFormat;
import jxl.format.UnderlineStyle;
import jxl.read.biff.BiffException;
import jxl.write.Label;
import jxl.write.WritableCell;
import jxl.write.WritableCellFormat;
import jxl.write.WritableFont;
import jxl.write.WritableSheet;
import jxl.write.WritableWorkbook;
import jxl.write.WriteException;
import jxl.write.biff.RowsExceededException;

public class WriteExcel {
    private static WritableCellFormat timesBoldUnderline;
    private static WritableCellFormat times;

    public static void modify(String outputFile){
        System.out.println("Out: " + outputFile);
        //String outputPath = Frames.path + "\\\" + Frames.javaFolder + "\\\" +
Frames.outFolder + "\\\" + Display.outputFileName + ".xls";
        File file = new File(outputFile);
        Workbook workbook;
        try {
            System.out.println("Name: " + file.getAbsolutePath() + "--" +
file.getName());

            workbook = Workbook.getWorkbook(file);

            File tempFile = new File("temp.xls");
            WritableWorkbook copy = Workbook.createWorkbook(tempFile,
workbook);

            WritableSheet sheet2 = copy.getSheet(0);

/*
            Workbook workbook1 = Workbook.getWorkbook(file);
            WritableWorkbook copy = Workbook.createWorkbook(file , workbook1);
            WritableSheet sheet2 = copy.getSheet(0);
*/

            createLabel(sheet2);
        }
    }
}
```

```

        createContent(sheet2);

        copy.write();
        copy.close();
        workbook.close();
        file.delete();
        tempFile.renameTo(file);
    } catch (BiffException e) {
        // TODO Auto-generated catch block
        e.printStackTrace();
    } catch (IOException e) {
        // TODO Auto-generated catch block
        e.printStackTrace();
    } catch (WriteException e) {
        // TODO Auto-generated catch block
        e.printStackTrace();
    }
}

public static void write(String outputFile) throws IOException, WriteException {
    File file = new File(outputFile);
    WorkbookSettings wbSettings = new WorkbookSettings();

    wbSettings.setLocale(new Locale("en", "EN"));

    WritableWorkbook workbook = Workbook.createWorkbook(file, wbSettings);
    workbook.createSheet("Report", 0);
    WritableSheet excelSheet = workbook.getSheet(0);
    createLabel(excelSheet);
    createContent(excelSheet);
    workbook.write();
    workbook.close();
}

private static void createLabel(WritableSheet sheet) throws WriteException {
    WritableFont times10pt = new WritableFont(WritableFont.TIMES, 10);
    times = new WritableCellFormat(times10pt);
    times.setWrap(true);
    WritableFont times10ptBoldUnderline = new WritableFont(WritableFont.TIMES, 10,
    WritableFont.BOLD, false, UnderlineStyle.SINGLE);
    timesBoldUnderline = new WritableCellFormat(times10ptBoldUnderline);
    timesBoldUnderline.setWrap(true);

    CellView cv = new CellView();
    cv.setFormat(times);
    cv.setFormat(timesBoldUnderline);
    cv.setAutosize(true);

    // Write a few headers

```

```

addCaption(sheet, 0, 0, "Notes:");
addCaption(sheet, 0, 1, "Period");
addCaption(sheet, Integer.parseInt(Display.outputColumnNumber), 1, Display.columnHeader);
//addCaption(sheet, 1, 1, Display.columnHeader);
}

private static void createContent(WritableSheet sheet) throws WriteException,
RowsExceededException {
    for (int i = 0; i < Frames.datas.size(); i++) {
        String sPeriod = Frames.datas.get(i).period;
        if(sPeriod .length()>4) {sPeriod = sPeriod .substring(0, 4);}
        addLabel(sheet, 0,i+2, sPeriod );
        addLabel(sheet, Integer.parseInt(Display.outputColumnNumber) ,i+2,
Frames.datas.get(i).str);
        //addLabel(sheet, 1,i+2, Frames.datas.get(i).str);
    }
}

private static void addCaption(WritableSheet sheet, int column, int row, String s) throws
RowsExceededException, WriteException {
    Label label;
    label = new Label(column, row, s, timesBoldUnderline);
    sheet.addCell(label);
}

private static void addLabel(WritableSheet sheet, int column, int row, String s) throws
WriteException, RowsExceededException {
    Label label;
    label = new Label(column, row, s, times);
    sheet.addCell(label);
}
}
.....

```

## CURRICULUM VITAE

### PERSONAL INFORMATION

Surname, Name :Etemadi, Ali  
Nationality :Iranian  
Date and Place of Birth :26 April 1983 , Oroumieh  
Marital Status :Single  
Phone : +90 554 832 7909  
Fax : +90 (312) 448 0081  
Email : alietemadi.83@gmail.com

### EDUCATION

Degree	Institution	Year of Graduation
PhD	METU, Civil Engineering- structures	2015
MS	I. Azad University of Mahabad, Civil Engineering- structures	2009
BS	I. Azad University of Mahabad, Civil Engineering	2006
High School	Andishe Borna High School, Oroumieh	2002

### WORK EXPERIENCE

Year	Place	Enrollment
2012-2014	Çankaya University, Department of Civil Engineering	Research Assistant
2009-	The Industrial Group of Mohammadzadeh (Bridge Construction)	Site Manager
2005-2008	Vila Tejarat Company (Shopping Center Construction Project)	Structural Consulting and Supervision

### FOREIGN LANGUAGES

Advanced English, Fluent Persian and Turkish

## **PUBLICATIONS & PROJECT WORK**

Gülkan P., and Etemadi A., 2014. “Lineer Olmayan Kayma Çerçeveleri İçin Yaklaşık Kat Arası Yer Değiştirme Spektrumu”, Project Report No. 111M551, (TÜBİTAK), The Scientific And Technological Research Council Of Turkey.

Etemadi A., Gülkan H. P., 2015. “Estimation of Seismic Drift Demands for Inelastic Shear Frame Structures”, World Academy of Science, Engineering and Technology (WASET), Civil and Environmental Engineering Vol: 2, No: 6, XIII International Conference on Civil, Structural and Earthquake Engineering (ICCSEE-2015), Toronto, Canada.

## **HOBBIES**

Archaeology, Tae Kwan Do, Swimming, Sculpture, Painting